CONCEPTUAL DESIGN OF THE VALMEER'S PUMP STORAGE STATION OF THE DELTA21 PLAN

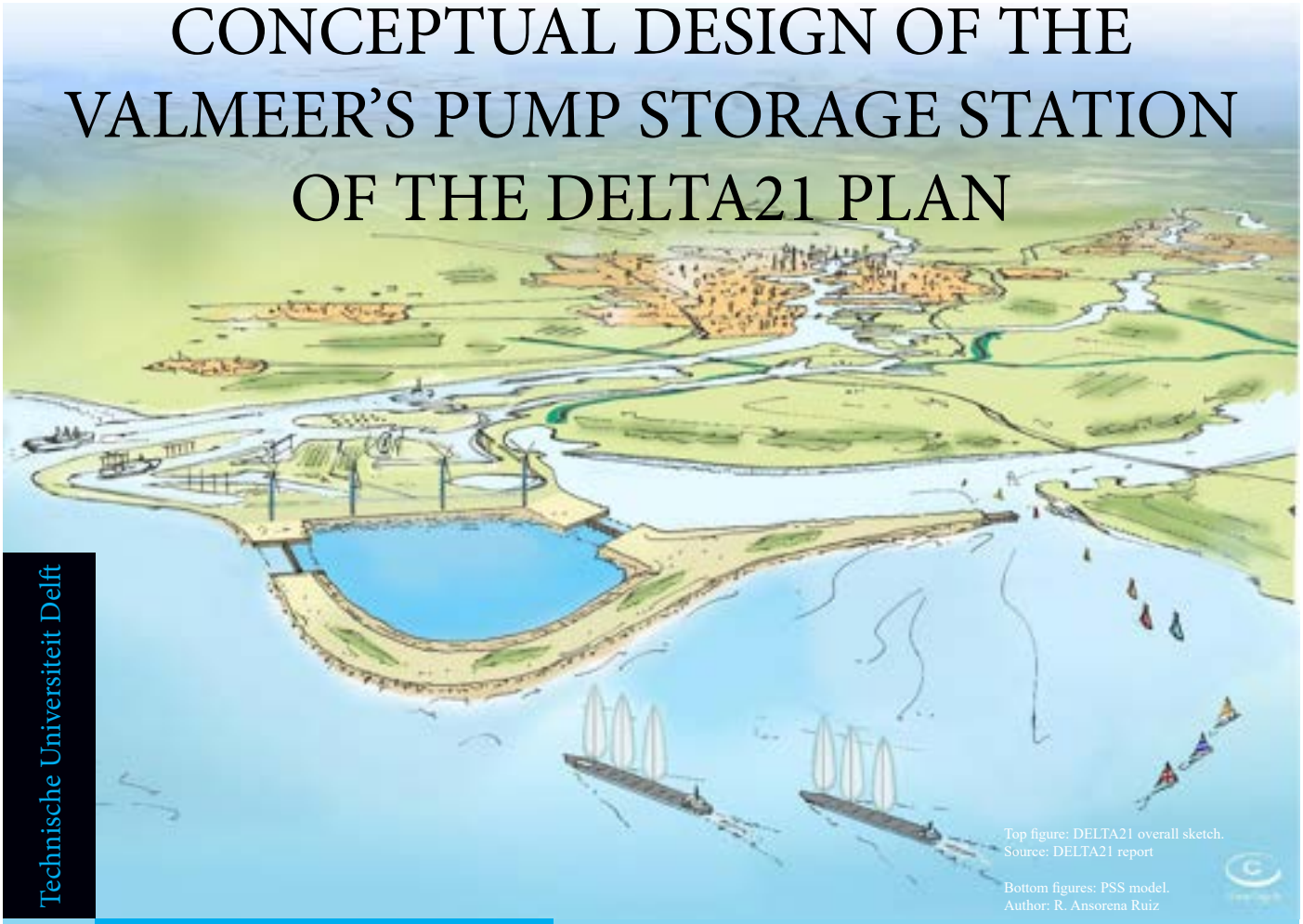

Top figure: DELTA21 overall sketch.
Source: DELTA21 report

Bottom figures: PSS model.
Author: R. Ansorena Ruiz

Technische Universiteit Delft

Ruben Ansorena Ruiz
Student number: 4718208

January 2020

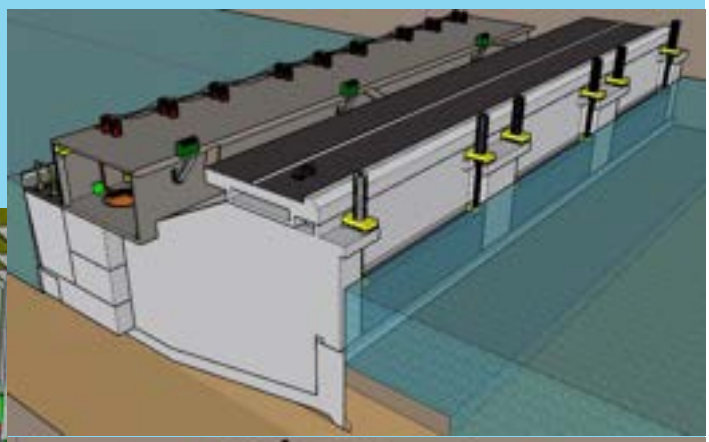

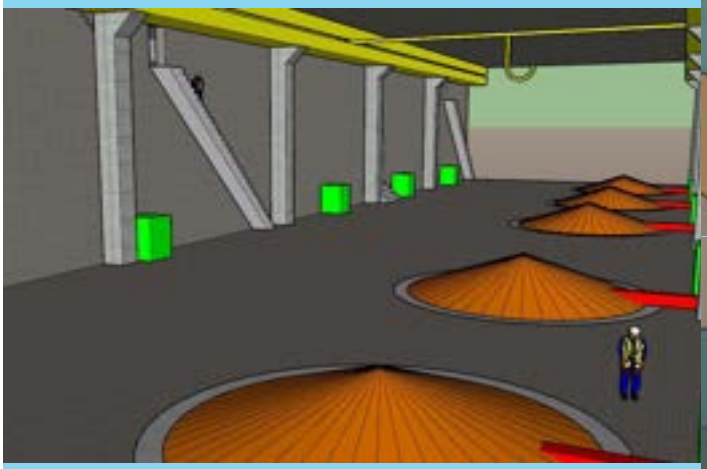

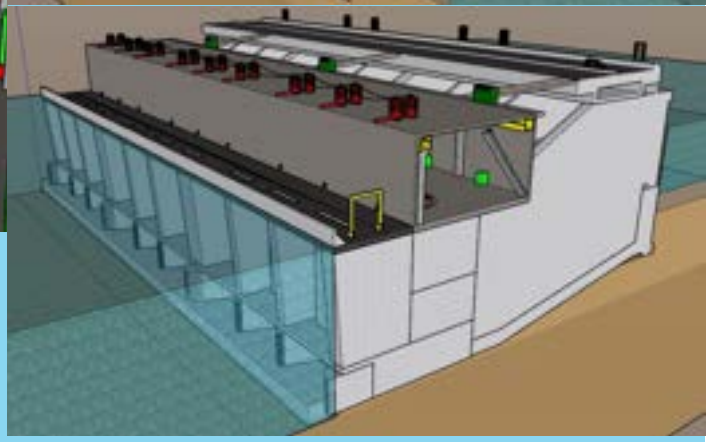

TU Delft

Conceptual design of the Valmeer's pump storage station of the DELTA21 plan

by

Ruben Ansorena Ruiz

Student number: 4728208

Delft University of Technology
January 2020

Thesis committee:	Prof. dr. ir. S.N. (Bas) Jonkman	TU Delft
	Dr. ing. M.Z. (Mark) Voorendt	TU Delft
	Dr. H.M. (Henk) Jonkers	TU Delft
	Ir. D. (Daan) van der Wiel	VolkerWessels Infra Competence Center
	Ir. H.A. (Huub) Lavooij	DELTA21

In collaboration with:

Preface

This document represents the MSc thesis needed to fulfill my academic requirements for completing the Master of Science in Hydraulic Engineering (Hydraulic Structures specialization) at the TU Delft.

This report is the result of 9 months of work done between Delft and Vianen, where the offices of VolkerWessels Infra Competence Center are situated. There I got professional advice and they all helped me with the development of this thesis. Besides, I have to mention that this thesis is part of the DELTA21 plan. Where students and other professionals are designing and/or researching other parts this bigger plan.

I am glad to finally present the result of my work. Doing a conceptual design of a structure like this one was not easy due to the time limit of 40 ECTS, especially at the beginning of the thesis when I used to "waste" time looking at some specifics that were vital for performing an adequate conceptual design. However, while developing the thesis, I improved my decision-making allowing me to make proper assumptions and organize the time I would spend in each activity in an efficient way. I consider this thesis finished because the following steps for having a more detailed design can be part of other MSc Thesis or Additional Thesis. I leave that responsibility to the rest of my student colleagues.

I would like to express my gratitude and respect towards the committee that help me arrive to where I am now. To Daan van der Wiel (VolkerWessels ICC) for not only the technical help and showing me real projects, but especially for helping me to feel comfortable at the offices where the common language is reasonably dutch. To Huub Lavooij and Leen Berke (DELTA21) for letting me be a part of their plan and give me all the freedom in terms of decision-making about my thesis, without requiring me to follow their most-preferred way, after all, that would have been better for them. To Mark Voorendt for being always able to chat about the thesis, being so responsive to emails and helping me to follow a structured design. To Henk Jonkers for giving me the guidelines I needed to jump into the LCA world and to perform my design not only focusing on monetary but also, on environmental costs. Finally, I'd like to thank the chairman Bas Jonkman for his useful and direct feedback during the multiple meetings we've had.

I cannot forget about my friends, you are my family abroad. I don't want to leave anyone out so I won't mention any names but special mention, to the NS56's crew with whom I've shared academic and extra-academic thoughts, parties, dinners, trips and lots of good times together since the beginning of our stay in the Netherlands. Thanks to all the hydraulic friends with whom I've passed through the toughest study times and projects but always found some time to chill and celebrate. To the Zamarrans team for bringing the tiqui-taka to the X's football fields and sincerely, to everyone I have shared some time with since I arrived in the Netherlands, thank you very much. Sharing experiences with people having other cultures, ideas and interests is for me what makes the living abroad really interesting and allows you to keep an open mind, and evolving as a homo sapiens.

I'd like to conclude the acknowledgments by thanking my family. Thanks, mom and dad for encouraging me to start university and support me on the tough times. Without you, I probably wouldn't have started university. Thanks to your sacrifices I've been able to graduate from a master's at the Technical University of Delft, feel proud. My most sincere love for my grandpas for all their love, kindness, comprehension and support.

I want to dedicate this thesis to you "tito", you couldn't see my academic journey coming to an end but I am sure you would have been the proudest grandpa ever.

Ruben Ansorena Ruiz.
Delft, 19^{th} January 2020

Summary

It is widely known that climate change will cause sea level rise and larger river discharges in the close future (because more precipitation during a shorter amount of time will happen). In the Netherlands, the delta works were developed to protect the hinterland from sea-water during storm surge situations. The storm surge barriers close and the water is kept at the sea. However, if large river discharges are present together with storm surge, the water level behind the barriers will rise because the closed barrier won't let the river water out. In delta areas, this is a major threat to water safety. To tackle these future problems Huub Lavooij and Leen Berke came up with the DELTA21 plan.

The plan is to build a storm surge barrier together with pumps that can evacuate the water from the river in the event of having both storm surge and large river discharges happening simultaneously. As this situation will happen once every ten years on average, there is a risk that the pumps might not function when needed if they were on hold for ten years. To tackle that problem and also producing green energy, a hydro pump storage basin is proposed to take advantage of the pumps already installed for flood protection. This hydro pump storage basin is called Valmeer. As this structure would be built next to the Maasvlakte 2, in a red Natura 2000 area, some ecological value must be gained with this project in return. That is why the Getijmeer (tidal lake) was created. This tidal lake would allow opening the Haringvliet sluices and thus recovering fish migration in that area. Bringing then the ecological, recreational and economic value to the Haringvliet area, which is currently closed to the sea. The objective of this thesis is to create a conceptual design of a hydro pump storage station able to turbine water in for energy generation and to pump it out for the same purpose and also for water safety.

For designing the plant, three locations and three different alternatives were considered. Finally, a pump storage station that is also a storm surge barrier is proposed in the northern part of the DELTA21 plan, next to the Maasvlakte 2. Aspects such as constructability, affection of sediment transport to the plant, wave loading and access to the plant were taken into account for choosing the location and the most suitable alternative.

The chosen alternative was found to be a good option if special care is taken about piping protection (the structure is subjected to head differences of 23 meters) and about methods to avoid water infiltration into the building pit during the construction of the plant (the building pit's floor is at NAP -32 m).

As a part of the design, a life cycle analysis on CO_2 emissions was performed. This showed that the hydro pump storage station can bring positive ecological value in terms of CO_2 emissions reduction for the grid of the Netherlands. Producing energy at 280 g of CO_2 / kWh at present grid conditions and at -140 g of CO_2 / kWh if renewable energy is used to power the pumps. The conventional fossil fuel energy-producing methods do it at between 500 and 1050 g of CO_2 / kWh.

Therefore this thesis shows that the DELTA21 plan is not only good for flood protection but for renewable energy generation. Contributing then to the United Nations Sustainable Development Goals of "affordable and clean energy" (energy generation function) and "life on land" (water safety function).

In the following page, a cross-section of the final conceptual design together with the seepage path is included.

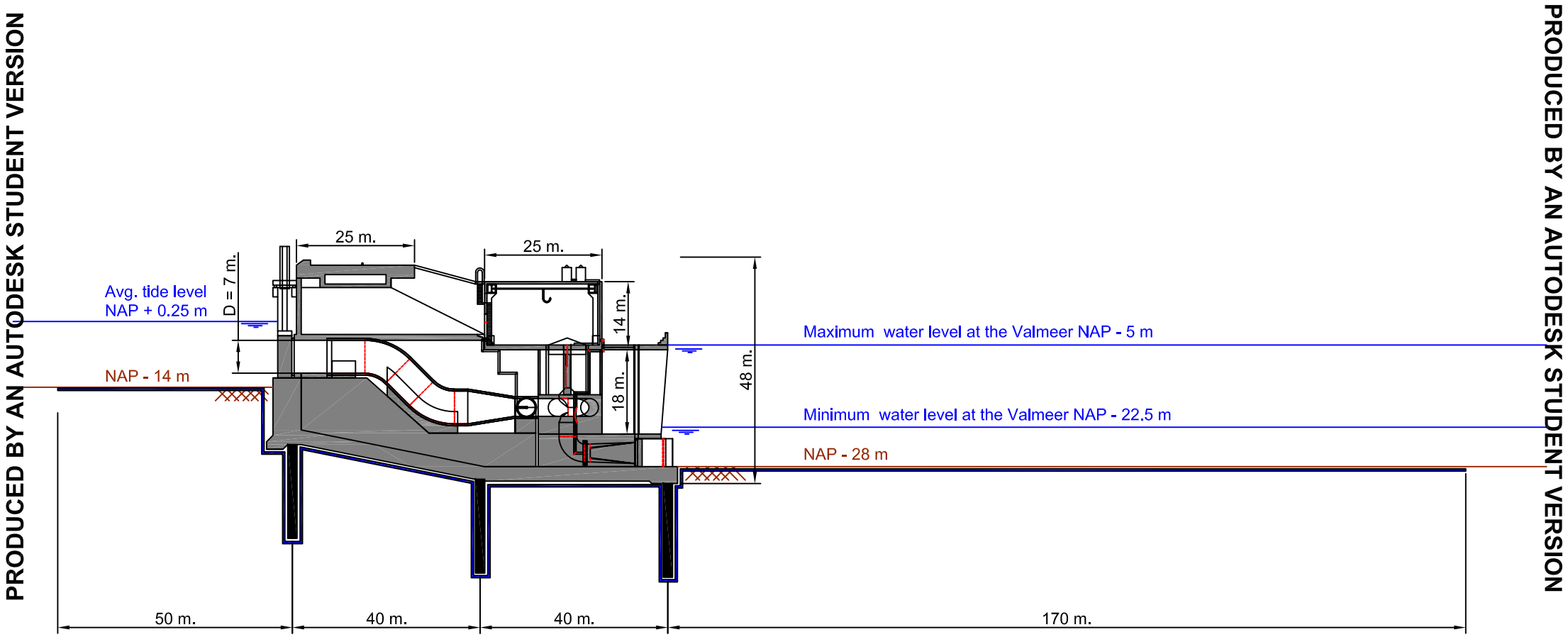

PRODUCED BY AN AUTODESK STUDENT VERSION

PRODUCED BY AN AUTODESK STUDENT VERSION

Table of contents

Chapter 1

Introduction

Nowadays it is widely assumed that climate change is a major threat all around the globe. For coastal areas, there are multiple consequences. For the aim of this study, the most important effects are sea level rise and the increase in the occurrence of extreme storm events, meaning that more and stronger storms (and therefore waves) will reach the coast (Villarini and Vecchi, 2012). Besides, as a consequence of climate change, extreme river discharges will also increase (van Vliet et al, 2013). Apart from the coastal erosion caused by sea level rise (Nicholls, 2010), in the delta area of the Netherlands, sea level rise threats also interior cities, especially the ones adjacent to the rivers, due to the expected larger river discharges in case of an extreme storm event.

Even by reducing the CO_2 emissions to zero, sea level rise will still happen (IPCC report, 2018). This is a well-known problem in the Netherlands and the dutch are continuously adapting to climate change. Currently, with the delta works, the dutch coast and interior areas are protected against flooding. However, if the future protective strategy is to keep raising and reinforcing dikes, 800 km of dike increases will be needed in the future (Lavooij, 2018).

Additionally, to fight climate change it is important to eliminate the use of fossil fuels and start generating renewable energy. To reach the goal of just warming the Earth to 1.5 degrees centigrade from pre-industrial levels, the global CO_2 emissions have to drop to zero by 2050 (IPCC report,2018).

In order to mitigate the above-mentioned issues, the DELTA21 plan arose from a discussion between its two initiators (Leen Berke and Huub Lavooij) at the beginning of 2015. The plan integrates different functions such as flood protection, storage and generation of energy, restoration of saline intrusion within the Haringvliet up to Tiengemeten and freshwater guarantee for Rotterdam and the surrounding areas. The DELTA21 plan is located in South Holland, west of the Haringvliet flood defense, southwest of the Maasvlakte (see Figure 1.1 below).

Figure 1.1: DELTA21's location

The whole plan can be divided into three elements: Valmeer (Energy Storage Lake, ESL), Getijmeer (tidal lake) and Haringvliet (former sea-arm). In the following picture, these 3 elements are shown as so as some important parts of the whole DELTA21 system:

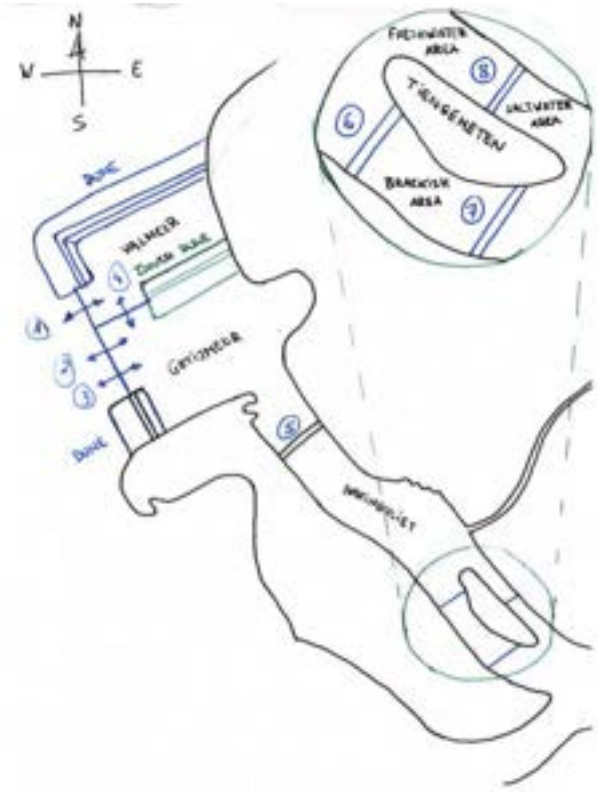

Figure 1.2: Sketch showing the elements of DELTA21.

The above numbers correspond to:

1. Inlet/outlet Valmeer
2. Inlet/outlet Getijmeer
3. Ship lock
4. Spillway
5. Haringvlietdam with discharge sluices and ship lock
6. Western brackish area dam
7. Eastern brackish area dam
8. Dam north of Tiengemeten

It is still a conceptual plan and it has to be looked at more deeply to see if its realization is feasible. The project proposed in this thesis addresses a conceptual design of one of the components of the DELTA21 plan: the hosting structure for the combined pumps/turbines of the energy storage lake (element 1 in Figure 1.2).

Chapter 2

Problem analysis and design objective

2.1 System breakdown structure

2.1.1 The DELTA21 main concept

The following information is of importance to understand the motivation of DELTA21, the information has been retrieved from the DELTA21 report on flood risk reduction (Lavooij et al., 2018).

DELTA21 plan takes into account the future needs of the Netherlands. It will allow us to avoid the raising and reinforcement of 800 km of dikes since proper water level control can be achieved by managing the water level at the Getijmeer. If DELTA21 is implemented, the normative water levels in the interior of the Haringvliet and upstream of the Maeslant barrier will be lowered. Leading to big savings in dike increase. Assuming an increase of 25 % in dike increase works after 2050 (due to sea level rise), and assuming that about 60 % of the budget will be used for dike increase, the implementation of DELTA21 will save around €2.2 billion from 2029-2050 and €6.3 billion from 2029-2100 in this matter (Lavooij, 2018).

In cities such as Dordrecht, with the present protective structures, flood risk reduction problems will arise soon if we take into account soil subsidence and sea level rise. In present times, the Maeslant barrier closes when the level at Hoek Van Holland is at NAP + 3 m. or when the water level at Dordrecht is at NAP + 2.9 m, that is once every 5 years. If we take into account a sea level rise of one meter, the frequency of closing will be increased to once every year, provoking a threat for the business in the Port of Rotterdam. After the implementation of DELTA21, the frequency of closing of the Maeslant barrier will be reduced by half. That is, once every 10 years and the water level at Dordrecht can remain at a maximum of NAP + 2.5 m even when the Maeslant barrier is open. This means that even in the event of failure of the Maeslant barrier (1/1000 or 1/2000 years), and having storm surge and high river discharge, flood risk reduction will still be ensured with only DELTA21.

2.1.2 The main components

The core of the DELTA21 program is the Energy Storage Lake (Valmeer). Here, the excess river runoff water can be pumped out of the system to avoid flooding of the upstream areas during closure of the inlet/outlet structure due to a storm surge. The great capacity of the pumps will allow them to get rid of the excess river discharge during extreme storm events (maximum discharge of 10.000 m^3/s). Additionally, during regular sea-conditions, water can be turbined into the Valmeer to obtain electrical energy. During the day (expensive electricity) the water is pumped into the Valmeer and during the night, it is pumped out (cheap electricity). The exterior part of the Energy Storage Lake will be composed of sprayed sandy dunes (see the "DUNE" element in Figure 1.2). The sand will come from the dredged material extracted from the Energy Storage Lake.

The Getijmeer will have a barrier open during regular conditions and closed during storm surge conditions. The water level upstream of the Haringvliet is controlled here by lowering the water level at the Getijmeer via letting water though the Valmeer's spillway. During regular conditions, the Getijmeer's gates will remain open allowing saltwater to come within the Haringvliet.

In principle, the storm surge barrier function will be carried out by the combination of the exterior dunes of

both Valmeer and Getijmeer, by the inlet/outlet of both Valmeer and Getijmeer and by the ship lock of the Getijmeer (DUNE, 1, 2, and 3 in Figure 1.2). DELTA21 will allow to leave the dike levels as they currently are even in the event of large (1 m) sea-level rise (Lavooij, 2018) and will cut by half the probability of closing the Maeslant barrier with respect to the present configuration, reducing it from 1/1 years to 1/2 years for the worst sea-level scenario (that is, for a SLS of 1 m.) (Lavooij, 2018).

Concerning the transition towards green energy, DELTA21 is also useful because it will generate hydro-electricity at the Energy Storage Lake since the beginning of its use. Eventually, windmills and solar panels can also be installed in the system.

DETA21 will also bring an ecological improvement. Since the already existing Haringvlietdam will lose its storm surge barrier function, its gates can be completely opened to allow saltwater intrusion back into the Haringvliet and restore fish migration. This is of importance not only ecologically, but for the local economy, since the ecological recovery will bring back business for, among others, fisheries and tourism. However, it is important to avoid contamination of fresh water supply to Rotterdam and its surroundings, for that reason, a set of three dams around Tiengemeten island will be built to allow for an adequate transition between fresh and saltwater. Saltwater won't go further east than Tiengemeten island and freshwater won't go further west than Tiengemeten island. In the south part of the island, two barriers will make up for a brackish water area where the exchange between salt and freshwater happens (see detail in Figure 1.2). On the north side, a channel will collect freshwater to supply Rotterdam and its surroundings.

To have a clearer image of all the different elements of the DELTA21 plan, an element tree is shown below (notice that the numbers in Figure 1.2 are also shown in the element tree):

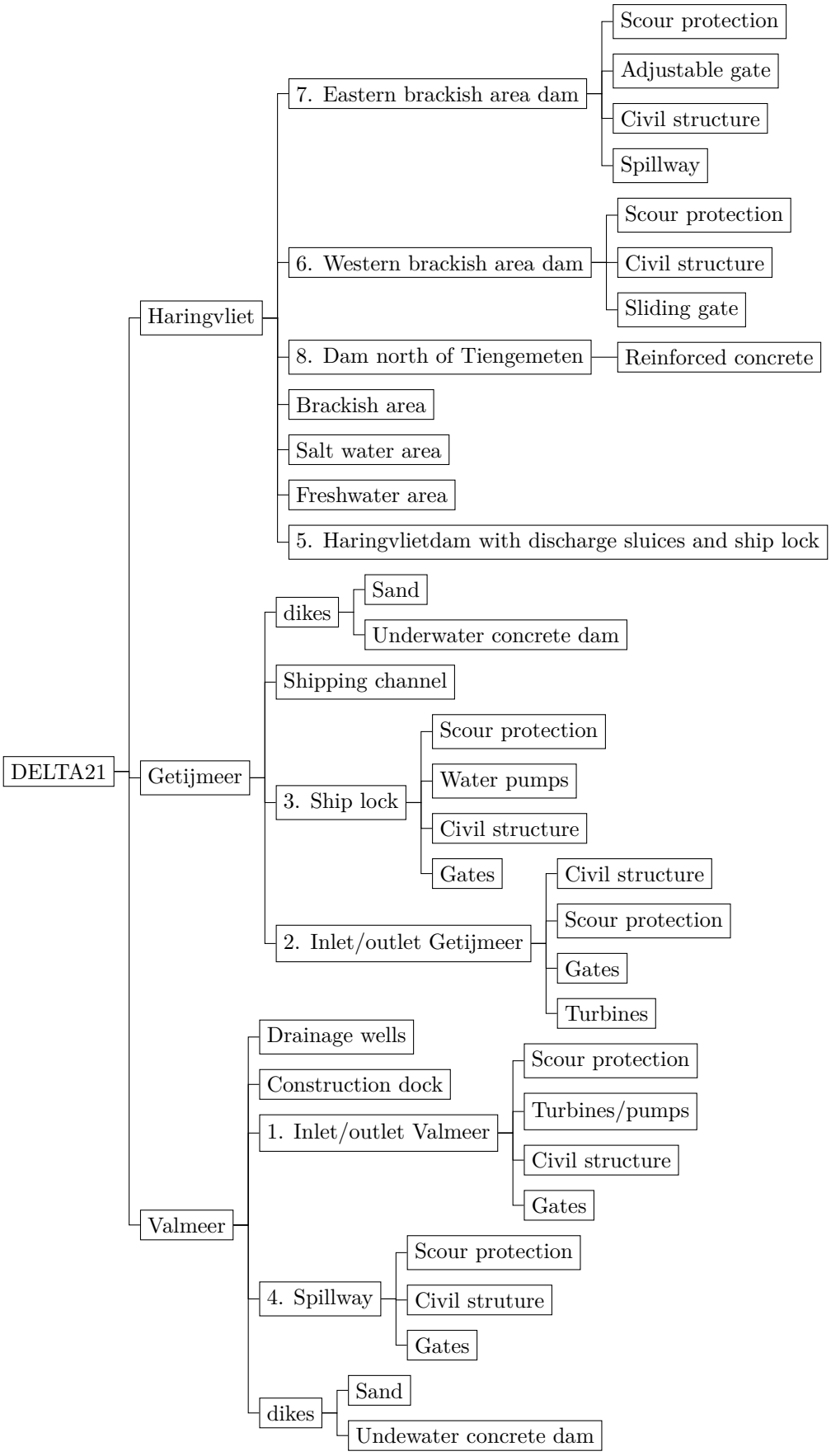

Figure 2.1: DELTA21 system breakdown structure

2.1.3 The Valmeer concept

In this thesis, the focus will be on the structures used to host the turbines/pump which will add/remove water to/out of the Valmeer. According to the preliminary DELTA21 plan, the Valmeer, also known as Energy Storage Lake has a maximum storage of 400 million m^3. The bottom of the basin will be at NAP -25 m, having some channeled areas down to NAP -27 m (see Figure 2.2). However, the minimum water level will be kept at NAP -22.5 m and the maximum at NAP -5 m. Therefore, the maximum amount of water head to be turbined will be of 17.5 m

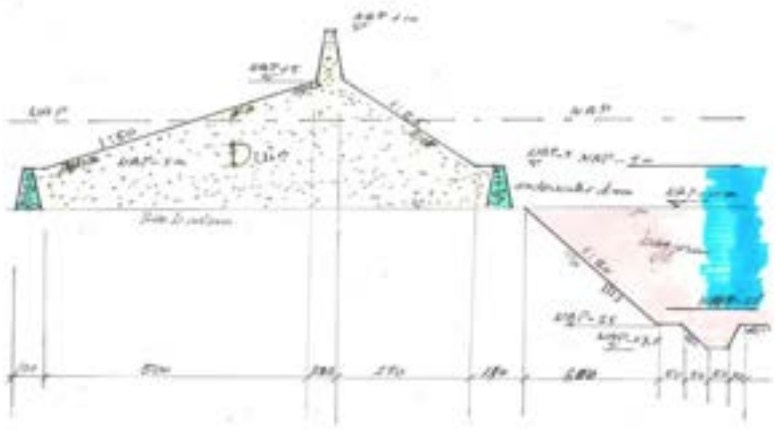

Figure 2.2: Cross section Valmeer protection dunes and storage basin. (Lavooij, 2018)

For turbining/pumping the water coming into/leaving the Valmeer, the initial idea was to install 93 pumps of 20 MW each (Lavooij, 2018). Also, the initiators planned to construct caissons around $3 \times 187 = 560$ m long to then install the pumps/turbines inside (Lavooij, 2018). However, other alternatives will be discussed further in this document (see SectionffunctionalDEsign). It is of importance to make the caissons accessible from above for maintenance purposes. Regarding the construction method, the initial idea is that these caissons will be built in three different phases. In a building pit, the first two parts will be constructed and then taken to position floating and carried by the use of tugboats. The third part will be cast in place since it can be done in the dry (see Figure 2.3). Anyways, other construction methods will also be considered (see Appendix I).

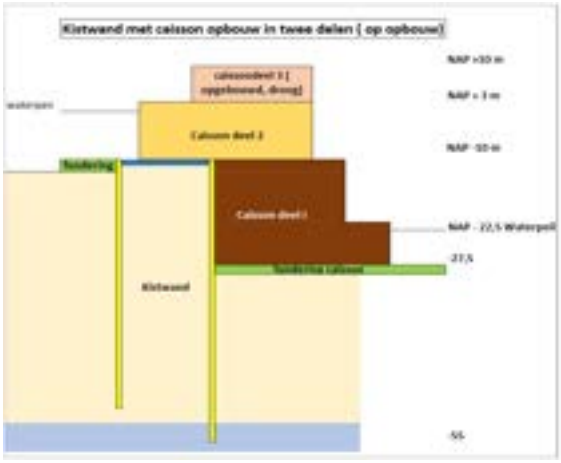

Figure 2.3: Construction sequence for the caissons (Lavooij, 2018)

2.2 System operation modes

To be able to obtain the water levels and boundary conditions, 4 different working scenarios for the DELTA21 system are currently considered. It is true that in reality, these 4 scenarios can be better defined (even new scenarios could be defined), but it has been considered that for the purpose of this thesis (and since other

students are working on this more accurate definition of the DELTA21 scenarios) which is the design of the ESL Power Plant, the following 4 scenarios are accurate enough to define the worst cases for designing the structure.

1. Regular sea conditions and low river discharge
2. Regular sea conditions and high river discharge
3. Sea storm and low river discharge
4. Sea storm and high river discharge

First, let's define the concepts of "sea storm", "Regular sea conditions", "low river discharge" and "high river discharge".

1. Sea storm conditions refer to the time period when a combination of design storm surge, sea level rise scenario and spring tide happen at once, leading then to the largest water level and wave forces at the sea-side.
2. Regular sea conditions happen most of the time and it comprises average wave heights and average astronomical tide level fluctuations.
3. High river discharge is defined as the case when the discharge at the Haringvliet is larger than 5.000 m^3/s. These discharges are not the most likely, but they are the most critical for flood risk reduction in the surrounding areas.
4. In contrast with the previous point, low river discharge is when the discharge at the Haringvliet is lower than 5.000 m^3/s. As so as the "Regular sea conditions" condition, low river discharge happens most of the time.

Now that the different scenarios are known, a description of how the elements are functioning is given in the following lines:

1. No storm surge and low river discharge ($Q < 5.000 m^3/s$)
   - The in- and outlet Getijmeer is open. The tide will flow in and out and energy is produced by the turbines.
   - The ship lock in the Getijmeer is in usage.
   - The spillway of the Valmeer is closed. No water exchange between Valmeer-Getijmeer.
   - The pumps/turbines of the Valmeer empty/fill the lake during specified hours.
   - The barriers in the haringvliet area are open and provide a minimum discharge of 40 m^3/s (to allow fish migration).
2. Regular sea conditions and high river discharge ($Q > 5.000 m^3/s$)
   - The in- and outlet Getijmeer is closed. The Getijmeer's water level will be reduced as specified.
   - The ship lock in the Getijmeer is in usage.
   - The spillway of the Valmeer is initially closed and the water level in Getijmeer will rise.
   - The pumps of the Valmeer empty the excess river discharge if needed.
   - The barriers in the haringvliet area are open and provide a maximum discharge of 10.000 m^3/s.

   Notice that in the case of such large river discharge (and/or storm duration) that the Getijmeer cannot store all the water, the spillway will be opened to transfer the excess water into the Valmeer.
3. Sea storm and low river discharge ($Q < 5.000 m^3/s$)
   - The in- and outlet Getijmeer is closed. The Getijmeer's water level will be reduced as specified.
   - The ship lock in the Getijmeer is closed.
   - The spillway of the Valmeer is closed and the water level in Getijmeer will start to rise. In this scenario, the Getijmeer will be able to store all the water coming from the river.

- The Energy Storage Lake minimum depth will be provided so that enough lateral stability is provided to resist water loads.
- The barriers in the haringvliet area are open and provide a minimum discharge of 40 m^3/s (to allow fish migration).

4. Sea storm and high river discharge ($Q > 5.000 m^3/s$)
    - The Maeslantkering is closed.
    - The in- and outlet Getijmeer is closed. The Getijmeer's water level will be reduced as specified.
    - The ship lock in the Getijmeer is closed.
    - The spillway of the Valmeer is opened and excess river discharge is coming into the Valmeer.
    - The pumps of the Valmeer empty the excess river discharge (if needed) with a maximum discharge of 10.000 m^3/s
    - The barriers in the haringvliet area are open and provide a discharge of 10.000 m^3/s.

2.3 Functions inlet/outlet of Valmeer

The main function of the Valmeer is a flood protection function. Estimated to happen once every ten years (Lavooij, 2018), the Valmeer will need to get rid of excess river discharges when the events of sea storm and extreme river discharges are happening simultaneously. This situation is depicted in the figure below:

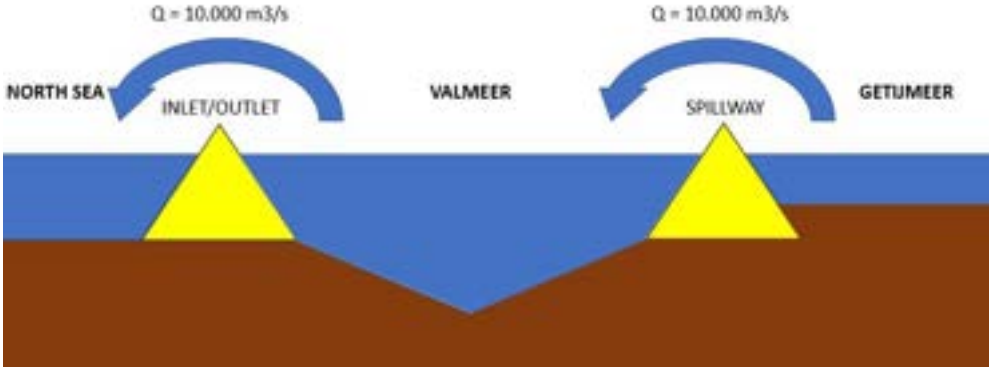

Figure 2.4: Conceptual representation of how the flood protection function is carried out in the DELTA21 plan

Furthermore, there is also an energy-related function: During periods of high electricity demand, the Valmeer concept generates electrical energy out of potential energy, which is produced during periods of low electrical energy demand (see Figure 2.5).

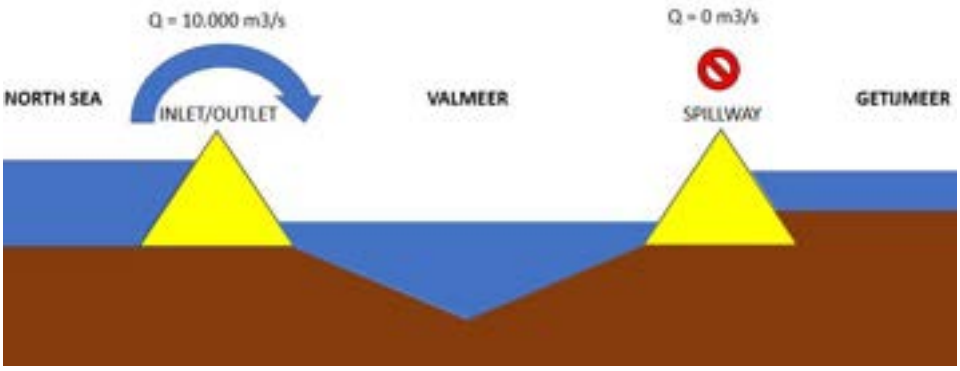

Figure 2.5: Conceptual representation of how the energy generation function is carried out in the DELTA21 plan

2.4 Problem statement

The problem statement for the caissons with the dual-mode turbines can be derived from the main functionality of the Valmeer shown above (see Section 2.3).

This is accomplished by adjusting the water level in the Valmeer: Energy can be produced by water flowing into the Valmeer during high electricity demand periods. This will raise the water level, which needs to be lowered again. This will be done during periods of low demand. The solution is probably cost-effective because electricity is less expensive during periods of low demand than during periods of high demand.
The problem statement is thus twofold:

- There is not yet a way to lower the water level in the Valmeer.
- There is not yet a way of getting electricity out of letting water into the Valmeer.

2.5 Design objective

The objective of the thesis is to create a conceptual design of a structure, being part of the DELTA21 Valmeer ring dike, that:

- Provides a way to lower the water level in the Valmeer to ensure flood protection of the hinterland during a storm surge combined with an extremely high river discharge;
- Generates electricity by allowing water to flow into the Valmeer
- Preserves the present ecological, nautical and flood protection systems.

2.6 Methodology

The final conceptual design has been achieved in three different steps:

1. Location selection: a location was selected according to the criteria shown in Chapter 5.
2. Functional design: a functional design is done for three alternatives constructed at the selected location and an alternative is selected (Chapter 6). Overall stability calculations were done to make sure the alternatives were stable. These are shown in Appendix L.
3. Structural design: the detailed structural calculations for the chosen alternative are performed. Only detailed structural calculations have been included for this alternative to reduce the final report's length and to optimize time use for this thesis.

The systems engineering method commonly used in civil engineering (Roozenburg & Eekels, 1995) has been used in Chapter 5 and 6). It comprises 5 different phases. In the following lines the different phases are listed:

1. Exploration of the problem: Chapter 2.
2. Generation of concepts: Section 5.1 and Section 6.1.
3. Verification of concepts: Section 5.2 and Section 6.2.
4. Evaluation of alternatives: Section 5.2 and Section 6.3.
5. Selection of the best alternative: Section 5.3 and Section 6.4.

The design aimed to reduce the life cycle emissions over the entire life cycle of the structure (Chapter 8).

Chapter 3

Requirements

Prior to the design it is of importance to define both functional and structural requirements of the structure. The functional requirements are given for the whole system of DELTA21. This will help the reader to understand how the DELTA21 system works. However, notice that the requirements used for the design of the hydro pump storage station are only the ones situated under "ESL Power Plant". The ones having the prefix "F" before them.

The structural requirements will be given exclusively for the structure object of study and not for the whole DELTA21 plan.

3.1 Functional requirements

- DELTA21

  1. The DELTA21 system has to protect the back country from high water on the north sea and the rivers.
  2. The DELTA21 system has to be able to produce 1.920 MW electricity during specified conditions.
  3. The DELTA21 system has to restore nature and fish migration into the Haringvliet, while maintaining the drinking water inlet points.

  - Valmeer
    - ESL Power Plant

    F. 1 - The ESL Power Plant has to be able to turbine water into the Valmeer from the north sea with a discharge of 10.000 m^3/s during specified boundary conditions.

    F. 2 - The ESL Power Plant has to be able to pump water from the Valmeer into the north sea with a discharge of 10.000 m^3/s during specified boundary conditions.

    F. 3 - The ESL Power Plant must function as part of a flood defense.

    F. 4 - The ESL Power Plant has to be able to produce 1.860 MW electricity during specified conditions.

    F. 5 - The structure needs to facilitate the traffic of people and vehicles over it.

    F. 6 - Operators, visitors and maintenance crew should be able to operate safely in and around the structure.

    F. 7 - Manual and remote operation for closing/opening the gates.

    - Spillway
      1. The spillway has to be able to let in water from the Getijmeer into the Valmeer with a discharge of 10.000 m^3/s during specified boundary conditions.
    - dikes
      1. The dikes have to function as part of a flood defence.
  - Getijmeer
    - Ship lock
      1. The Getijmeer's ship lock shall allow the ship passage between north sea and Getijmeer during specified conditions.

2. The Getijmeer's ship lock has to function as part of a flood defence with a chance of failure of 1/10.000 year.

* Shipping channel
  1. The Getijmeer's shipping channel shall allow for ship transit at the specified conditions.
* In-/outlet
  1. The Getijmeer in-/outlet has to allow a flow in and out of 10.000 m^3/s under specified boundary conditions.
  2. The Getijmeer in-/outlet has to function as part of a flood defence with a chance of failure of 1/10.000 year.
  3. The Getijmeer in-/outlet has to produce 60 MW electricity during specified conditions.

– Haringvliet

* Western brackish area dam
  1. The "western brackish area dam" has to allow for a minimum discharge of 40 m^3/s and a maximum of 5.000 m^3/s.
  2. The "western brackish area dam" has to stop freshwater from reaching the west area of the Haringvliet.
  3. The "western brackish area dam" has to allow salt water into the west area of the Haringvliet.
* Eastern brackish area dam
  1. The "eastern brackish area dam" has to allow for a minimum discharge of 40 m^3/s and a maximum of 5.000 m^3/s.
  2. The "eastern brackish area dam" has to stop salt water from reaching the east area of the Haringvliet.
  3. The "eastern brackish area dam" has to allow fresh water into the east area of the Haringvliet.
* Dam north of Tiengemeten
  1. The "dam north of Tiengemeten" has to act as a barrier to separate fresh from salty water. Impermeable structure with no water flows through/over it.
* Brackish area
  1. The "brackish area" has to allow for a proper (layered) exchange between fresh and salt water.

3.2 Structural requirements

- Constructability: The structure needs to be able to be constructed with conventional or specific methods. In case specific methods are used, these need to be properly described.
- Stability: The structure and/or its parts must not fail due to overturning, sliding, sinking or buckling under the action of loads.
- Strength: The structure needs to safely resist the stresses induced by the loads in the different structural members and its connections.

3.3 Required failure probability

To get the normative water levels, first, the failure probability of the structure needs to be obtained. According to the Waterwet there are three different categories for primary flood defenses:

- Type A: Water barriers that directly protect against "outside water" and are part of a "dike ring".
- Type B: Water barriers that protect against "outside water" and connect different "dike rings". These are barrier dikes, dams and movable flood barriers (Ministerie van Infrastructuur en Milieu, 2016).
- Type C: Water barriers that are part of a "dike ring" but are not adjacent to "outside water"

Appendix 1 of the Waterwet shows the flood defenses and their failure probability:

Figure 3.1: Location of a, b and c barriers in the system of primary flood defenses

The Haringvliet dam is a type-B water barrier since it is connecting two "dike rings" and it is in contact with "outside water". The Valmeer ring and the Geitijmeer's dam will replace this barrier and therefore will also be a type-b water barrier. In the figure below, a detail around the project's location is shown:

Figure 3.2: Location of a, b and c barriers in the system of primary flood defenses

The probability of failure for the Haringvlietdam is 1:1000 per year. Therefore, Since the DELTA21 plan replaces this barrier, the whole DELTA21 will be designed for the same failure probability. For failure probabilities, there are the "Signaleringswaarde" (in English, signal value) and "Ondergrens" (in English, lower limit) that give the minimum and maximum failure probabilities respectively. For design purposes, the Ondergrens value will be used. The Ondergrens is the maximum allowable value for the failure probability of the structure. This failure probability is the one that corresponds to the last year of its life because long-term effects such as sea level rise and material degradation are thus included in the design.

So the probability of the whole system of barriers creating DELTA21 is 1:1000 per year. But for the design of the power plant, a different failure probability will be considered. The Werkwijzer Ontwerpen Waterkerende Kunstwerken (November 2018) provides some guidelines into how to get the failure probability for an element of a system with a certain failure probability. Following section 2.6 of the previously mentioned document, first, the failure probability of each failure mechanism has to be defined. Then, the second step is to determine the failure probability per failure mechanism for individual works of art or structural component. In the document, some guiding values are given for the importance of each failure mechanism and the division of the elements. Those values will be used in this project. However, the realization of a deeper probabilistic analysis is recommended to find the actual failure probabilities of each component.

Following the Werkwijzer Ontwerpen Waterkerende Kunstwerken document then, the first step is to divide the DELTA21 system into different sections. The system has been divided into three sections:

Figure 3.3: Division of DELTA21 into sections

Each section contains:

- Section 1: dike and power plant
- Section 2: Spillway and dike
- Section 3: dike and Getijmeer's inlet

The Werkwijzer Ontwerpen Waterkerende Kunstwerken document says: "Een seriesysteem is zo sterk als de zwakste schakel: als één schakel faalt, faalt het systeem. De overstromingskans is zodoende gelijk aan de kans dat ten minste één van de onderdelen van het traject faalt.", in english: " A series system is only as strong as the weakest link: if one link fails, the system fails. The probability of flooding is therefore equal to the probability that at least one of the parts of the route will fail." Therefore, the probability of failure for the section 1 in Figure 3.3 is also 1:1000 per year. The next step is to find the failure probabilities for different failure methods. For that, the default failure probability budget from the WBI2017:

Type of barrier	Failure mechanism	Other structure from dikes
Dike or artwork	Overflow or wave overtopping	24%
Dike	Bursting and piping	24%
	Macro-instability	4%
	Damage to the covering and erosion of the dyke body	10%
Artwork	No closing	4%
	Piping	2%
	Constructive failure	2%
Dune	Dune erosion	0%
Other		30%
Total		100%

Table 3.1: Default failure probability budget from the WBI2017

The last step is to obtain the failure mechanism of each component. This is done following the next formulation:

$$P_{eis,kw} = \frac{P_{eis}}{N} = \frac{P_{max} \cdot w}{N} \tag{3.1}$$

Where:

- $P_{eis,kw}$: Failure probability for the failure mechanism under consideration for an individual work of art per year. [-]

- P_{eis}: Failure Risk for the failure mechanism under consideration at trajectory level per year. [-]
- P_{max}: Maximum permissible probability of flooding of the dyke route (specified in law as a lower limit) per year. [-]
- w: Failure probability factor for the relevant failure mechanism [-]
- N: Length effect factor for the failure mechanism considered [-]

And the length factor can be found in the WBI2017 as:

Overflow or overtopping	N = 1-3
No closing	$N = max(1; 0.5 \cdot n_{kw,2a})$ $n_{kw,2a}$: Number of works of art whose probability of failure is not negligibly small according to the simple test (-)
Constructive failure	N = 3
Piping	There are no regulations in the WBI2017

Table 3.2: Length effect factors in the WBI2017. The reader is referred to the Wekwijzer document for further details.

In the following tree a division of the elements as so as their failure probability is shown.

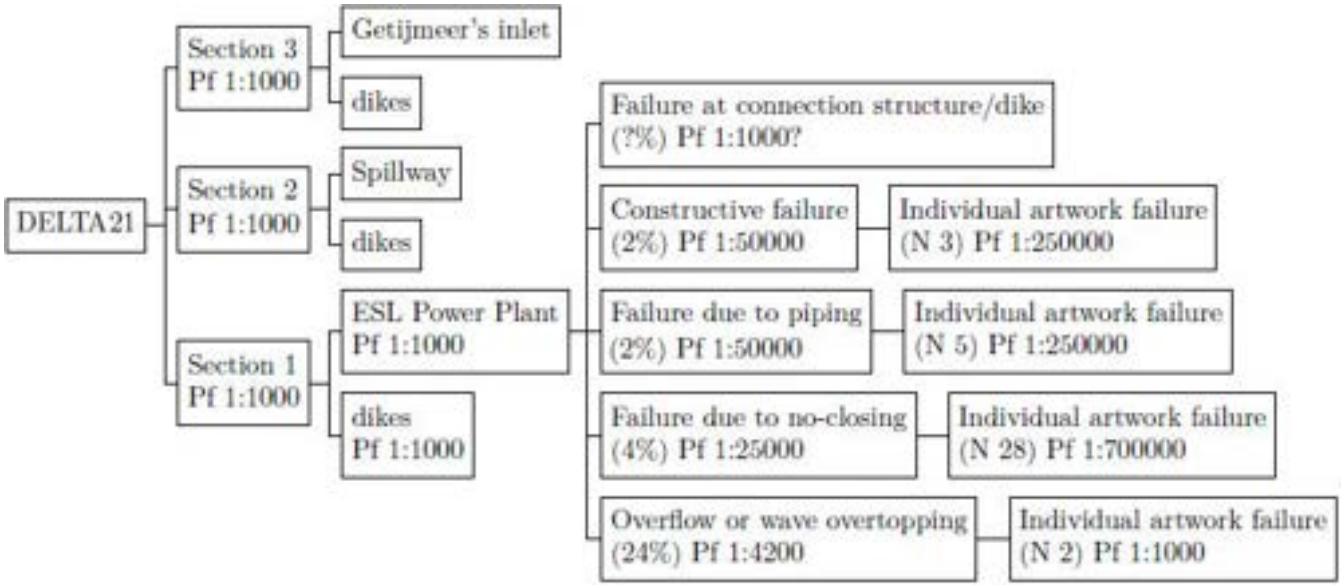

Figure 3.4: DELTA21 system breakdown structure regarding flood defense function. Probability of failure expressed per year.

As a recap, the structure object of design will be designed for a failure probability of 1:1000 per year. However, for overtopping the failure probability will be of 1:4200 per year. No further analysis of failure probabilities will be done about this structure on this thesis since it depends on several factors. Further research on the management of water levels within the Valmeer and the use of pumps for pumping water out and reducing failure probabilities is recommended.

It would be of interest to see what happens if Section 1 in Figure 3.3 would fail. A large water wave entering the Valmeer could make the whole DELTA21 system fail.

Chapter 4

Boundary conditions

4.1 Bathymetry

In an engineering project, the bathymetry plays an important role for wave propagation. Additionally, the water depth will influence the type of structure and building method.

The bathymetry at the area of study is shown below. For a detailed image, see Appendix B.2.

Figure 4.1: Detail of the bathymetry at the project's area. Retrieved from: https://webapp.navionics.com/?lang=en#boating\spacefactor\@m{}6key=wh%7B%7CH%7Blr%5D

As it can be observed, the deeper areas are at the level of the seaward part of the Maasvlakte 2. The depth of the seabed is gradually increasing from aprox. NAP -2 m/4 m in the south east to aprox. NAP -15 m in the northern area of the ESL.

4.2 Topography

The topography in this project won't be as important as the bathymetry due to the coastal nature of the work. However, the topography will be needed to design the access roads to the work site among other uses.

As for the bathymetry, a figure containing the topography next to the worksite is shown below. See Appendix B.3 for larger resolution of the drawing.

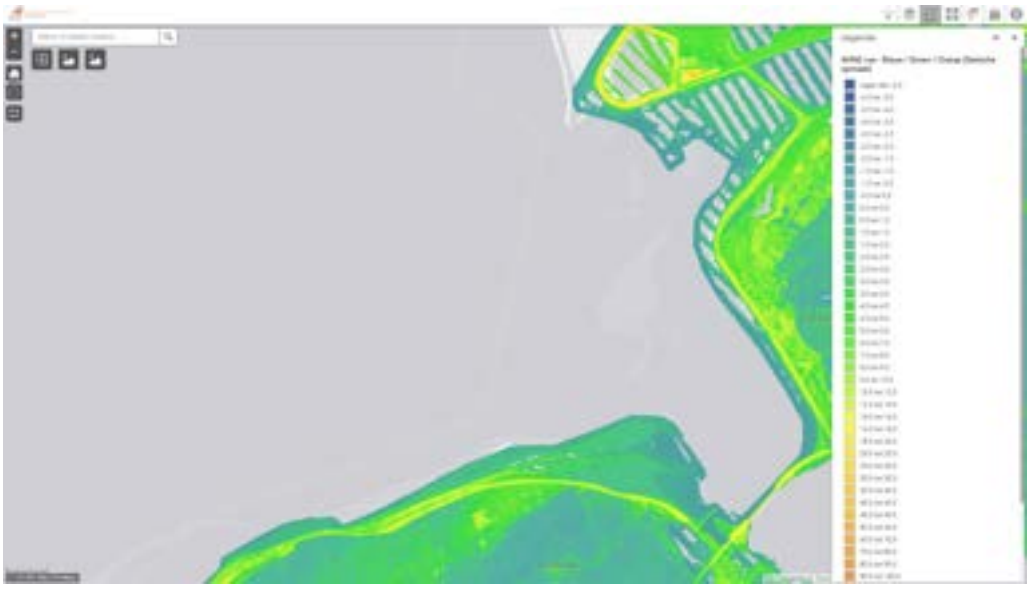

Figure 4.2: Detail of the topography at the project's area. Retrieved from: Actuel Hoogtebestand Nederland, webpage: http://www.ahn.nl/index.html

In short, the surrounding area to the project's location is characterized for being part of the Delta flood protection system of the Netherlands. Hence, the are surrounding the work site will be composed by defensive dikes.

4.3 Soil profile

To know which materials, soil types and geological formations are around the worksite, this section has been added to the boundary conditions.

In the following figure, a detail of the Holocene elements around the work area is shown. See Appendix B.4 to see the complete document.

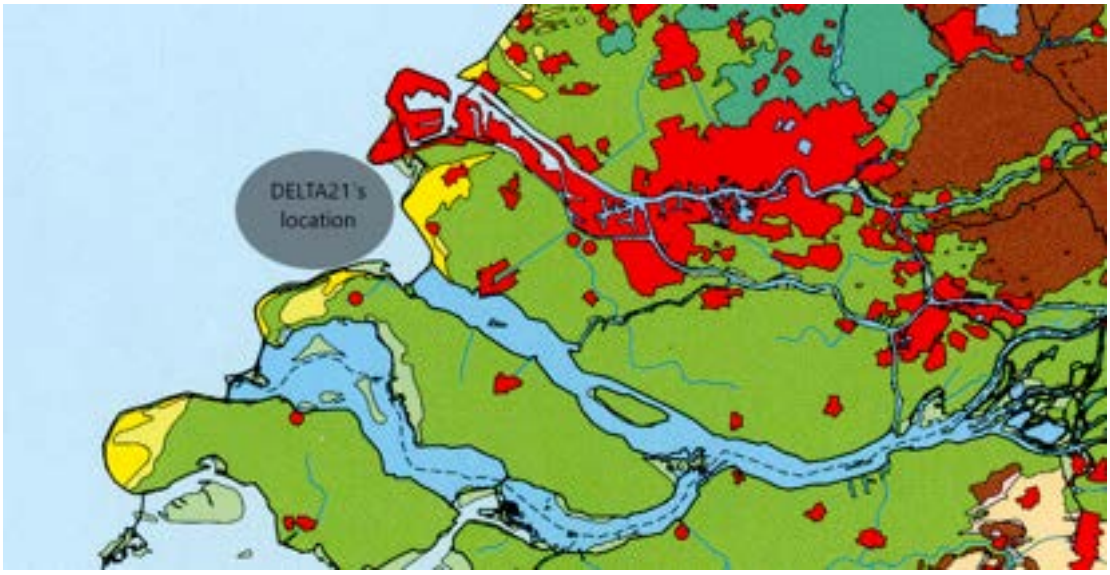

Figure 4.3: Holocene landscape. Source: TU Delft Library

For the project's area, the dominant Holocene landscape consists of the following three elements: High dunes (dark yellow), Sand-walls and low dunes (light yellow) and tidal area and river plains (green).

In the following figures, a representation of the longitudinal profile of the underground part of the soul is shown (see Figure 4.4), the next figure is a cross-section containing the layers of the soil profile (see Figure 4.5):

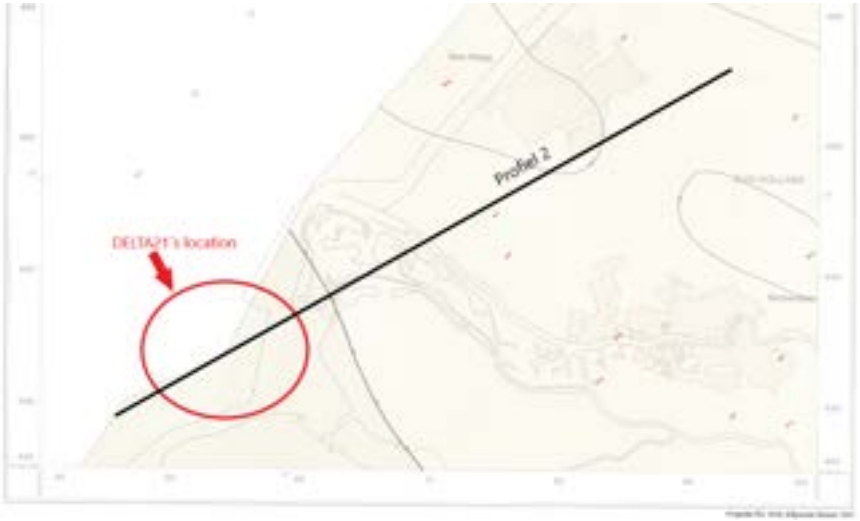

Figure 4.4: Longitudinal profile representation of the "profiel2" (see Figure 4.5)

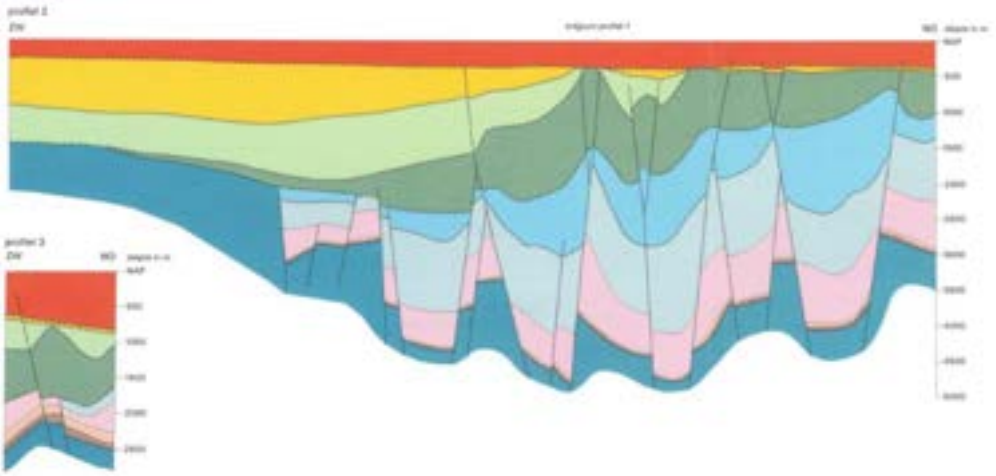

Figure 4.5: Soil profile from "profiel 2" (see Figure 4.4)

The southwestern part of the profile is composed of the following materials:

- Upper North Sea Group (surface - 250 m): This is the newest sedimented group. It lays disconformably over the middle group. Below, different boreholes data is shown for the work area. Besides, the assumed soil profile for calculations is presented (see Figure 4.8)
- Lower and Middle North Sea Group (250 m-1000 m): The lower part of the North Sea Group lays unconformably over the Chalk group. The lower and middle groups are separated from each other by unconformities. The lower group was deposited during the Late Paleocene and the Eocene whereas the middle group during the Oligocene. Because of erosion and its minimal deposition, this layer is not too thick compared with the others.
- Chalk Group (1000 m-1500 m): This group consists mainly of light-colored, hard, fine-grained bioclastic limestone and marly limestone.
- Rijnland Group (1500 m-1600 m): This group's age ranges from the Valangian to Albian. It is composed of glauconite-bearing sandstones, siltstones, claystones, and marls. In the work area, this group only consists of a small intrusion (around 100 m thick layer).

- Limburg Group (1600 m - 2250 m): This group is the oldest geological unit. The group is composed of grey to black claystones, siltstones, and sandstones.

The Upper layer is the most important one when designing civil works. The data of the different soil layers was obtained from DINOloket (https://www.dinoloket.nl/ondergrondgegevens). In the following figure, the position of the boreholes considered is shown:

Figure 4.6: Position of the boreholes used for defining a design soil profile. They are the ones shown in a darker color

Then, the borehole data can be observed below:

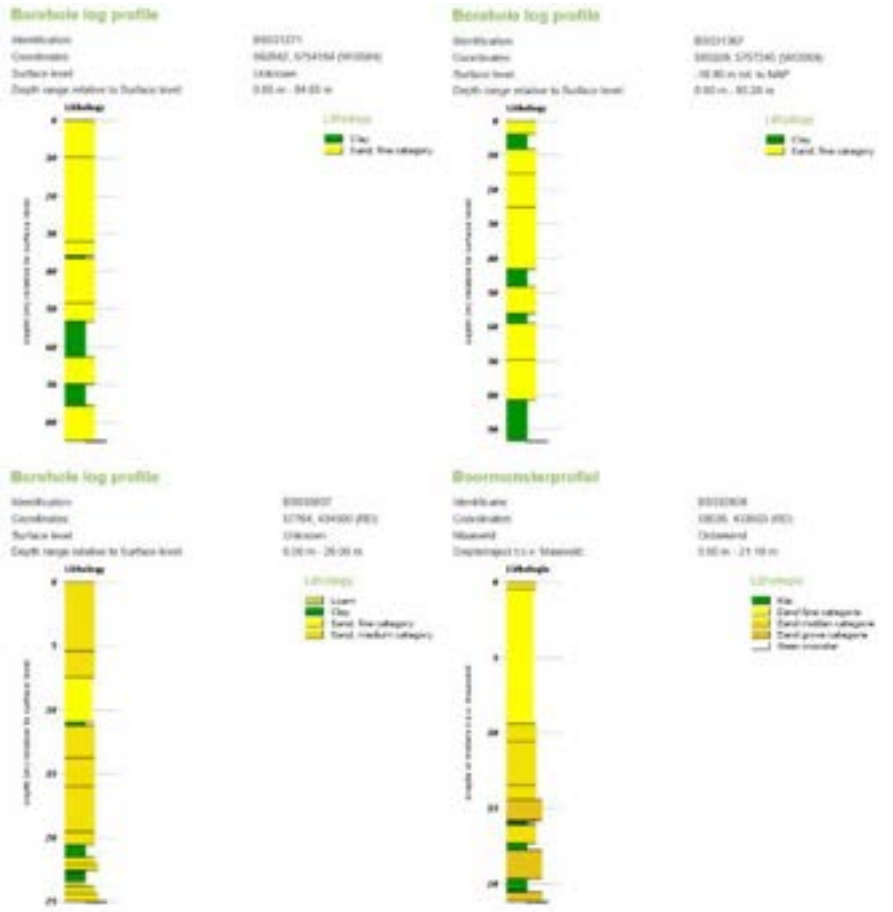

Figure 4.7: Data from boreholes. A, B, C and D from left to right, up to down.

From the pictures above can be noticed that the surface level of the boreholes is unknown. However, for this thesis, the surface soil level would be at the seabed's level. That is, for boreholes A and B, that are at a depth of 14m, the borehole surface is at NAP -14 m. For C and D, the borehole surface is at NAP -5 m

For consistency and simplicity, the soil profile has been assumed to be the following one:

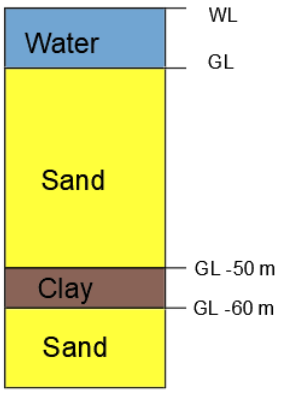

Figure 4.8: Model for soil profile

4.4 Astronomical tide

The astronomical tide levels were obtained from the DELTA21 report (Lavooij, 2018). First, some figures are given for the Hoek van Holland and then the astronomical tide at the Valmeer's position is shown:

Locatie:	High water	Low water
Hoek van Holland, spring	LAT +2.2 m; NAP + 1.3 m	LAT +0.3 m; NAP -0.6 m .
Hoek van Holland, neap	LAT +1.8 m; NAP +0.9 m	LAT +0.3 m; NAP -0.6 m.
Hoek van Holland, average	LAT +2.0 m; NAP +1.1 m	LAT +0.3 m; NAP -0.6 m.
Valmeer, spring	LAT +2.6 m; NAP +1.5 m	LAT +0.3 m; NAP -0.8 m.
Valmeer, neap	LAT +2.1 m; NAP +1.0 m	LAT +0.4 m; NAP -0.7 m.
Valmeer, average	LAT +2.35 m; NAP +1.25 m	LAT +0.35 m; NAP -0.75 m.

Table 4.1: Tidal fluctuations at Hoek van Holland and Valmeer

4.5 Sea level rise

Sea level rise estimations are included within Hydra-NL software. However in this section, an explanation about how the sea level rise estimation is done is included.

Hydra-NL considers the KNMI'06 (Koninklijk Nederlands Meteorologisch Instituut, Royal Dutch Meteorological Institute in English) scenarios. These scenarios are summarized in the following table:

KNMI'06 scenario	[G] Low(2050)	[G] Low(2100)	[W+] High(2050)	[W+] High(2100)
Increase in global temperature	+1°C	+2°C	+2°C	+4°C
North Sea SLR	15 to 25 cm	35 to 60 cm	20 to 35 cm	40 to 85 cm

Table 4.2: KNMI'06 Components for mean sea level rise (cm) for two time periods (2050 and 2100) and two temperature scenarios (low and high). Listed are the low and high values of a range determined by 10%/90% confidence limits for all components. Source: KNMI, 2006.

The above sea level rise figures are the lower and upper value corresponding to a 10%-90% uncertainty range. The model used was the CMIP5 and it was complemented by an analysis of the involved process, their uncertainty and their relative contribution to sea level rise. The processes taken into account for the analysis are:

oceans, glaciers and ice-caps, ice sheets, landwater changes, atmospheric pressure loading. However, changes in the Earth surface elevation are ignored. This changes may come from glacial isostatic adjustment, drying of peat, sinking due to heavy building, etc. As this surface elevation changes are ignored, the sea level rise calculated in the KNMI is absolute sea level rise.

In the next lines, the processes taken into account are explained:

- Oceans: The ocean expansion by temperature and salinity changes is taken into account. Coupled Atmosphere-Ocean General Circulation Models (AOGCMs) are used. An accurate 3D definition for water temperature and salinity in the oceans is needed to calculate the ocean expansion. Ocean circulation changes introduce more complexity (and hence uncertainties) to the model.

- Glaciers and Ice-caps: This process looks at the behaviour of glaciers and ice-caps separated from the Antarctic Ice Sheet (AIS) and Greenland Ice Sheet (GIS). This glaciers have a short-time response to temperature changes. The contribution of this process to sea level rise can just be based in temperature (Van del Wal and Wild, 2001; Slagen and Van de Wal, 2011). Also AOGCMs are used to compute the contribution of glaciers and ice-caps to sea level rise.

- Ice-sheets: The contribution of the Greenland and Antarctic ice sheets is taken into account here. The AIS and GIS could highly contribute to sea level rise. It is estimated that the GIS can raise the sea level 7 m, whereas the AIS can do it up to 60 m. For the calculations the AIS is divided between the Western AIS (WAIS) and Eastern AIS (EAIS), this last one being ten times bigger than both WAIS and GIS. The EAIS is the least sensitive to temperature changes in a centennarial scale, whereas the WAIS is subjected to temperature changes in a short-time scale. Nevertheless, for the calculation of sea level rise, both the contribution from WAIS and EAIS is taken into account. The contributions of the ice sheets to sea level rise are divided into ”surface mass balance” and ”rapid dynamical changes”.

- Landwater changes: Changes in water storage in land. This term includes changes in the amount of water stored in lakes, river, wetlands as well as snowpack in high altitude and latitude areas. Anthropological contributions such as groundwater extraction, runoff change due to land-use changes, dam building, etc are also included.

- Atmospheric pressure changes: The contribution of pressure can influence locar water levels. A pressure drop of 1 mbar increases the water level by 1 cm (inverse barometer effect). Due to climate change, more moisture is present in the atmosphere, which increases the atmospheric pressure and hence reduces sea level rise. This contributions is computed from pressure and moisture fields of AOGCMs.

The scenario that will be used for the design of the structure will be the G scenario looking at year 2100. The water level, wave height and wind speed obtained in the following sections has been adjusted for the climate change scenario G of the KNMI’06 report for the year 2100. For this G scenario the sea level rise is in the range of 35 to 60 cm.

4.6 Normative water levels

The normative water levels then will be obtained for a failure probability of 1:1000 per year using Hydra-NL software. The same failure probability will indeed be used for wind speeds and wave height.

Hydra-NL specifies hydraulic data for the existing flood defences. For the design of the ESL powerplant the data of two nearby locations will be used. In the following figure, the different locations used for obtaining water level figures as so as wave height, direction and wind speed are shown.

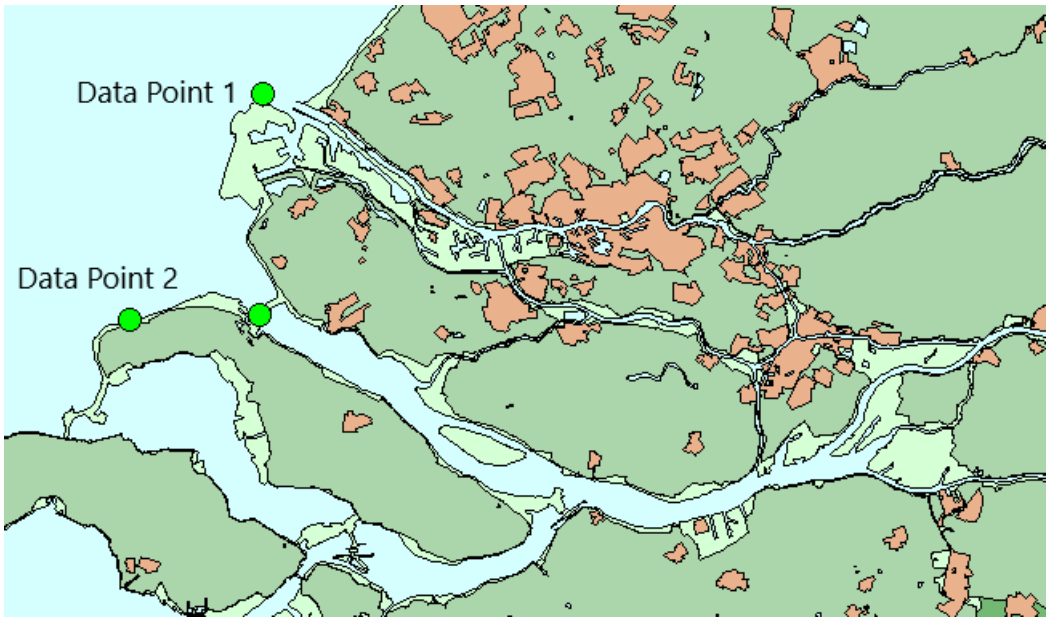

Figure 4.9: Data points from Hydra-NL

The water level was then obtained for Data Point 1 and 2. For Data Point 1 and for a return period of 1000 years, the water level was NAP +4.6 m. For Data Point 2 and the same return period, the water level is NAP + 4.4 m. Therefore the water level at the structure's location was assumed to be the average of those two water levels. The water level for design then will be NAP + 4.5 m.

4.7 Wave height, wind speed and direction

Again, to define the design wave height, wind speed and directions at location of the Data Points (see Figure 4.9 above), the software Hydra-NL was used.

In the previous section, it was stated that the design wave heights will be obtained for a return period of 1000 years. The software Hydra-NL already gives wave height for that frequency. The wave data at Data Point 1 will be used for the waves reaching the northern dune and the power plant in case it is located at the north-side of the Valmeer. On the other hand, Data Point 2 data will be used for the waves reaching the powerplant in case it is located at the southwest side of the Valmeer.

The third data point (third green point in Figure 4.9) was excluded because of the influence of both shallow water and diffraction. Data Point 2 is at a shallow water area which will influence on the wave height, however, the wave direction shows that waves are just affected by shoaling and breaking. Finally, Data Point 1 is the one that resembles deep water conditions the most. This is because the data is obtained at a deeper water area (20 to 16 meters depth). At this depth, using the simple rule of "$H_b = 0.8 \times h$" (Rusell, 1840). Where: "H_b" is the wave height when breaking and "h" the water depth, we see that waves of 18*0.8 = 14.4 meters could come to this point undisturbed by breaking. So, any 14.4 meters wave or lower will arrive to this point without breaking. However, the wave height is still influenced by shoaling, even though not as much as the wave heights at Data Point 2.

In conclusion, both Data Points 1 and 2 will be looked at for the design. For the parts of the structure facing the North Sea at depths of 20 to 16 meters, data from Data Point 1 will be used. For elements of Valmeer in shallow areas, the data from Data Point 2 will be used.

4.7.1 Wave climate from Data Point 1

The wave height for a return period of 1000 years is 7.9 meters. In the following table, the data from Hydra-NL is shown (notice that 360 degrees coincides with North direction):

r degrees	zeews m+NAP	windsn m/s	Hm0 m	bijdrage ov. freq (%)
30	1.54	29.5	7.88	0.0
60	1.51	29.6	7.88	0.0
90	1.49	29.6	7.88	0.0
120	1.52	29.6	7.88	0.0
150	--	--	--	0.0
180	--	--	--	0.0
210	--	--	--	0.0
240	6.48	44.6	7.88	0.0
270	4.33	37.3	7.88	0.1
300	3.38	27	7.88	35.3
330	3.30	24	7.88	46.3
360	2.90	23.8	7.88	17.9

Figure 4.10: Data for Data Point 1 and a return period of 1000 years. Source: Hydra-NL

The dominant wave height come from the NNW and WNW directions.

4.7.2 Wave climate from Data Point 2

The wave height for a return period of 1000 years is 3.2 meters. In the following table, the data from Hydra-NL is shown (notice that 360 degrees coincides with North direction):

r degrees	zeews m+NAP	windsn m/s	Hm0 m	bijdrage ov. freq (%)
30	3.57	20	3.22	0
60	3.57	20	3.22	0
90	3.57	20	3.22	0
120	3.57	20	3.22	0
150	4.72	43.1	3.22	0
180	4.66	44.1	3.22	0
210	5.07	35	3.22	0
240	4.14	39.2	3.22	0
270	3.88	30.2	3.22	4.6
300	3.73	25.9	3.22	38.8
330	3.64	23.1	3.22	52.2
360	3.47	24.5	3.22	4.4

Figure 4.11: Data for Data Point 2 and a return period of 1000 years. Source: Hydra-NL

We can observe that the most dominant waves come from the NNW and WNW directions.

4.8 Weather at the work site area

A brief climate study is included in this section to get an idea of how can be the working conditions at the work site. It has been assumed that the weather conditions such as temperature and rainfall at the work-site are going to be similar to the ones of the city of Rotterdam. Therefore, the weather stations of Rotterdam and its averages will be used in this analysis.

The Rotterdam area is characterized by a sub-oceanic climate, humid and rainy, influenced by the North Sea. It has mild cold (not freezing) winters with minimum temperatures averaging 1 °C and maximum temperatures averaging 7 °C. During summer the temperature rises, averaging maximum temperatures of 22 °C during the day which drop to minimum averages of 12 °C specially during the night. In the following table, the average temperatures are shown:

Month	Jan	Feb	Mar	Apr	May	Jun	Jul	Aug	Sep	Oct	Nov	Dec
Min (°C)	1	1	3	4	8	11	13	13	11	8	4	1
Max (°C)	6	7	10	14	18	20	22	22	19	15	10	7

Table 4.3: Average temperatures at the Rotterdam area. Source: https://www.climatestotravel.com/climate/netherlands/rotterdam

Month	Jan	Feb	Mar	Apr	May	Jun	Jul	Aug	Sep	Oct	Nov	Dec
Prec. (mm)	70	60	65	45	60	65	75	80	85	90	85	80
Days	12	10	12	9	9	10	10	10	12	12	13	13

Table 4.4: Average rainfall at the Rotterdam area. Source: https://www.climatestotravel.com/climate/netherlands/rotterdam

The water temperature is an important factor to take into account for factors such as concrete hardening or safety of the working crew, among others. Therefore, a brief description of the average water temperatures at the Maasvlakte is given: The minimum water temperatures range from 3 to 9 °C. at February 17th (in average) whereas the maximum temperature is reached around August 17th. In this period the water temperature ranges from 16 to 20 °C. Having this minimum temperatures we can conclude that the appearance of ice is unlikely.

4.9 Land subsidence

The land in The Netherlands is subsiding. Recent discoveries by the Netherlands Center for Geodesy and Geo-informatics (NCG) have shown that the rate of subsidence is larger than expected. These discoveries are published in the Dutch Land Subsidence Map (Bodemdalingskaart Nederland) available at: https://bodemdalingskaart.nl/portal/

The new map shows the rate of land subsidence in the whole country of The Netherlands. It differs both land subsidence due to "deep causes" and "shallow causes". Deep causes represent land subsidence due to oil and gas extraction whereas shallow subsidence represent subsidence at the first meters of soil. The shallow subsidence was found to be larger than expected and in some areas is even larger than the deep subsidence. This is caused by the lowering of ground water table and the settlement of peat and clay areas. To make things worst, climate change accelerates this process of subsidence by drying the soil (lowering of the groundwater table) and allowing a larger amount of soil grains to settle, filling the previously water-filled spaces. Below, a figure containing the land subsidence at the project's area is shown (read areas mean lots of subsidence, whereas green areas mean soil uplift):

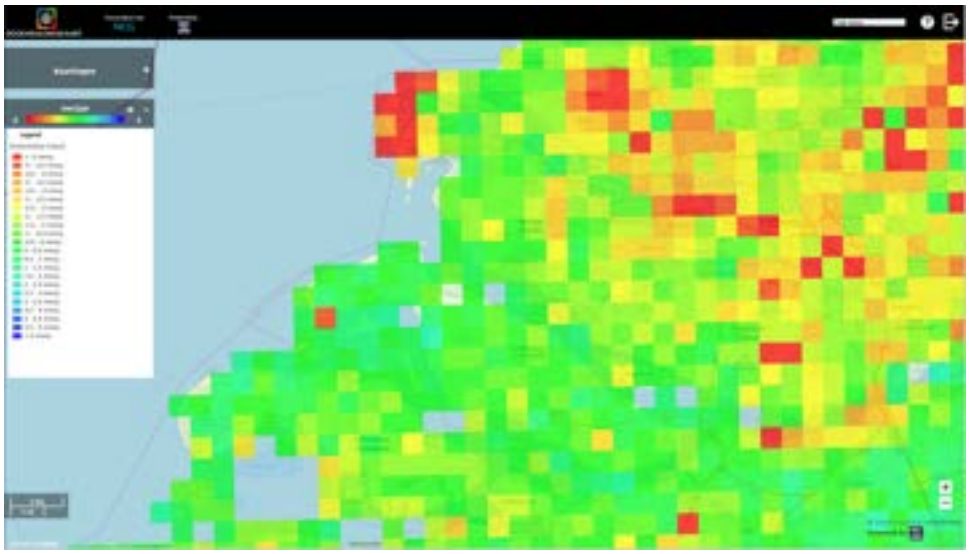

Figure 4.12: Land subsidence map at the project's location. Source: https://bodemdalingskaart.nl/portal/index

As we can observe, there is not information about land subsidence at the exact location of the project. However at the surroundings of the project's location, the subsidence rate is within 0.7 mm/year and -0.7 mm/year. No subsidence has been taken into account for the present design.

4.10 Ice loading

Ice loads follow from the Richtlijnen Ontwerp Kunstwerken ROK 1.4. In section 5.9: Specifieke belastingen op natte kunstwerken (in english, specific loads in wet engineering works) the different loads are shown:

1. Ice thermal expansion: Applied in the longitudinal direction of the lock, 0.2 meters below upper water level. Load: 50 kN/m.
2. Ice floating pieces: Perpendicular to the gate, at the height of the upper water level. Load: 50 kN/m.
3. Ice growth: vertical direction, evenly distributed over the underwater lines. Load: 10 kN/m.

Notice that the Valmeer's power plant gates must be calculated on all mentioned ice loads, however, loads 1 and 2 do not have to be combined with each other.

For the calculation of column walls, calculations must be made with a horizontal pressure load of 400 kN/m due to ice at the level of the expected water level.

4.11 Earthquake risk analysis

In order to assess the probability of earthquakes affecting the construction area, the Eurocode 8 is followed. The earthquake hazard is determined by a single parameter: the reference peak ground acceleration (α_{gR}) (Solomos G. et al, 2008). Each European state has its own national annexes with different seismic areas. For The Netherlands, the seismic zonation map is the following:

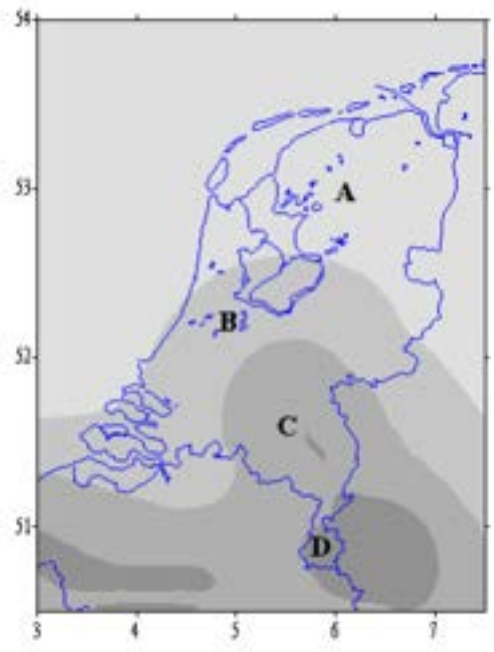

Figure 4.13: The seismic zonation map is based on a seismic hazard study with a 10 % probability of exceedance in 50 years (return period 475 years). Source: deCrook, T. (1996)

The above seismic zones have the following ground acceleration values:

- Zone A: PGA = 0.10 m/sec^2 (0.010 g)
- Zone B: PGA = 0.22 m/sec^2 (0.022 g)

- Zone C: PGA = 0.50 m/sec^2 (0.050 g)
- Zone D: PGA = 1.00 m/sec^2 (0.100 g)

Now, for the project's location (See 1.1) the ground acceleration is: α_{gR} = 0.10 m/sec^2 (0.022 g). This figure will be the one used for future earthquake-related calculations.

4.12 Comment on boundary conditions considered for design

First, notice that two important assumptions have been considered when taking into account boundary conditions:

- Water depth = 14 m.
- Soil profile (see Figure 4.8)

The water depth, in reality, will vary depending on the part of the structure as so as the soil profile. More soil probes need to be taken for the following design loops. The soil profile is quite important because it influences where the impermeable clay layer is. Having this influence in the depth at which the Valmeer can be excavated as so as the methods for reducing or stopping infiltration in the dry-dock when constructing the structure.

Second, the other important boundary conditions for design are the water level and wave height and period. All these factors influence the design wave pressures acting on the structure and therefore its stability and strength calculations. This important design boundary conditions can be seen below:

- Northern part of the DELTA21: H_s = 7.9 m; T_p = 11.3 s; WL = 4.5 m
- South western part of the DELTA21: H_s = 3.2 m; T_p = 11.2 s; WL = 4.5 m

Chapter 5

Choice of the Hydro Pump Storage Station location

The location where the structure will be built affects its construction and design in several ways. Placing the structure at areas of larger waves influences, for instance, the final size of the structure. Besides, different locations cause different flow paths within the basin. Therefore an adequate location selection is key for further design the final structure. The aspects that were taken into account when choosing location are: "Exposure to wave loading", "Accessibility for maintenance", "Accessibility for construction", "Outflow affection to the surroundings", "Flow within Valmeer (spillway to pump station", "Reduction of environmental impact" and "Soil properties". In this chapter, first, the different locations for building the power station will be shown. For each location, a brief description stating advantages and disadvantages is given. Second, it is explained what are the different aspects used for the location selection and why are they given the weight they have for the MCA. Finally, After analyzing all these aspects, a grade for each factor will be given and multi-criteria analysis will be used to choose an adequate location.

5.1 Potential locations for constructing the ESL's Power Plant

Three different locations were considered for the power plant positioning. In the following figure we can see these locations:

Figure 5.1: Possible locations for building the structure

Each location has its own characteristics. In the following sections these are given:

5.1.1 Alternative locations

Location 1: North

This location represents the deepest possible construction area, the seabed depth is at an average depth of NAP -14 m. This will be favorable for excavation volumes but the contrary happens for building-pit construction. Additionally, this area is directly exposed to waves coming from the NNW direction (the most common waves during storm conditions). Also as the depth is of 14 m, the waves will reach the structure without breaking. If we go back to Section 4.7, the incoming design wave height is of 7.8 m and any wave larger than (H_b = 0.8*h, rule of thumb for wave breaking depth) 11.2 m will reach the structure undisturbed by breaking. Also, this location is the closest to land from all the locations considered. This is not only favorable for any kind of construction method, but also for maintenance and equipment (mainly cables from generators to the grid) installation. Besides, the larger the depth, the better for the floating caisson construction method. Finally, the water flow when pumping the water out of the Valmeer can cause a cross-current in the approach channel of the Port of Rotterdam.

Location 2: Middle

Location 2 and Location 2 are quite similar one to the other. The main differences are the available depth of the seabed at each location and the affection of the flow leaving the power plant. For Location 2, the average depth is 10 m. The water flow is assumed not to affect the already existing beach at Ouddorp, but it can affect shipping in that area. A big advantage of this location is regarding wave attack. As mentioned above, the main wave direction is coming from the WNW-NW directions, which coincides with the direction of the power plant at this location. This means that the waves will refract and shoal before reaching the structure. (In order to obtain the wave loading, the wave height obtained from Data Point 2 (see Figure 4.9) is used due to the similar depth conditions.) But not everything is positive about this location, for instance, the power plant would be built far from land (about 7 to 10 km) which will influence the cable installation and maintenance strategies.

Location 2: South

Location 2 has the same properties for wave loading and maintenance as Location 2. The only differences are that this location is at a depth of 5 meters and that the beach at Ouddorp can be affected by the flow of pumping water out the Valmeer. The depth difference plays an important role when considering some construction methods. For instance, for the floating caissons into the position method, a depth of 5 m will be not good enough for transporting the caissons by floating. However, if the Valmeer is excavated first, the elements can be floated from inside the basin.

5.2 Evaluation criteria and weighting factors

In this section, a brief explanation of what the different weighting factors of the evaluation criteria are given.

- Exposure to wave loading: This factor accounts for the ocean climate. If larger waves are expected, the grade for this location is small. Wave loading affects the structure's size and therefore materials and time used for construction are also affected. Since costs are a deciding factor in most of the construction projects, this factor will be given a weight of 25 % in the MCA.

- Accessibility for maintenance: Ease for providing maintenance to the elements of the power plant. If elements are far from land, large distances will need to be covered for carrying out maintenance works. Ships or vehicles will be needed for maintenance, whereas if the structure is connected or closer to land, those ships won't be needed and maintenance costs will be reduced. Besides, the closer the structure is to land, the faster the emergency services will arrive at the site. For this category, the closer to land the better. As the life of the structure is so large and maintenance is expected to happen quite often (167 turbines will be installed), this factor will be given a weight of 20 % for the MCA together with the accessibility for construction explained below.

- Accessibility for construction: Similar to the previous point, but applied to the construction process. The closer to land, the better for construction. Less material displacement and easier installation of the cable units needed to bring the electrical energy from the turbines to the grid. The weight for this factor in the MCA will be 20 % together with the accessibility for maintenance. This has been done because the

construction accounts for a large initial investment. However, in the long term maintenance costs can become more critical. Ans a difficult accessibility means more costs

- Sedimentation at the structure's inlet: The net alongshore sediment transport on the coast of the Netherlands is towards the north-east direction (source: coastal dynamics course lecture notes, TUDelft). Therefore, there is a risk that at locations 2 and 3 sediment will accumulate. If we add that a trench needs to be dredged down to NAP -14 m at these locations to allow water to enter without air (to avoid cavitation) into the Valmeer, sedimentation is expected at the inlet of the structure. This sedimentation in low quantities would not affect the turbines (as specified by Pentair), but eventually, it can become a problem. To avoid this problem, regular dredging for maintenance would be done and taking into account the large dimensions that this structure will have, the volume to dredge could become significant. Therefore giving high maintenance costs in the future. Location 1 seems more favorable in this aspect. A weight of 20 % will be given to this factor.

- Outflow affection to the surroundings: Having a discharge of 10.000 m^3/s could cause large currents at the exit and entrance of the power plant. Affecting the shipping at the Port of Rotterdam is not an option due to the importance of this port for the Netherlands and Europe. The ports approach channel is located at $\approx$ 5.5 km from the structure on its closer side and $\approx$ 6.0 km on its farther side. Affecting a beach is also a negative factor since it affects recreation and can cause unexpected sediment movement. The beach is located at $\approx$ 8 km on its closer side and $\approx$ 10 km on its farther side. Finally, recreational shipping affection is also negative, but to a lesser extent. For the MCA this factor weights 13 %. Preliminary calculations were performed for this factor. However, further deeper analysis is recommended.

- Flow within Valmeer (spillway to pump station): When the spillway and pumps are working at the same time, a current connecting the two elements could be created. The closer a location is to the spillway, the worst. Bed protection can reduce the flow affection to erosion, but this would increase the construction costs. For the MCA this factor weights 7 %. The grade given here is based only on distance, however, further research on this is advised. Besides, the spillway is supposed to have a fixed position. This could change since the whole of the DELTA21 project still at a preliminary stage.

- Reduction of environmental impact: This factor will give high grades to places where the environmental impact is minimized. Since all the possible locations are in a Red Natura 2000 and not much difference can we find between the locations with respect to environmental impact, this factor will be given a weight of 5 %

- Soil properties: This factor is important for construction, the better the soil, the lower the costs for foundations and possible future settlements. However, in this project, the whole DELTA21 area is considered to have the same soil properties. So no difference is felt in the analysis and therefore a weight of 5 % is given to this factor

5.3 MCA for the best location selection

In the following table, the grade for each location and deciding factor is given.

Location	Exposure to wave loading	Accessibility for maintenance and construction	Sedimentation at the structure's inlet	Outflow affection to the surroundings	Flow within Valmeer (spillway to pump station)	Reduction of environmental impact	Soil properties	TOTAL SCORE
Weight of criteria	25.0%	20.0%	20.0%	15.0%	10.0%	5.0%	5.0%	100%
Location 1	6	9	9	6	9	6	8	7.0
Location 2	9	6	6	9	7	6	8	6.8
Location 3	9	6	6	8	6	6	8	6.7

Figure 5.2: MCA analysis for location selection

Therefore, as we can see above, the better location according to our criteria is Location 1. This location and its boundary conditions will be the one considered for the designs.

Chapter 6

Functional design

In the present chapter, first, the different conceptual designs for the alternatives are shown. Second, it is explained how the technical requirements are met. Then, to select an alternative, two loops are done. The first loop studies the ease and/or complications of constructing each alternative, in this first loop, some alternatives are discarded. In the second loop, a score is given to each alternative and criteria. An MCA is performed and the alternative with a better score is selected.

Accurate costs are not calculated because of both time limitations and the difficulty of getting an accurate costs estimation by comparison with other structures. This is due to the singularity of this structure. However, the most expensive parts of the works will be described and they will be considered for the MCA.

6.1 Concept development

3 different alternatives have been considered for the design of the ESL's power plant:

1. The construction is a flood defense (independently stable)
2. The construction is not a flood defense (the dike is, and the construction is placed within the Valmeer)
3. The construction is part of a flood defense in combination with the dike

6.1.1 Alternative 1: Power plant is a flood defense (independently stable)

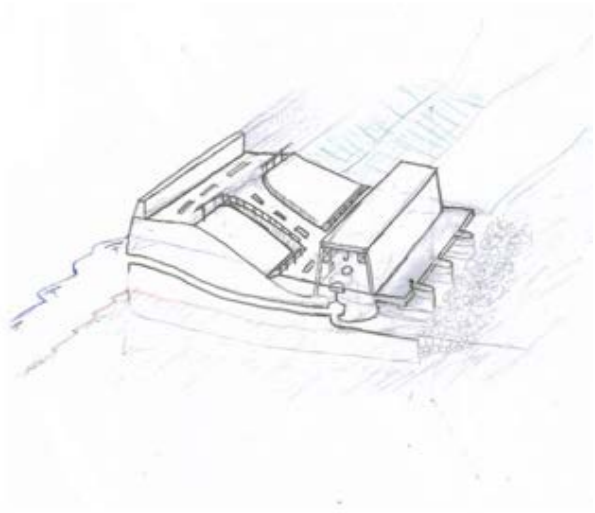

Figure 6.1: 3D conceptual design of the Alternative 1.

This alternative consists of a power plant integrated within the flood defense. The whole structure will need to be stable by itself. This alternative would be similar to the already existing hydroelectric power plants. In this case, though, the head differences are smaller than those of conventional hydroelectric power plants. Two construction methods were considered for this alternative: In situ and prefab construction method. The in situ alternative will be constructed in a building pit located at the structure's final position. The prefab alternative will be done similar to the conventional immersed tunnels construction method. A building pit will be constructed for developing the different segments which then will ba transported and placed at its final position.

6.1.2 Alternative 2: Power plant is not a flood defense (the dam is, and the power plant is constructed within the Valmeer)

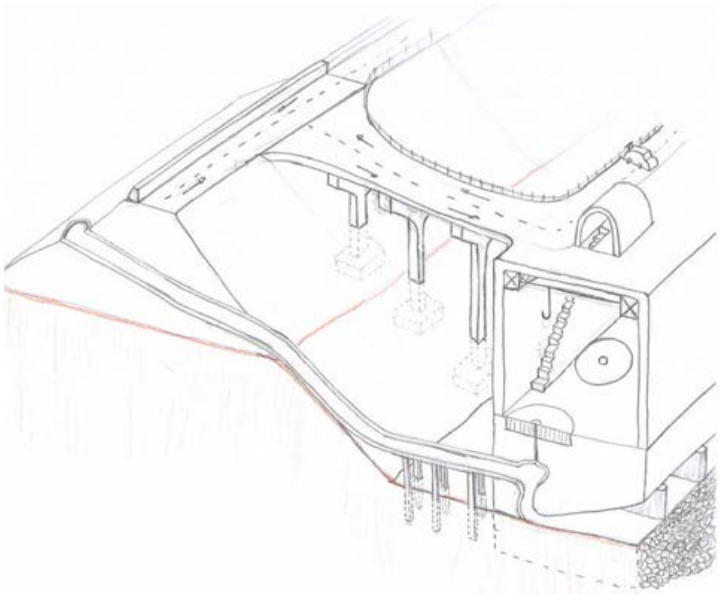

Figure 6.2: 3D representation of Alternative 2.

The pumping/turbining function in the present alternative is carried out by a power plant placed within the Valmeer. The water will be taken in/out of the Valmeer by a 1500 meters long penstock. The flood defense function is taken by the dike that now will surround the whole Valmeer (all but a small gap used for the spillway). To access the power plant, there have to be roads links between the dike, which is connected to the land, and the power plant.

Since the power plant will be built after the dike is done, the penstock would need to be installed within the dike. A tunnel has to be built. This can be both expensive and risky.

6.1.3 Alternative 3: Power plant is part of a flood defense in combination with the dune

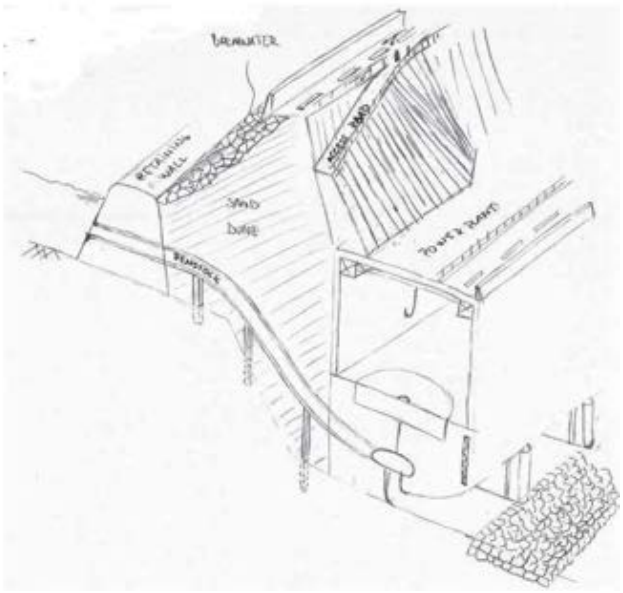

Figure 6.3: 3D conceptual design of Alternative 3

This alternative consists mainly in four different elements: Retaining wall containing the power plant's inlet, power plant able to also act as a retaining wall, penstock's positioning structure and sand fill (see figure below):

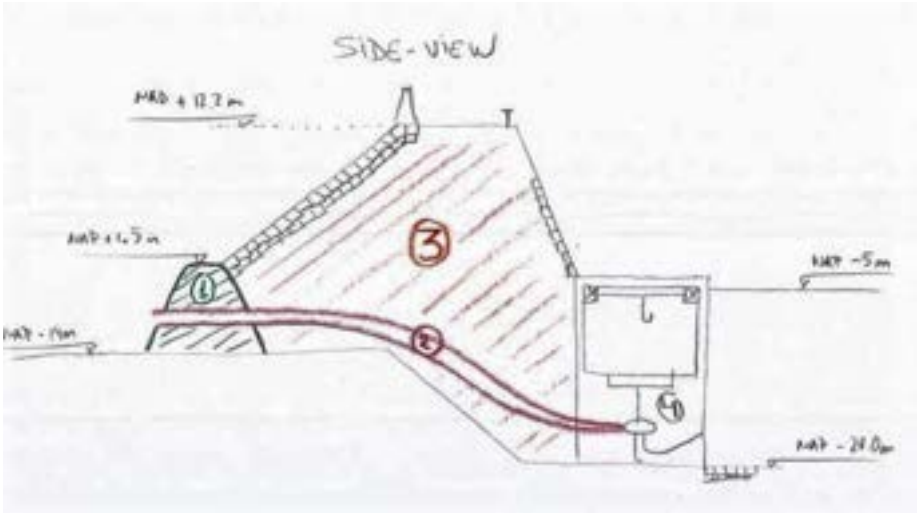

Figure 6.4: Different elements of the Alternative 3

This is a tricky alternative in terms of stability calculations. The idea is to have two retaining walls (numbers 1 and 4 in the figure above) and fill in between (3). The flood defense is defined as the whole system.

For the in situ alternative a huge building pit will be needed due to the dimensions of the alternative. For the prefab method, the issue will be on the connection of all the different elements. There are 4 different elements (see figure above) which in turn would be composed of at least 2 elements each. This element's connection using vessels needs to be extremely accurate and can be costly.

6.2 Verification of the concepts regarding the functional requirements

The ESL power plant has the following basic functions during its usable lifetime (see Section 3.1):

- F. 1 & F. 2: Discharge in/out the Valmeer
- F. 3: Flood defense
- F. 4: Electricity generation
- F. 5: Accessibility to the ESL power plant
- F. 6: Maintenance works
- F. 7: Gates operation (opening/closing)

Sections from 6.2.1 to 6.2.6 show how the functional requirements are met. "The discharge in/out the Valmeer" and "Electricity generation" sections will show how to meet these requirements for all the alternatives. The "flood defense", "Accessibility to the ESL power plant", "Maintenance works" and "gate operation" will be given for each particular alternative.

6.2.1 F. 1 & F. 2: Discharge in/out the Valmeer

To provide a total discharge of 10.000 m^3/s, different options are possible. For different discharges, a different number of turbines is needed to provide the working discharge of 10.000 m^3/s. Besides, the suction inlet tube dimensions as so as the depth at which the turbine/pump caisson has to be placed vary. When the discharge of the turbine/pump increases, a wider and deeper structure is needed to place the turbines. However, that increase in width is balanced by the reduction of the number of turbines needed. The table below shows that the larger the discharge of an individual pump, the narrower the final width of the power plant and the deeper it needs to be installed (To see further calculations the reader is referred to Appendix C.3).

Parameter (units)	Alternative 1	Alternative 2	Alternative 3	Alternative 4	Alternative 5
Discharge per pump (m^3/s)	27	60	100	160	200
Power per pump (MW)	5.0	11.1	18.5	29.6	37.0
Total number of pumps needed	371	167	100	63	50
Max. rpm per turbine (rpm)	144	97	75	59	53
Impeller inlet diameter (m)	2.57	3.84	4.95	6.26	7.00
Submergence, s in Figure 6.5	2.4	3.6	4.7	5.9	6.6
Distance water surface, bottom of structure, t in Figure 6.5	3.7	5.5	7.1	9.0	10.0
Bottom level of structure, NAP -x m in Figure 6.5	-26.2	-28.0	-29.6	-31.5	-32.5
Width of singe turbine (m)	8.9	13.3	17.2	21.8	24.4
Width estimation of power plant(m)	3320	2228	1722	1372	1218

Table 6.1: Individual turbine/pump affection to power plant dimensions and positioning

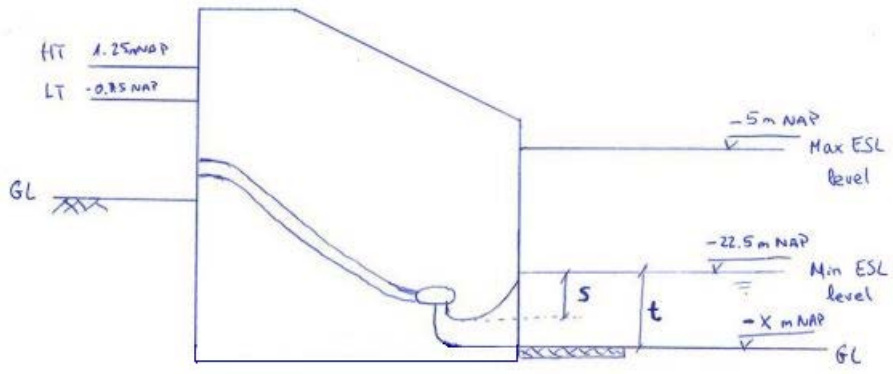

Figure 6.5: Representation of submergence values for power plant

For this thesis, the discharge per turbine/pump will be 60 m^3/s, having a total of 167 turbine/pumps installed. The power plant width is approximately 2228 m and it is installed at a depth of NAP -32 m. Nevertheless, further research for choosing an adequate turbine/pump discharge and type is recommended.

6.2.2 F. 3: Flood defense

- Alternative 1: The power plant is at the same time a flood defense.
- Alternative 2: The flood defense function is taken by the dike. So the defense against flooding is still ensured.
- Alternative 3: The flood defense function is provided by the ensemble of all the elements shown in Figure 6.4. failure of one element will lead to failure of the whole flood defense system.

6.2.3 F. 4: Electricity generation

The power plant needs to have a total power installed of 1860 MW. Pentair recommended to install multiple 5 MW turbines (27 m^3/s). However, in the previous section can be seen that the final individual discharge selected is 60 m^3/s. Therefore, as the power of the turbines grows exponentially with its discharge, the power of the 60 m^3/s turbine/pump is 11.1 MW. This gives a total of 1853 MW for 167 turbines. Since the turbines needed come from the needed discharge of 10.000 m^3/s, the total number of turbines will still be 167 and the power plant will have a capacity of 1853.

The equipment needed to carry the electricity from the generator to the grid is the following one:

- Speed increaser: necessary for low-speed turbines ($\leq$400 rpm). Increases the turbine speed to meet the rotator speed.
- Generator: Converts mechanical power generated by the turbine into electrical power. Consists of two parts: stator and rotor. The stator is the fixed part of the generator whereas the rotor is the rotating assembly, it is connected to the turbine by a connecting shaft. The generator is cooled by passing air through the stator and rotor coils.
- Buswork, circuit breakers, and disconnects: Buswork consists of the electrical conduits and transfer power output from the generator to the step-up transformers. Disconnectors and circuit breakers are switches that connect/disconnect generator and power grid.
- Transformers: Electrical device that increases the generator output voltage to match the voltage level of the transmission line. Usually, place close to the generators to minimize loses. Transformers are often cooled with oil-to-air fan type radiators.
- Switchyard: Consists of line circuit breakers and disconnect switches.

6.2.4 F. 5: Accessibility to the ESL power plant

Access for the workers of the power plant as so as for the maintenance crew and even visitors needs to be provided. There will be two different roads considered for this design. One will be the public road, used for the visitors to travel around the Valmeer. This road will give access to the beaches and recreational areas created around the Valmeer. Besides, an additional maintenance road will be considered. This road will allow the maintenance crew to drive without facing regular traffic. As this road would be miss-used if it was only used by maintenance crew and workers of the plant, two bike lanes together with a walking path will be added. This is done to ensure low traffic and fast access to any place within the power plant. This road will be used for emergencies, maintenance works and pedestrians and cyclists.

- Alternative 1: The road will be constructed on the crest of the power plant's structure. This road contains two lanes for regular traffic and another for maintenance, pedestrians and cyclists. Parking on the maintenance lanes will be possible if it is done without obstructing the rest of the lane. The access to the interior of the power plant will be from some ramps which connect the road to the upper part of the powerhouse. This alternative provides a stiff base for building the road (when compared to the other alternatives where the road will be constructed over loose material, probably sand).

- Alternative 2: The public road will be constructed on top of the dike. Access roads will be needed to provide access to the power plant which is situated inside the Valmeer. The access road goes from the top of the dike to the top of the power plant. For that reason, 4 bridges (one every 500 meters) connecting the dike and the power plant will be built. On top of the power plant the "maintenance road" will be built so that the maintenance crew can easily go from one point to another of the power plant without needing to go back to the dike road. The access to the interior of the power plant is from the top.
- Alternative 3: The public road will be installed on top of the dike. To provide access to the maintenance road, 4 access roads on the slope of the dike (see Figure 6.3) are needed. Construction of a road on a sandy slope can be an expensive work (which will not be good taking into account that it just constitutes an access road and not the main road). Anyways, the access to the power plant still ensured for this alternative. As so as for the previous alternative, the maintenance road is built on top of the power plant and the access to the power plant is from above.

6.2.5 F. 6: Maintenance works

In general terms, the maintenance within the power plant is the same for all alternatives since the elements composing the power plant similar. important differences will be explained when maintaining the main gate's mechanical system and the penstock. Once the power plant has been accessed to, maintenance of the turbines/pumps can be done from the inside using a traveling crane to lift the turbine/pump. This method has been designed due to the large number of turbines present in the power plant. To lift the turbine/pump, it is necessary to first close the valve gate and the roller gate (see Figure 6.6). Then, the water within these two gates is pumped out and the turbine can be lifted using the traveling crane. For both the valve gate and roller gates, special chambers will be constructed to host the motors of the gates. These chambers will have enough space to allow for maintenance works. Besides, the surrounding of the gate needs to be accessible so that gate maintenance is possible.

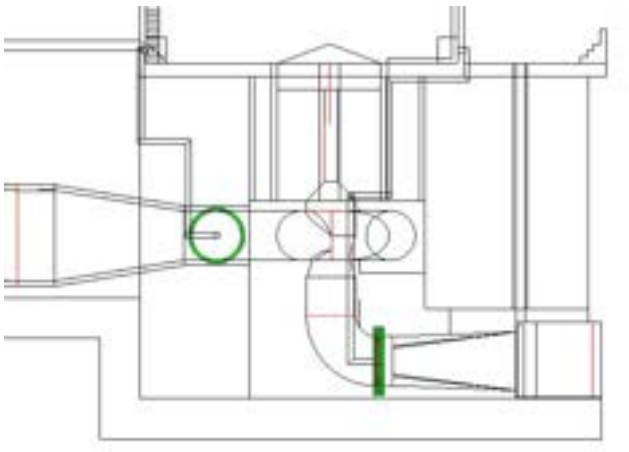

Figure 6.6: Maintenance gates (represented in green color)

Providing maintenance to other parts of the structure such as main gate and penstock differs for each alternative.

- Alternative 1: The maintenance is the easiest for this alternative. The penstock can be accessed from inside the dam. Access to the inside and outside of the penstock will be possible for the maintenance crew. Regarding the main gate's maintenance, some access chambers will be provided to access the gate and the mechanical equipment.
- Alternative 2: Alternative 2 and 3 have some challenges when maintaining the main gate and penstock. For this alternative, since the penstock is within a dune, a surrounding structure has to be constructed to access the exterior part of the penstock for maintenance purposes. Regarding main gate maintenance, a support structure has to be built within the dune. This will have to have all the necessary room for hosting the gate's motors, hydraulic and electrical systems. Space will also be needed for the maintenance crew to perform their work successfully. The access to this room is more complicated than the access to the power plant. Some paths will allow pedestrians to arrive to the abutment with the maintenance

material. In case heavy material is needed, cranes or ships will be used to bring it down to the abutment. No roads will be built at the sea-side of the dune.

- Alternative 3: The penstock maintenance will be done again by constructing an auxiliary structure around it. The main gate will be enclosed in the abutment next to the sea. Access to it will be provided from the top. As for Alternative 2, access lanes will be provided for pedestrians. Therefore, if heavy machinery or parts need to be replaced, cranes and/or ships will be used.

In conclusion, Alternative 1 is the most favorable regarding maintenance aspects. Especially for maintaining the main gate and penstock.

6.2.6 F. 7: Manual and remote operation for closing/opening the gates.

To ensure the proper operation of the gates a control room from which all gates can be both opened and closed will be installed. The gates need to be controlled from the control room, the powerhouse and manually at the gate's position.

This is possible for all the alternatives. However, for alternatives 2 and 3, the manual opening of the main gates will be more difficult to do since the gates are far (at the abutment) from all the other power plant elements.

6.3 Evaluation of the verified concepts with help of evaluation criteria

The three alternatives will be evaluated for both in situ and prefab construction methods. Therefore, the total number of alternatives to be evaluated is 6.

- Alternative 1, in situ construction method
- Alternative 1, prefab construction method
- Alternative 2, in situ construction method
- Alternative 2, prefab construction method
- Alternative 3, in situ construction method
- Alternative 3, prefab construction method

The evaluation of the alternatives will be done in two different loops. In the first loop, the advantages and disadvantages of each alternative will be shown. Then, the alternatives having disadvantages that make the construction of an alternative more laborious or very complicated in comparison with the others, will be discarded. In the second loop, an MCA scoring the advantages and disadvantages of each remaining alternative will be done. Notice that only relative costs will be included in this MCA. Finally, the alternative with a better score will be chosen.

The reader is referred to Appendix H to see in detail the different categories considered for the functional analysis. Only the results of these analyses are shown here.

6.3.1 Loop 1

In this loop, the following alternatives were already discarded:

- Alternative 2, in situ construction method
- Alternative 2, prefab construction method
- Alternative 3, in situ construction method
- Alternative 3, prefab construction method

In the following paragraphs, a brief explanation of why these alternatives were discarded is given.

Regarding Alternative 2, the prefab construction method has been discarded for mainly one reason: underwater installation of the penstock through the dike. A challenging situation which will translate into expensive construction methods. Realizing this alternative will be simpler in the dry, especially because the dike can act as a part of the construction pit and then, only the other 3 dikes will be needed as temporary constructions. Working in the dry, the still challenge of installing the penstock through the sand becomes more doable. Besides the installation of the penstock, the construction of the enclosing structure for the main gate will be the second-largest challenge since it has to be constructed on the seaside. That means that another construction pit at the sea-side of the dike will be needed and that the main gates will be installed far away from the main structure. For that reason, the electric and mechanical circuits will need to be transported all the way there.

Regarding Alternative 3, both construction methods will be difficult to realize. The in situ method comes with the first problem that would be building a huge building pit due to the slope of the dike. The first estimations for the power plant's length is around 160 meters (as a comparison, please notice that Alternative 1 length is around 80 meters). Comparing with the other two alternatives, the construction pit will have to be two (or even 3 if compared to Alternative 1) times larger. Additionally, this alternative is composed of 4 different elements whose connections need to be precise. This will be especially difficult for the prefab construction method. On the one hand, the penstock will have to be built over special pillars (or supporting structure). Besides, the penstock needs to be connected to the abutment at the seaside and the power plant at the Valmeer's side. Difficult operation taking into account the building tolerances and amount (and size) of elements to connect. Once connected, the space between abutment and power plant can be filled with sand to create the dike (see Figure 6.4). About the gate installation, installing a gate on an abutment is doable, however, the abutment will have to have large dimensions to host all the necessary equipment for opening and closing the gates.

6.3.2 Loop 2

The next 2 alternatives will be graded in this section for the MCA and costs over value analysis:

- Alternative 1, in situ construction method.
- Alternative 1, prefab construction method.

An extended construction methodology for each alternative is shown in Appendix I. And in the Appendix J, the floating stability of the caissons for the prefab construction method is shown. In this chapter, just the most significant differences between both construction methods are shown.

For the MCA then, the most significant differences for the remaining two alternatives are given a score. In the following lines, these differences are pointed out:

- Overall dimensions and number of wells for construction dock: Larger construction dock dimensions will lead to more water infiltration and therefore more wells and pumping capacity needs to be installed to de-water the pit. Besides, larger dimensions mean more costs and construction time of the dry-dock. As it can be seen in Appendix I, the building pit dimensions are similar for both alternatives. For the prefab method, the area of dry dock can be reduced by decreasing the number of compartments and the number of elements to be built at once. However, if this technique applies, the dry docks will have to be provided with a gate and a pumping system.
- Depth of construction: The depth at which the site can be excavated varies for both in situ and prefab construction methods. The deeper the construction, the more difficult to keep the dock dry. Thus more expensive. In the Appendix E calculations are shown to ensure that uplift of the soil is not a problem for any alternative. The in situ method needs to excavate down to NAP -32 m, whereas the prefab method just needs a dry dock with the bottom level at NAP -19 m.
- Elements connection: The in situ alternative will not have different elements to connect. Everything is properly connected on-site. The prefab alternative will have to be built by parts and then transported and lowered to its final position. This alternative is composed of 56 bottom caissons (84 m x 50 m x 18.4 m) and other 56 top caissons (84 m x 50 m x 18.1 m). Both vertical and horizontal connections need to be watertight to ensure continuity of the powerhouse. After the top caisson is constructed the rest of the plant will be finished in situ on the dry. Besides, the abutments needed to connect the structure to the dike will be easily constructed in the dry. This will be more difficult for the prefab method.

- Machinery used for construction of the structure: In this category, after knowing all the machinery that will be involved in the construction process, a focus is put on the different machinery used. For instance, the prefab method will use specific vessels to transport the power plant segments into position. This machinery will mean additional costs for the prefab alternative. Below the reader can find an extended list of the machinery considered.
  - Tugboats
  - Machine to lower elements
- Foundation preparation: For the in situ method, the foundation will be constructed directly over the sand bed. However, for the prefab method, a rock/sand foundation will need to be placed before lowering the bottom element. This foundation needs a clean and even surface to properly transfer the loads from the caisson to the subsoil (Rasmussen, 1997).
- Construction time: Assumed to be similar for both alternatives. The in situ construction has the advantage that everything is constructed at its final position so we don't have to transport any elements. The contrary happens for the prefab method, but if we consider a smaller dry dock and an efficient construction method, the construction time would be similar to the in situ method.
- Construction costs: these won't be calculated, but an estimation on what can be more expensive is done below:
  - Dry dock: The dry dock is larger and deeper for the in situ alternative, so it'll be more expensive.
  - Foundation preparation: The prefab method needs specific machinery for its realization. The in situ method needs no special foundation. A shallow foundation will be built on top of the sand bed.
  - Machinery for construction: Special machinery will be used for the prefab construction method. This machinery is the one needed to transport and lower the elements to position.
  - Material costs: Both in situ and prefab alternatives have a similar amount of materials, so no distinction is done in this aspect.

  Both construction methods have some expensive and cheap parts. Following the expert's judgment, the cheapest alternative is Alternative 2.

To make a decision, the above pros and cons were given a score. Besides, each category has its weight which has been assigned following the importance of a category in the final design. Recommendations from experts have been followed to reach a reasonable weight distribution. The alternative with the overall greater score below will be the selected one.

Category	Alternative 1, in situ	Alternative 1, prefab
Construction dock (overall dimensions, amount of wells and costs) [15%]	8	8
Construction dock (depth of construction) [15%]	5	8
Elements connection [15%]	9	5
Machinery used for construction of structure [10%]	8	6
Foundation preparation [15%]	9	7
Construction time [10%]	6	7
TOTAL	7.7	6.7

Table 6.2: Pros and cons of each alternative

Regarding costs and assuming that for each alternative, the material costs will be similar, just the construction of the hydro pump water storage plant (in situ and using prefab caissons) are considered. The turbines, surrounding dikes, and other works are not included in this costs approximation. As explained in Appendix I, these costs depend on the chosen construction strategy for the prefab alternative. However, following expert's recommendations and being conscious about the uncertainty of this result, the prefab method has been chosen to be 1.2 times more expensive than the in situ construction method. Thus, the value over costs of each alternative would be:

- In situ construction method: $\frac{V}{C} = \frac{7.7}{1} = 7.7$
- Prefab construction method: $\frac{V}{C} = \frac{6.7}{1.2} = 5.6$

These results can be plotted for a better comparison (There are two results so it is clear that the in situ alternative will be chosen):

Figure 6.7: Value over costs analysis for in situ and prefab construction methods

6.4 Selection

The selected alternative is then Alternative 1. A cross-section of early design stages is shown to already get an idea of how the power plant will be. Only the cross-section together with the water and ground levels is shown because this was one of the first designs. At the beginning of the next chapter, the final section together with measurements, water and ground levels are present. To see the different elements of the plant, the reader is referred to Appendix K.

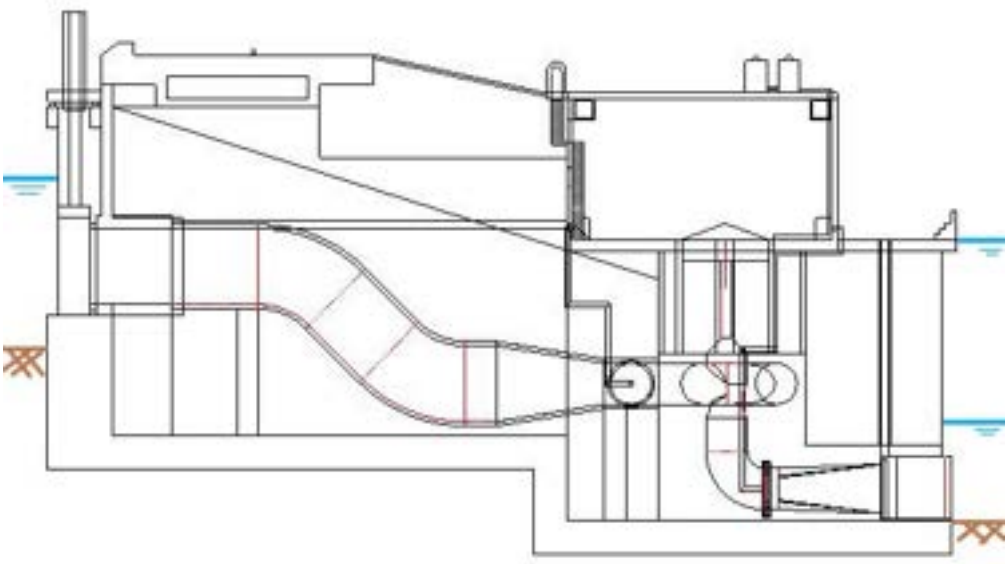

Figure 6.8: Chosen alternative for further design

Chapter 7

Structural design

In the present chapter, the general stability and reinforcement calculations are shown for the chosen alternative.

The stability calculations ensure horizontal, rotational and vertical stability of the structure. Additionally, bed protection at the sides of the structure as so as the piping protection are also included in this section.

The reinforcement calculations have been performed using MatrixFrame software (student version) and following the Eurocode 2 as a guideline for reinforcement. Additionally, the reinforcement at the connections between different elements is done using the strut-and-tie model. The gate's design is also included in this section.

7.1 Construction sequence

This section aims to show the reader the different construction steps through figures. This is a summary of the detailed explanation present in Appendix I.

7.1.1 Step 1: Temporary roads, concrete production plant, and offices preparation

All the necessary temporary constructions are constructed as the building pit is being constructed.

7.1.2 Step 2: Building pit construction

An accurate cross-section of the building pit is given in Figure I.2 where the adequate slopes are shown. Here just a representation of the building method is depicted.

Step 2a: Dredging and simultaneous dike formation

Notice that this is done meanwhile the temporary constructions are being done because only dredgers are needed.

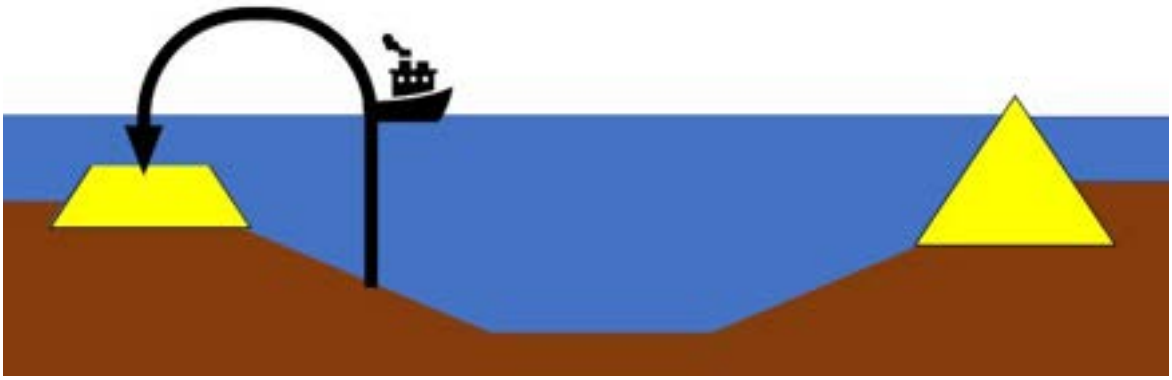

Figure 7.1: Construction step 2a.

Step 2b: Screens installation to reduce seepage

Due to the large infiltration expected and to reduce the discharge of the wells, it is recommended to install some sheet piles and/or diaphragm walls. Diaphragm walls are recommended to be built under the structure since they can also be used as a tool to increase the piping seepage length as it will be recommended in Section 7.2.4 below.

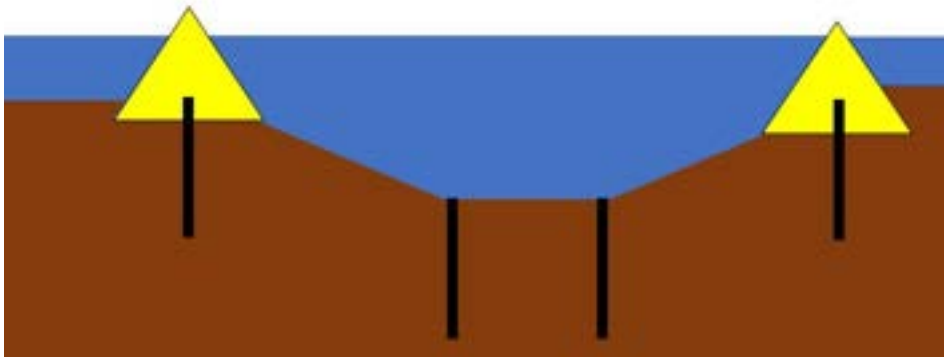

Figure 7.2: Construction step 2b

Step 2c: Wells installation and dewatering by pumps

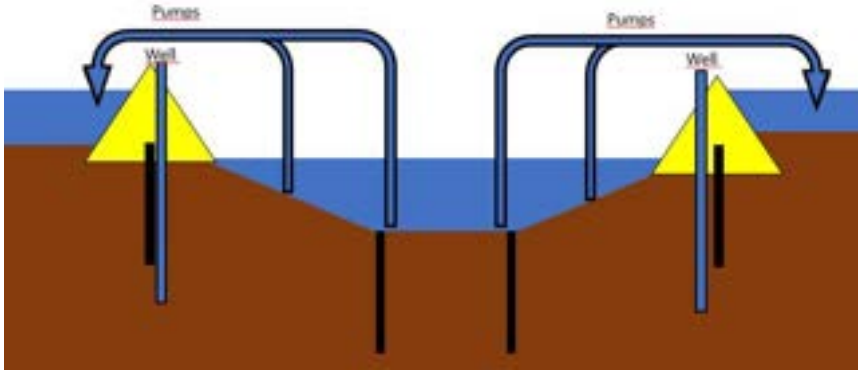

Figure 7.3: Construction step 2c.

Step 2d: permanent dewatering by wells to lower the water table

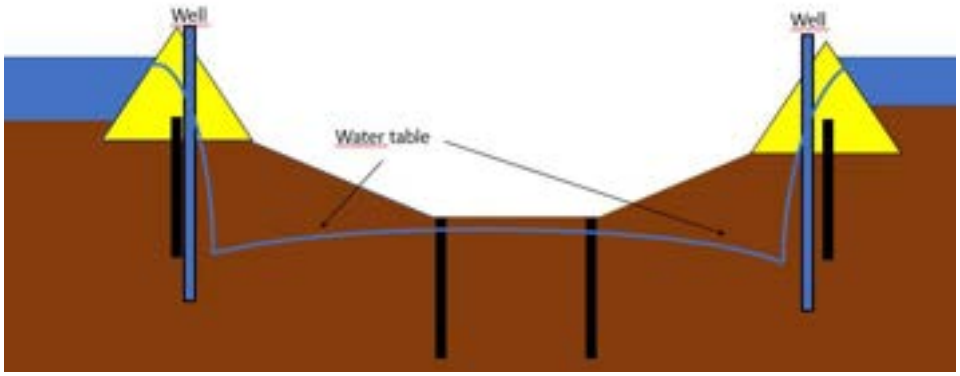

Figure 7.4: Construction step 2d.

7.1.3 Step 3: Piping protection installation (1^{st} positioning)

The piping protection is installed under the shallow foundation and rolled next to it to not interrupt the operation of the machinery. It will be extended later on. This is done on both sides (sea-side and Valmeer's side) of the structure.

Figure 7.5: Construction step 3.

7.1.4 Step 4: Power plant construction in situ

The erection of the plant will be done using traveling formwork. After the shallow foundation is finished (To see the plant's elements go to Appendix K). The vertical walls will be erected. These are the skeleton of the structure and they are needed to give strength to the entire structure. After that, the caissons for the pumps/turbines will be cast in situ (the turbine/pump company provides the design of these caissons). Then the compartments and the penstock supporting structure are built. The penstock is built on top of that. The penstock is made out of steel and each part will be bolted one to another. Meanwhile, on top of the pump/turbine caissons, the shaft room is built. Once it is finished, the crane room is built over it. With these elements, the concrete works of the dam are finished. In the following figures, 4 phases of the construction are shown.

Step 4(a): Shallow foundation + vertical walls construction

Figures 7.6 and 7.7 are part of the same building sequence. The penstock will be installed before the horizontal roof above it.

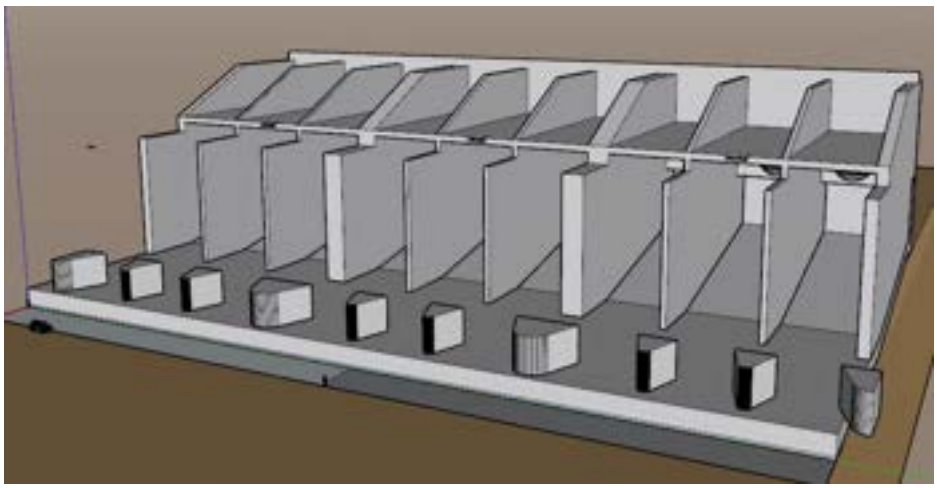

Figure 7.6: Construction step 4a.

Step 4(b): Fill compartments + penstock support structure construction + penstock installation

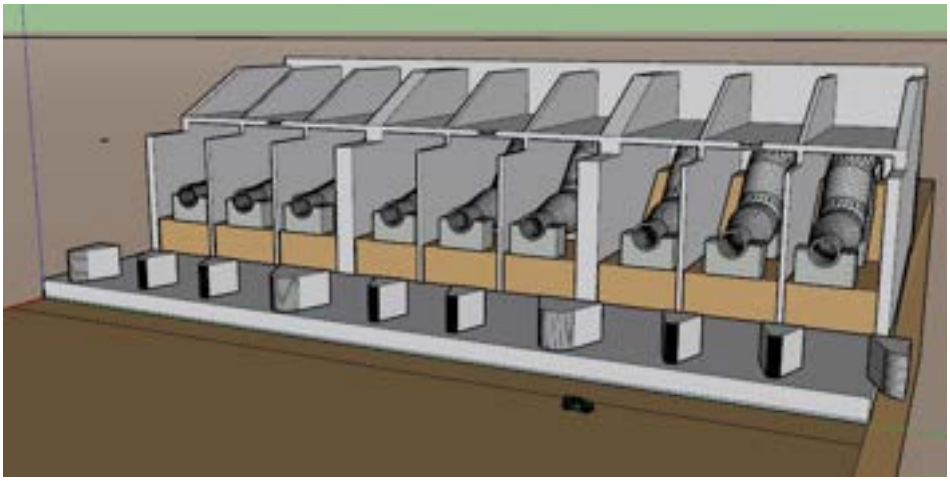

Figure 7.7: Construction step 4b.

Step 4(c): Caissons for pump/turbine + shaft room + Valmeer gates structure construction

Figure 7.8: Construction step 4c.

Step 4(d): Crane room construction

Notice that this is the worst case scenario for vertical stability (see Section L.6.3)

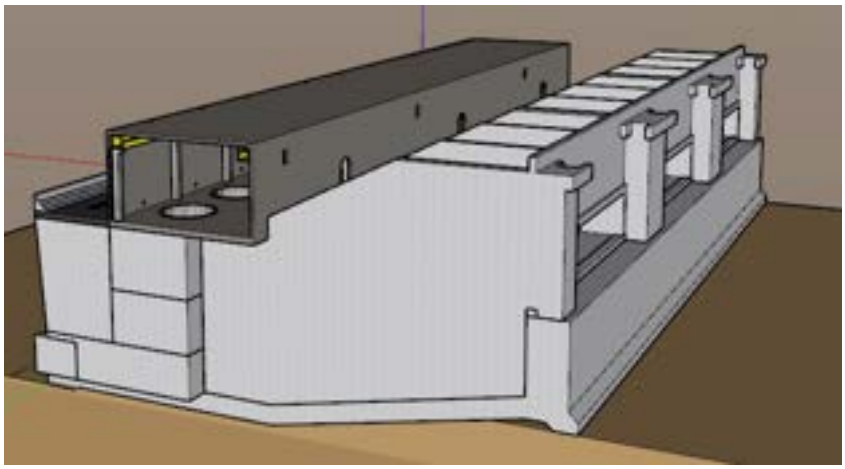

Figure 7.9: Construction step 4d.

7.1.5 Step 5: Extension of all piping protection (2^{nd} and final positioning)

Now that the concrete works are finished, the piping protection can be laid down. At first, the protection is placed until the limits of the building dock. Then, after the disassembly of the dry dock, the rest of the piping protection will be installed towards the Valmeer side, since at the sea-side some dredging would be needed for installing the protection (see Section 7.2.4 below for a detailed drawing of the piping protection).

7.1.6 Step 6: Gates installation, sand refill at plant's sea-side and bed protection installation at both sides of the plant

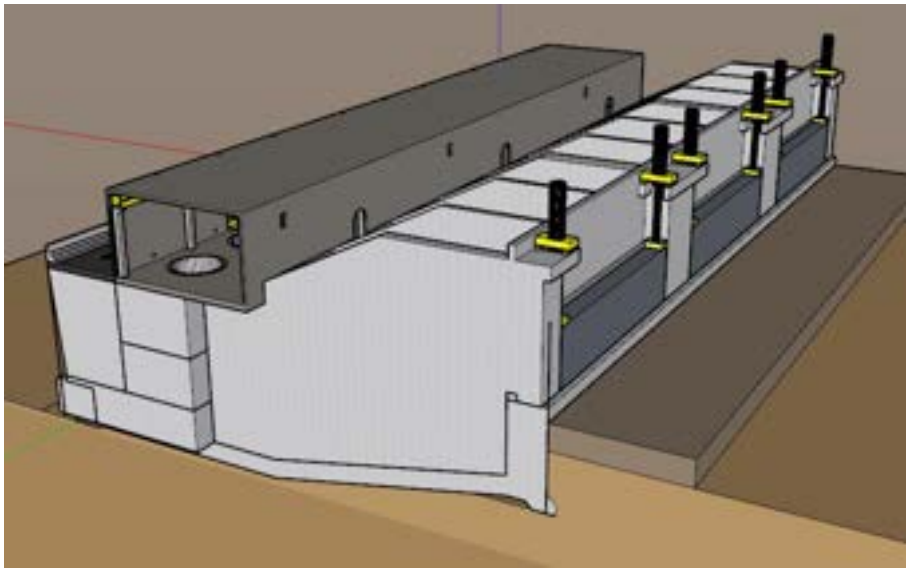

Figure 7.10: Construction step 6.

7.1.7 Step 7: Disassembly of dry dock and road deck installation

The road deck is installed by a crane vessel.

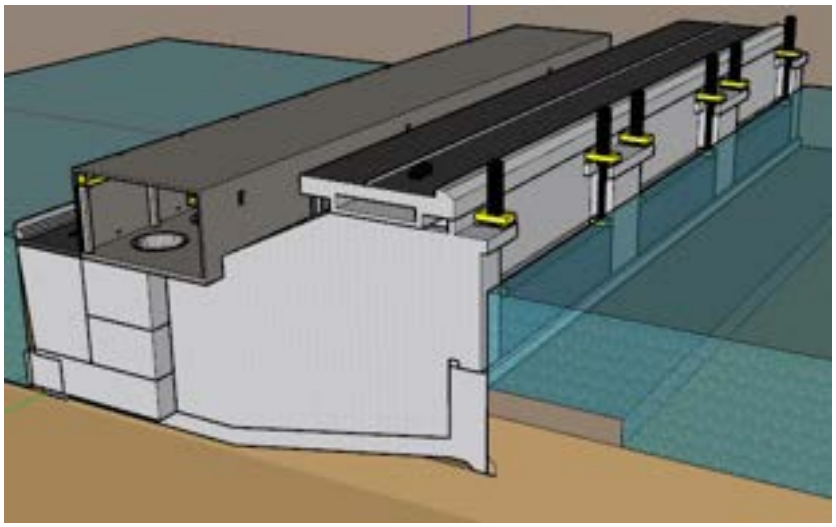

Figure 7.11: Construction step 7.

7.1.8 Step 8: Works finalization

The last elements are positioned in the plant.

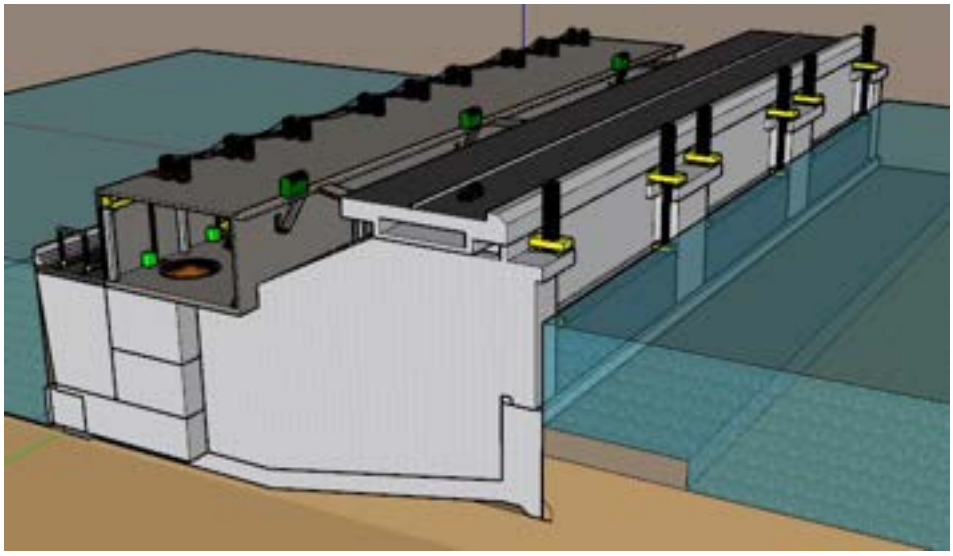

Figure 7.12: Construction step 8.

7.2 General stability calculations

In Section 6.4 can be seen that the chosen alternative is Alternative 1 built in-situ. In the present section, Alternative 1 is shown after some design loops have been performed. The design iterations were done using an excel spreadsheet and looking at the 3D model. Several design loops have been done. The formulation used to check the structure's stability is the one present in the Appendix L.6. The final cross-section together with approximate dimensions can be seen below (To see the different elements of the plant, the reader is referred to Appendix K.):

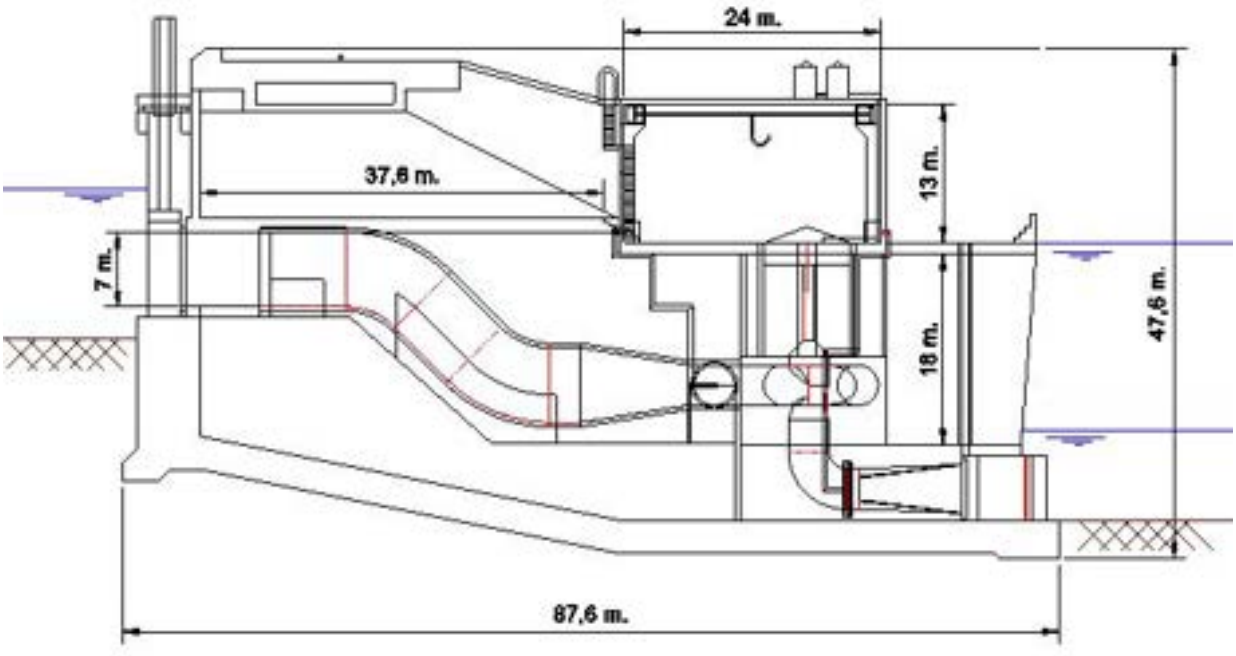

Figure 7.13: Cross section showing final power plant's design

The calculations performed for the alternative include the following sections:

- Horizontal stability
- Rotational stability
- Vertical stability
- Piping protection
- Bed protection at the in-/outlet of the structure

After performing several design iterations, the horizontal stability was found to give the largest weight and therefore it was the critical check.

For that reason then, in the following lines, the horizontal stability calculations are first shown. There, the procedure to arrive at a stable weight is shown. The stable weight will be of 37400 kN/m (see 7.2.1). In the rotational and vertical stability section, it will be shown that this weight per meter is enough to meet the requirements for rotational and vertical stability. Remember that the most critical parameter was horizontal stability.

The weight of the plant was obtained from the volumes of the elements of the power plant. These volumes come from the modeled 3D plant. Remember that the model represents 3 modules of the structure. Accounting for a total of 148 meters. The total number of modules needed for the total structure is 56. The model is composed of 178236 m^3 of reinforced concrete, 56115 m^3 of compartments which will be filled with sand and 1631 m^3 of steel elements such as cables, tubes, and gates. Therefore, the structure's weight per meter is:

$$W_{structure} = \frac{178236m^3 \cdot 25kN/m^3 + 56115m^3 \cdot 17kN/m^3 + 1631m^3 \cdot 75kN/m^3}{148} = 37379kN/m \approx 37400kN/m^3$$

7.2.1 Horizontal stability

Sketch failure mechanism

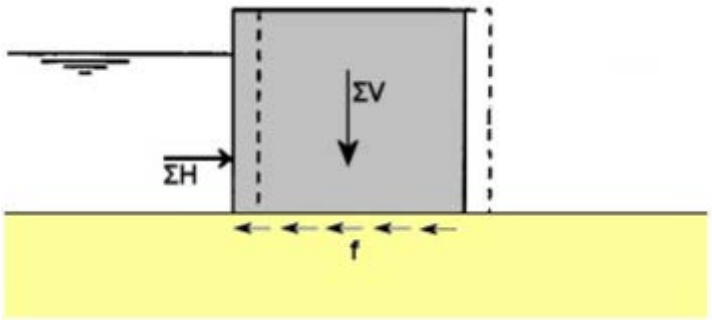

Figure 7.14: slip-off principle sketch. Source: Hydraulic Structures Manual

$$\sum H \leq f \cdot \sum V \tag{7.1}$$

Critical load case (construction step 8)

Two models of forces were considered to find the worst-case scenario for horizontal stability. The worst-case comes when the resultant horizontal forces are maximum and the resultant vertical forces are minimum. In the first load case considered, the head difference is governing (maximum lateral loads but maximum vertical load, buoyancy force is minimum) and in the second, maximum wave height does (not maximum horizontal forces, but minimum resultant vertical force, buoyancy is maximum). At first glance, the first load case seems to be more critical, since the head difference is maximum and quite large, however, buoyancy might play an important role reducing the weight of the structure and therefore the two load case s are studied:

1. Regular working conditions: In this load case, the maximum water head difference is present. For these working conditions, the design water level and wave height will have a return period of 10 years (Assumed regular conditions design case. At this wave heights and water levels, the plant should still operate to obtain energy).

2. Storm surge conditions: In this load case, the wave loading is maximum. The design wave height will have a return period of 1000 years

These two load cases will be considered to check the horizontal stability of the structure. The goal is to see which load case gives the larger structure dimensions and weight and then use that weight for design. Thus, making sure that the structure will hold the forces present at any future condition.

In the following lines, the stability calculations are shown for both load cases.

Regular working conditions

The water level at Valmeer is at NAP -22.5 m for providing potential energy to the water. The head difference is maximum at this stage. As previously mentioned, the design wave and water level are the ones corresponding to 1/10 years.

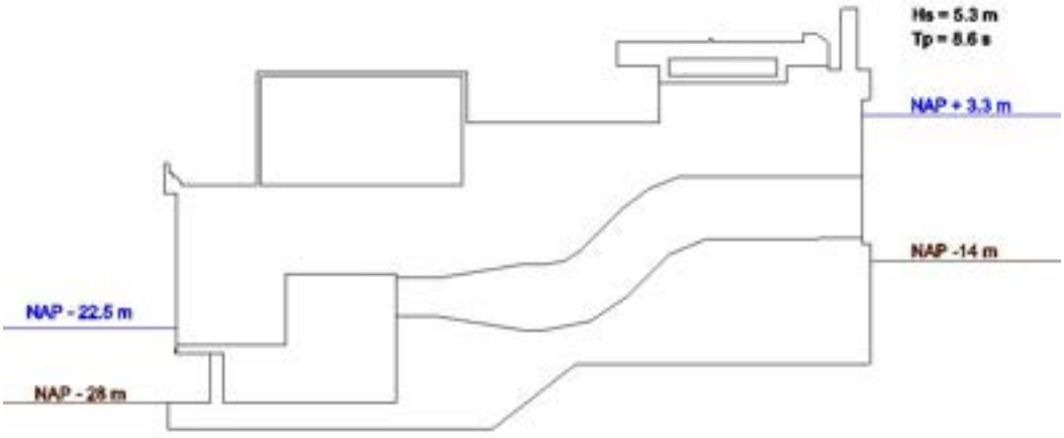

Figure 7.15: load case regular conditions.

In the following figure, a representation of all the forces acting on the structure is shown. To see where these forces come from, the reader is referred to Appendix L.6:

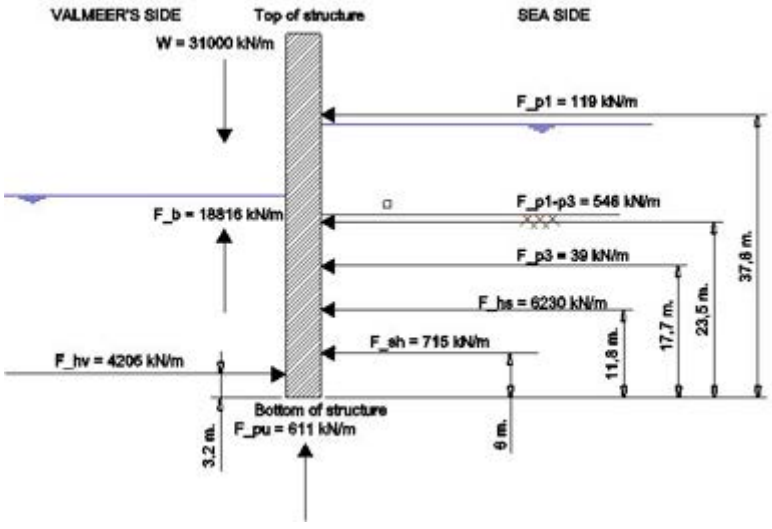

Figure 7.16: Forces considered for overall stability of the structure. Graphic representation.

Taking this into account and following the formulations shown in the beginning of this section, the stability calculations will be done. First, the resultant horizontal and vertical force has to be computed:

$$\sum H = F_{p1} + F_{p1-p3} + F_{p3} + F_{hs} + F_{sh} - F_{hv} = 7243\ kN/m$$

$$\sum V = W - F_b - F_{pu} = 12138\ kN/m$$

Then, the horizontal stability is met if:

$$\sum H \leq \nu \cdot \sum V; 7243\ kN/m \leq 0.6 \cdot 12138\ kN/m = 7283\ kN/m$$

Thus, horizontal stability is ensured.

Storm surge conditions.

The water level at Valmeer is at NAP -5 m for providing maximum lateral stability. The design wave and water level are 1/1000 years.

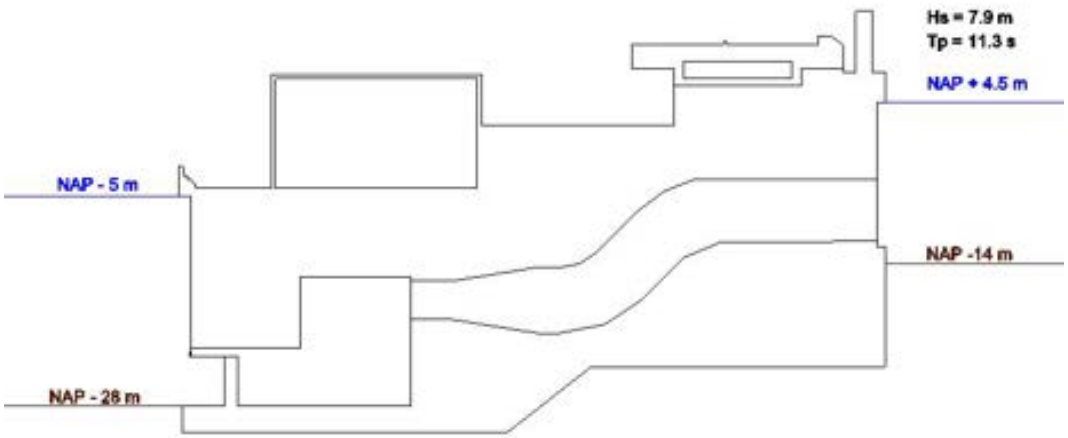

Figure 7.17: load case storm surge situation

A representation of the above forces is shown below:

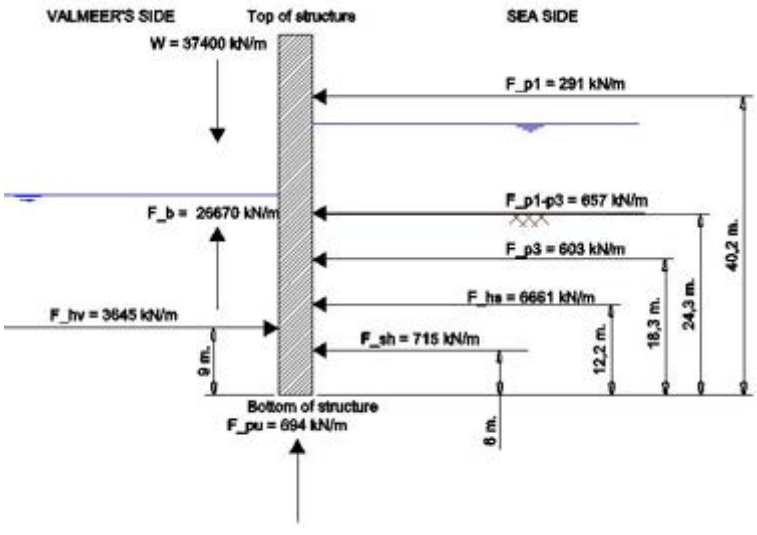

Figure 7.18: Forces considered for overall stability of the structure. Graphic representation

Taking this into account and following the formulations shown in the beginning of this section, the stability calculations are done. First, the resultant horizontal and vertical force have to be computed:

$$\sum H = F_{p1} + F_{p1-p3} + F_{p3} + F_{hs} + F_{sh} - F_{hv} = 5976\ kN/m$$

$$\sum V = W - F_b - F_{pu} = 10036\ kN/m$$

Then, the horizontal stability is met if:

$$\sum H \leq \eta \cdot \sum V; 5976\ kN/m \leq 0.6 \cdot\ 10036 kN/m =\ 6022 kN/m$$

Thus, horizontal stability is ensured.

Conclusions from horizontal stability checks

The initial assumption that the regular conditions load case would be more critical due to the head difference is not true. Head difference plays an important role because of the large resultant hydrostatic loads that are created. However, a large head difference also means less buoyancy (see Equation L.6 to see how buoyancy is calculated), which in turn, resulted to be disadvantageous for the structure's stability (the horizontal stability check was found to be the most critical for stability, therefore the less buoyancy the better). For this reason, for each load case, the stability calculations have been obtained for a varying water level within the Valmeer.

The results are the following for both Regular and storm surge conditions:

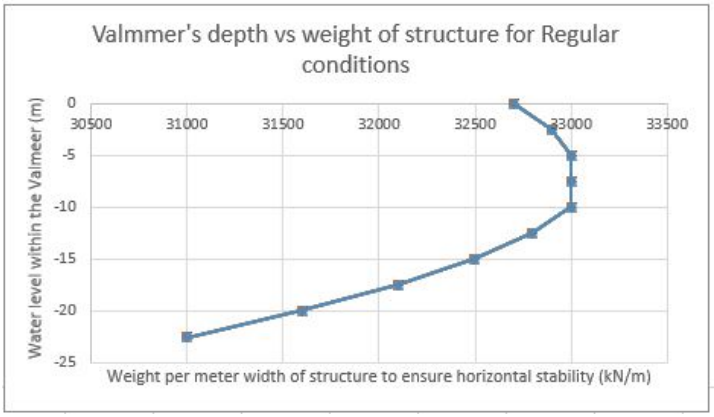

Figure 7.19: Valmeer's depth vs weight of structure for Regular conditions

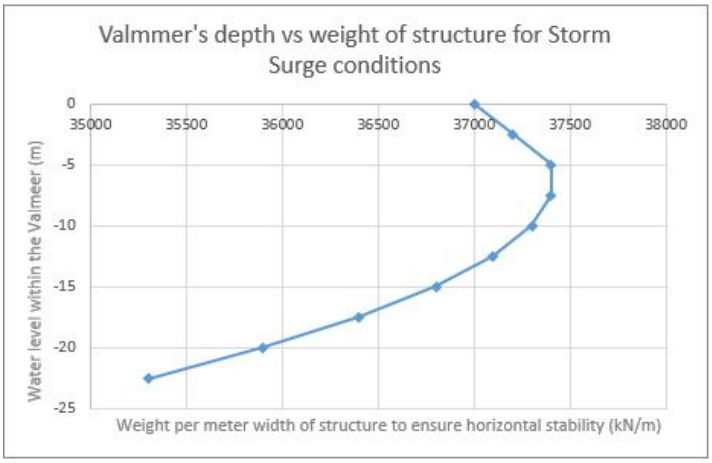

Figure 7.20: Valmeer's depth vs weight of structure for Regular conditions

In these figures, it can be seen that the buoyancy influence on stability is noticeable. To the surprise of the author, the structure is more stable (less weight needed for stability) when the water level differences between the sea and the Valmeer are maximum. The worst-case scenario happens for storm surge conditions and a water level inside the Valmeer between NAP -5 m and NAP -7.5 m. For these water levels, the contribution of the lateral load by raising the water within the Valmeer is counteracted by the large buoyancy force product of having such high water levels at both sides of the structure. Therefore a large weight per unit meter of structure is needed for the structure to be stable. When the water level goes higher (in the real case cannot go higher than NAP -5 m, but it is interesting to see what would happen), the water inside the Valmeer seems to counteract the loss of weight from the buoyant forces by an increase in lateral load. The opposite happens when the water level drops below NAP -7.5m. The low water level inside the Valmeer causes loss in lateral stability but, in turn, the loss in buoyant force is more critical and makes the structure more stable (less weight is needed for stability).

The selected weight per meter that the structure needs to have to be stable is then the corresponding to storm surge conditions (H_s = 7.9 m, T_p = 11.3 s) and a water level within the Valmeer between NAP -5 m and NAP -7.5 m. The weight per meter needed for stability is then 37400 kN/m.

However, some techniques can be applied to lower the influence of the buoyant forces:

1. Make an impervious Valmeer. If the Valmeer is impermeable, at the sea-side the water buoyant forces acting at the structure will be zero, and therefore only the water level within the Valmeer will produce buoyant forces

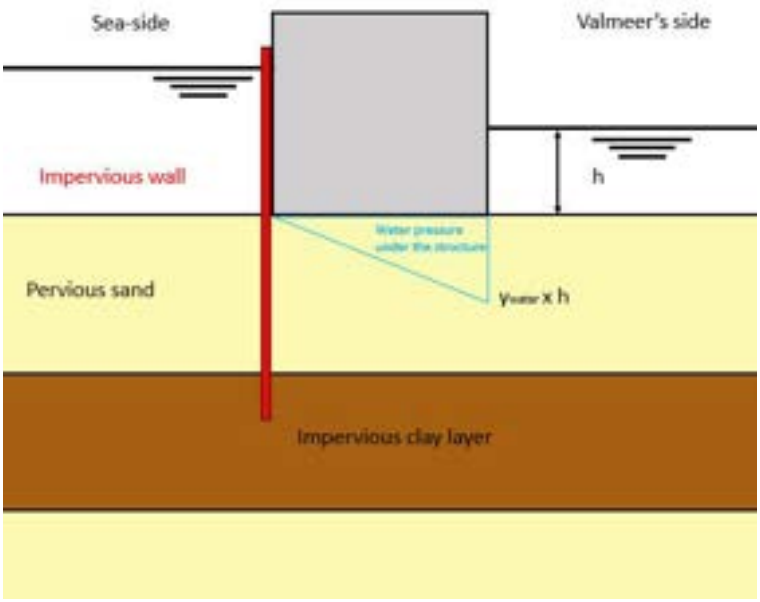

Figure 7.21: Sketch showing the effect of having an impervious Valmeer

   However, this is quite hard (almost impossible) to realize since it will require to build a wall from the top of the water level down to the clay layer (around 64 meters deep wall) along 2764 meters of structure. Another possibility is to create an impervious layer under the structure, and drive sheet piles down to it, but this would require a huge amount of grout (around 2.3 million m^3 for a 1 m thick impervious layer under the building pit).

2. Reduce the buoyant force by installing sheet piles under the structure. This strategy is more interesting since this sheet piles are needed for piping protection. However, the buoyant force reduction will not be very significant.

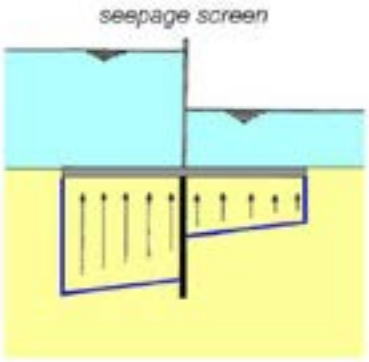

Figure 7.22: Sketch showing the effect of having a single sheet pile under the structure. Source: CIE 3330, Hydraulic structures slides. (Voorendt, 2018)

If the Valmeer cannot be impermeable, it is interesting to know that the water level within the Valmeer doesn't have to be raised to NAP -5 m to have more favourable conditions to hold back the storm surge, as it was expected since the beginning. It was demonstrated above that the most favourable case for providing lateral stability to the structure is when the water level in the Valmeer is minimum (NAP -22.5 m). This means that the water level of the Valmeer can be lowered to NAP -22.5 m to resist better the loads and to increase the storing capacity of runoff water of the Valmeer. Then maybe the pumps would not need to be used until a really large river discharge is present. However, lowering the water level at maximum during storm surge conditions is not a good strategy regarding piping (see piping protection Section 7.2.4 below). Therefore the recommendation is to have a water level inside the Valmeer of NAP -19 m during storm conditions to have the same head difference as during regular conditions and thus use this case for piping calculations. This is not in the scope of this thesis and therefore no further mentions about it will be done.

From now on, the storm surge conditions can happen together with having water levels within the Valmeer between NAP -5 m and NAP -22.5 m.

7.2.2 Rotational stability

Sketch failure mechanisms

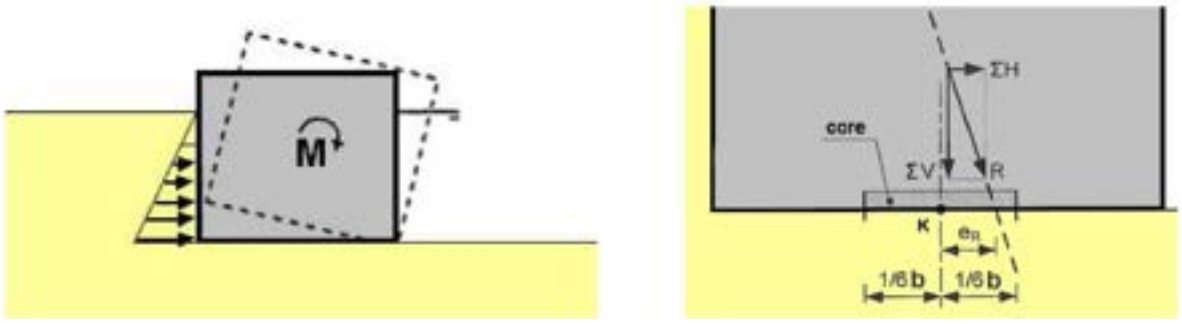

Figure 7.23: Rotational stability sketch.Source: Hydraulic Structures Manual

$$e_R = \frac{\sum M}{\sum V} \leq \frac{1}{6}b \quad [m] \tag{7.2}$$

Critical load cases (construction step 8)

Now that the worst-case for selecting the weight of the structure was developed, in the following sections, the checks for the other stability requirements are shown.

In the present section, the worst-case loading regarding rotational stability is considered. Rotational stability is more critical when the rotational moment is maximum and the vertical resultant force is minimum. Maximum

rotational moment happens when the head difference is maximum (only lateral loads are considered) but minimum vertical resultant force happens when the water levels at both sides of the structure are maximum. Using the experience gained in the previous check, the rotational stability checks will be done for the storm surge case and different water levels within the Valmeer.

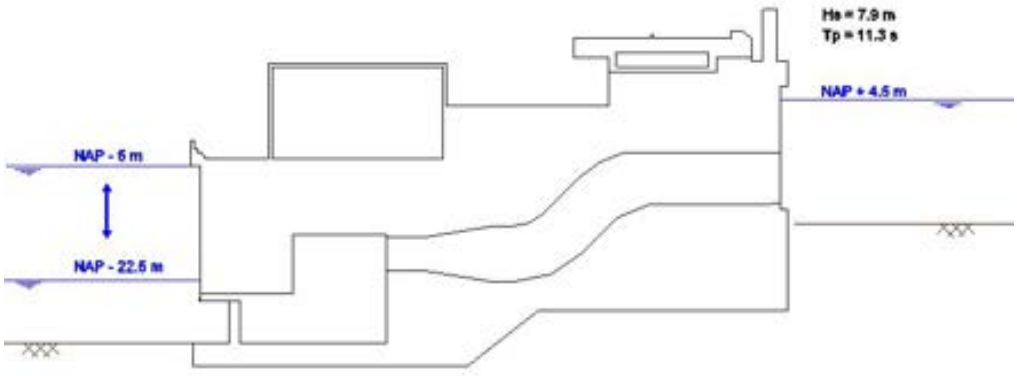

Figure 7.24: load case considered to check whether rotational stability is met

In the following lines, first a figure considering the safety factor against rotational stability for each water level will be shown. Then, the rotational stability calculations will be shown for the worst case scenario.

Safety factor against rotational stability for storm surge conditions and different water levels inside the Valmeer

Rotational stability checks are done following the formulation present in Section L.2.2. There, it can be seen that:

$$e_R = \frac{\sum M}{\sum V} \leq \frac{1}{6}b \quad [m]$$

Therefore, the e_R will be used as the design unit. e_R has been calculated for storm surge conditions and the different water levels that can be present within the Valmeer. The safety factor (SF) has been defined as:

$$SF = \frac{b/6}{e_R}$$

This means that for the limit of $b/6 = e_R$, the safety factor will be one, as the e_R value decreases, the safety factor increases. The results of the analysis can be observed below:

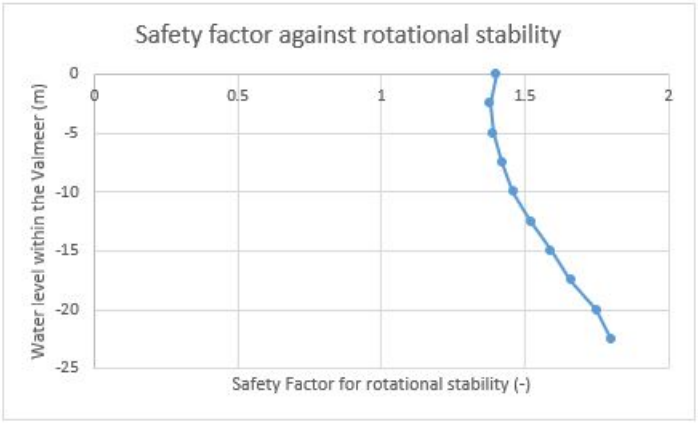

Figure 7.25: Safety factor against rotational stability

As we can see above, the safety factor against rotational stability is always greater than 1. Thus, the rotational stability of the structure is ensured. The worst-case scenario happens when the water level within the Valmeer is at NAP -5 m (it is actually at NAP -2.5 m, but this water level is not allowed within the Valmeer). This

coincides with the worst case scenario for horizontal stability. The calculation performed for this worst-case scenario is shown in Appendix L.6.

7.2.3 Vertical stability

Sketch of failure mechanism

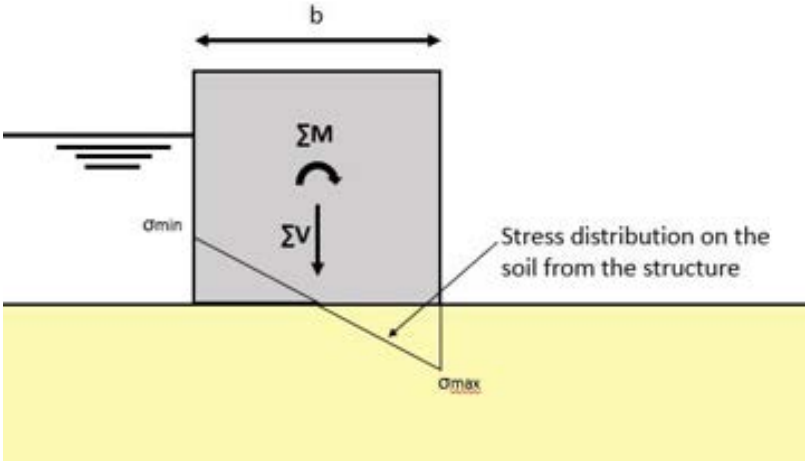

Figure 7.26: Vertical stability sketch

The stress created on the soil by the structure must not exceed the maximum soil bearing capacity ($\sigma_{k,max} < p'_{max}$). Otherwise the soil will collapse. The maximum load on the soil is calculated as:

$$\sigma_k, max = \frac{F}{A} + \frac{M}{W} = \frac{\sum V}{b \cdot l} + \frac{\sum M}{\frac{1}{6} l b^2} \quad [kN/m^2] \tag{7.3}$$

On the other hand, as the soil cannot take negative stresses, the minimum load acting on the soil has to have a positive sign ($\sigma_k, min > 0$. Only compressive stresses allowed). The minimum soil load is calculated as:

$$\sigma_k, max = \frac{F}{A} - \frac{M}{W} = \frac{\sum V}{b \cdot l} - \frac{\sum M}{\frac{1}{6} l b^2} \quad [kN/m^2] \tag{7.4}$$

Worst load cases for vertical stability

This section will check if the maximum and minimum soil pressure stay below the $p'_{max} = 400$ kN/m^2 (densely packed sand bearing capacity assumption from CUR, 2010) limit and above zero (no tensile stresses can develop in the soil).

The maximum soil pressure happens when the vertical resultant force and the rotational moment are maximum. The vertical force is maximum just after finishing of the structure construction. Since water is not surrounding the structure and therefore no buoyant force makes the structure "lighter". Maximum rotational moment happens for the case of having storm surge and a water level within the Valmeer of NAP -22.5 m. Therefore, a calculation only including selfweight will be done and then another calculation will be done for the case of having storm surge and a water level within the Valmeer of NAP -22.5 m.

The minimum soil pressure happens when the vertical resultant force is minimum and the rotational moment is maximum. The vertical force is minimum for the case when maximum water levels are present at both sides of the structure. The maximum rotational moment happens when the structure is subjected to storm surge conditions and the water level within the Valmeer is minimum. Therefore again, the case of having storm surge conditions will have to be checked for the different water levels inside the Valmeer.

Thus, the following load cases are considered:

- The structure has just been constructed and there is not water around it. (construction step 4(d)).
- Storm surge and water level within Valmeer between NAP -5 m and NAP -22.5 m.

Maximum pressure acting on the soil

First, the vertical stability is calculated for the case when the structure has just been constructed and there is no water surrounding it. The structure's selfweight was 37400 kN/m. Therefore, the pressure over the soil comes from dividing the weight by the length of the structure:

$\sigma_k, max = \frac{37400 kN/m}{84m} = 445\ kN/m2$

As we can see, if the whole weight of the structure is present, the soil will fail in compression. However, the road will be installed after the structure is surrounded by water. From Sagemo & Storck (2013) we know that the installed bridge weight per meter is 24.71 tons/m, which results in:

$24.71\ tons/m \cdot 1000\ kg/ton \cdot 10\ kN/kg = 2471\ kN/m$

Now the soil pressure is computed as:

$\sigma_k, max = \frac{37400 kN/m - 2471 kN/m}{84m} = 416\ kN/m2$

Which still not feasible. One more thing can be done though. The power plant contains some compartments that will be filled with sand (to provide more weight and therefore stability). These compartments can be filled up after the water is surrounding the structure since they are only needed for providing stability during the design storm situation. The weight of each of these compartments can be calculated from:

$W_{compartment} = V_{compartment} \cdot \gamma_{sand} = 6235\ m^3 \cdot 17\ kN/m^3 = 105995\ kN$

The volume is obtained from the AutoCAD model and the unit weight of the fill in material (sand) has been assumed. The weight per meter of structure is then computed as:

$$W_{compartmentPerMeter} = \frac{W_{compartment} \cdot N_{compartments}}{Width_{plant}} = \frac{105995 \cdot 9}{148} = 6445\ kN/m$$

The width of the compartment has also been calculated from the AutoCAD model. Thus, if the compartments are empty and only filled in after the bulding pit is flooded, the "dry" weight of the structure is now:

$W_{structure} = 37400 kN/m - 2471 kN/m - 6445 kN/m = 28484\ kN/m$. Giving now a soil pressure of:

$\sigma_k, max = \frac{28484 kN/m}{84} = 339\ kN/m^2$

Now, the soil can take the pressure of the structure.

The other load case comprise the maximum rotational moment. That load case can be seen below:

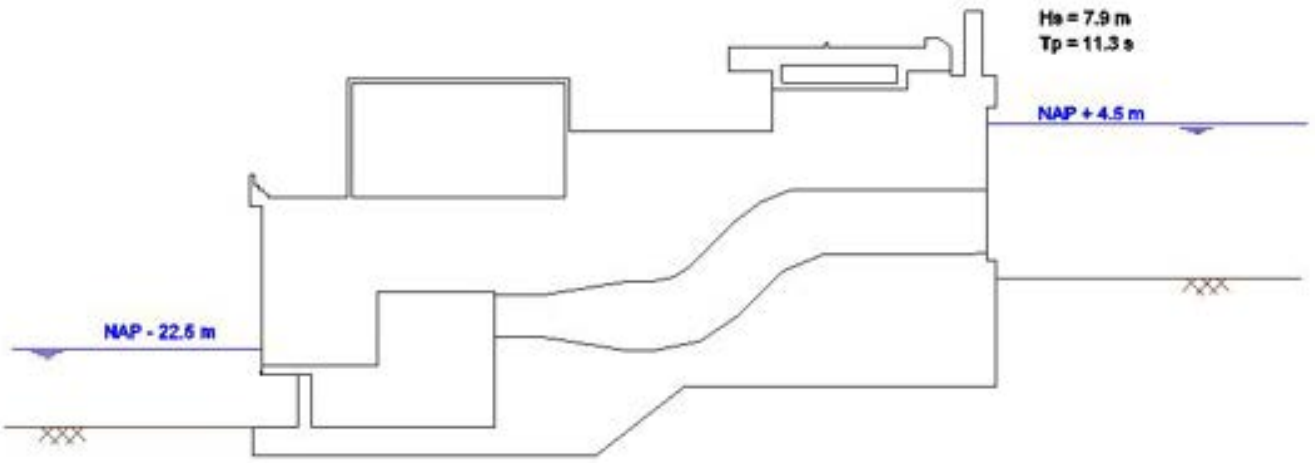

Figure 7.27: load case for maximum rotational moment. Storm surge and low water level within Valmeer.

For this loadcase, the maximum pressure is (see Appendix L.6 for calculations):
$\sigma_k, max = 319\ kN/m^2/m$

Minimum pressure acting on the soil

Following Section L.2.2 the minimum soil pressure can be calculated with the following equation:

$$\sigma_k, max = \frac{F}{A} - \frac{M}{W} = \frac{\sum V}{b \cdot l} - \frac{\sum M}{\frac{1}{6} l b^2} \quad [kN/m^2]$$

To obtain the minimum pressure, the load case of having storm surge will be checked for finding the minimum stability for different water levels inside the Valmeer. The result of the calculations can be seen in the figure below:

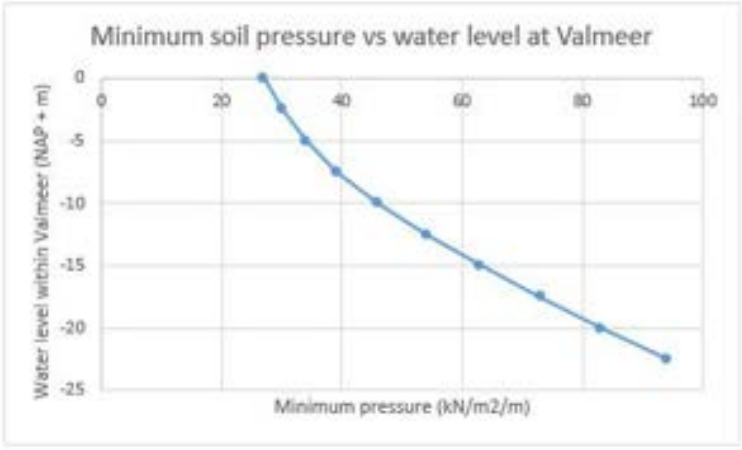

Figure 7.28: Minimum soil pressure depending on water level at Valmeer

It can be observed that in this case, the minimum pressure increases when increasing the depth of the Valmeer. Again, the contribution of the buoyant force is governing. At a water level within the Valmeer of NAP -5 m, the minimum soil pressure still above zero, so no tensile stresses are develop on the soil. The vertical stability of the structure is then ensured.

7.2.4 Piping protection (construction step 8)

The piping calculations have been done following Lane's formula. As stated in Appendix L there are another more accurate formulations such as the Hans Sellmeijer formulation (1988) but they require more soil informa-

tion. As this is not available and the present design is conceptual, Lane's theory will be used. The formulation can be seen below. For a better definition of the theoretical background of these formulas, the reader is referred to Appendix L.

$$L \geq \gamma \cdot C_L \cdot \delta H \quad [m]$$

$$L = \sum L_{vert} + \frac{1}{3} \sum L_{hor} \quad [m]$$

In this case, it is easy to find the critical load case since according to Lane's formula the piping length depends mainly on the head difference. So the larger head difference that the system will face will be used for the piping calculation. The maximum head difference will happen for the conditions of storm surge and low water level. This conditions are taken as design conditions beacause it is a possible situation and the wordt one. Further research is recommended on this aspect, since by managing water levels within the Valmeer a reduction in pipin protection can be achieved (see piping conclusions below). Below the design water levels are shown:

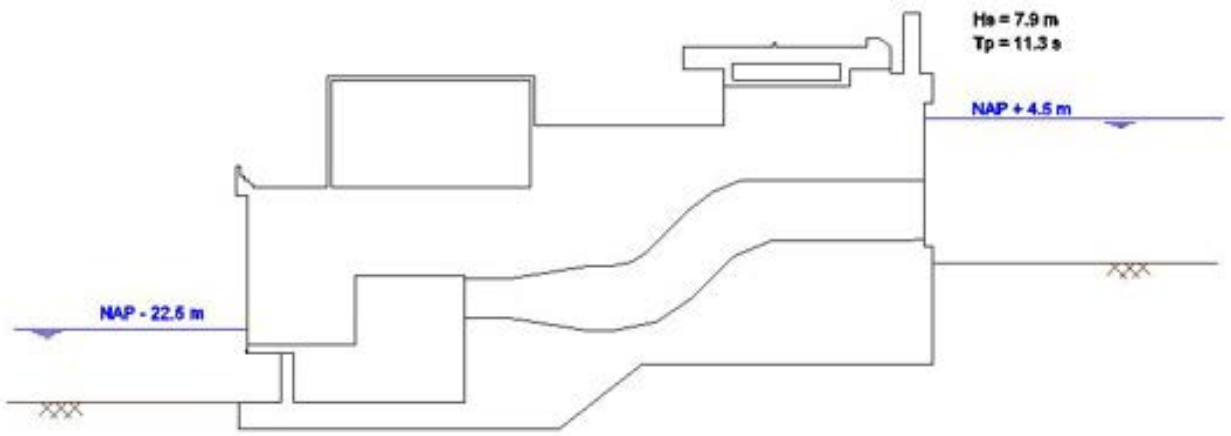

Figure 7.29: load case for piping calculations. Storm surge and low water level within Valmeer.

Assuming that the soil below the structure is "middle fine sand" and following lane's formulation the seepage length is then:

$L = \gamma \cdot C_L \cdot \delta H = 1.5 \cdot 6 \cdot (4.5 - (-22.5)) = 243\ m$

Middle fine sand was considered (C_L in the above equation is equal to 6), therefore the maximum allowed hydraulic gradient is (from the table in Section L.2.2) 16.7 %. The actual hydraulic gradient is:

$i_{actual} = \frac{4.5-(-22.5)}{243} = 11.1$ % Therefore the maximum allowed is not reached.

The total protection length can be obtained from Equation L.15, also shown in the beginning of this section. At the sea-side of the structure, 18 meters of vertical protection will be installed, on the Valmeer's side another 4 meters of vertical protection are applied. Then, 243 - 4 - 18 = 221 meters are still needed. Since these will be installed horizontally, Lane recommends $L_{hor} = 3 \cdot L = 3 \cdot 221\ m = 663$ meters of horizontal piping protection. Equation L.15 is then: $L = 18 + 4 + \frac{1}{3} \cdot 663 = 243\ m$ which meets Lane's formulation. The total piping length protection is then 663 + 18 + 4 = 685 meters long without applying any other measures. Below, different strategies are recommended to reduce the piping protection length.

Conclusions from the piping calculations

Having a shallow foundation gives the above-calculated necessary piping length protection without applying extra measures. Here recommendations are given to reduce the piping protection. First, some alternative techniques using sheet pile walls and diaphragm walls are give. Then, the advantages and disadvantages of those

techniques are explained. To finish, a recommendation is given to change the design load case.

According to Lane's theory, the vertical screens are more effective against piping than the horizontal ones (L_{hor} is divided over 3). Therefore the following strategies are recommended:

1. Installation of 32 m long sheet pile wall (or diaphragm wall) down to the impermeable clay layer. This would stop piping since water won't pass through the impermeable clay layer. However, digging sheet pile walls this depth could not be possible. Then diaphragm wall could be a better option but the slurry pressure to counterbalance the water pressures before reaching the clay layer needs to be approximately 640 kN/m^2. A big advantage of this method is that the seepage within the building dock would be significantly reduced. Easing the dewatering process.

2. Installation of 20 m long sheet pile wall (or diaphragm wall). This technique won't avoid fully piping but it will reduce the amount of piping protection needed. Different techniques can be applied:

   (a) 2 lines of 20 meters sheet piles: 2x20 m sheet pile reduces protection to L = 2x20x2 + 18 + 4 + 1/3 * 423, having then 423 m of horizontal protection. Sheet pile area needed = 110.560 m2 (2 x 2764 m x 20 m) [16 football fields].

   (b) 3 lines of 20 meters sheet piles: 3x20 m sheet pile reduces protection to L = 3x20x2 + 18 + 4 + 1/3 * 303. having then 303 m of horizontal protection. Sheet pile area needed = 165.840 m2 (3 x 2764 m x 20 m) [24 football fields].

   (c) 4 lines of 20 meters sheet piles: 4x20 m sheet pile reduces protection to L = 4x20x2 + 18 + 4 + 1/3 * 190. having then 190 m of horizontal protection. Sheet pile area needed = 221.120 m2 (4 x 2764 m x 20 m) [32 football fields].

   (d) 5 lines of 20 meters sheet piles: 5x20 m sheet pile reduces protection to L = 5x20x2 + 18 + 4 + 1/3 * 63 , having then 63 m of horizontal protection. Which would be provided just with the base of the structure, so no extra horizontal protection would be installed. However, a huge amount of steel would be needed and installing 5 sheet pile files would be very expensive. Sheet pile area needed = 276.400 m2 (5 x 2764 m x 20 m) [40 football fields].

GENERAL DRAWBACKS:
The installation of the sheet pile walls need a precise placing operation but according to professionals it can be done.
Furthermore, the more sheet piles installed under the structure, the better regarding buoyancy because the water pressures will take longer to develop because of the influence of the impermeable screen that the sheet piles create. In Figure 7.22 the effect of the sheet piles installation under the structure is already mentioned. However, this issue should be further researched to see the effects in buoyant forces.

As a last remark, the design water levels for piping can be different because during storm conditions the water level in the Valmeer can be raised to increase protection against piping by reducing the water head difference. Then, the other design condition will be the daily situation. But it would be interesting to check whether piping will occur in daily situations. For daily conditions, during 2 hours a day the water level difference is 22.5 meters. Research should be done to figure out adequate strategies to reduce the piping protection. This is not the main focus of this thesis, so for this thesis, the following piping protection is recommended (without doing any costs analysis, just considering the shorter piping protection length):

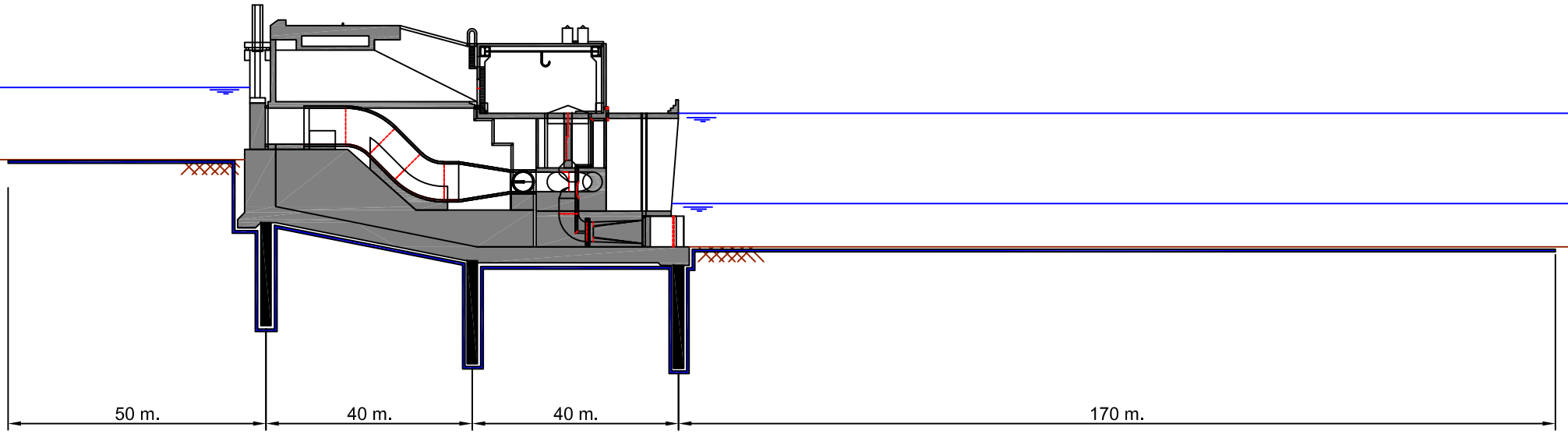

7.2.5 Bed protection at the in-/outlet of the structure

Bed protection is needed for two different phenomena. The scour holes which develop by the action of waves on vertical walls and the erosion of the bed caused by water flows velocities. This happens when water leaves the Valmeer during pumping (or enters during turbining). For these last cases, the following two scenarios will be considered:

1. Maximum discharge leaving the Valmeer. Erosion at sea-side of the structure.
2. Maximum discharge entering the Valmeer. Erosion at Valmeer-side of the structure

The scour depth due to wave action is already calculated in Figure L.17. The wave conditions of the final structure coincides with the ones of preliminary calculations. Therefore, a scour hole of 2.4 meters is expected to happen during critical conditions (if the storm duration is long enough for the hole to develop).

In the following lines, the reasoning for obtaining the bed protection length from flow velocities is shown.

Maximum discharge leaving the Valmeer

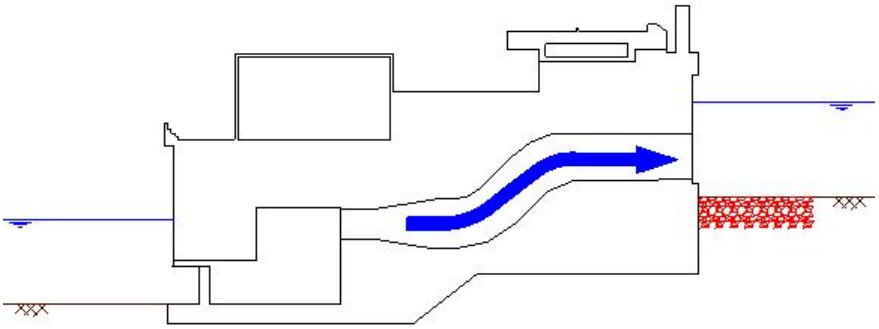

Figure 7.30: Representation of water leaving the Valmeer. The bed protection zone is signaled in red color.

When water is leaving the Valmeer it is exited by pipes with a diameter of 7 meters. The flow velocity at this pipe is then calculated as:

$v = \frac{Q}{A} = \frac{60}{\pi \cdot 7^2/4} = 1.6\ m/s$

To reduce this velocity at the exit, 3 pipes are diverted into a rectangular "inlet structure" with dimensions of 37 m × 7 m. Ideally, the "inlet structure" would reduce the flow velocity to:
$v = \frac{Q}{A} = \frac{60 \cdot 3}{37 \cdot 7} = 0.70\ m/s$

However, the velocity reduction won't happen instantaneously. For that reason, a reduction in flow velocity of a 25 % with respect to the velocity at each tube is assumed for the socour calculations. Then, the design velocity of the water leaving the Valmeer will be 0.75 × 1.6 m/s = 1.2 m/s.

Following Equation L.20, the critical velocity for initiation of motion of the sand particles (D_{50} = 1 mm) at the end of the bed protection is calculated:

$u_c = 88.3\sqrt{0.1 \cdot 0.6 \cdot 0.001} = 0.70\ m/s$

Then, the maximum scour hole depth is calculated as:

$h_{max} = 18.5 \cdot \frac{0.5 \cdot 3 \cdot 1.2 - 0.70}{0.70} = 1.6\ m$

Check $0.5 \cdot \alpha \cdot u > 0$: $0.5 \cdot 3 \cdot 1.2 = 1.8 > 0$.

Finally, the bed protection length is at least:

$L \geq 1.2 \cdot 10 \cdot 1.6 = 19.6\ m \approx 20\ m$

Therefore, at the sea-side, the bed protection length has to be of 20 m.

Maximum discharge entering the Valmeer

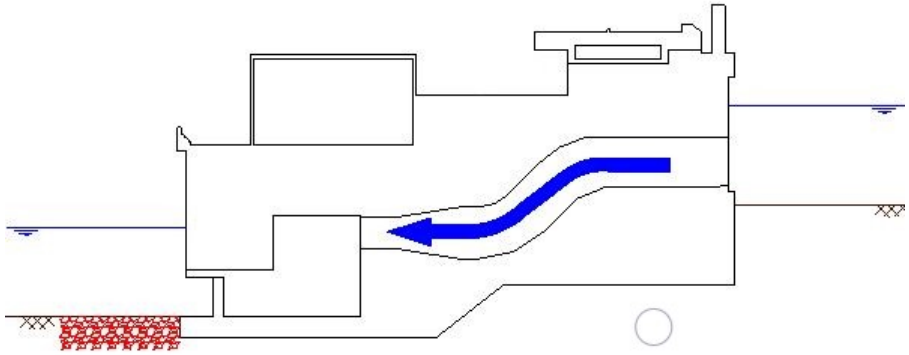

Figure 7.31: Representation of water coming into the Valmeer. The bed protection zone is signaled in red color.

The water enters the Valmeer at a lower velocity than it leaves. The draft tube is designed to reduce the flow velocity at maximum to maximize the kinetic energy obtained at the turbine. The flow velocity is calculated from the geometry of the formed suction intake (see Figure C.7):

$v = \frac{Q}{A} = \frac{60}{13.3 \cdot 6} = 0.75\ m/s$
The critical velocity for initiation of motion for the sand particles present at the end of the bed protection is the same as for the previous case: 0.70 m/s.
In this case though, due to the reduction of the flow velocity, the maximum scour hole depth is:

$h_{max} = 18.5 \cdot \frac{0.5 \cdot 3 \cdot 0.75 - 0.70}{0.70} = 0.66\ m$

Check $0.5 \cdot \alpha \cdot u > 0$: $0.5 \cdot 3 \cdot 0.75 = 1.1 > 0$.

Finally, the bed protection length is at least:

$L \geq 1.2 \cdot 10 \cdot 0.66 = 7.7m \approx 8.0\ m$

Therefore, inside the Valmeer, the bed protection length has to be of 8 m.

7.3 Strength calculations

The reinforcement calculations include the following:

- Gate design
- Reinforcement of the main wall

Each item above will be part of a different section. Within a section, the worst load case will be shown with a sketch. Then the forces will be calculated and the gate geometry and necessary reinforcement will be shown. No more strength calculations are added due to time limitations and lack of academic interest.

7.3.1 Gate Design

Vertical lift gates have been chosen for the Valmeer's pump storage station. The information for the selection of a gate has been obtained from Daniel & Paulus (2018). Vertical lift gates allow for large spans, which in this case was very convenient to reduce the number of installed gates. 54 gates are installed along 2,7 kilometers of the plant. A drawback of this is that cylinders able to lift up heavy gates are needed. However, these gates

have similar dimensions to the Oosterschelde Barrier. Thus, its realization is possible. Besides, vertical lift gates just need a pier in which to lift and a cylinder, all in the vertical direction, leaving space in the back for the penstock and the access road. Maintenance, reparation, or replacing operations are simple in comparison with other gates suited for large spans such as sector gates. Finally, the simplicity of vertical gates make them relatively cheap in comparison with sector or rotatory gates. In the following figure, a sketch of the gate is shown. The gate is lifted vertically by two cylinders that rest over the piers. These cylinders rotate in two axis as shown in Figure 7.32 below. The gate rests on the "inlet structure" element of the structure (see Figure 7.33).

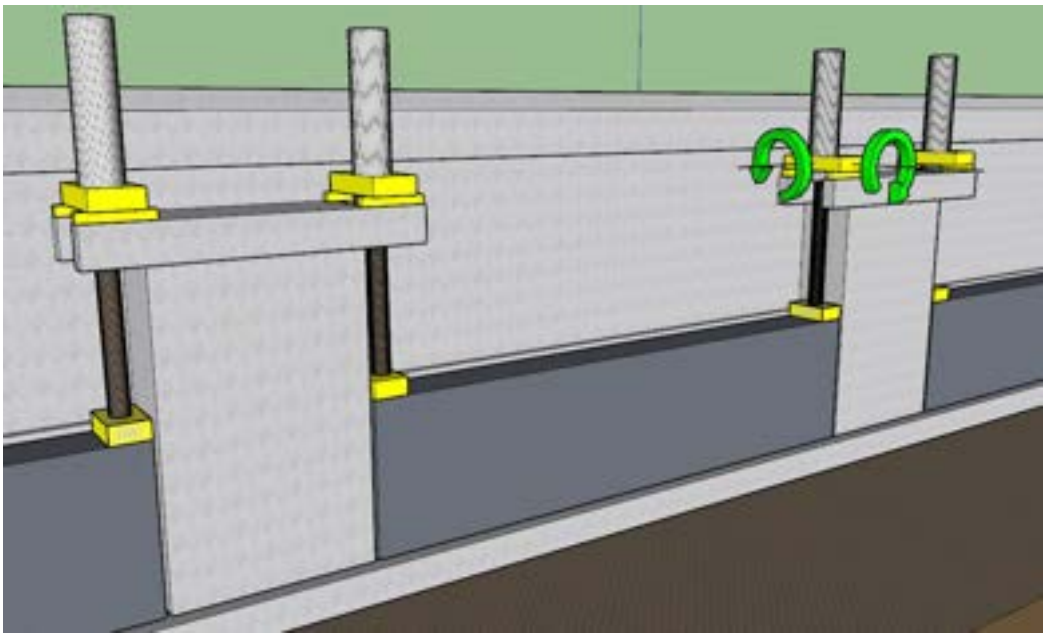

Figure 7.32: Sketch showing the main gate and the cylinders

This structure is composed of gates with dimensions of 38 m (width) × 9 m (height). The top of the gate is at NAP -3 m and the bottom at NAP -12 m. This gate is supported by the inlet structure behind it. Its span is 36.5 m and 7.5 m in the horizontal and vertical direction respectively. The span can be reduced by constructing two vertical walls between the penstocks exit that are shown in Figure 7.33 below. However, then this wall would need to have the strength to handle the forces acting on the wall. This strength would have to be checked for both compression and buckling. For this reason, and because vertical lift gates can have large spans, the span of 36.5 meters is chosen for design. In the Figure 7.33 below, an schematization of the gate is shown:

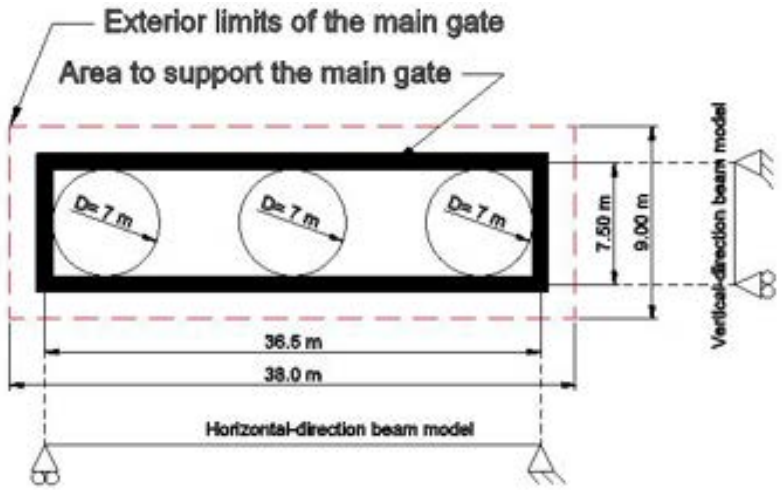

Figure 7.33: Schematization of the main gate. Showing the beam-model used for bending moment and shear force diagrams calculation

The worst-case scenario that the gate will be under during its lifetime is the one where the design storm surge is present ($H_s = 9$ m, $T_p = 11.3$ s, $WL = \text{NAP} + 4.5$ m):

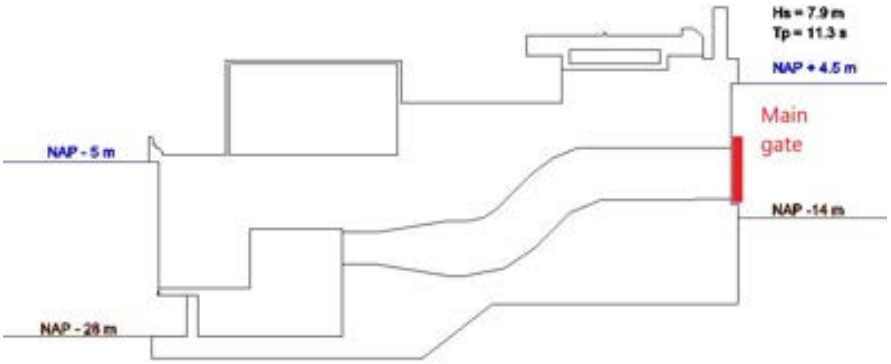

Figure 7.34: load case storm surge situation

In this section, again, the results from the calculations are shown, for further calculations see Appendix L.6. The pressures acting on the gate are as follow:

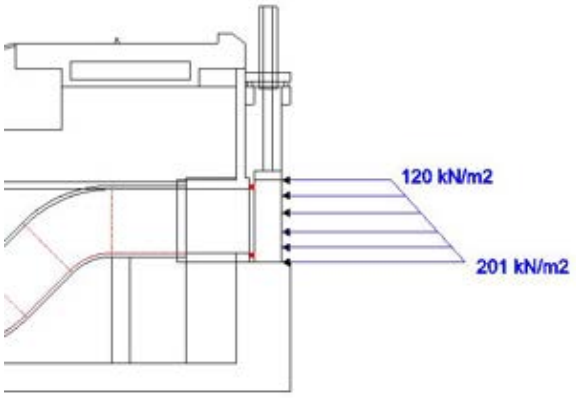

Figure 7.35: Resultant pressure acting on the gate. The gate supports are shown in red

The bending diagram of the loads acting on the gate (see Figure L.59 will be divided between 3 sections. For doing this, the bending moments are calculated at 4 and 11 meters from the support:

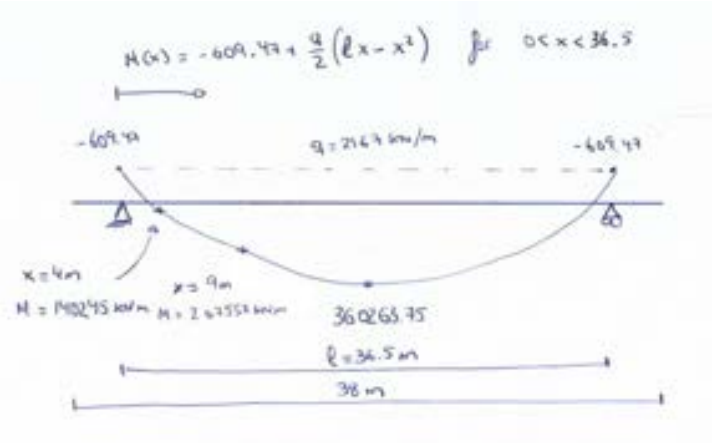

Figure 7.36: Bending moment at 4 and 9 meters from the support

Then, we can divide the above bending moments over the length of the gate. The new model considering 3 different gate sections is shown:

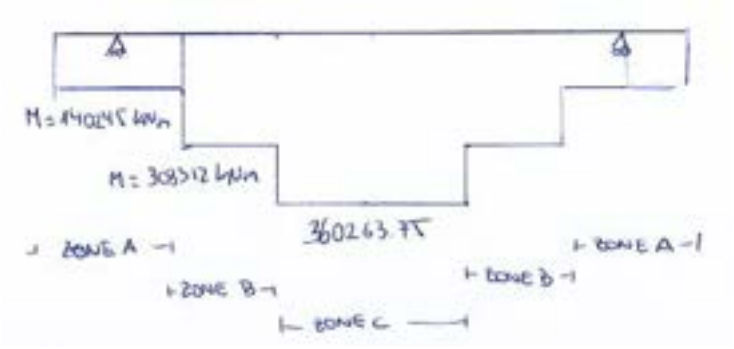

Figure 7.37: Final bending moment distribution considered for the main gate's design.

The needed section modulus at each zone is as follows (assuming that the gate's steel yields at a stress of 240 MPa):

Zone A: $W_A = \frac{M_{EdA}}{\sigma_{steel}} = \frac{140245 \times 10^6 Nmm}{240 N/mm^2} = 584 \times 10^6\ mm^3$
Zone B: $W_A = \frac{M_{EdB}}{\sigma_{steel}} = \frac{267557 \times 10^6 Nmm}{240 N/mm^2} = 1114 \times 10^6\ mm^3$
Zone C: $W_A = \frac{M_{EdC}}{\sigma_{steel}} = \frac{360264 \times 10^6 Nmm}{240 N/mm^2} = 1501 \times 10^6\ mm^3$

The steel plate used for design will still be the 60 mm one. Besides, the width of the flange is fixed to be 280 mm so only the height of the flange will change. The height is varied instead of the width because at zone A, reducing the flange of 280 mm can be problematic for buckling. This change for each zone is as follows:

- Zone A: $h_{fA} = 750\ mm$
- Zone B: $h_{fB} = 1150\ mm$
- Zone C: $h_{fC} = 1400\ mm$

Below the 3D gate is shown again as so as a vertical cut to show the dimensions:

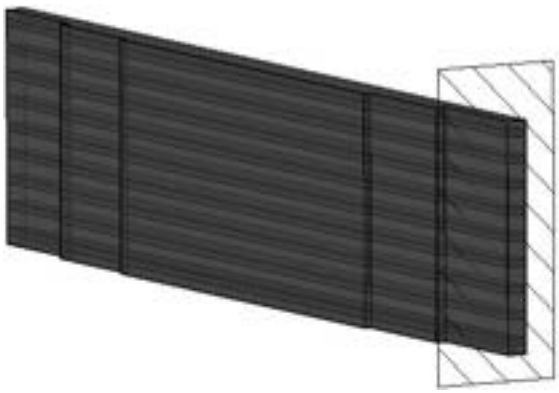

Figure 7.38: 3D representation of the gate showing cutting plane.

In the picture above, we can see an area that represents the cut above-represented:

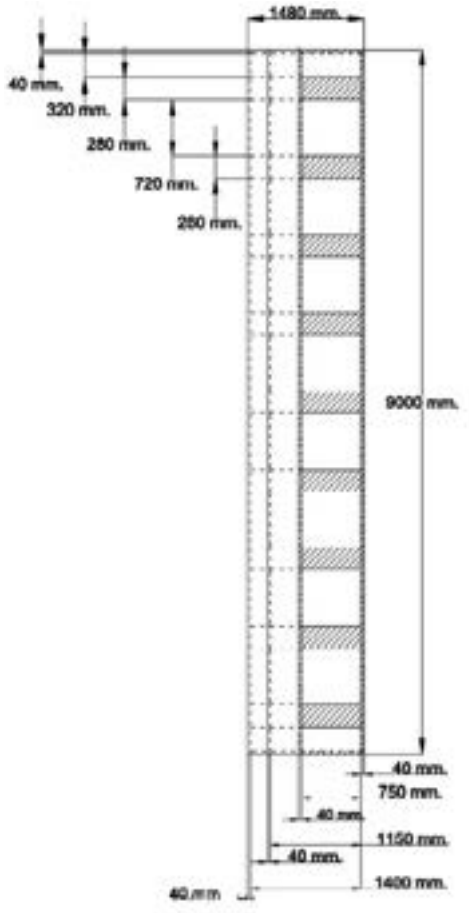

Figure 7.39: Gate's vertical section including measurements

The forces are transmitted to the pillars as shown in this image:

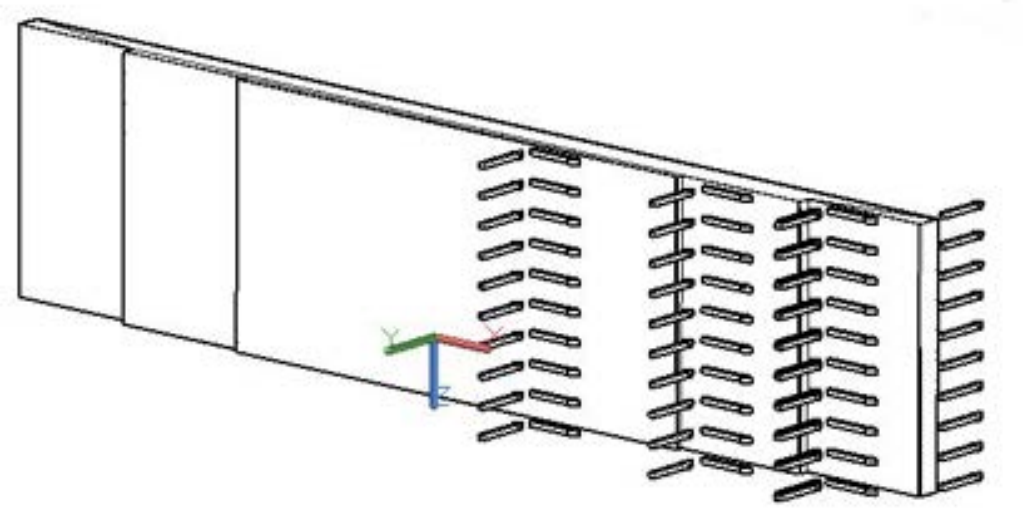

Figure 7.40: Flow of forces acting on the gate

The forces acting perpendicularly to the gate are transmitted via the horizontal flanges to the sides, where the forces are transmitted to the structure.

With this last figure, the gate design is complete.

7.3.2 Reinforcement calculations for the "water retaining wall"

The present section includes the flow of forces for the "skeleton" of the structure (see Figure 7.41). This skeleton is composed of the piers, the wall between the piers that stops the water from passing into the Valmeer ("water retaining wall"), the vertical walls and horizontal slabs, and finally the caisson for the turbine, where the last forces will be transmitted to the ground. In this section, reinforcement calculations for the wall between the piles are included. No more reinforcement calculations are included since it is time-consuming and it does not provide much value for this conceptual design.

To calculate reinforcement, the structure is subjected to the larger load that can happen during its lifetime. That is, during storm surge conditions. The water level inside the Valmeer doesn't play an important role in the reinforcement of the sea-side part of the structure. They will play an important role in the reinforcing of the Valmeer-side part. However, for the purpose of this thesis and time limitations, this loads won't be considered.

In the following figure, the loads considered for the design of each element is shown.

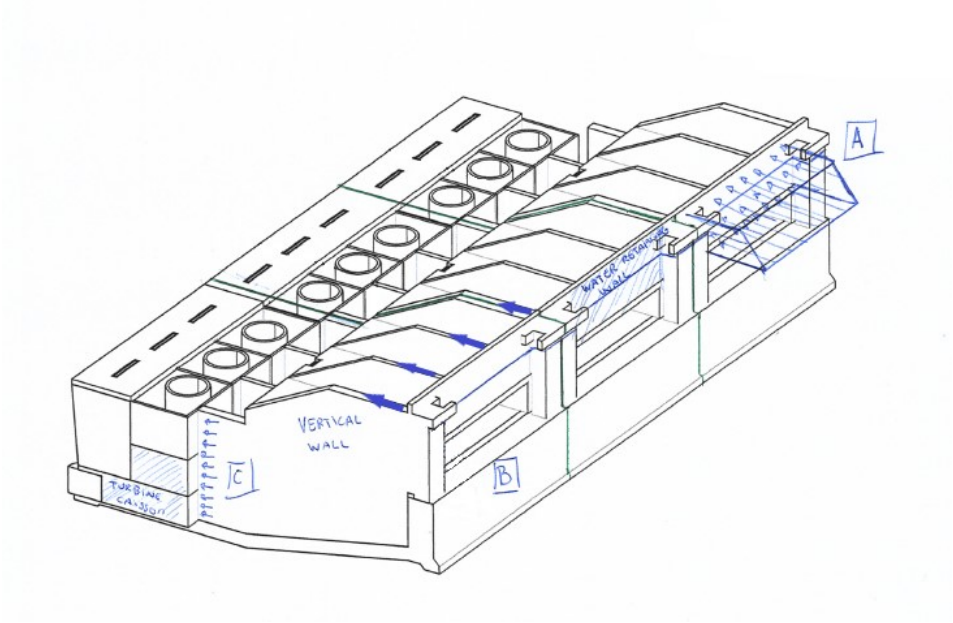

Figure 7.41: General view of the loads considered for reinforcement calculations

The above A, B and C areas mean the following:

- A: the load comes from the combination of the hydrostatic load and wave pressures present during storm surge conditions (H_s = 9 m, T_p = 11.3 s, WL = NAP + 4.5 m). This wall will be analyzed considering a beam model solved with the MatrixFrame software. The load considered in the beam model will be the resultant of the wave pressures acting on the water retaining wall. The beam will be modeled as a beam with fixed-end supports (at the thick walls behind the pillar) and fixed pin supports in between (at the walls between the pillars). This model is conservative. A realistic model would include a plate analysis having three fixed-ends (the sides are connected to the pillars and the bottom part to the inlet structure) and a free one (the top level is free) having the actual total pressures acting on it (a representation of this can be seen in Appendix L.6, Figure L.78). However, this is more time consuming and is recommended to be done when the design of the structure is at a further stage. A safety factor of 1.5 will be applied to this load.

- B: the load comes from the support reaction forces obtained from A. By dividing these reaction forces between the height of the wall, the force distribution per meter is obtained. This distributed load should be used at further design stages for the strength calculations of this element.

- C: the load comes from the vertical wall and they are divided between the caisson and the wall above this caisson (see Figure 7.41).

Design of the water retaining wall

The load from the water pressures acting on the wall is 938 kN/m. This load is distributed over the width of the water-retaining wall and will be used for the bending moment calculation. A safety factor of 1.5 is applied to the load. However, remember that this model is already conservative, a more realistic model of the wall is the one shown in Figure L.78 and not considering a beam. The load case introduced in MatrixFrame is the following:

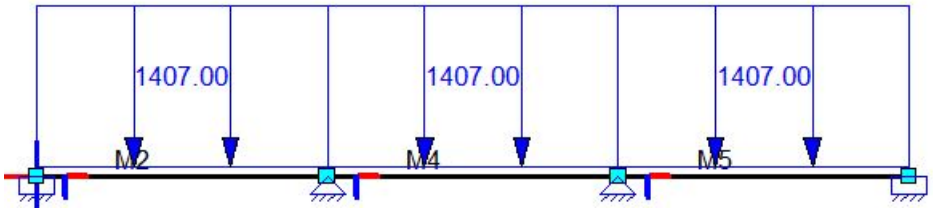

Figure 7.42: Load case considered for the water-retaining wall. MatrixFrame input.

The beam considered for design has fixed ends and fixed pin support in between. The cross-section is a 19.3 m wide (height of the water retaining wall) and 2.3 m in height (the thickness of the water-retaining wall is of 2.3 meters). Notice that the cross-section geometry doesn't affect the bending moment but will be considered later on for the reinforcement calculations. The resulting bending moment from MatrixFrame is as follows:

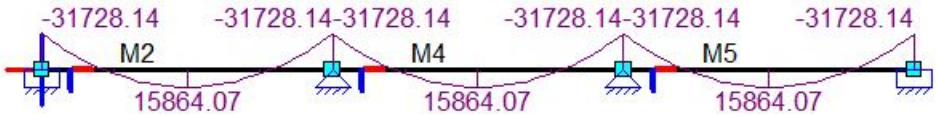

Figure 7.43: Bending moment diagram of the water-retaining wall. MatrixFrame output.

Therefore, the design bending moment for the water retaining wall is 31728 kNm (negative bending moment at the position of the walls). The shear diagram also follows from MatrixFrame:

Figure 7.44: Shear force diagram of the water-retaining wall. MatrixFrame output.

The steel yield strength considered is 500 MPa (Average of reinforcing steel characteristic yield strength present in Annex C of the Eurocode 2.) and the design yield strength is then: $f_{yd} = f_{yk}/\gamma_s = 500MPa/1.15 = 435\ MPa$. The design young's modulus of the reinforcing steel is assumed to be 200 GPa (in accordance with EC2). The necessary reinforcement for both bending and shear is shown below (to see detailed reinforcement calculations go to Appendix L.6, Section L.7.2): The necessary reinforcement for both bending and shear is shown in the figures below:

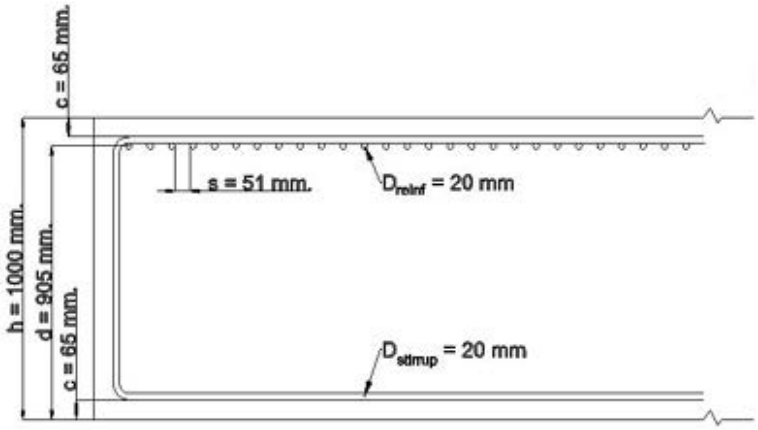

Figure 7.45: Reinforcement needed to resist the design bending moment. Vertical cut of the water-retaining wall.

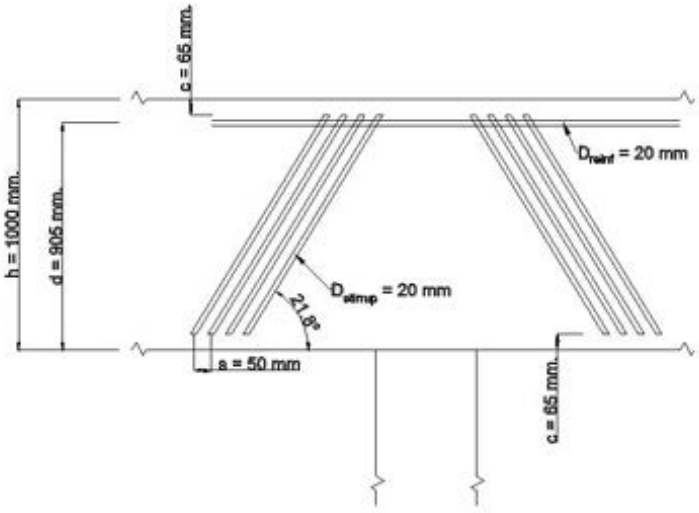

Figure 7.46: Reinforcement needed to resist the design shear force. Horizontal cut of the water-retaining wall. Notice that the angle is not represented with its actual tilting to better fir the bars.

With these figures, the reinforcement of the water retaining wall against bending moment and shear force is ensured.

Design of the vertical wall

The forces for calculating the reinforcement of the vertical wall comes from the reaction forces of the above load case (see Figure 7.42). Notice that these forces are calculated per meter width of the water retaining wall. The reaction force from MatrixFrame are:

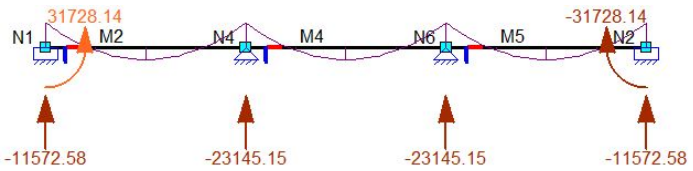

Figure 7.47: Reaction forces from the load case shown in Figure 7.42 for vertical wall design.

The vertical wall design is not included in this thesis.

Chapter 8

Life Cycle Assessment (LCA) of the pump storage station

In this chapter, a life cycle assessment of the pump storage plant is performed. This analysis is done to see which are the largest sources of CO_2 emissions during the entire life cycle of the structure. In an early stage of the design, the CO_2 emissions were already calculated for the construction stage of the life cycle. This information was used to design for minimizing the CO_2 emissions in other design loops. Besides, the emissions for the entire life cycle of the structure give an idea of how this structure ranges among other electricity generation technologies in terms of CO_2 emissions per kilowatt hour of electricity produced.

8.1 Introduction

The structure under study in this thesis is the pumping station with the largest pumping capacity (10.000 m^3/s) in the world. The IJmuiden, the largest European pumping station has a maximum discharge of 260 m^3/s, almost 40 times lower. Additionally, this structure is also one of the largest hydroelectric pump-storage stations in the world (1.853 MW) and the largest one when taking into account that is is built in the sea and not taking advantage of the head difference mountains provide. This makes the hydro pump storage station one of the most unique structures in the world and thus predictably one of the most expensive ever made. However, this financial issue can be justified by the ecological gains (nature restoration and generation of clean energy).

Nowadays global climate change has become a major threat to the environment and the economic development of the world. To address the problem, environmental factors must be considered in several different types of decisions made by businesses, individuals, and public administrators and policymakers (Finnveden at al. 2009). Hydro pump storage power stations use energy to pump water out of a basin to then turbine it in and obtain clean energy on demand. Thus, it can be used as a clean energy battery. In this section, the environmental impact of the Valmeer's power station will be analyzed throughout the whole life cycle of the structure. Then, the results will be compared to the already existing energy generation methods.

There are several methods to evaluate the environmental impact of a product (structure). LCA is a methodology for evaluating the environmental loads of processes and products during their whole life-cycle (Castells, 2003). The assessment includes the entire life-cycle of a product, process or system encompassing the extraction and processing of raw materials; manufacturing, transportation and distribution; use, reuse, maintenance, recycling and final disposal (Consoli et al., 1993). LCA methodology is based on ISO 14040 and consists of four distinct analytical steps: defining the goal and scope, creating the life-cycle inventory, assessing the impact and finally interpreting the results (ISO 14040, 2006). ISO 14040 defines LCA as: "A technique for assessing the environmental aspects and potential impacts associated with a product, by compiling an inventory of relevant inputs and outputs of a product system, evaluating the potential environmental impacts, and interpreting the results of the inventory analysis and impact assessment phases. LCA is often employed as an analytical decision support tool."

In this chapter, the complete LCA will be developed. First, the reader can see a brief description of the literature review done. Then the LCA steps from ISO 14040 will follow: Goal and scope definition, inventory analysis, impact assessment and results interpretation.

8.2 Literature review

The goal of this literature review is finding already existing technologies and methods that aim to reduce the environmental impact of structures similar to Valmeer's power plant. Materials such as Rock filled concrete or the use of stainless steel in the splash zone is analyzed. Besides, already existing LCA's in the hydropower (storage, pump storage, and run-of-river plants) industry have been looked at to find what are the major environmental impacts in the life cycle of this type of structure. Alpine hydropower has been used as a close enough system to obtain information about pumped storage hydropower stations in the sea due to the lack of information available for this kind of system. Besides, the construction methods are similar for both alpine and sea pump storage stations. Finally, the environmental costs of producing electricity with fossil fuels and renewable energy was also analyzed.

Hydropower is, globally, the largest renewable energy source (Turconi el at., 2013). However, hydropower plants have caused worldwide concern with regard to environmental issues (Zhang et al., 2007). Life cycle assessments of hydroelectric plants show that GHG emissions occur at all use phases in a power plant's life (Steinhurst et al., 2012).

Several papers divide hydropower emissions into different phases of the construction, use and dismantling process such as Material production, material transportation, construction, operation and maintenance and dismantling (Zhang et al., 2015; Zhang et al., 2007; Flury & Frischknecht, 2012). These phases will be the ones used in the present analysis. In the following lines, the most significant environmental costs of each phase is commented (the information was retrieved from Zhang et al., (2015), Zhang et al., (2007), Lui et al., (2013), Flury & Frischknecht, (2012):

- Material production phase: The large amount of concrete used, makes this material the most negative regarding environmental issues mainly due to its cement content.
- Material transport phase: The largest source of GHG emissions during transport is the fuel combustion caused by vehicles.
- Construction phase: The machinery fuel used is the main pollutant.
- Operation and maintenance phase: Several processes lead to emissions in alpine hydropower. The aerobic and anaerobic decomposition of organic matter that is flooded due to the construction of a reservoir, the nutrient inflow from upstream, plants and plankton growing in the water, vegetation that quickly grows on exposed land around the shore, when the water level is low and is flooded again when the water rises (Fearnside 2004; Mäkinen & Khan 2010; Turconi et al., 2013). For the present project, however, no dry land will be flooded as the Valmeer is constructed on the sea. This will significantly reduce the emissions during operation and maintenance (respecting alpine hydropower) since the aerobic and anaerobic decomposition of organic matter is the main contributor to emissions in alpine hydropower. Especially in tropical regions (Mäkinen & Khan 2010; Soumis et al. 2005).
- Dismantling phase: While Bioscience (2002) published a special issue about dam decommissioning, there still exists a general lack of information about the impacts from decommissioning and its global environmental implications (Hart & Poff, 2002). To date, a successful large hydro dam has never been demolished. The average height of removed dams in the United States is 6.5 m (IRN 2005). Authors such as Pacca (2007) show that for alpine hydropower, the sediments accumulated behind the dam have lots of CO_2 that can be released after its dismantling. For the present project though, this will not be an issue since no sediment accumulation is expected within the Valmeer. Other factors such as dismantling and recycling of the materials used after its lifetime for such a structure are not clear. Currently, this is not a common practice, but in the future, the concrete used might be recycled due to the improvement of technology. For the present analysis, this will not be taken into account due to the uncertainty of this happening and the LCA analysis will be a cradle-to-grave analysis.

The concrete industry is responsible for 5 % of the anthropogenic carbon dioxide emissions (Mahasenan & Humphreys, 2003). Nonetheless, authors such as Flower & Sanjayan, 2007 researched methods to reduce these emissions. They state that replacing a portion of the cement used by fly ash and ground granulated blast furnace slag (GGBFS), can reduce the concrete production emissions by 13-15 % and 22 % respectively, in typical concrete mixes. These methods are especially attractive for areas where not the best quality concrete is required.

Another option to reduce the emissions by the use of concrete, Chinese authors recommend the use of Rock-fill concrete (RFC). This material is composed of a mix of rock larger than 30 cm and self-compacting concrete (SCC). The SCC's fills in the spaces between the rocks and forms a compact material. Between 55 % and 60 % of RFC is filled by rock blocks, which leads to a great reduction of cement content (Huang, 2008). An et al (2014) studied the integrated performance of RFC by conducting tests on its compaction, compression strength, tensile strength, and permeability. Results indicated that RFC meets the requirements of hydraulic concrete. With two types of construction technology in practical application, RFC exhibits remarkable advantages, such as high construction efficiency, low cost, low heat of hydration, and low environmental load. These advantages contribute to simpler construction management and easier quality control, signifying that RFC is a promising technology in hydraulic engineering. Therefore, RFC will be considered for the mass concrete parts of the structure.

Additionally, Val & Stewart, 2003 recommend the use of stainless steel reinforcement for the splash zone if the construction costs using stainless steel are no more than about 14 % higher than the construction costs of using carbon steel reinforcement. This is due to the maintenance costs of carbon steel reinforcement over the lifetime of marine structures. The large initial investment of stainless steel is balanced by the maintenance costs of carbon steel over the lifetime of marine structures.

Another positive finding in the literature is that large hydropower plants perform better than smaller ones regarding emissions and other environmental aspects (Zhang et al., 2007). Because of their inherent economies of scale, larger hydropower projects often perform better than smaller ones in terms of both energy efficiency and GHG emissions (Zhang et al., 2007).

This literature review was used for two different purposes

1. Knowing how are the LCAs done globally to then being able to compare the results of this LCA to other LCAs.
2. Finding ways of reducing the CO_2 emissions using new materials and/or techniques.

8.3 LCA Goal and scope definition

8.3.1 System description

The Valmeer's power plant object of design is part of the DELTA21 project. This structure is both a flood defense and a pumped-storage hydropower station. The structure's dimensions are 2764 m wide, 84 m long and 44.75 m high. Its flood protection function needs to ensure water tightness of the structure and allow for the pumping of water out of the basin. For the energy generation function, the power station needs to be able to let water pass through a turbine to generate energy and then to export water out of the basin to create the needed head difference to later turbine the water.

8.3.2 Scope

The life cycle assessment follows the Valmeer's power plant over a period of 150 years. Let's keep in mind that this is the time for the analysis, the lifetime of the structure can be larger. But analysis for later than 150 years from now will be excessively uncertain. By doing this we're on the safe side of the calculations. Remember that the larger power-plants perform better than smaller ones regarding environmental issues (Zhang et al., 2007).

The function considered for this analysis will be the energy generation. The system is assumed to be working 22 hours a day (11 hours of pumping and 11 hours of turbining) for 350 days a year. Even though the plant is supposed to be working daily over the year, it is important to take into account that some days the system would need maintenance and therefore it won't be working at maximum capacity every day. Besides, during the design storm days (an average of once every ten years), power won't be produced and water will only be pumped out of the system. That is why a year of 350 days has been taken.

The goal of this LCA is to calculate the emissions per kWh of energy produced to compare with other electricity generation alternatives to optimize (lower the environmental footprint of) the phases with the most emissions.

8.3.3 Functional unit

A functional unit of a product system is a quantified description of the performance requirements that the product system fulfills.

One kWh of electrical energy is a common functional unit in LCA studies on electrical power generation (IEA, 2002). Therefore the functional unit will be the kWh that is available at the grid connection (generated kWh after losses). Thus, the energy loss in the turbine and pump are taken into account.

8.3.4 System boundaries

The following cradle to grave analysis considers all phases of the Valmeer's power plant life cycle:

1. Extraction and processing of construction materials
2. Transport of construction materials and necessary supplies. The transport will be divided between:
   (a) Transport from production point to construction site
   (b) Transport within the construction site
3. Construction containing all of the procedures that utilize construction machinery.
4. Operation and maintenance stage (O&M)
5. Decommissioning

The main structure and so as turbines, generators, and extra needed equipment will be included in the design.

Some papers don't include the on-site transport of materials because the distance is insignificant when compared to the distance covered to bring the materials to the worksite. For the present project, due to the dimensions of the structure, the transport distances on-site are relevant and therefore they are included in the design.

The analysis has been defined as a cradle to grave. Hence, by the end of the lifetime of the structure, it is assumed to be dumped to landfill. This is because in present times it is very (environmentally) costly to recycle materials (especially if they have been in contact with the sea for large amounts of time). However, future technology might allow recycling most of the materials used for constructing the power plant (in 150 years from now). Then, in case technology develops and allows for recycling of (parts of) the structure the total CO_2 emissions will decrease. This makes this analysis conservative regarding dismantling CO_2 emissions. In the following figure, a flow diagram of the LCA is shown:

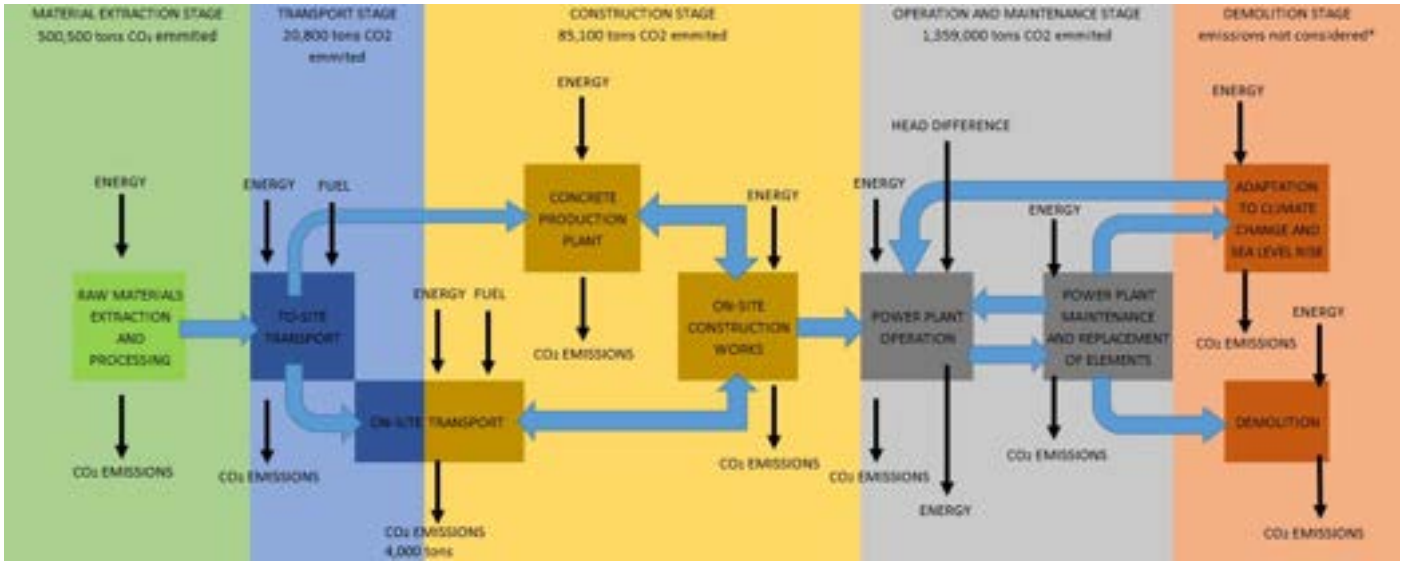

Figure 8.1: LCA flow diagram, the top black arrows represent inputs and the bottom arrows outputs

8.3.5 Exclusions

Lack of data might drive the study in the wrong direction, or change its goal and scope (Scheuer et al., 2003). This lack of data can be from the life cycle inventories (LCI) available and/or the lack of design depth the structure is currently at (conceptual design). Additionally, there are some other materials and activities whose emissions have been considered to be negligible when compared to other materials and or activities. Due to this lack of data, and the assumption (based on what others LCA considered) that these units will score low on the LCA, the following has been excluded from the LCI:

- Factors not related to the structure's design such as furniture, street lights, sidewalks, etc.
- Formwork use: Excluded because it has been assumed to be used in several construction sites and therefore the individual fabrication emissions are divided among all. Giving a small fraction to each site. Thus making it negligible.
- Control room equipment: it can have significant pollutants for human health but regarding CO_2 emissions this is negligible.
- Emissions associated with the construction of the machinery: This equipment has been assumed to be used in other projects so that the amount of emissions from construction associated with each construction site is negligible.
- Paints and lubricants used on system equipment such as turbine are ignored (Pascale et al., 2011)
- Wells installation emissions: emissions from drilling are omitted mainly due to a lack of emission data on drilling equipment.
- Concrete production plant assembly. Lack of data about assembly of concrete production plants and its components' LCI have made the author of the analysis to leave this factor out.
- In general, any kind of material that accounts for less than 5 % of the total mass of the structure.

8.4 Inventory analysis

According to ISO14040, 2006, the inventory analysis contains the "data collection and calculation procedures". Choosing the most appropriate data is critical since it will be what is used to quantify the emissions of a product (Kasreen et al., 2009). Small variations in the emissions per unit when multiplying by the amount of unit used can lead to huge emission differences.

The data from the Idematapp database has been used for this design. According to the official website: "Idemat (short for Industrial Design & Engineering MATerials database) is the LCI (Life Cycle Inventory) set of databases of the Delft University of Technology and maintained by the Design for Sustainability Group of the faculty of Industrial Design Engineering." This database still lacks information about specific civil engineering machinery and materials. For instance, turbine manufacturing emissions are not included in the database. However, this will be calculated looking at literature and making some design assumptions that will be indicated below.

In the following sub-sections, the different emission factors are listed depending on the phase they have been used on.

8.4.1 Material production stage

In the following table, a summary of the materials extracted, emission factors and data source is given. Below the reasoning followed to obtain/calculate the unit is given.

INVENTORY OF MATERIAL PRODUCTION				
Meterials	Unit	Emission factor	Unit	Data source
Reinforced concrete	m3	150	kg CO2-eq / m3	Idematapp2020
Steel	kg	2	kg CO2-eq / kg	Idematapp2020
"Road mix"	m	23,100	kg CO2-eq / m	Sagemo & Storck (2013)
Turbine	#	10,000,000	kg CO2-eq / 168 turbines	Assumption. See section J.3.1
Rock bed protection	kg	0.0586	kg CO2-eq / kg	Nationale Milieu database (NMD) versie 2.3
Sand (dikes)	m3	0	kg CO2-eq / m3	Assumption. See section J.3.1

Figure 8.2: LCI for material production

Following professor H.M. Jonkers' (professor at the TU Delft for the Materials and Environment section) recommendation, the reinforced concrete data from Idematapp2020 is very conservative for the Netherlands. In the Netherlands, the use of Blast Furnace Slag (BFS) cement causes fewer emissions. The recommendation from the professor was to reduce the emissions from the Idematapp database by a 70%: 0.3 * 499 = 150 kg CO_2-eq / m^3.

The "road mix" unit comes from Sagemo & Stork, 2013. In their master's thesis, a comparison between different kinds of road decks is done. This comparison analyzes the life cycle costs as so as life cycle assessment for 4 different types of bridge decks. It has been assumed that the concrete and steel bridge deck analyzed in Sagemo & Stork, 2013 resembles the one that will be installed on the Valmeer's power plant. This is because the bridge deck analyzed will be a four-lane deck (like the one of the Valmeer's power plant) with a span of 22 m (the bridge deck installed in the Valmeer's pump storage station will have a 17 meters span, conservative assumption since probably the installed bridge will have to stand lower loads and therefore will have less material, but this assumption is considered good enough for the present analysis). The analysis shows that the total emissions for a concrete and steel bridge are 1.26 $\times 10^6$ kg CO_2-eq. The length of the road was 54.5 m. Thus, an estimate on emissions per meter of deck can be calculated as: 1.26 $\times 10^6$ / 54.5 = 23.1 $\times 10^3$ kg CO_2-eq/m. This is taking into account a design lifetime of 100 years.

Regarding turbine manufacturing emissions, Pentair provided an estimation based on "Manufacturing a pump/turbine unit will produce approximately 0.2 [%] of CO2 emission compared to the emission of the energy consumption at 100 [%] (continuous) operation (assuming coal power plant)". This approximation gives a total of 1,422,000 tons CO_2-eq. However, the recommendation of Pentair was to check these numbers. To do that, a fast calculation of the turbine emissions can be done assuming that the whole turbine is made out of steel (professor Jonkers recommendation):

$$CO_2\ Emissions = weight\ of\ steel\ of\ turbine \times Steel\ emissions$$

Pentair provided a way of estimating the weight of a turbine. They say a turbine of 5 MW weights around 100 kN (including both the pump and the rotor). For an 11 MW turbine, the figure of 200 kN is assumed. Therefore an 11 MW will have a weight of 20,000 kg. The emissions of 20,000 kg of steel are:

$$CO_2\ Emissions = 20000\ kg_{steel} \times 2 \frac{kgCO_2 - eq}{kg_{steel}} = 40,000\ kgCO_2 - eq$$

The above are the emissions for one turbine. But this only accounts for material extraction. To take into account the material processing, using the available data of Ideamatapp2020, and from the drawing and rolling units of steel (processes that are present in the fabrication of turbines, among others), an average of 0.45 kg CO_2-eq/kg is used. So the contribution of material processing (this is a low estimation, more process than the ones considered take place such as welding and assembling using different machinery, etc) is of:

$$CO_2\ Emissions = 20000\ kg_{steel} \times 0.45 \frac{kgCO_2 - eq}{kg_{steel}} = 9,000\ kgCO_2 - eq$$

Again, for a single turbine. So, the total emissions of manufacturing a turbine would be: 40,000 kgCO_2-eq + 9,000 kgCO_2-eq = 49,000 kgCO_2-eq. For the 167 turbines: 167 turbines $\times$ 49,000 kgCO_2-eq/turbine = 8,203 tons CO_2. Order of magnitude 3 times smaller than the approximation given by Pentair. Therefore, the emissions given from Pentair's approximation are very conservative. The assumed emissions value will be

10,000 tons CO_2 to take into account extra processes in the manufacturing of the turbine. Further research is recommended in this field.

The rock bed protection data was obtained from the staff in VolkerWessels Infra Competence Center using the DuboCalc software.

Emissions from obtaining sand have bed assumed as zero because the sand is taken from the seabed on-site by a Trailed Suction Hopper Dredger (TSHD). Therefore, the emissions from the THSD activity will be assumed to include the extraction, transportation, and deposition of material (sand).

8.4.2 Material transportation stage

Multiple studies don't look at the emissions of transporting the goods on-site because these are neglected when compared to the transport of goods from the manufacturing place to the worksite. For the present project, however, due to the large dimensions of the structure, the transport on-site will also cause significant emissions that need to be considered in the LCA. Thus, in this subsection, the transportation of products and materials from its manufacturing point to (and within) the worksite is given. To make a distinction, a division between the transported goods to the site and the transported goods on-site is done.

To-site transport

The figure below shows a summary of the data used and it's source for the transport of goods and products from its manufacturing site to the worksite.

INVENTORY OF MATERIAL TRANSPORT TO CONSTRUCTION SITE							
Materials		From-to	Transport mode	Distance (km)	Data source	Emission factor (kg CO2-eq/tkm)	Data source
Concrete	cement	IJmuiden - Maasvlakte 2	Railway*	120	Assumed	0.0297	Idematapp2020
	gravel	Limburg - Maasvlakte 2	Railway*	200	Assumed	0.0297	Idematapp2020
	sand	Rotterdam area - Maasvlakte 2	Inland Bulk carrier	50	Assumed	0.0300	Central Commission for
	water	Collected from pipes at Maasvlakte 2	Pipes	0	Assumed	-	the Navigation of the
Steel	reinforcing	IJmuiden - Maasvlakte 2	Railway*	120	Assumed	0.0297	Idematapp2020
	gates a	IJmuiden - Rotterdam area	Railway*	120	Assumed	0.0297	Idematapp2020
	gates b	Rotterdam area - Worksite	Barge	55	Assumed	0.0203	Idematapp2020
Road deck		Spanbeton - Worksite	Barge	90	Assumed	0.0203	Idematapp2020
Turbine		Winterswijk - Maasvlakte 2	Railway*	240	Pentair, 2019	0.0297	Idematapp2020
Rock bed protection		Ardennen	Railway*	235	Assumed	0.0297	Idematapp2020

Figure 8.3: LCI for transport of materials from production site to work site

* Only railway emissions considered. For getting material on/off the trains, other transportation modes such as trucks or cranes are used. However, considering that the transportation emissions to get material to the train or off the train are negligible when compared to the total emissions of transporting the goods and products by rail. Thus, only railway emissions have been taken into account.

On-site transport

The figure below shows a summary of the transportation of materials within the worksite.

INVENTORY OF MATERIAL ON-SITE TRANSPORT							
Materials	Transport mode	Distance (km)	Emission factor	Unit	Data source	Diesel consumption	Data source
Concrete	pump concrete truck	1394779	0.08	tkm	Idematapp2020	34.0 l/100km	Zhengzhou Focus Machinery Co
Steel	truck	1881	0.07	tkm	Idematapp2020	27.4 l/100km	Scania webpage
Rock bed protection	truck	17026	0.07	tkm	Idematapp2020	27.4 l/100km	Scania webpage
Turbine	Crane						

Figure 8.4: LCI for on-site transport of materials

In the following lines, it is shown how the distance and emissions of on-site transport are calculated.

The on-site distance is defined from the number of rides a transport unit has to make:

$$Number\ of\ rides = \frac{Amount\ of\ material\ to\ transport}{Capacity\ of\ an\ individual\ transport\ unit}$$

$$On\ site\ Distance = Number\ of\ rides \times Average\ distance$$

The average covered distance has been taken as twice (trucks have to drop the material and then come back to take more material) the distance to the midpoint of the structure:

$Average\ distance = 2 \times \frac{2764\ km}{2} = 2764\ km$

In the following table the calculations for obtaining the on-site covered distance is shown:

ON-SITE TRANSPORTATION DISTANCES									
Equipment	Amount of material transported	Unit	Capacity	Unit	# of Rides	Avg. distance / ride	Unit	Total distance	Unit
Pump concrete truck	2,523,117	m3	10	m3	252,312	2.764	km	697,390	km
Steel truck	19,054,700	kg	28	ton	681	2.764	km	1,881	km
Bed protection Lorry	172,473,600	kg	28	ton	6,160	2.764	km	17,026	km

Figure 8.5: Distance covered on-site

The turbines are assumed to be loaded at the land-most side of the structure and transported using the maintenance crane installed in the powerhouse. Some emissions from electricity then should be accounted for, but these are assumed to be negligible compared to the other on-site transportation emissions.

8.4.3 construction stage

For this stage, the machinery's fabrication emissions as so as the fuel consumption is taken into account. Due to the lack of precise data about construction machine's emissions during construction and operation, only the main machinery has been taken into account for the LCA. In the following figure the main machinery used for construction is presented:

EQUIPMENT USED IN THE CONSTRUCTION STAGE OF THE POWER PLANT									
Item	Equipment	Unit	Productivity	Unit	Data source	Diesel consumption	Electricity consumption	Unit	Data source
dredging & dike creation	Trail suction hopper dredger	m3	3300	m3/h	van der Schrieck, 2016	5000	0	l/h	van der Schrieck, 2016
Dike construction	Bulldozer	m3	40	m3/h	www.cat.com	55		l/h	Kecojevic & Komljenovic, 2011
	Vibro roller(sand)	m3	45	m3/h	www.methvin.org	12.5		l/h	www.sakainet.co.jp
Dam construction	Concrete vibrator		9.68	h/100m3	Zhang et al., 2015		12	kWh	Zhang et al., 2015
Building pit dewatering	Wells elecricity generator	#	100	m3/h	Assumed from HSM, 2019		12	kWh	www.bedu.eu

Figure 8.6: LCI for on-site transport of materials

8.4.4 Operation and maintenance stage

To compute the emissions for the lifetime of the structure, the design life of the structure was assumed to be 150 years. Then, for each year, the emissions are calculated including maintenance activities. The activities considered for the emission analysis during operation and maintenance are the following ones:

- Energy used for pumping: The pumping operation uses electrical energy from the grid to transport water from the Valmeer to the sea. Therefore the emissions from the used electricity will be taken into account.
- Energy obtained from turbining: When turbining water into the Valmeer, the turbines together with the generators and transformers create electrical energy that is given to the grid. Therefore, there are no emissions in this operation. Energy is given to the grid. To take this into account, the system is assumed to "rest" emissions from the grid.

- Emissions by maintenance works: Machinery, products, transportation modes are only some of the contributors to emissions in the maintenance phase. For maintenance, the following is considered:
  - Turbine/pump replacement every 50 years. The emissions considered are the emissions from manufacturing and transporting the turbines to the site.
  - Turbine/pump regular inspection every 10 years. As these works depends on the situation of the individual turbines, the emissions have been assumed. The assumption is that those emissions are 5% of the emissions from replacing the turbines/pumps.
  - Main gates replacements every 100 years. The emissions considered are emissions from manufacturing and transporting the gates to the site.
  - Main gates regular inspection every 10 years. Emissions are assumed to be 5% of the main gate replacement emissions.
  - Turbine gates replacement every 50 years. These gates' lifetime is lower since they are being used on a daily basis. Again, the emissions considered come from the manufacturing of the gates and transportation to the site.
  - Turbine gates regular inspection every 10 years. Emissions are assumed to be 5% of the turbine gates replacement emissions.

A summary of the above is shown in the following table:

EQUIPMENT MAINTENANCE		
Activity	Frequency	TonCO2 activity
turbine/pump inspection	10 years	501
turbine/pump replacement	50 years	10,029
Main gates inspection	10 years	1,912
Main gates replacement	100 years	38,249
Turbine gates inspection	10 years	637
Turbine gates replancement	50 years	12,750

Figure 8.7: Maintenance strategy

Factors such as electricity consumption due to lights, control room, and other factors are not considered. Furthermore, concrete maintenance methods are also not considered for the design mainly due to a lack of data in this matter. Both in emissions and maintenance frequencies.

After all the emissions are calculated, the total of emissions can be obtained. Then, these emissions are divided by the amount of energy produced during the lifetime to see the CO_2 emissions per kWh of energy produced. This is a widely used unit to compare the CO_2 emissions between different energy generation technologies. Amponsah et al. (2014) reviewed the current understanding and estimates of greenhouse gas emissions from multiple renewable energies and heat generation technologies. Their findings are summarized in the following figures:

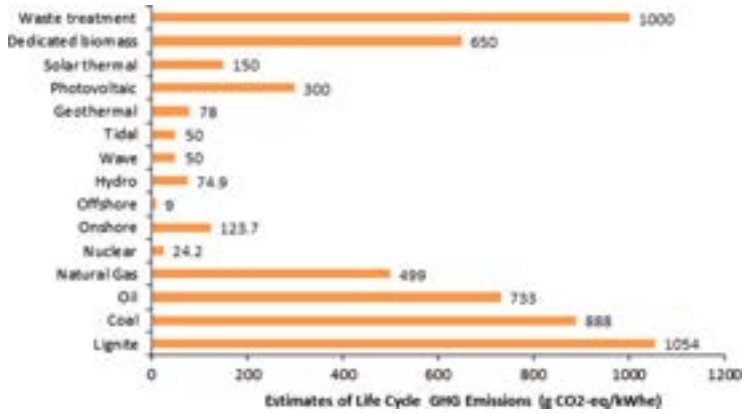

Figure 8.8: Maximum GHG emission levels of electricity generation methods. Amponsah et al., 2014

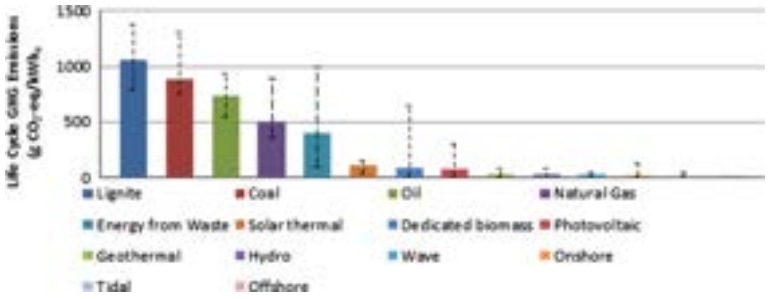

Figure 8.9: Life cycle GHG emission estimates of electricity generation methods including its confidence intervals. Amponsah et al., 2014

8.4.5 Dismantling stage

The present cradle to grave analysis doesn't consider any emissions from dismantling nor recycling/reuse of materials and parts of the structure.

8.5 Impact assessment

In this section, the calculations to obtain the emissions during construction and operation and maintenance are shown. After having the life cycle inventory (see Section 8.4), just by obtaining the amount of materials, distance covered by transport and fuel usage of machinery and transportation, the total emissions for construction can be calculated. For the material stage, the quantities of reinforced concrete, steel, road mix, turbine, and rock bed protection are obtained from the current design of the structure. Once each quantity is shown with its adequate units, the analysis can be done as:

INVENTORY OF MATERIAL PRODUCTION					
Meterials	Total amount	Unit	Emission factor	Unit	Total emissions (t CO2-eq)	Contribution
Reinforced concrete	2,523,117	m3	150	kg CO2-eq / m3	378,468	75.6%
Steel	19,054,700	kg	2	kg CO2-eq / kg	38,109	7.6%
"Road mix"	2,764	m	23,100	kg CO2-eq / m	63,839	12.8%
Turbine	168	#	10,000,000	kg CO2-eq / 168 turbines	10,000	2.0%
Rock bed protection	172,473,600	kg	0.0586	kg CO2-eq / kg	10,102	2.0%
Sand (dikes)	12,173,000	m3	0	kg CO2-eq / m3	-	0.0%
				TOTAL	500,517.94	100.0%

Figure 8.10: CO_2 emissions during material extraction

The material that most contributes to the total material emissions is the reinforced concrete. This is expected because of the cement within the concrete. Cement is responsible for 74 % to 81 % of total concrete CO_2

emissions (Flower & Sanjayan, 2007).

The following step is to calculate the amount of emissions by transportation. These can be divided into two:

1. Equipment emissions: Emissions from manufacturing a vehicle.
2. Fuel emissions: Emissions from the fuel-burning action.

The vehicle emissions need to be multiplied by the amount of ton-kilometers (tkm) a transport mode has to do. To calculated that, the following expression was used:

$$Quantity(tkm) = Total\ amount\ of\ material\ transported(tons) \times Distance\ covered\ by\ transport\ mode$$

For the fuel emissions, the amount of fuel used for transportation is obtained. The fuel consumption can be seen in Figure 8.3. Once the amount of fuel (or electricity in case railway transport is used) is obtained, the emissions can be calculated from the following relationships:

- Electricity emissions per kWh: This emissions factor has been obtained from the European Environmental Agency (EEA) average. The value is 0.2958 kg CO_2/kWh. In idematapp2020 the emissions value for the "Electricity Industrial Western Europe (ENTSO-E)" are 0.13 kg CO_2/MJ = 0.468 kg CO_2/kWh. Which according to the EEA (https://www.eea.europa.eu/data-and-maps/daviz/co2-emission-intensity-5#tab-googlechartid_chart_11_filters=%7B%22rowFilters%22%3A%7B%7D%3B%22columnFilters%22%3A%7B%22pre_config_ugeo%22%3A%5B%22European%20Union%20(current%20composition)%22%5D%7D%7D corresponds to levels of 1994. That is the reason why the emissions from the EEA instead of the ones from Idematapp2020 have been used.
- Fuel emissions per liter: These emissions have been obtained from Idematapp2020: 3.66 kg CO_2/kg. This results in: 3.66 kg CO_2/kg × 0.830 kg/l = 3.04 kg CO_2/l.

The total transport emissions from manufacturing to site and on-site are shown in the following tables:

INVENTORY OF MATERIAL TRANSPORT TO CONSTRUCTION SITE

Materials		From-to	Transport mode	Distance (km)	Quantity (tkm)	Emission factor (kg CO2-eq/tkm)	Emission transport (ton CO2-eq)	Fuel consumption	Units	Fuel used (l/kWh)	Fuel emissions (TonCO2)	Total emissions (TonCO2)	Weight
Concrete	cement	IJmuiden - Maasvlakte 2	Railway*	120	41,855,489	0.0297	1,243	0.02	kWh/tkm	837,110	248	1,491	7.2%
	gravel	Limburg - Maasvlakte 2	Railway*	200	286,905,874	0.0297	8,521	0.02	kWh/tkm	5,738,077	1,697	10,218	49.2%
	sand	Rotterdam area - Maasvlakte 2	Inland Bulk carrier	50	38,232,823	0.0000	1,744	0.00999	l/tkm	375,113	2,004	3,778	18.2%
	water	Collected from pipes at Maasvlakte 2	Pipes	0	-	-	-	-	-	-	-	-	0.0%
Steel	reinforcing	IJmuiden - Maasvlakte 2	Railway*	120	95,071,981	0.0297	2,824	0.02	kWh/tkm	1,901,421	562	3,386	16.3%
	panes a	IJmuiden - Rotterdam area	Railway*	120	2,286,564	0.0297	68	0.02	kWh/tkm	45,731	14	81	0.4%
	panes b	Rotterdam area - Worksite	Barge	50	1,048,008	0.0203	21	0.00999	l/tkm	10,375.28	57	58	0.3%
Road deck		Spanbeton - Worksite	Barge	90	5,116,520	0.0203	104	0.00999	l/tkm	50,751	179	183	1.4%
Turbine		Wintersrijk - Maasvlakte 2	Railway*	240	801,600	0.0297	24	0.02	kWh/tkm	16,032	5	29	0.1%
Rock bed protection		Ardennen	Railway*	255	40,531,296	0.0297	1,204	0.02	kWh/tkm	810,625.92	240	1,444	7.0%
											TOTAL	20,768	100%

Figure 8.11: CO_2 emissions during transportation from manufacturing place to worksite

INVENTORY OF MATERIAL ON-SITE TRANSPORT

Materials	Transport mode	Distance (km)	Emission factor (Unit	Total emissions (Ton CO2)	Diesel consumption (l/100km)	Diesel used (l)	Diesel emissions (TonCO2)	Total emissions (TonCO2)	Weight
Concrete	Pump concrete truck	1,394,779	0.08 tkm	1,339	34	474,225	1,266	2,605	65%
Steel	Truck	1,881	0.07 tkm	4	27.4	51,539	138	141	4%
Rock bed protection	Truck	17,026	0.07 tkm	17	27.4	466,502	1,246	1,262	31%
Turbine	-			0				-	0%
							TOTAL	4,008.7	100%

Figure 8.12: CO_2 emissions during on-site transportation

The last contribution to CO_2 emissions in the construction stage are the machinery emissions. Using the production and fuel consumption of these machines, the emissions can be obtained as:

EQUIPMENT USED IN THE CONSTRUCTION STAGE OF THE POWER PLANT											
Item	Equipment	Quantity	Unit	Productivity	Unit	Diesel consumption	Electricity consumption	Unit	Total diesel (ton)	Total electricity (kWh)	Emissions (TonCO2)	Weight
dredging & dike creation	Trail suction hopper dredger	22,780,000	m3	3300	m3/h	12	-	ton/day	6,903	0	18,431	22%
Dike construction	Bulldozer	7,593,333	m3	40	m3/h	55	-	l/h	8,687		23,194	27%
	Vibro roller(sand)	7,593,333	m3	45	m3/h	12.5	-	l/h	1,755		4,686	6%
Dam construction	Concrete vibrator	2,422,193	m3	9.68	h/100m3	-	12	kW		2,813,619	832	1%
Building pit dewatering	Wells elecricity generator	61	#	100	m3/h	-	12	kW		128,246,400	37,935	45%
										TOTAL	85,078	100%

Figure 8.13: CO_2 emissions during construction of the structure

Notice that emissions from machinery manufacturing hasn't been taken into account due to the lack of data and the complication of obtaining accurate emission factors.

Finally, the emissions from the operation and maintenance stages are calculated. On Appendix N, two pages show the projected emissions for each year of the lifetime of the structure. The maintenance strategy can be found in Figure 8.7.

The yearly emissions are calculated from: emissions from pumping mode, minus, emissions saved from turbining mode. These last emissions come from the assumption that if there would not be zero-emissions energy from turbining water into the Valmeer, the electricity would come from the grid and therefore it would have some emissions costs (the ones from the European grid). The yearly emissions can then be calculated from:

- Power of the pump: 11.1 MW
- Power of the turbine: 11.1 MW
- Efficiency of the pump: 93 %
- Efficiency of the turbine: 74 %
- Work hours pumping mode: 11 h/day
- Work hours turbine mode: 11 h/day
- Work days pump mode: 350 days/year
- Work days turbine mode: 350 days/year
- CO_2 emissions from electricity: 0.0002958 ton CO_2/kWh

Thus,

Emissions from pumping mode $= \frac{11.1MW \times 1000KW/MW}{93\%} \times 11h/day \times 350day/year \times 0.0002958tonCO_2/kWh \approx 13,600\ tonCO_2/year$

Emissions from turbining mode $= 11.1MW \times 1000KW/MW \times 74\% \times 11h/day \times 350day/year \times 0.0002958tonCO_2/kWh \approx 9,400\ tonCO_2/year$

Total yearly emissions = 13,600 - 9,400 = 4,200 ton CO_2 per year.

To these yearly emissions, every 10, 50 or 100 years the emissions of maintenance have to be added (see Appendix N to see the maintenance strategy considered). After adding all these contributions, the total CO_2 emissions can be added. The result is a total of 1,360,000 tons of CO_2 (to see the detailed year-by-year emissions the reader should look at Appendix N).

The electricity produced over all the lifetime of the structure comes from the turbining operation and it is calculated as:
$11.1\ MW \times 1000\ KW/MW \times 74\ \% \times 11\ h/day \times 350\ day/year \times 150\ years = 4,769,000,000\ kWh$

It can be concluded that this power station produced energy at an environmental costs of $\frac{1,360,000,000,000[gCO_2]}{4,769,000,000[kWh]}$ = 280 g CO_2 / kWh.

8.6 Results interpretation

The above analysis is part of the preliminary design of the Valmeer's hydro pump storage station. The results are summarized in the table below:

General stage	Tons CO2 emitted	percentage of the total	Stage of life cycle	Tons CO2 emitted	percentage of the total
Stages for construction of the pump storage plant	610,373	45%	Material production	500,518	36.7%
			Material transport to site	20,769	1.5%
			Material transport on-site	4,009	0.3%
			Construction equipment	85,078	6.2%
Operation and Maintenance stage	754,660	55%	yearly emissions from plant	628,136	46.0%
			maintenance	126,524	9.3%

Figure 8.14: Summary of the result of the LCA

Above can be seen that the large amount of concrete produced and used is one of the largest emitting factors together with the yearly emissions from the pumping (and turbining) operation. For this last emissions, the initiators of DELTA21 are looking for methods to power the turbines using renewable energy (this is further discussed below). Regarding material production, it is clear than concrete amount for both economical and environmental reasons need to be reduced at maximum on the following design stages. Concrete reduction can come from reducing the thickness of the walls to the minimum possible and not using this material to just providing weight to the structure. Instead, more compartments for fill material can be constructed. These compartments are now filled with sand, but rock-filled-concrete (already mentioned in 8.2) should also be considered since it can provide weight with less volume when compared with sand. Therefore, the compartments can also be smaller.

On the other hand, the lesser emitting stage is material transport (both to-site and on-site). This contrast some authors' analyses such as Zhang et. al., (2015) for whom the lesser emissions were the material extraction. However, in the present analysis, concrete production is taken into account in this phase. In Zhang et. al., (2015) just the extraction of the cement and granular materials is accounted for. Furthermore, these authors used the data from already-built projects which included a detailed list of transportation both to-site and on-site and construction machinery. In the present LCA, these transportation methods and construction machinery emissions come from preliminary design and only the most important transport and machinery have been considered. For a project like the present one, these emissions are expected to increase. A further analysis of the construction method and emissions is recommended in the future.

Construction equipment emissions could also be reduced by using electric dredgers. This technology might be available for the time the project construction starts. However, as we can see above, the construction machinery is not the most pollutant factor and therefore it won't make a big difference to use these green dredgers. If they are too expensive, conventional dredgers should be still be used.

The regular working conditions emissions per kWh were calculated previously, giving a total of 280 g CO_2 / kWh. With this figure, we can compare the Valmeer's pump storage station to the other generation technologies present in figures 8.8 and 8.9 obtained from Amponsah et al., (2014). These authors considered the same phases as the ones present in this LCA. Besides, the energy generated payback has been also considered in the renewable energy generation technologies present in Amponsah et al., (2014). Therefore a realistic comparison can be done and it can be concluded that the Valmeer's hydro pump storage station produces fewer emissions than average photovoltaic energy technologies and similar to the average solar thermal. Besides, it has the advantage of being able to store energy and use it on demand. The storage of energy is not included in the CO_2 emissions analysis of the other technologies and the construction of batteries will cause more CO_2 emissions. And not only that but also, the production of other contaminants coming from the batteries production and dismantling stages.

Using renewable energy for powering the pumps and therefore considering that the yearly emissions for plant operation are zero, the emissions would drop considerably. Thus, the emissions per kilowatt-hour would then be -140 g CO_2 / kWh. The DELTA21 initiators are already looking for renewable energy generation methods

to power the pumps (currently they are looking at wind and/or solar energy). If this is done, we can see that the present project emissions per kilowatt-hour are below zero. Something that is not happening in the figures 8.8 and 8.9. This is because the life expectancy of the solar and wind technologies present in Amponsah et. al., (2014) is rather low. For a life expectancy of 50 years and regular conditions, the emissions of the plant are around 500 g of CO_2 per kWh. But this is unrealistic for a pump storage station.

Adaptation is not taken into account for emissions calculation but it is present at the LCA chart because it is an interesting strategy for alternatives with such a large lifetime. The climate change scenario considered for this design is the G scenario from the KNMI'06. However, some uncertainty is present when deciding which climate change scenario to choose. If the climate change scenario is worst than the expected one, the structure's lifetime would be reduced. However, if the structure can be adaptable to these changes (both in water level height and wave loading on the structure) the lifetime can remain the same or even enlarged. An increase in water level is countered by changing the road deck to one with a higher freeboard. At the same time, larger wave loads will have to be stood. This can be done by increasing the averaged weight per meter of structure using heavier fill-in material in the compartments. However, notice that also the reinforcement of the structure will change. For the water retaining wall, the reinforcement is currently calculated for loads of the climate change G scenario, if these loads increase, additional reinforcement will be needed, exterior prestressing or exterior additional girders can be installed for this purpose. Adaptation is, therefore, an interesting strategy to take into account but it is not further developed in this thesis. It is given as a possible CO_2 emissions reduction strategy for the end of the structure's lifetime.

To finish, analysis of other pollutants must also be done to make a full comparison between energy-generating technologies. Only considering this analysis, the nuclear energy ranges quite low in total CO_2 emissions. However, nuclear energy produces pollutant waste and radiation, which are very negative for human health. Therefore, the CO_2 emissions should not be the only factor at which look at.

Chapter 9

Conclusions and recommendations

9.1 Conclusions

The design of the Valmeer's hydro pump storage station considered three different alternatives:

- Power plant is a flood defense
- Power plant is not a flood defense
- Power plant is a flood defense in combination with the dune

The alternatives 2 and 3 have clear advantages in the amount of concrete used. Respecting alternative one they use less concrete material and therefore it is clear from the LCA that they will score better environmentally regarding material use. However, the realization of these alternatives has other complications. They have a larger footprint, and different parts need to be connected. This will difficult the construction operation when compared to Alternative 1, which will mean more costs and more time of machinery use. The Alternative 1 is the more compact one, it can be entirely constructed in one building pit (also the smallest in comparison with the one that would be needed for alternatives 2 and 3) and maintenance is easiest to carry out. Maintenance is another important factor regarding CO_2 emissions (almost a 10 % for the chosen alternative. See Figure 8.14) and these emissions will raise for alternatives 2 and 3 because maintenance of the foreshore of the dunes will be regularly needed. Therefore Alternative 1 was chosen.

The most interesting findings during the development of this thesis are mentioned below.

In the early stages, it was found that the discharge chosen for each pump/turbine has a big influence on the final dimensions of the hydro pump storage station. For larger individual discharge, the amount of pumps needed is smaller and the width of the flow exit structure increases. The result of this is a considerable reduction in the plant's width (for 27m3/s turbine/pump the total width is 3320 meters whereas for a 160 m3/s turbine/pump the total width is 1372 meters, a reduction of 60 %, see Appendix C.3). However, when increasing the discharge of the individual pumps/turbines, the submergence and thus the depth at which these have to be installed increases. For that reason, 60 m^3/s pump/turbine has been chosen for this design. For this discharge, the bottom of the station is situated at NAP -32 m. The maximum allowed according to the performed soil uplift calculations.

When performing the stability calculations was found that the most stable load case is when the water level at the Valmeer is minimum, even though it was mentioned above, that due to piping the water level will be lowered to a maximum of NAP -19 m. This allows the Valmeer to have some storage capacity during storm surge conditions and large river discharge. This will reduce the failure probability of the system if the maximum discharge is kept at 10.000 m^3/s because the failure of some pumps will not lead to failure of the whole system, as it would happen if the water level would be at NAP -5 m for maximum stability. Further analysis is recommended in re-defining the working conditions of DELTA21 during storm surge and high river discharge knowing that the water level within the Valmeer during these conditions can be lowered to NAP -19 m. Even the maximum design discharge can be reduced if the energy generation function of the Valmeer doesn't need to have 1860 MW of power installed.

To finish this chapter, one last mention regarding the life cycle analysis (LCA) is done. The LCA shows that the Valmeer's power plant already, in this conceptual design stage, ranges among other renewable energy generation technologies in terms of CO_2 emissions during its lifetime. The largest contributions to CO_2 emissions are the amount of concrete used and the electricity used to power the pumps. The concrete amount used should then be reduced at maximum, but the concrete use will be reduced at the maximum for both environmental and economic reasons already. Regarding electricity used, the DELTA21 initiators are already looking for ways of getting the energy for pumping from wind and other renewable energy technologies. This is highly recommended since as it was shown in the LCA chapter conclusions, that the emissions per kWh of electricity produced (if renewable energy is used to power the pumps since the beginning of the operation and during all its lifetime) would drop to -140 g CO_2 / kWh, removing then emissions from the Dutch grid.

The above-written issues make the construction of the Valmeer's power plant a challenging engineering work. But, the advantages show that this project could be very beneficial for the water safety and green energy generation of the Netherlands.

9.2 Recommendations

Some aspects need to be looked at in more depth to ensure that Alternative 1 can be constructed.
First of all, regarding the construction of the building pit itself, two issues arise: The depth at which it has to be excavated (NAP -32 m) and the way of getting rid of the water infiltration within it. The large excavation depth can cause soil uplift problems. Especially if we consider that only one soil profile has been considered for the calculation. In reality, the impermeable clay layer may vary in depth and thus the maximum excavation depth. However, methods such as sequential excavation can tackle this issue. A bigger challenge will be to reduce water infiltration within the building pit. It is unrealistic to drive a sheet pile or diaphragm wall down to the clay layer to make the pit completely impervious (which would be ideal, but experts from the TU Delft and Volker Wessels Infra Competence Center disagree whether this is possible. If possible, it would be extremely expensive). The recommendation of the author on this matter will be to install sheet piles to reduce the infiltration discharge within the Valmeer, to then dewater the pit using pumps and well to reduce the water table below the surface of the pit.

Second, the buoyancy of the structure was found to be negative for the stability calculations. A large amount of water is surrounding the structure and creates large buoyant forces. Two techniques have been discussed in Section 7.2.1 but the author recommends to install sheet piles under the structure to reduce the buoyant force and thus give more stability to the structure.

The last stability issue is piping. There is a large maximum water level difference happening during storm conditions and low water level within the Valmeer. The author recommends that during these conditions, the water level within the Valmeer must be set at a minimum of NAP -19 m. In this way, the water level difference during these conditions is the same as during regular working conditions during high tide. In this way, the piping protection needed will be reduced and the Valmeer still has a large storage capacity during storm surge and high river discharge conditions (from NAP -19 m to NAP -5 m). The piping protection will be composed of 3 sheet piles of 20 meters located 100 meters apart one from another and an impervious layer extending 303 meters horizontally (see Section 7.2.4 to see a drawing showing the piping protection and the seepage path).

Notice that the sheet piles used for piping help to both, reducing the water infiltration within the building pit during construction of the plant, and reducing the buoyant forces acting on the structure.

Below, a cross section of the final conceptual design together with the seepage path is included.

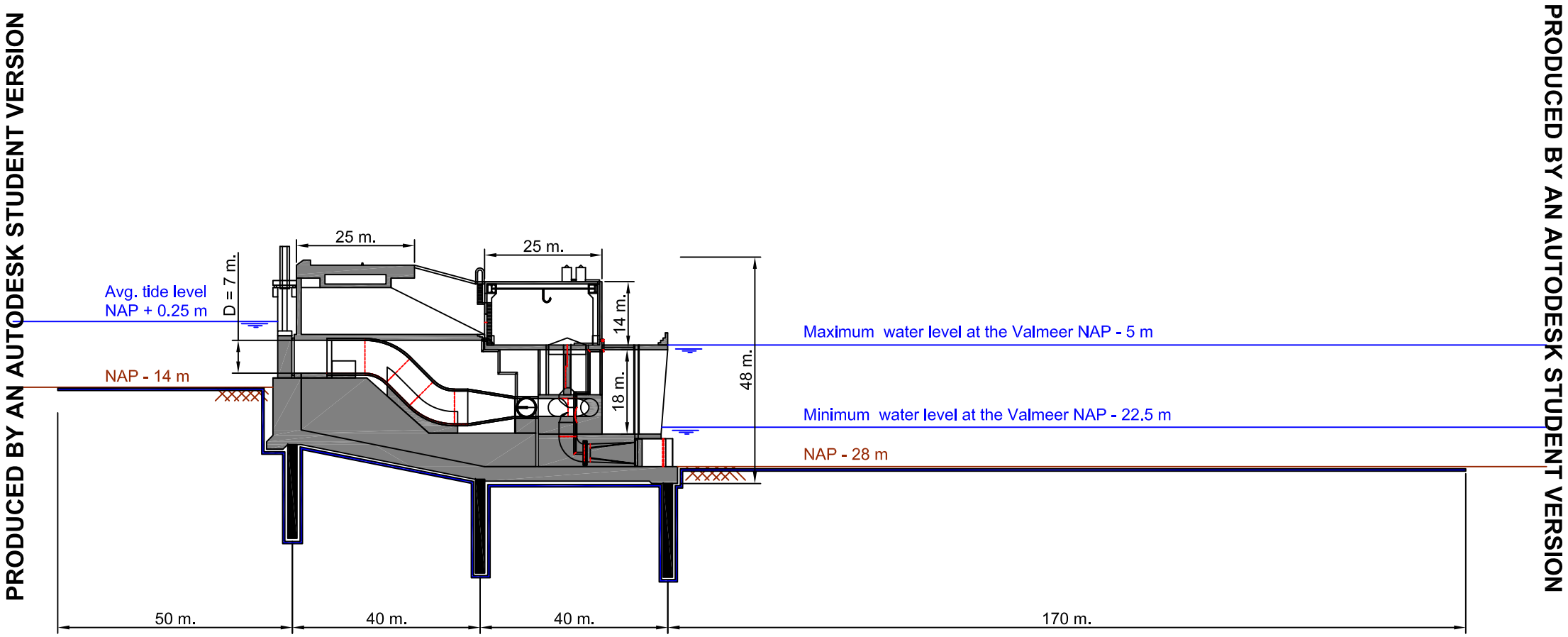

PRODUCED BY AN AUTODESK STUDENT VERSION

PRODUCED BY AN AUTODESK STUDENT VERSION

References

- Agarwal, T. (2012). Review of pump as turbine (PAT) for micro-hydropower. International Journal of Emerging Technology and Advanced Engineering, 2(11), 163-169.
- Amponsah, N. Y., Troldborg, M., Kington, B., Aalders, I., & Hough, R. L. (2014). Greenhouse gas emissions from renewable energy sources: A review of lifecycle considerations. Renewable and Sustainable Energy Reviews, 39, 461-475.
- An, X., Wu, Q., Jin, F., Huang, M., Zhou, H., Chen, C., & Liu, C. (2014). Rock-filled concrete, the new norm of SCC in hydraulic engineering in China. Cement and Concrete Composites, 54, 89-99.
- Bisch, P., Carvalho, E., Degee, H., Fajfar, P., Fardis, M., Franchin, P., ... & Somja, H. (2012). Eurocode 8: seismic design of buildings worked examples. Luxembourg: Publications Office of the European Union.
- Castells, F. (2003). Integrated life-cycle and risk assessment for industrial processes. CRC Press.
- Church, J.A., P.U. Clark, A. Cazenave, J.M. Gregory, S. Jevrejeva, A. Levermann, M.A. Merrifield, G.A. Milne, R.S. Nerem, P.D. Nunn, A.J. Payne, W.T. Pfeffer, D. Stammer and A.S. Unnikrishnan, 2013: Sea Level Change. In: Climate Change 2013: The Physical Science Basis. Contribution of Working Group I to the Fifth Assessment Report of the Intergovernmental Panel on Climate Change [Stocker, T.F., D. Qin, G.-K. Plattner, M. Tignor, S.K. Allen, J. Boschung, A. Nauels, Y. Xia, V. Bex and P.M. Midgley (eds.)]. Cambridge University Press, Cambridge, United Kingdom and New York, NY, USA.
- Consoli et al. (1993). Guide Lines for Life-Cycle Assessment: A 'Code of Practice'. Society of Environmental Toxicology and Chemistry SETAC: Pensacola, FL, USA.
- Daniel, R., & Paulus, T. (2018). Lock gates and other closures in hydraulic projects. Butterworth-Heinemann.
- De Vlieger, I., Panis, L. I., Joul, H., & Cornelis, E. (2004). Fuel consumption and CO2-rates for inland vessels. WIT Transactions on the Built Environment, 75.
- deCrook, T. (1996). A seismic zoning map conforming to Eurocode 8, and practical earthquake parameter relations for the Netherlands. Geologie en Mijnbouw, 75(1), 11-18.
- Deltadienst of Rijkswaterstaat. (1973). The realization and function of the northern basin of the delta project. Government Publishing Office, The Hague.
- Ellen MacArthur Foundation, http://www.ellenmacarthurfoundation.org/
- Esteban, M., Takagi, H., & Shibayama, T. (2009). Methodology for the simulation of the construction of a breakwater taking into account climate and construction accident risks. Coastal engineering journal, 51(01), 49-68.
- International Energy Agency (IEA), (2002). Environmental and health impacts of electricity generation: a comparison of the environmental impacts of hydropower with those of other generation technologies. Retrieved from https://www.ieahydro.org/media/b9067994/A%20Comparison%20of%20the%20Environmental%20Impacts%20of%20Hydropower%20with%20those%20of%20Other%20Generation%20Technologies%20.pdf
- de Ingenieur. (2015). Lievense, the man of the storage basin. Retrieved from: https://www.deingenieur.nl/artikel/lievense-de-man-van-het-opslagbekken.

- Fearnside, P. M. (2004). Greenhouse gas emissions from hydroelectric dams: controversies provide a springboard for rethinking a supposedly 'clean'energy source. An editorial comment. Climatic Change, 66(1), 1-8.
- Fernandez, J., Blanco, E., Parrondo, J., Stickland, M. T., & Scanlon, T. J. (2004). Performance of a centrifugal pump running in inverse mode. Proceedings of the Institution of Mechanical Engineers, Part A: Journal of Power and Energy, 218(4), 265-271.
- Flury, K.,& Frischknecht, R. (2012). Life cycle inventories of hydroelectric power generation. ESU-Services, Fair Consulting in Sustainability, commissioned bye Oko-Institute eV, 1-51.
- Flower, D. J., & Sanjayan, J. G. (2007). Green house gas emissions due to concrete manufacture. The international Journal of life cycle assessment, 12(5), 282.
- Huang, M., An, X., Zhou, H.,& Jin, F. (2008). Rock-fill concrete, a new type of concrete. Proceeding of International fib Symposium2008, 1047-1049.
- International Rivers Network (IRN). (2005). "The U.S. experience. Reviving the world's rivers: Dam removal." http://www.irn.org/revival/decom/index.asp?id=/revival/decom/brochure/rrpt2.html June 1, 2005.
- ISO 14040 (2006). Environmental Management Life Cycle Assessment Principles and Framework; International Standards Organization: Brussels, Belgium.
- Katsman, C. A., Sterl, A., Beersma, J. J., Van den Brink, H. W., Church, J. A., Hazeleger, W., ... & Lowe, J. (2011). Exploring high-end scenarios for local sea level rise to develop flood protection strategies for a low-lying delta—the Netherlands as an example. Climatic change, 109(3-4), 617-645.
- Kecojevic, V., & Komljenovic, D. (2011). Impact of bulldozer's engine load factor on fuel consumption, CO2 emission and cost. American Journal of Environmental Sciences, 7(2), 125-131.
- Keoleian, G. A., Kendall, A., Dettling, J. E., Smith, V. M., Chandler, R. F., Lepech, M. D., & Li, V. C. (2005). Life-cycle cost model for evaluating the sustainability of bridge decks.
- Khasreen, M. M., Banfill, P. F., & Menzies, G. F. (2009). Life-cycle assessment and the environmental impact of buildings: a review. Sustainability, 1(3), 674-701.
- KNMI (2014): KNMI'14: Climate Change scenarios for the 21st Century – A Netherlands perspective; by Bart van den Hurk, Peter Siegmund, Albert Klein Tank (Eds), Jisk Attema, Alexander Bakker, Jules Beersma, Janette Bessembinder, Reinout Boers, Theo Brandsma, Henk van den Brink, Sybren Drijfhout, Henk Eskes, Rein Haarsma, Wilco Hazeleger, Rudmer Jilderda, Caroline Katsman, Geert Lenderink, Jessica Loriaux, Erik van Meijgaard, Twan van Noije, Geert Jan van Oldenborgh, Frank Selten, Pier Siebesma, Andreas Sterl, Hylke de Vries, Michiel van Weele, Renske de Winter and Gerd-Jan van Zadelhoff. Scientific Report WR2014-01, KNMI, De Bilt, The Netherlands. www.climatescenarios.nl
- Knutson, T., Camargo, S. J., Chan, J. C., Emanuel, K., Ho, C. H., Kossin, J., ... & Wu, L. (2019). Tropical Cyclones and Climate Change Assessment: Part I. Detection and Attribution. Bulletin of the American Meteorological Society, (2019).
- Lavooij, H., Berke, L., Tonneijck, M., de Boer, H., Vrijling, H. (2018). DELTA21 deelrapport waterveiligheid.
- Ligterink, N. E., Smit, T., & Spreen, J. S. (2017). Insight into the energy consumption, CO2 emissions and NOx emissions of rail freight transport (No. TNO 2017 R11679). TNO.
- Liu, C., Ahn, C. R., An, X.,& Lee, S. (2013). Life-cycle assessment of concrete dam construction: comparison of environmental impact of rock-filled and conventional concrete. Journal of Construction Engineering and Management, 139(12), A4013009.
- Mahasenan, N., Smith, S., & Humphreys, K. (2003, January). The cement industry and global climate change: current and potential future cement industry CO2 emissions. In Greenhouse Gas Control Technologies-6th International Conference (pp. 995-1000). Pergamon.
- Mäkinen, K.,& Khan, S. (2010). Policy Considerations for Greenhouse Gas Emissions from Freshwater Reservoirs. Water alternatives, 3(2).

- Michalowski, R. L. (2005). Coefficient of earth pressure at rest. Journal of geotechnical and geoenvironmental engineering, 131(11), 1429-1433.
- Ministerie van Infrastructuur en Milieu. (2016). Achtergronden bij de normering van de primaire waterkeringen in Nederland. (Hoofdrapport).
- Nicholls, R. J., & Cazenave, A. (2010). Sea-level rise and its impact on coastal zones. science, 328(5985), 1517-1520.
- Pacca, S. (2007). Impacts from decommissioning of hydroelectric dams: a life cycle perspective. Climatic Change, 84(3-4), 281-294.
- Poff, N. L.,& Hart, D. D. (2002). How dams vary and why it matters for the emerging science of dam removal: an ecological classification of dams is needed to characterize how the tremendous variation in the size, operational mode, age, and number of dams in a river basin influences the potential for restoring regulated rivers via dam removal. BioScience, 52(8), 659-668.
- Possibilities for reducing fuel consumption and greenhouse gas emissions from inland navigation, Report by the Inspection Regulations Committee for the 2012 Autumn Meeting (Annex 2 to protocol 2012-II-4 of the Central Commission for the Navigation of the Rhine, 29 November 2012)
- Rasmussen, N. S. (1997). Concrete immersed tunnels—forty years of experience. Tunnelling and underground space technology, 12(1), 33-46.
- Rijkswaterstaat & Rijksinstituut voor Volksgezondheid en Milieu (2015). Circular economy in the Dutch construction sector (RIVM-rapport Vol. 2016-0024). Retrieved from Rijksinstituut voor Volksgezondheid en Milieu website: https://www.rivm.nl/bibliotheek/rapporten/2016-0024.pdf
- Rijkswaterstaat (2017). Richtlijnen Ontwerp Kunstwerken. Document number: RTD 1001:2017, versie: 1.4.
- Roozenburg, N. F., & Eekels, J. (1995). Product design: fundamentals and methods (Vol. 2). John Wiley & Sons Inc.
- Rastler, D. M. (2010). Electricity energy storage technology options: a white paper primer on applications, costs and benefits. Electric Power Research Institute. :Pumped hydro energy storage is the largest capacity and most mature energy storage technology currently available
- Sagemo, A. & Storck, L. (2013). Comparative study of bridge concepts based on life-cycle costs analysis and life-cycle assessment. (Master's thesis, Chalmers University of Technology, Götemborg, Sweden). Retrieved from: http://publications.lib.chalmers.se/records/fulltext/182549/182549.pdf
- Scheuer, C., Keoleian, G. A., & Reppe, P. (2003). Life cycle energy and environmental performance of a new university building: modeling challenges and design implications. Energy and buildings, 35(10), 1049-1064.
- Shi, C., Li, Y., Zhang, J., Li, W., Chong, L., & Xie, Z. (2016). Performance enhancement of recycled concrete aggregate–a review. Journal of Cleaner Production, 112, 466-472.
- Slangen, A. B. A., and R. S. W. Van de Wal, 2011: An assessment of uncertainties in using volume-area modelling for computing the twenty-first century glacier contribution to sea-level change. The Cryosphere, 5, 673–686, doi:10.5194/tc-5-673-2011.
- Solomos, G., Pinto, A., & Dimova, S. (2008). A review of the seismic hazard zonation in national building codes in the context of eurocode 8. JRC Scientific and Technical Reports.
- Soumis, N., Duchemin, É., Canuel, R.,& Lucotte, M. (2004). Greenhouse gas emissions from reservoirs of the western United States. Global Biogeochemical Cycles, 18(3).
- Steinhurst, W., Knight, P.,& Schultz, M. (2012). Hydropower greenhouse gas emissions. Conservation Law Foundation, 24, 6.
- Turconi, R., Boldrin, A.,& Astrup, T. (2013). Life cycle assessment (LCA) of electricity generation technologies: Overview, comparability and limitations. Renewable and sustainable energy reviews, 28, 555-565.

- Val, D. V.,& Stewart, M. G. (2003). Life-cycle cost analysis of reinforced concrete structures in marine environments. Structural safety, 25(4), 343-362.
- Valsecchi, C., Ten Brink, P., Bassi, S., Withana, S., Lewis, M., Best, A., ... & Soares, C. D. (2009). Environmentally harmful subsidies (EHS): Identification and assessment. Final report for the European Commission's DG Environment.
- Van Lagen, G. (2016). Immersed tunnels subjected to a sunken ship load.
- Van de Wal, R. S. W., and M. Wild, 2001: Modelling the response of glaciers to climate change by applying volume-area scaling in combination with a high resolution GCM. Clim. Dyn., 18, 359–366, doi:10.1007/s003820100184.
- van Vliet, M. T., Franssen, W. H., Yearsley, J. R., Ludwig, F., Haddeland, I., Lettenmaier, D. P., & Kabat, P. (2013). Global river discharge and water temperature under climate change. Global Environmental Change, 23(2), 450-464.
- Villarini, G., & Vecchi, G. A. (2012). Twenty-first-century projections of North Atlantic tropical storms from CMIP5 models. Nature Climate Change, 2(8), 604.
- Watersnoodmuseum (2018). Haringvliet dam. Retrieved from https://watersnoodmuseum.nl/en/knowledgecentre/haringvliet-dam/
- Yang, S. S., Derakhshan, S., & Kong, F. Y. (2012). Theoretical, numerical and experimental prediction of pump as turbine performance. Renewable Energy, 48, 507-513.
- Zhang, Q., Karney, B., MacLean, H. L.,& Feng, J. (2007). Life-cycle inventory of energy use and greenhouse gas emissions for two hydropower projects in China. Journal of Infrastructure Systems, 13(4), 271-279.
- Zhang, S., Pang, B.,& Zhang, Z. (2015). Carbon footprint analysis of two different types of hydropower schemes: comparing earth-rockfill dams and concrete gravity dams using hybrid life cycle assessment. Journal of Cleaner Production, 103, 854-862.
- Zhu, B., Wang, X., Tan, L., Zhou, D., Zhao, Y., & Cao, S. (2015). Optimization design of a reversible pump–turbine runner with high efficiency and stability. Renewable Energy, 81, 366-376.

Appendices

Appendix A

Reference projects

The present appendix serve as base knowledge for the design of the ESL Power Plant for the turbines/pump of the Valmeer. Because of its head difference and discharges, the ESP Power Plant lies between both conventional tidal power plants and pump-storage hydroelectric plants. For that reason, some of the already existing tidal power plants and pump-storage hydroelectric plants are looked at in the following lines, paying attention to aspects such as: discharge, water level difference at each side of the structures and energy generation figures. These will be taken into account to have an idea of the dimensions and possible configurations for the structure aim of study.

A.1 Conventional tidal power plants

A.1.1 Swansea Bay Tidal Lagoon, Whales

The following information has been retrieved from: http://www.tidallagoonpower.com/projects/swansea-bay/

Figure A.1: Plan-view Swansea Bay Tidal Lagoon. Source: http://www.tidallagoonpower.com/projects/swansea-bay/

Swansea Bay Tidal Lagoon will be the world's first tidal lagoon power plant.

This tidal lagoon comprises a U-shaped breakwater which, together with the land area, creates a closed lagoon to create a water level difference with the sea. This water level difference (potential energy) will allow the electricity creation when turbining the water through the lagoon's inlet.

When the turbine gates are closed for 3 hours, a 4 meters difference in water level can be achieved. Power then is created as the water goes through 60m long horizontal tubes, rotating 7.2 m diameter hydro turbines. These turbines are low-head Kaplan turbines, able to generate 320 MW with an actual production of 530 GWh/year

turbinig an average of 3000m^3/s.

However these are just calculated figures and the actual ones are yet to be discovered when the plant starts to work. The construction started in 2018 and it is expected to cost around 1.3 billion $.

A.1.2 La Rance Tidal Power Station, France

The following information has been retrieved from:
https://www.edf.fr/en/the-edf-group/industrial-provider/renewable-energies/marine-energy/tidal-power
and
https://tethys.pnnl.gov/annex-iv-sites/la-rance-tidal-barrage;https://www.power-technology.com/features/tidal-energy-cost/;

Figure A.2: La Rance Tidal Power Station. source: https://tethys.pnnl.gov/annex-iv-sites/la-rance-tidal-barrage

Opened in 26th November 1966, La Rance Tidal Power Station was the first tidal power station in the world and it is the second largest operative tidal power plant. This facility is situated on the esturary of the Rance river.

The power is generated by water flowing through the 332.5 m long dam built at the river. The maximum flow that can p[ass through the tidal power plant is 9600 m^3/s. The average tidal range of the estuary is 8m, having a maximum of 13.5m at spring tide. With its 24 turbines able to generate 240 MW, it can give an output og 600 GWh/year.

The structure was constructed using the dry island construction method. The costs of this tidal power plant was around 100 million €from 1966, so the equivalent to 910 million €in 2019.

A.1.3 Sihwa Lake Tidal Power Station

Information retrieved from:
https://tethys.pnnl.gov/annex-iv-sites/sihwa-tidal-power-plant and
https://www.hydropower.org/blog/technology-case-study-sihwa-lake-tidal-power-station

Figure A.3: Sihwa Lake Tidal Power Plant, Gyeonggi Province, South Korea. Source: https://www.powermag.com/sihwa-lake-tidal-power-plant-gyeonggi-province-south-korea/

The Sihwa Lake was part of a land reclamation project by the government of South Korea. A seawall 12.7 km long was constructed in 1994 to give birth to the Sihwa Lake. The lake would protect the land from flooding at the same time as acting as a fresh water buffer.

Yet once the seawall was closed, the natural tidal flows were cut and the wastewater from industrial complexed increased. By 1997, the delay in the construction of wastewater treatment plants made the lake's water so contaminated that it could no longer be used. To counteract these effects, the gates of the lake were opened to allow salt-water intrusion. However, this was no enough to palliate the pollution in the lake. Therefore, the plan of building the Tidal Power Plan came in 2002 and construction started in 2004. The tidal lake would increase the flow exchange in 200%.

The construction method was dry island. An artificial island was constructed and then, the tidal power plant was constructed in the dry. The construction costs rose up to 500 million euros and after its completion in 2011, it has been the largest tidal power plant in the world, having 10 pumps of 24.5 MW each providing a power output of 245 MW (4 MW larger than the La Rance Tidal Power Plant. See **??**). Each 7.5 m diameter turbine operates at a maximum discharge of 481.1 m^3/s, giving a total maximum discharge of 4800 m^3/s. The operative head difference is of 5.82 meters and the annual energy production is around 550 GWh.

A.1.4 Annapolis Tidal Station

The Annapolis Tidal Station is the first and only tidal power station in North America. It was built in 1985 and it has an energy output of 20 MW, giving an annual production of 32.9 GWh. There are no available data about discharges nor tidal difference but it is constructed in the Bay of Fundy. At the location of the tidal power plant, the average tidal range is 8 meters. In the following image, the location of the power station and the tidal range in the bay of Fundy is shown:

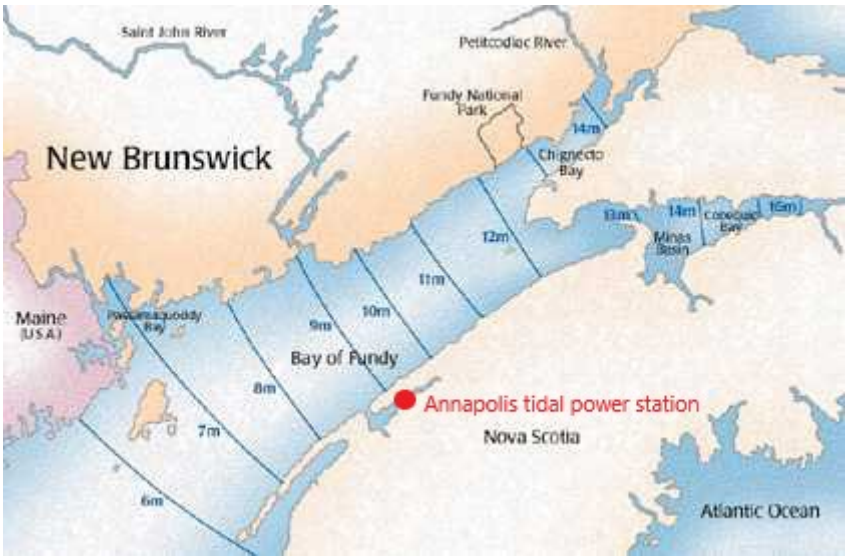

Figure A.4: Location of Annapolis tidal power station at the Bay of Fundy.

A.2 Pump storage hydroelectric station at the sea

The following pump storage hydroelectric stations are just projects, i.e. they were never constructed due to different limitations. However, even if they were not realized, the studies can be used to see what are the costs of pump hydropower storage systems and the issues and advantages of this technology. Furthermore, there are not lots of pump storage hydroelectric stations apart from the ones built at the mountains taking advantage of the large head different they can provide. This lack of real data, makes the one from projects more likable. Anyways, the next section (see A.3) will talk about actual pump storage hydroelectric stations built at the mountains.

A.2.1 Plan Lievense

All information retrieved from: Rijkswaterstaat, Hollandsche Beton Groep NV, Ballast Nedam Groep NV, & Raadg. Ing. Bur. Lievense. (1985). Pomp accumulatie centrale Noordzeekust (Hoofdrapportage fase 1).

Lievense launched the idea of building a a pumped accumulation plant for the Netherlands in 1979.

Figure A.5: General representation of the plan Lievense. Source: https://www.deingenieur.nl/artikel/lievense-de-man-van-het-opslagbekken

The main idea was to construct a 100 km long and 14 m high dike ring in the Markermeer. The dike would

host between four and five hundred wind turbines and contain four water power stations (De Ingenieur, 2015).

Figure A.6: Dike section of the Valmeer with the pumping system (Illustration by the Das brothers). Source: https://www.deingenieur.nl/artikel/lievense-de-man-van-het-opslagbekken

The design included the use of 134 Francis turbines, working at a total discharge of between 3000 and 7000 m^3/s in a basin 500m wide and 10 m deep. The total storage capacity is of 20GWh for a head range variation of 75 to 56 meters. Even though for this option, high dikes would needed. That is why in 2007 the idea of digging a 40 m deep basin and using the excavated material to build the surrounding dikes arised. With this new plan, the plant would be able to produce 18 GWh per day. The total cost of the project were estimated to be between 4276 and 3367 million euros.

A.2.2 Taiwan integrated Energy and Service island

Information retrieved from: Beurskens, J., De Haan, S., Bauer, P., & Dieleman, R. (2014). Taiwan integrated energy storage island. Alliander

Currently Taiwan is almost fully reliant of the import of energy. To deal with that, the Taiwanese want to increase the locar energy production, mainly using wind and solar energy up to 7.3 GW in 2030. This need to look for clean energy generation motivated the design of this energy island.

Figure A.7: Artist impression of the multifunctional island by Reinout Prins (Source: Beurskens et al., 2014)

The design comprises a 40 to 31 meters depth basin with an area of reservoir of 32.6 km^2 able to produce 20 GWh of storage capacity. The turbine type was chosen to be francis, installing a total of 125 12MW turbines.

Total costs for this project were estimated to be in the range of 3000 million euros. However the annual benefits were estimated to be around 200 million euros, giving a payback period of 26 years.

A.3 Pumped storage stations built taking advantage of the head difference provided by mountains

These kind of structures are usually made taking into advantage the head difference provided by mountains. They are composed of the following elements: Lower lake, upper lake, penstock connecting the two deposits and the reversible pump/turbines.

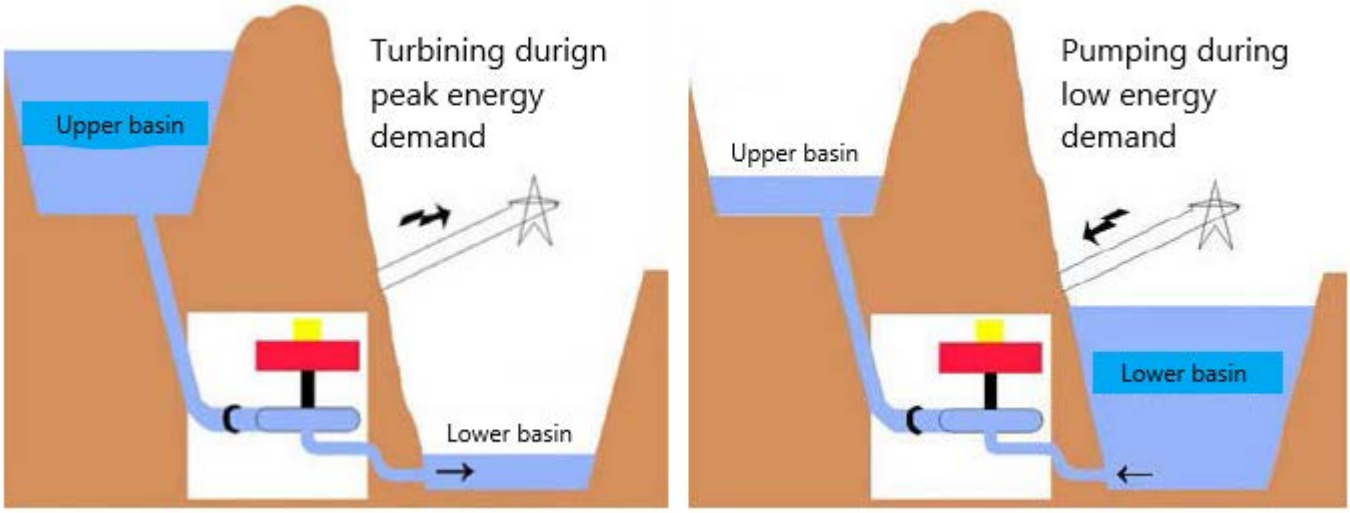

Figure A.8: Pump storage hydroelectric estation elements and working scheme. Source: notes from the class "Aprovechamientos Hidroelectricos" from University of Cantabria (Garcia, 2017)

These kind of centrals are net consumers of energy. However, due to the difference in the electricity prices during periods of high/low demand, they are cost-efficient. Besides, for getting more economic performance, the water in the above lake can then be used for irrigation or water supply purposes if that is economically profitable.

The hydromechanic equipment consists of a reversible pump/turbine and an electric machine (motor and generator). For reversing the flow's direction, the inlet gates are closed and then the turbine/pump change rotation direction and the gates are opened again.

These kind of centrals work with large head differences, in contrast to the head difference at the Valmeer (4.2 to 24 meters). However, the main idea is the same. In the following sections, some of the largest pumped-storage stations are shown (All the information was retrieved from https://elperiodicodelaenergia.com/las-10-mayores-centrales-hidroelectricas-de-bombeo-del-mundo/):

Bath County Pumped Storage Station, United States of America

This station is known to be the largest pumped storage station in the world. It consists of two lakes separated by approximately 380 meters in height.

Figure A.9: Aerial view of the Bath County Pumped Storage Station

Its construction, with an original capacity of 2100 MW, started in march 1977 and was completed in december 1985 having a cost of 1.600 million US dollars. Voith - Siemens improved the already installed Francis pump-turbines between 2004 and 2009, increasing the energy generation of each turbine to 500.5 MW and the pumping power to 480 MW. Having a total of 6 turbines, the installed capacity became 3003 MW.

Tianhuangping Pumped Storage Station, China

Figure A.10: Tianhiangping Pumped Storage Station

This station has an installed capacity of 1836 MW and uses six reversible Francis turbines made by Kvaerner. Its construction started in 193 and the project was completed in 2004. The station is directed by Shenergy CO Ltd. and costed a total of 1080 million US dollars.

Situated in Daxi Creek, the dam Tianhuangping gives place to the lower lake. The dam is 72 m high and 577 long, storing up to 6.8 million m^3.

From the lower lake, the water is pumped to the upper lake, able to store 6.7 milliom m^3. From there, the water falls through two pipes 882 m long with a 7 m diameter. Before arriving to the pump/turbines, each of these two pipes are diverted into 6 different pipes which reach the 306 MW reversible turbine units.

Grand'Maison Pump Storage Station, France.

Figure A.11: View of the dam and reservoir of the Grand'Maison Storage Pump Station.

The Grand'Maison Pumped Storage Station is property of the public french electric company "EDF". It was constructed between 1878 and 1985 and the energy production started in 1987. Its installed capacity is 1800 MW which makes it the largest hydroelectric power plant in France.

Grand'Maison is a dam with a height of 140 meters from the river water surface and 160 meters from its base. It is 550 long and the storage basin behind it is able to host 140 milliom m^3 of water. The central has levels above and below the soil surface. In the upper level, there are 4 generator of 150 MW Pelton turbines that are used for conventional hydroelectric generation.

The underground level contains eight 150 MW Francis turbines that can be used for either energy generation or water pumping to the upper lake.

Both energy generation and water pumping can be activated within seconds. In an annual base, the station generates 14220 GWh of electricity and consumes 1720 GWh.

Dinorwig Pumped Storage Station, United Kingdom.

Figure A.12: View of the reservoir of the Dinorwig Storage Pump Station.

The Dinorwig Pumped Storage Station has a capacity of 1728 MW and it is situated at the north of Wales. The station was constructed on an old slate quarry. The project started in 1974 and costed 425 million pounds. The construction time was 10 years and it constituted the largest-ever civil engineering project given by the UK's government at the moment.

The work was done by a joint venture between Alfred McAlpine, Brand and Zschokke. They had to move 12 million tons of rock. The station has 16 km of tunnels, a million tons of concrete, 200000 tons of cement and 4500 tons of steel.

The electric central is connected to the grid by 400 kV cables installed underground in order to preserve the beauty of the place it is situated in. The hydroelectric station is composed of six 300 MW GEC generators connected to reversible Francis's turbines. With the six units a load from 0 to 1.800 MW can be achieved in 16 seconds.

A.3.1 Similarity between Valmeer's PP and already existing constructions

It is important to notice the singularity of the ESL's Tidal Power Plant of the Valmeer. This pumped tidal plant ranges between the conventional tidal power plant stations and the pump storage hydroelectric stations. From the tidal power plants, comes the idea of getting energy from a relatively low head difference (between 24 and 4.2 meters in head difference for the Valmeer). Whereas from the pump storage hydroelectric plant, the idea of pumping during low electricity demand hours and turbining during high electricity demand hours is taken. However, these last-mentioned power pants usually work at water level differences larger than the 24m available at the Valmeer.

The most similar projects are the ones that were left as a design idea. See sections A.2.1 and A.2.2. However, these were never realized, so there are not real projects that we can compare to in this study.

Appendix B

Maps used for boundary conditions

B.1 Introduction

In this appendix, a more detailed image of the maps used for defining the boundary conditions are shown.

B.2 Bathymetry


NAVIONICS
Products
Features
Chart Viewer
My Card
Support
Account
Lng
Pilot LNG Carriers
(See Lower Zooms)
Pilot Boarding
Oil and Gas Fields
Gas
Hoek van Holland
Yangtzekanaal
Europoort
Maasvlakte
Nieuwe Waterweg
Brede Water
Slufter
Nature Reserve
Polder Strijpe
Polder Nieuwe Gote
Maeuverhoorn
Grondpolder
Bokkepolder
Zuiderdiep
Harlingen
Route
Menu

B.3 Topography

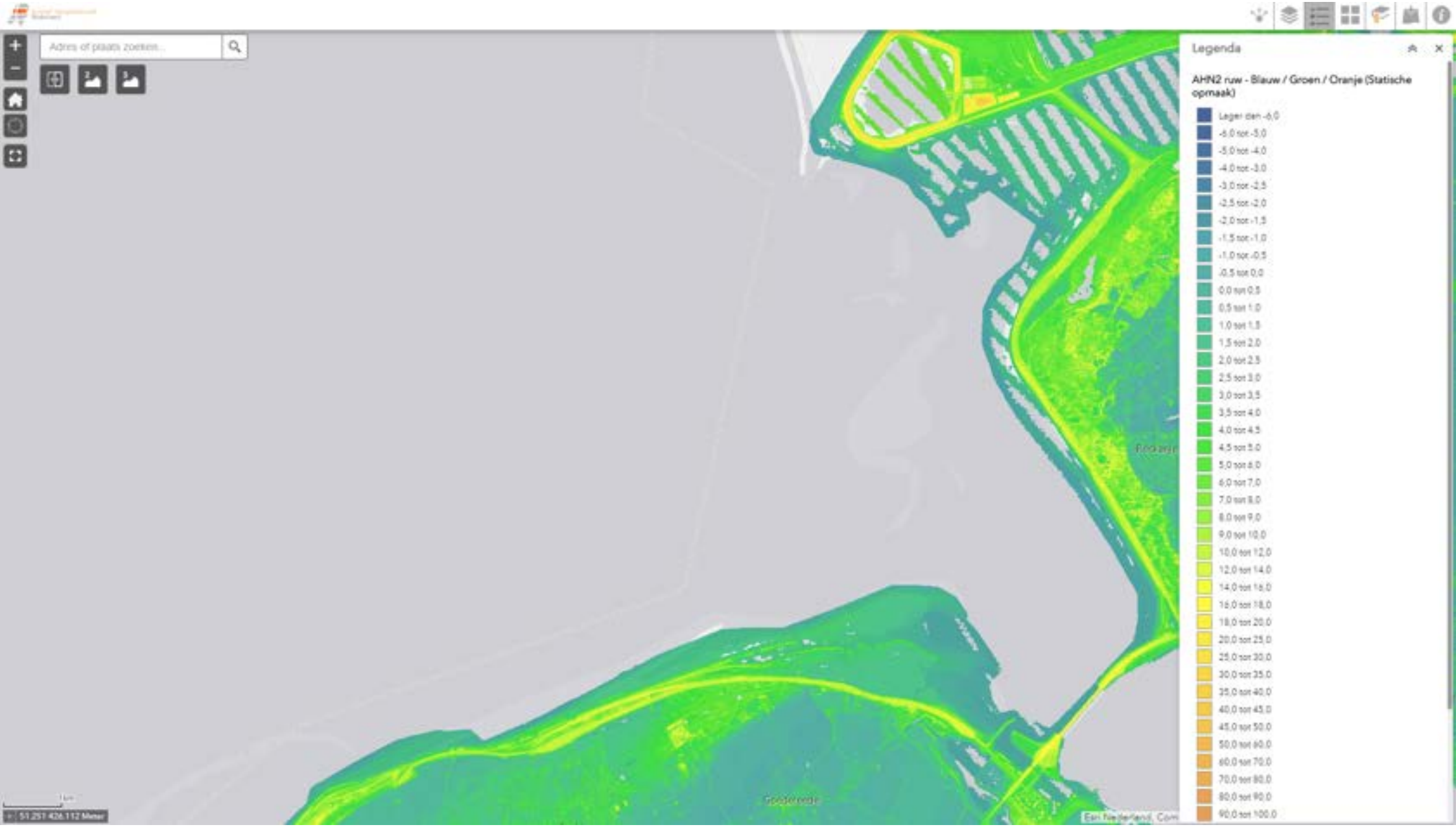
Adres of plaats zoeken...
Legenda
AHN2 ruw - Blauw / Groen / Oranje (Statische opmaak)
Lager dan -6,0
-6,0 tot -5,0
-5,0 tot -4,0
-4,0 tot -3,0
-3,0 tot -2,5
-2,5 tot -2,0
-2,0 tot -1,5
-1,5 tot -1,0
-1,0 tot -0,5
-0,5 tot 0,0
0,0 tot 0,5
0,5 tot 1,0
1,0 tot 1,5
1,5 tot 2,0
2,0 tot 2,5
2,5 tot 3,0
3,0 tot 3,5
3,5 tot 4,0
4,0 tot 4,5
4,5 tot 5,0
5,0 tot 6,0
6,0 tot 7,0
7,0 tot 8,0
8,0 tot 9,0
9,0 tot 10,0
10,0 tot 12,0
12,0 tot 14,0
14,0 tot 16,0
16,0 tot 18,0
18,0 tot 20,0
20,0 tot 25,0
25,0 tot 30,0
30,0 tot 35,0
35,0 tot 40,0
40,0 tot 45,0
45,0 tot 50,0
50,0 tot 60,0
60,0 tot 70,0
70,0 tot 80,0
80,0 tot 90,0
90,0 tot 100,0

B.4 Soil Information

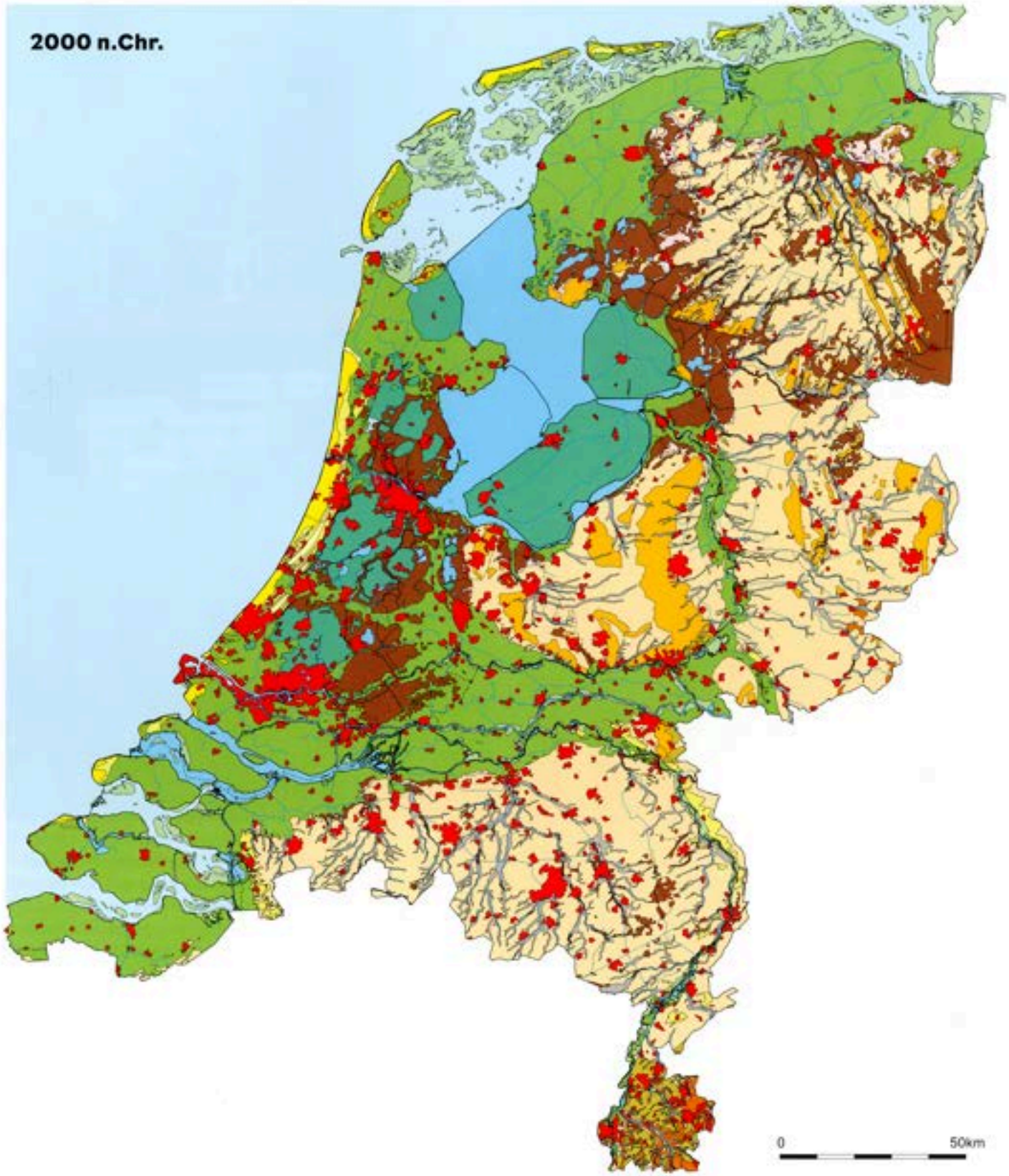
2000 n.Chr.
0
50km
Holoceen landschap
Hoge duinen
Strandwallen en lage duinen
Strandvlaktes
Getijdengebied en riviervlakte
Getijdengebied en riviervlakte, bedijkt
Droogmakerij
Veengebied
Stedelijk gebied
Stad
Buiten- en binnenwater
Waterlopen
Pleistoceen landschap
Riviervlakte en beekdalen
Dekzandgebied beneden 16 m -NAP
Dekzandgebied tussen 16 en 0 m -NAP
Dekzandgebied boven 0 m NAP
Rivierduinen
Stuwwallen, gestuwde keileemheuvels en -ruggen
Lössgebied
Gebieden met Tertiaire en oudere afzettingen

Appendix C

Pump/turbine working discharge selection

C.1 Introduction

This appendix contains the formulation used to calculate the characteristic design parameters of the turbine/pumps. These calculations were performed following the document "Notes on configuring, modeling and testing of rotodynamic pumps (Arnold, 2017)" provided during a meeting with Pentair. This appendix first shows the formulations used to design the turbine characteristics and then, those values are given for different pump discharges. Finally, a design discharge will be chosen and future recommendations are given.

The designed pumps will work as Pump-As-Turbine (PAT). The turbine will be designed to work efficiently in pump mode. For generating energy, the rotor changes the rotation direction and the motor acts as a conventional generator of a hydroelectric power plant. Therefore a centrifugal pump can work in reverse mode as a Francis turbine (Agarwal, 2012). The use of a pump as a turbine reduces the efficiency when turbining but the capital costs are significantly reduced (Fernandez et al., 2004).

C.2 Theoretical background

To obtain adequate turbine/pump geometries, first, the working environment has to be defined (see Figure C.1). The maximum water level at the Valmeer is situated at NAP -5m, whereas the minimum, is at NAP -22.5. Considering average tidal levels (see astronomical tide Section 4.4), the water level at sea-side varies daily from NAP +1.25m to NAP -0.75m. This means that the maximum water head difference available in the basin is 23.75 m and the minimum is 4.25 m.

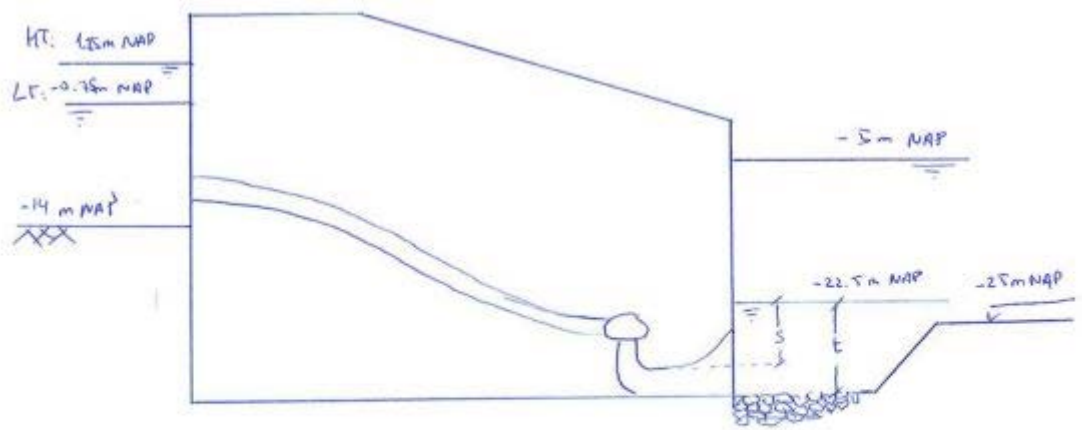

Figure C.1: Daily water level variations considered for the design of the turbines/pump

The first design parameter to obtain is the specific speed or impeller shape number (Ω_s). This number indicates what is the impeller shape that best fits taking into account discharge (Q), rotation speed (Ω) and water head difference (H):

$$\Omega_s = \frac{\Omega\sqrt{Q}}{(gH)^{3/4}} \text{ [-]} \tag{C.1}$$

In the following figure, different shapes for different specific speeds are shown:

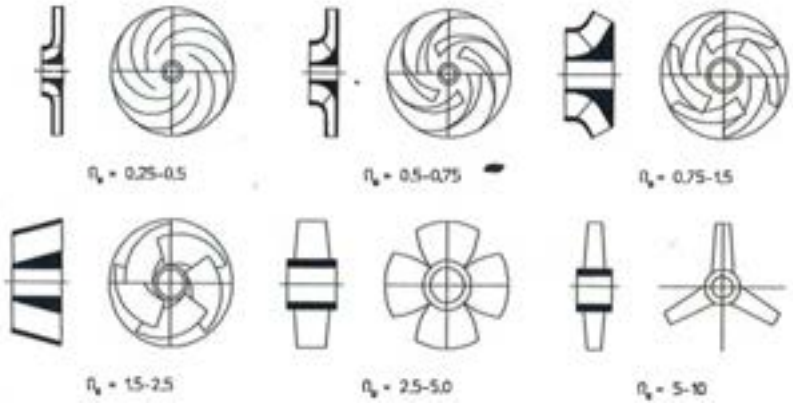

Figure C.2: Impeller shapes depending on specific speed

Since the water head difference is variable, the design has been performed for the average water head difference (i.e. 14m). Then, to have a constant specific speed, the rotation speed (Ω in Equation C.1) will change depending on the head difference. For the design head difference, the rotation speed is set as the maximum rotation speed (N_{max}) and is calculated as:

$$N_{max} \approx \frac{750}{\sqrt{Q}} \text{ [-]} \tag{C.2}$$

From the specific speed together with the discharge, efficiency can be calculated as:

$$\eta \approx 0.95 - 0.05Q^{-1/3} - 0.125[log(\Omega_s)]^2 \text{ [-]} \tag{C.3}$$

Finally, the impeller inlet (D_{s1}) and outlet diameters (D_{s2}) can be calculated from:

$$D_{s1} \approx 2\left(\frac{1}{1-\lambda^2}\right)^{1/3}\left[\frac{Q}{\Omega}\right]^{1/3} \text{ [-]} \tag{C.4}$$

Where: $\lambda \approx 0.5[1 - \exp -\Omega_s]$ [-]

$$\frac{D_{s2}}{D_{s1}} = \left(\frac{f_d}{2}\right) + \sqrt{\left(\frac{f_d}{2}\right)^2 + \frac{1}{\eta f_s}\left(\frac{1}{\Omega_s}\right)^{4/3}} \text{ [-]} \tag{C.5}$$

Where:

- Diffusion ratio $f_d \approx 0.85$ [-]
- Slip factor $f_s \approx 0.85$ [-]
- Efficiency $\eta \approx 0.85$ [-]
- Hub-shroud ratio $\lambda \approx 0.85$ [-]

Once the impeller inlet diameter (Equation C.4) is known, the geometry of the concrete volute pump can be obtained. This geometry, following recommendation from professionals, will be a mix between the draft tube geometry, typical from hydropower and the concrete volute pump geometry, typical from pumping stations. The different measurements are obtained as a function of the impeller inlet diameter.

On the one hand, the draft tube geometry will be used for the part next to the turbine. The draft tube is designed to reduce the velocity of the fluid at the outlet. In this way, the kinetic energy loss is reduced and this is converted into potential energy. Thus increasing the net head that the turbine will obtain the energy from. Following König (1985), the design of the draft tube is:

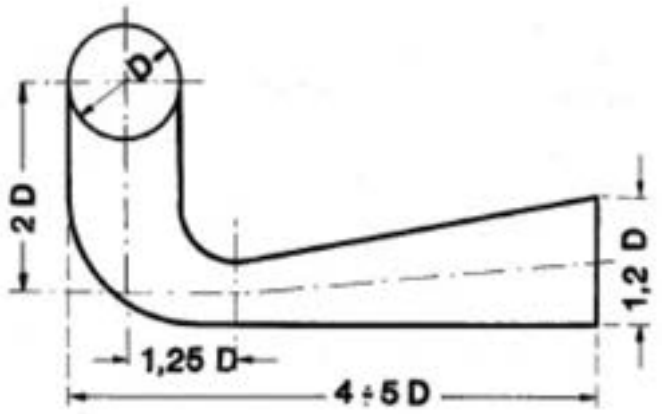

Figure C.3: Draft tube geometry (König, 1985)

On the other hand, the formed suction intake geometry is used to "improve flow conditions to the pump." (US Army Corps of Engineers, 1994). Pentair provided an excel spreadsheet that calculated the geometry of the formed suction intake in terms of impeller inlet diameter. See below:

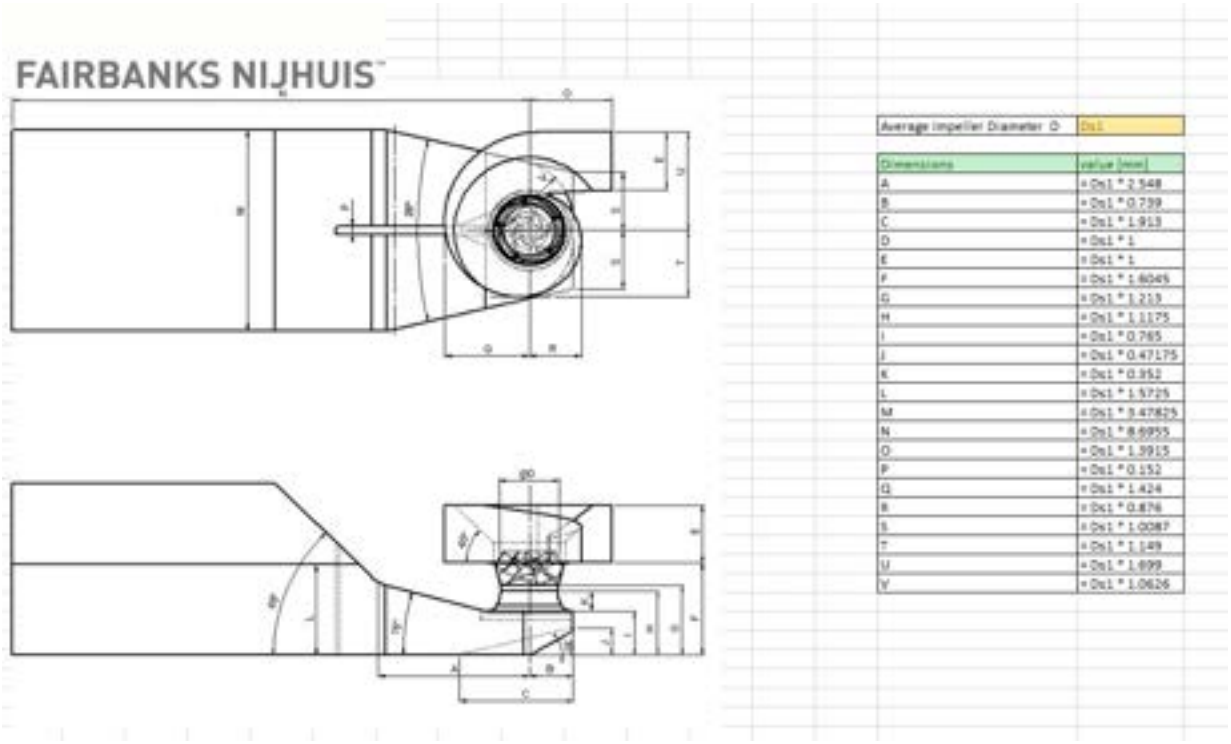

Figure C.4: Spreadsheet for concrete volute pump dimensions calculation

Besides, other values such as submergence and the bottom level of the turbine/pump caisson are of great importance for the design. Those values were obtained from the U.S. "Army Corps of Engineers, 1994: Mechanical and electrical design of pumping stations. Appendix I":

Submergence, $s = 0.94 \cdot D_{s1}$
water surface to bottom on caisson, t = $1.43 \cdot D_{s1}$

As mentioned above, the geometry is a mix of draft tube and formed suction intake. The part next to the turbine will be long, following a draft tube geometry in order to reduce the outflow velocity. Then, the next part will follow the formed suction intake geometry in order to allow for a proper catchment of water when functioning in pumping mode. According to the US Army Corps of Engineers: "reduces excavation and increases the available static suction head on the pump impeller".

In order to calculate the power of the turbines, it is known that for a discharge of 27 m3/s, the power of the turbine/pump unit if of 5MW (Pentair, 2019). Besides, the power increase is proportional to the discharge, thus if the discharge doubles, the power also does and so on.

C.3 Power plant width depending on turbine size

In this section, the relationship between the turbine/pump size with the overall power plant width is given. Basically, by increasing the discharge turbines can work with, the size of the suction inlet tube, as so as the depth at which the turbine/pump has to be place increases. However, the number of turbines/pumps to be used drastically reduces. Therefore, as the following table shows, the total power plant width reduces when increasing the turbine/pump capacity.

Parameter (units)	Alternative 1	Alternative 2	Alternative 3	Alternative 4	Alternative 5
Discharge per pump (m^3/s)	27*	60	100	160	200
Power per pump (MW)	5.0	11.1	18.5	29.6	37.0
Total number of pumps needed	371	167	100	63	50
Max. rpm per turbine (rpm)	144	97	75	59	53
Impeller inlet diameter (m)	2.57	3.84	4.95	6.26	7.00
Submergence, s in Figure C.5	2.4	3.6	4.7	5.9	6.6
Distance water surface, bottom of structure, t in Figure C.5	3.7	5.5	7.1	9.0	10.0
Bottom level of structure**, NAP -x m in Figure C.5	-26.2	-28.0	-29.6	-31.5	-32.5
Width of singe turbine (m)	8.9	13.3	17.2	21.8	24.4
Width estimation of power plant***(m)	3320	2228	1722	1372	1218

Table C.1: Individual turbine/pump affection to power plant dimensions and positioning

* This discharge was the one recommended from Pentair.

** The level of excavation of the basin will be 4 meters deeper. This 4 meters are part of the base of the structure.

*** Width estimation of power plant obtained from: Total number of pumps needed × Width of single turbine (m).

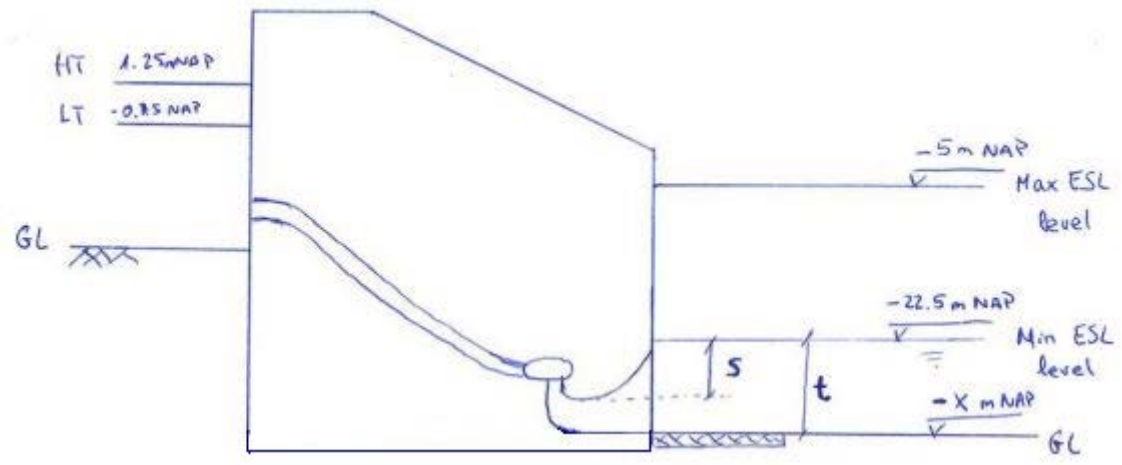

Figure C.5: Representation of submergence values for power plant

It is important to take into account that when going deeper with the turbines, some extra excavations would need to be done next to the exit from the turbines. The good news is that not all the Valmeer would need to be excavated. Only a portion large enough to reduce the water speed at the turbine's exit down to a safe value (for erosion) would suffice. See picture below:

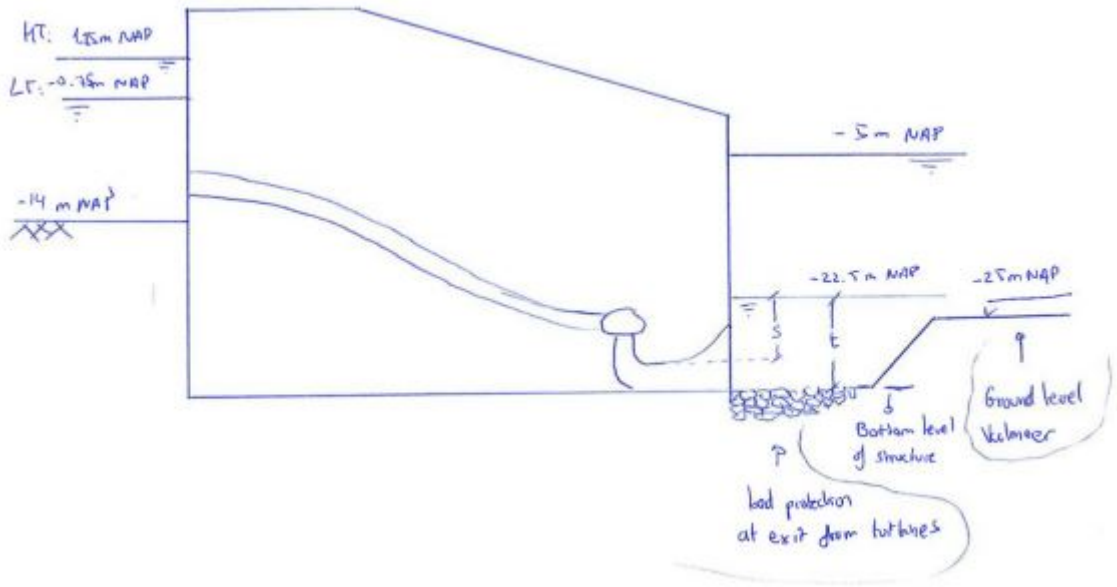

Figure C.6: Consequences of installing the turbines/pump deeper

However, the problem with excavating deeper is that the more soil we remove from the basin, the less resistance the basin floor has against uplift. After some preliminary calculations (see Appendix E) the Valmeer can be excavated down to NAP -32.4m without any soil eruption problems (assuming a clay layer from NAP -64m to NAP -74m and sand on top of that).

Taking the above into account, the chosen individual pump discharge for design will be 60 m^3/s. That will reduce the width of the structure by 1/3 with respect to the 27 m^3/s turbine recommendation from Pentair. Besides, the number of turbines is reduced from 371 to 167, which improves considerably the time maintenance will take for the total number of turbines. A larger discharge wasn't chosen because there is some uncertainty about how stable would be the floor going to deeper depths. See Appendix E. Further analysis is recommended in this aspect.

Regarding efficiency, this is maximum for the design discharge in pumping mode. The efficiency, calculated using eq. C.2. Resulting in a 93% efficiency. The efficiency for turbining mode is hard to predict without performing calculations and/or testing the pumps as turbines. However, the manufacturer Pentair assures the efficiency loss for their pumps working as turbines is of 10 % "if the rotational speed is varied at different heads". However, they could not provide data proving this and the reviewed literature (Zhu et al., 2015; Yang et al,. 2012; Agarwal, 2012) shows that for low heads the efficiency of the turbine mode is significantly reduced. Following recommendations of professor Bricker from the TU Delft (lecturer of Waterpower Engineering), the assumed efficiency loss for turbine mode will be 20%. Thus, the turbining efficiency will be (93% *(1-0.2)) 74%.

As mentioned above, the geometry is a mix of draft tube and formed suction intake. The part next to the turbine will be a long draft tube geometry to reduce the outflow velocity. Then, the next part will follow the formed suction intake geometry to allow for a proper catchment of water when functioning in pumping mode. According to the US Army Corps of Engineers: "reduces excavation and increases the available static suction head on the pump impeller". The final geometry assumed for this project can be seen below.

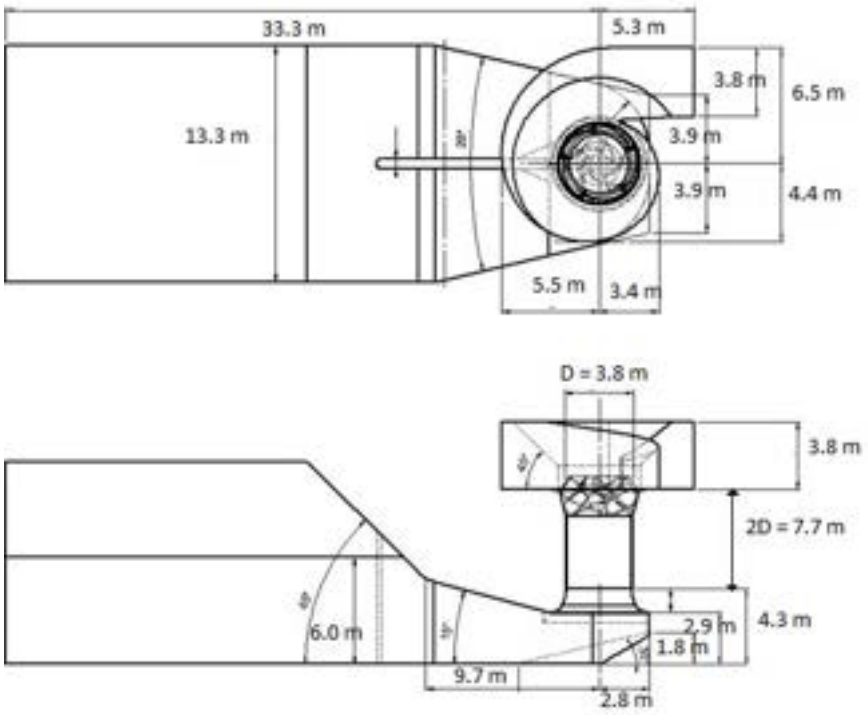

Figure C.7: Combination of draft tube and formed suction intake geometries

C.4 Recommendations

The above geometry will be used for the present thesis. However, further research on designing a turbine/pump and geometries around it to maximize the efficiency for both working modes is recommended.

Authors such as Zhu et al., 2015 investigate on runner geometries that maximize efficiency for the turbine mode. They found that a negative blade lean translates into good efficiency and stability in the operations. However, this study was done for medium to high head differences. Therefore, research needs to be done to ensure this geometry works for low-heads. If not, new runner geometries can be investigated.

Appendix D

Head losses

D.1 Theoretical background for water head loss calculations

When turbining water to obtain electricity, it is important to have adequate water head differences. The natural water head difference (distance between top surface of water at both sides of the power station) can be significantly reduced if the system causes large water head loses. In order to reduce this at maximum, an analysis of the losses has been included in this report.

The head loses were computed using the Darcy-Weisbach equation:

$$h_L = f\frac{L}{D}\frac{v^2}{2g} \tag{D.1}$$

Where:

- h_L [m] = friction losses
- f [-] = friction factor
- L [m] = pipe's length
- D [m] = pipe's diameter
- v [m] = flow velocity within the pipe

The *friction factor* (f) is dependent on Reynolds number and the relative roughness of the pipe's material. It can be accurately obtained using Colebrook equation. This method however requires iteration using Moody's chart so for this preliminary designs, the simpler Blasius (1911) formula will be used:

$$f = (100 \cdot Re)^{-1/4} \tag{D.2}$$

where:

$$Re = \frac{v * D}{\nu} \tag{D.3}$$

ν in the above equation is the cinematic viscosity. For water it has a value of 10^{-6} m^2/s.

With the above formulations, the friction losses within the pipe can be obtained. However, there are local loses at the entrance, bends and constrictions that need to be taken into account. These local loses can be calculated as:

$$h_L = K_L\frac{v^2}{2 \cdot g} \tag{D.4}$$

Where K_L is the local friction coefficient. In the following table, some values for K_L are shown:

Component	K_L
Well-rounded inlet	0.04
Gradual constriction	0.025
Bend	0.3

Table D.1: Local friction coefficient for pipe's elements

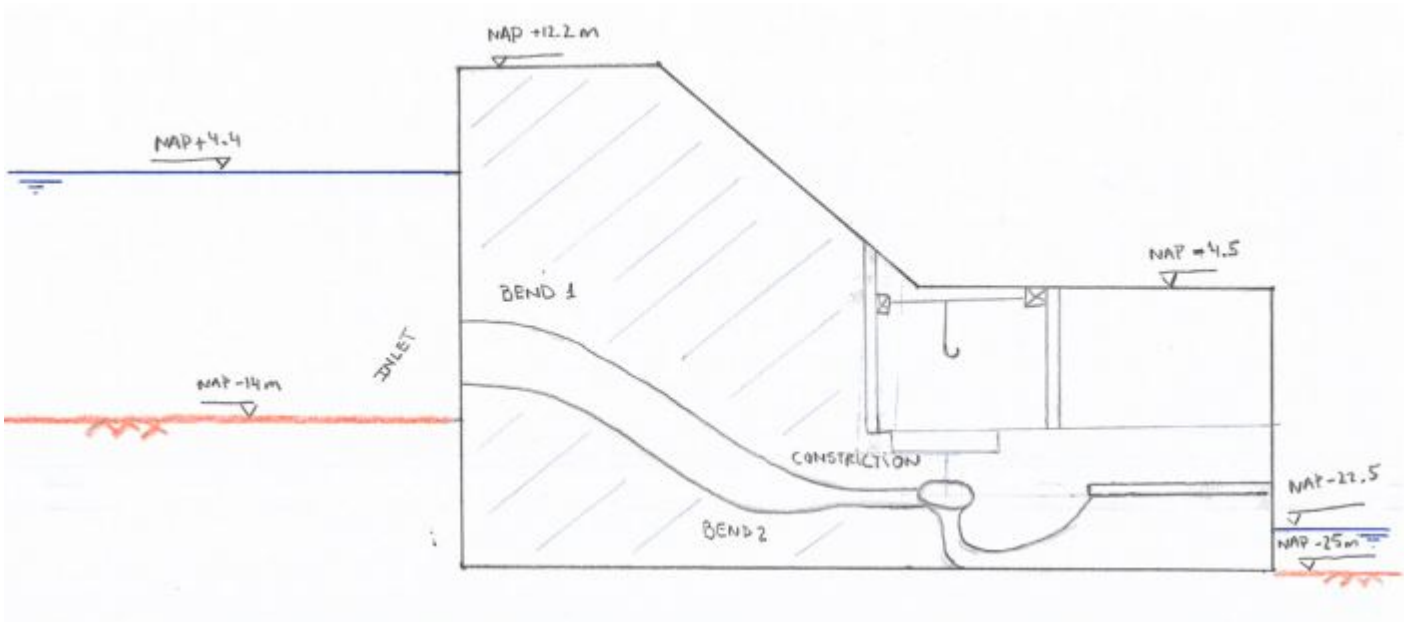

Figure D.1: Sketch showing the pipe's geometry

D.2 Head loss for Alternative 1

The first step for calculating head loses is to get a first estimate of the pipe's length. Then, the localized loses such as the ones from the inlet, bends or pipe's contractions are shown. Outlet losses are neglected since the design of the turbine/pump casing is design to reduce head loss at maximum. The speed at which water leaves the power station makes the losses at the outlet negligible.

In the following image, the layout for the pipes is shown: For Location 1, the estimation for the pipe's length is 42.5 meters. Besides, we can see that there are two bends, one inlet and one consticion that need to be taken into account for calculating the local (or minor) loses.

As mentioned before, the head loses were computed using the Darcy-Weisbach equation:

$$h_L = f \frac{L}{D} \frac{v^2}{2g}$$

Where:

- $f = (100 \cdot Re)^{-1/4}$
- $Re = \frac{v*D}{\nu}$
- $\nu = 10^{-6}$ m^2/s
- L [m] = 42.5
- D [m] = 3.5
- v [m/s] = 2.8

Giving a loss within the pipe of $h_L = 0.03$ m. The next step is to calculate the local loses. For the geometry present in Figure D.1 and using Equation D.4, the following calculation results:

LOCAL HEAD LOSES					
	factor	element D	velocity within element	Head loss	
element1	0.04	3.5	2.8	0.02	INLET
element2	0.025	2.5729	5.2	0.03	GRADUAL CONTRACTION LOSS
element3	0.3	3.5	2.8	0.12	BEND 1
element4	0.3	3.5	2.8	0.12	BEND 2
TOTAL				0.29	

Figure D.2: Localized loses

Therefore, the total losses from friction and geometry disturbances are 0.32 m under the currently defined geometry. Which is acceptable ($\leq$1% of the total head).

D.3 Head loss for Alternative 2

In order to obtain an approximation of the pipe length, it is assumed that the pipe is installed over the sand slope within the valmeer and at the lower part of the dike. Then, depending at the depth that the penstock is installed, different pipe lengths will result:

- Bottom of dike (situated at a depth of NAP -14m): 1545 m
- Within the dike (situated at a depth of NAP -10m): 1325 m
- Within the dike (situated at a depth of NAP -5m): 1050 m

In addition to the pipe's length, the diameter and geometry of the pipe will define the total head loss. In this preliminary design, the geometry was considered to have an inlet, two bends and a constriction to pass from the initial diameter to the impeller outlet diameter (see representation below).

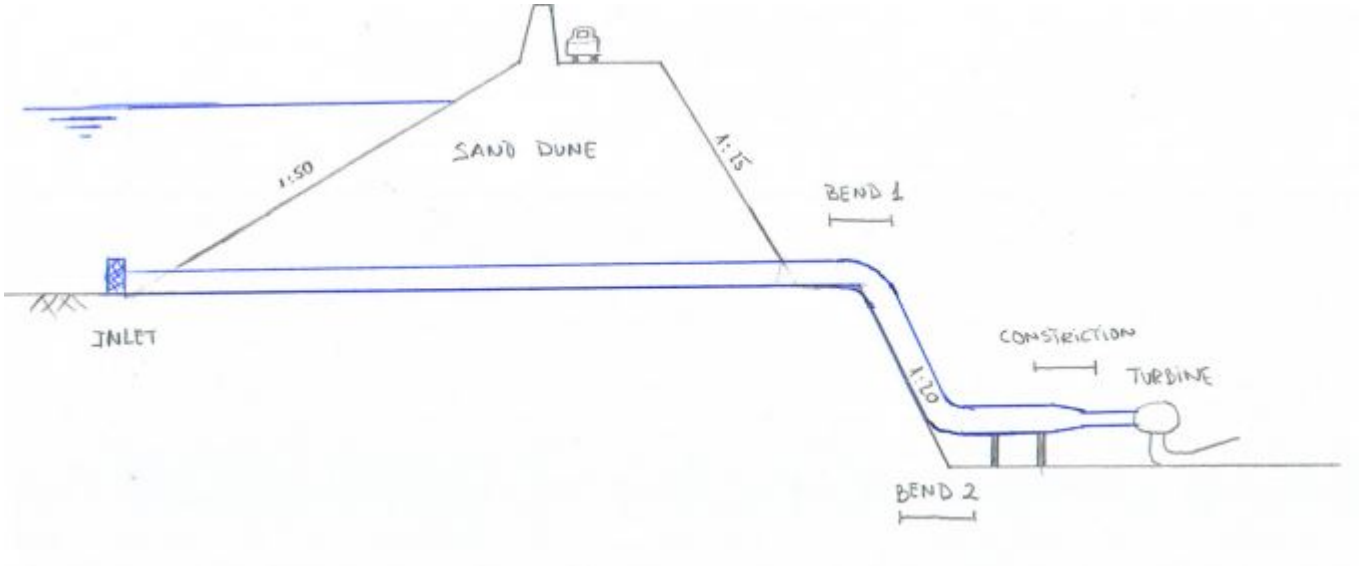

Figure D.3: Representation of the pipe's geometry for Alternative 2

In order to obtain the head losses, the Darcy-Weisbach (see Equation D.1) formulation has been used:

$$h_L = f\frac{L}{D}\frac{v^2}{2g}$$

Where:

- $f = (100 \cdot Re)^{-1/4}$
- $Re = \frac{v*D}{\nu}$

- $\nu = 10^{-6}$ m^2/s
- L [m] = 1545, 1325, 1050
- D [m] = 5
- v [m/s] = 1.4

Giving a loss within the pipe of $h_L = 0.18$m, 0.16m and 0.22m. for the lengths of 1545, 1325 and 1050 respectively. The next step is to calculate the local loses, which are all the same since the diameter chosen is 5m for all pipe lengths. For the geometry present in Figure D.3 and using Equation D.4, the following calculation results:

LOCAL HEAD LOSES					
	factor	element D	velocity within element	Head loss	
element1	0.04	5	1.4	0.00	INLET
element2	0.025	2.5729	5.2	0.03	GRADUAL CONTRACTION LOSS
element3	0.3	5	1.4	0.03	BEND 1
element4	0.3	5	1.4	0.03	BEND 2
TOTAL				0.10	

Figure D.4: Localized loses

Therefore, the total losses from friction and geometry disturbances are 0.28m, 0.25m and 0.22m under the currently defined geometry. Which is acceptable ($\leq$1% of the total head). The main difference against the previous alternative's loses is that in order to provide that 1% head loss value, the pipe's diameter has to be 5m.

D.4 Head loss for Alternative 3

The head loss for Alternative 3 is similar to the one in Alternative 2. The penstock is also buried on the sand dune and it is composed of the same elements as Alternative 2. The only different parameter in both alternatives is pipe's length, but from Alternative 2 to 3 this change is negligible.

D.5 Head loss for final alternative

Finally, the head losses are also obtained. It is clear that head loss is not a stability parameter for the structure, it is only used as a tool to check whether the penstock geometry is acceptable regarding losses or not. As already mentioned in Section D. The head loss within the penstock comes from the Darcy-Weisbach equation (eq. D.1). To obtain the losses, first, the Reynolds number is calculated:

$Re = \frac{1.6*7}{10^{-6}} = 1.09 \times 10^7$

The friction factor can be approximated with the simple Blasius (1911) formula without need of iterating in Moody's chart:

$f = (100 \cdot 1.09 \times 10^7)^{-1/4} = 0.00550$

Finally, the losses within the pipe can be calculated from the Darcy-Weisbach equation:

$h_L = f\frac{100}{7}\frac{1.6^2}{2 \cdot 9.81} = 0.010m = 10cm$

Additionally, the local losses due to the two bends, the constriction and the inlet-/outlet of the structure are calculated from Equation D.4:

$h_L = \sum K_L \cdot \frac{v^2}{2 \cdot g} = \sum(0.04 + 0.025 + 2 \cdot 0.3) \cdot \frac{1.6^2}{2 \cdot 9.81} = 0.25m$

The local losses have a larger contribution that losses inside the penstock, this makes sense due to the relatively low velocity inside the penstock, narrower penstock diameter would give larger inner losses. The total head loss is then: 0.25 m + 0.01 m = 0.26 m. This is an acceptable amount since represents a 2% of the average head difference. This losses are considered acceptable.

Appendix E

Depth of Valmeer basin

E.1 Introduction

This Appendix contains the calculations performed to see down to which point the Valmeer bottom level can be excavated (without any soil improvement method). First, a calculation is shown to check if there will be soil uplift during regular working conditions of the system. Then calculations will show the maximum depth at which the bottom of the dry dock can be. Both for in situ construction method and for prefab method. For the calculations, the soil profile shown in Figure 4.5 is used. The following figure shows the model used for the soil uplift calculations:

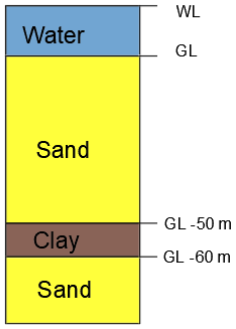

Figure E.1: Model used for soil uplift calculations

E.2 Soil uplift during regular working conditions

Considering that the water pressures for uplift act at the impermeable clay layer and that the ground level and water level are at NAP -14m and NAP +0.25 respectively (average level between high and low tide for average tidal range. See Table 4.1), the maximum excavation depth can be obtained from the equilibrium between the upwards pressure under the clay layer (p_{water}) and the downward pressure from the water, sand and clay weight (p_{weight}). In the following figure, the model used for calculating soil uplift is shown:

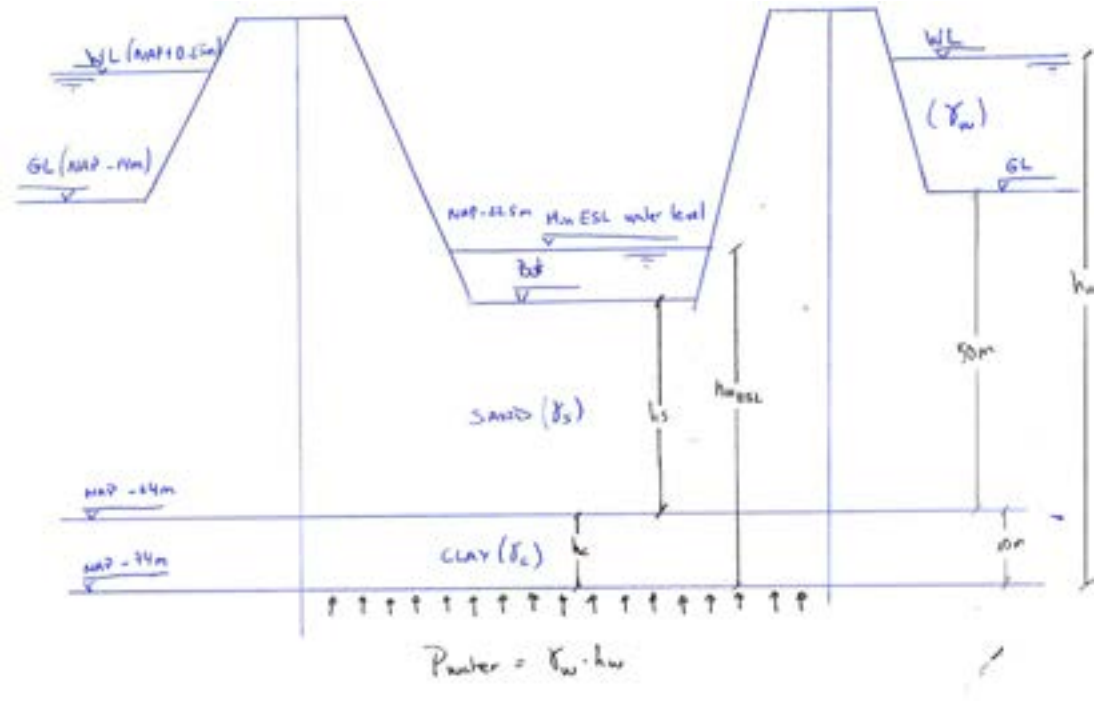

Figure E.2: Model used to obtain maximum excavation depth from pure equilibrium

Where:

- Sand unit weight (γ_s) = 20 kN/m^3
- Clay unit weight (γ_c) = 19 kN/m^3
- Water unit weight (γ_w) = 10 kN/m^3
- Water column (h_w) = 50 + 10 + 14.25 = 74.25 m
- Sand layer thickness (h_s) = 50 - (GL - Bot) = 50 - (-14 - bot)
- Clay layer thickness (h_s) = 10 m
- Water column inside ESL (H_wESL) = -22.5 - (-74) = 51.5 m

To know the calculations are on the safe side, a safety factor of 1.1 will be used. Then, we can solve the equality $1.1 \cdot p_{water} = p_{weight}$ from:

$1.1 \cdot p_{water} = h_w \cdot \gamma_w$

$1.1 \cdot p_{weight} = h_{wESL} \cdot \gamma_w + h_s \cdot (\gamma_s - \gamma_w) + h_c \cdot (\gamma_c - \gamma_w)$

resulting in:

$1.1 \cdot h_w \cdot \gamma_w = h_wESL \cdot \gamma_w + h_s \cdot (\gamma_s - \gamma_w) + h_c \cdot \gamma_c$

$1.1 \cdot 74.25 \cdot 10 = (-22.5 - (-74)) \cdot 10 + (-Bot - (-64)) \cdot (20 - 10) + 10 \cdot (19 - 10)$

$$Bot = NAP\ - 42.8\,m$$

The above calculations show that during regular conditions (water level lowered to a maximum of NAP -22.5 m), the bottom of the basin could be down to NAP -42.8 m. The basin needs to be excavated down to NAP -32m to locate the alternative so for daily conditions, soil uplift won't cause trouble. Lets now check for constructing period, which will be the most critical.

E.3 Maximum excavation depth within a dry dock (in situ method)

Since for dry dock construction method the bottom level needs to be situated at NAP -32 m, the water level needs to be lowered to NAP -32.5 m (the extra 0.5 meters extra will ensure having a dry dock, Hydraulic Structures Manual (2019)). The model used for the calculations is shown in the next figure:

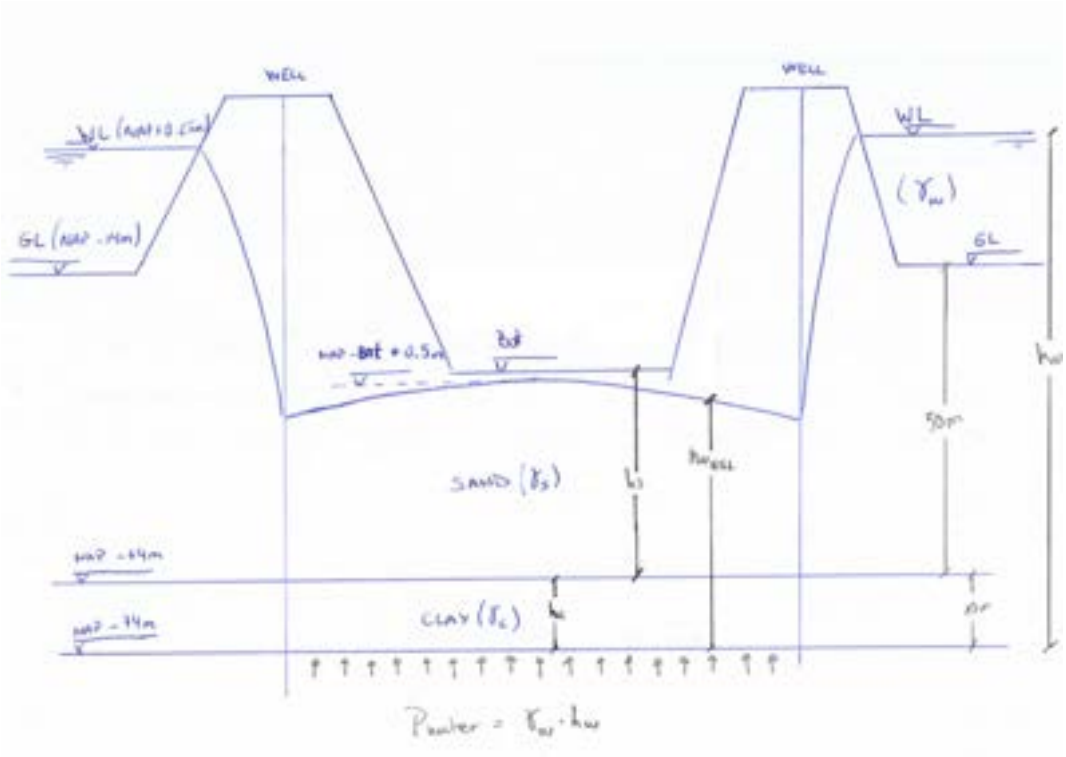

Figure E.3: Model used for soil uplift calculation when dry dock is emptied

Where:

- Sand unit weight (γ_s) = 20 kN/m^3
- Clay unit weight (γ_c) = 19 kN/m^3
- Water unit weight (γ_w) = 10 kN/m^3
- Water column (h_w) = 50 + 10 + 14.25 = 74.25 m
- Sand layer thickness (h_s) = 50 - (GL - Bot) = 50 - (-14 - Bot)
- Clay layer thickness (h_s) = 10 m
- Water column inside ESL (H_wESL) = -(Bot + 0.5) - (-74) = 74 -Bot -0.5

To know the calculations are on the safe side, a safety factor of 1.1 will be used. Then, we can solve the equality $1.1 \cdot p_{water} = p_{weight}$ from:

$1.1 \cdot p_{water} = h_w \cdot \gamma_w$

$1.1 \cdot p_{weight} = h_{wESL} \cdot \gamma_w + h_s \cdot (\gamma_s - \gamma_w) + h_c \cdot (\gamma_c - \gamma_w)$

resulting in:

$1.1 \cdot h_w \cdot \gamma_w = h_wESL \cdot \gamma_w + h_s \cdot (\gamma_s - \gamma_w) + h_c \cdot \gamma_c$

$1.1 \cdot 74.25 \cdot 10 = (74 - Bot - 0.5) \cdot 10 + (-Bot - (-64)) \cdot (20 - 10) + 10 \cdot (19 - 10)$

$$Bot = -32.4mNAP$$

So, according to these calculations, the maximum level the excavation can reach without having soil uplift is NAP -32.4m. As it was mentioned before, the needed excavated depth is NAP -32 m. Thus, soil uplift shouldn't be a problem. On the one hand, it is important to take into account that in these calculations factors such as shear resistance of the soil (which would be an extra resistant load) are not accounted for. On the other hand, the calculations were done for the assumed average soil profile. Having a clay layer not as deep as the one used for these calculations will reduce the safe excavation depth and vice-versa. After all, the excavation to NAP -32 m is assumed to be safe. Extra calculations are recommended to ensure there will be no failure for excavating to this depth (this is not in the scope of this thesis).

Following recommendations of Ir. K.J. Reinders (professor at TU Delft) an excavation like this should be doable. In case soil uplift would be a problem she recommended a segmental construction method, meaning that the bottom can be excavated to NAP -30 m (safe) and then segments to NAP -32m can be excavated and then filled with concrete. In this way, the foundation of the structure could be built without soil uplift problems.

E.4 Maximum excavation depth for the prefab construction method

For the prefab construction method, the soil still needs to be excavated to NAP -32 m in order to place the structure's foundation. However, the elements are floated and then positioned, so the water level stills at NAP + 0.25 m. In the previous section soil uplift calculation was done for a low water level (NAP -32.5) and the safe excavating depth was NAP -32.4m. From this it can be inferred that soil uplift won't be an issue for this construction method. The next equations prove this:
$1.1 \cdot h_w \cdot \gamma_w = h_{wESL} \cdot \gamma_w + h_s \cdot (\gamma_s - \gamma_w) + h_c \cdot \gamma_c$

$1.1 \cdot 74.25 \cdot 10 = (74.25) \cdot 10 + (-Bot - (-64)) \cdot (20 - 10) + 10 \cdot (19 - 10)$

$$Bot = -65.6mNAP$$

Clearly there will not be any soil uplift problems for this alternative.

Appendix F

Waves and wave period inside the Valmeer

F.1 Introduction

In this appendix, the calculations performed to obtain the wave height and period within the Valmeer are shown. These wave heights and periods are obtained from the wind speed and fetch available at the Valmeer.

F.2 Calculations

Wave height, period and direction define the load applied on maritime structures. This information is usually taken from buoys on the sea and then analyzed to obtain design wave heights. However, when building a new structure in a lake/pond, the wave height in the interior of the lake cannot be taken from this buoys. In this case, the wave height can be obtained from the wind speeds generated at the lake/pond area and the available fetch length.

In this report, the wave height within the Valmeer was obtained using the Young and Verhagen (1996a) modified by Breugem and Holthuijsen (2006) formulation. These formulations are used to obtain the dimensionless wave height and peak period.

$$\tilde{H} = \tilde{H}_{\infty}\left[tanh(k_1\tilde{F}^{m_1})\right]^{p} \tag{F.1}$$

$$\tilde{T} = \tilde{T}_{\infty}\left[tanh(k_2\tilde{F}^{m_2})\right]^{q} \tag{F.2}$$

Where:

- Dimensionless fetch, $\tilde{F} = \frac{gF}{U_{10}^2}$
- U_{10}: Wind velocity 10 m above the water surface.
- F: Available fetch length.
- $\tilde{H}_{\infty}$: 0.24
- k_1: 4.14×10^{-4}
- m_1: 0.79
- p: 0.572
- $\tilde{T}_{\infty}$: 7.69
- k_2: 2.77×10^{-7}
- m_2: 1.45
- p: 0.187

This equations are valid for deep water and all sea states (meaning fully developed states - which are unlikely to happen - and transition between states).

After obtaining the dimensionless wave height and wave period, the actual wave height and period can be calculated from:

$$\tilde{H}_{mo} = \frac{gH_{mo}}{U_{10}^2} \tag{F.3}$$

$$\tilde{T}_{peak} = \frac{gT_{peak}}{U_{10}} \tag{F.4}$$

The wind speed values have been obtained from Hydra-NL for a 1/1000 frequency. The wind speed in data point 2 (see Section 4.7) has been used for obtaining wave height within the Valmeer since the point is next to the basin and have the necessary wind direction data (180°). The design wind speed is then 44.1 m/s

The fetch was obtained from the geometries of the existing Valmeer's layout (see Figure 5.1), for Location 1, the distance fetch would go up to 6000 m (see Figure F.1). The wind velocity was taken for the same direction to the perpendicular of the storm surge barrier (See image below). The wind speeds can be observed at Figure 4.11.

Figure F.1: Largest distance for wind wave generation hitting the power plant

Therefore, using the above mentioned values and equations, the wave height and period for the worst case scenario is:

- Location 1: $H_{ESL} = 2.6$ m, $T_{ESL} = 5.2$ s

Appendix G

Overtopping analysis

G.1 Introduction

In this section, the calculations performed to obtain the top levels of the structure at the sea-side and at the Valmeer's side are included. This calculations analyze the overtopping discharges and volumes allowed to take place.

G.2 Calculations

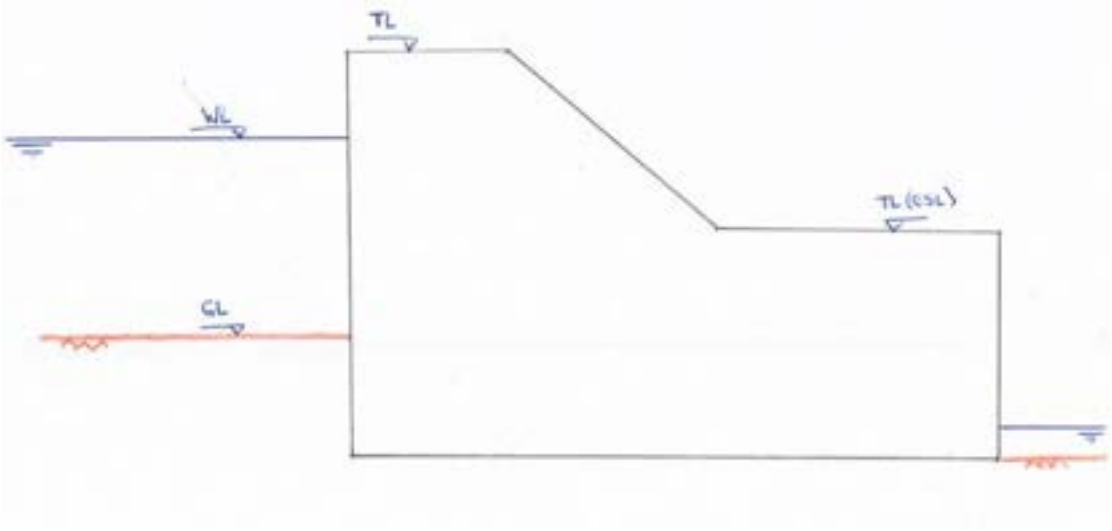

Figure G.1: Sketch showing the top levels of structure at sea-side (TL) and at the ESL's side (TL(ESL)) as so as the ground level

To obtain the top level of the structures, overtopping calculations are performed. In the following figure we can see that two different levels of structure will be obtained. The level at sea-side and the level at Valmeer's side. This last water level will be obtained taking into account that the overtopping will be calculated for storm conditions (see previous Appendix F to see how the design wave height inside the Valmeer is obtained from the expected wind and fetch) and an allowed overtopping discharge of 100 l/s/m. This is chosen because during storm conditions, the overtopping at Valmeer's side will only affect the rear part of the structure and this part will have closed access to vehicles and pedestrians during this conditions. Furthermore, there are not important structural or electrical elements that need to be protected. The water will leave via some trenches that need to be calculated according to this overtopping discharge (this is not part of this thesis). Regarding the top level at sea-side, the following scenarios are taken into consideration:

- SLS overtopping: Regular conditions present and overtopping discharge of 0.3 l/s/m (safe limit for people on top of sea-walls, EurOtop (2018))

- Allowed discharge into the Valmeer: Storm surge conditions and maximum allowed discharge of 500 m^3/s = 181 l/s/m (5% of maximum discharge capacity on pumping mode. It is assumed that if 500 m^3/s of overtopping discharge happens, the discharge coming into the Valmeer will not be a problem for the system, it can be evacuated back to the sea)
- ULS overtopping: Storm surge conditions present and maximum overtopping volume allowed of 8 m^3/m. This maximum overtopping value comes from the following overtopping volumes from the EurOtop (2018):
  - V_{max} between 10 to 20 m^3/m for rubble mound breakwaters; H_{m0} ¿ 5 m, rear side designed for wave overtopping.
  - V_{max} between 5 to 30 m^3/m makes significant damage or sinking of larger yachts; H_{m0} ¿ 5 m.

  Therefore, an amount of 8 m^3/m seems reasonable to avoid structural damage of the plant during storm conditions.

Notice that for well-protected crests and inner slopes in ULS, the EurOtop (2018) recommends using a discharge of 200 l/s/m. Thus, it is reasonable that this discharge is used for the ULS state of the dikes next to the structure (another student is working on this design) and, therefore, to have a similar height (aesthetic reasons), it can be chosen as an overtopping discharge also for the ULS case of the structure. However, the design overtopping discharge for the "allowed discharge into the Valmeer" (181 l/s/m) is smaller than 200 l/s/m. Therefore, this is a more restrictive design condition and it will be used for the structure's and dikes' design. Further analysis to see what will be the maximum discharge allowed into the Valmeer due to overtopping during storm surge conditions is recommended because the current "allowed discharge into the Valmeer" was assumed. For the ULS case of the structure then, the analysis would include overtopping volumes instead of discharges.

First, overtopping is used to get the interior top level and SLS and "allowed discharge" freeboards. According to equation 7.2 of the EurOtop (2018) manual, the overtopping can be calculated from:

$$\frac{q}{\sqrt{g \cdot H_{m0}^3}} = 0.054 \cdot exp\Big[-(2.12 \frac{R_c}{H_{m0}})^{1.3} \Big] \tag{G.1}$$

The above equation depends on overtopping discharge (q), significant wave height (H_{m0}) and freeboard (R_c). Therefore, a freeboard height can be calculated for the overtopping discharge and wave height present at the situations described above.

- TL(ESL): q = 100 l/s/m, H_s = 2.6 m. Then, R_c = 2.1 m
- SLS overtopping: q = 0.3 l/s/m, H_s = 3 m. Then, R_c = 7 m
- Allowed discharge into the Valmeer: q = 181 l/s/m, H_s = 7.9m. Then, R_c = 8.8 m

Second, the maximum overtopping volumes is calculated following the two-steps described in section 7.4.2 "Overtopping volumes at plain vertical walls" of the EurOtop (2018) manual:

The first step is to calculate the number of overtopping waves, this is calculated from the ratio of overtopping waves (N_ow) over incoming waves during a storm (N_w). To calculate this ratio, first we need to see if there are impulsive or non-impulsive wave conditions. $[h^2/(H_{m0} \cdot L_{m-1,0})]$ ¿ represents non-impulsive conditions. For the present case:

$[h^2/(H_{m0} \cdot L_{m-1,0})] = [14^2/(7.9 \cdot 123)] = 0.202$

So, impulsive conditions are present. Therefore, the ratio N_ow/N_w can be calculated using equation 7.25 of the EurOtop (2018) manual. IN the calculation below, a freeboard (R_c) of 7.9 meters is considered:

$N_{ow}/N_o = max\Big[\exp -1.21(R_c/H_{m0})^2; \quad 0.024 \cdot (h^2/(H_{m0} \cdot L_{m-1,0}) \cdot R_c/H_{m0})^{-1} \Big] = max\Big[\exp -1.21(7.9/7.9)^2; \quad 0.024 \cdot (14^2/(7.9 \cdot 123) \cdot 7.9/7.9)^{-1} \Big] = max\Big[0.30; \quad 0.12 \Big] = 0.30$

This means that a 30% of the incoming waves are overtopping waves. The total of incoming waves is calculated assuming a storm duration of 6 hours (remember that the wave period for a H_{m0} = 7.9 m is 11.3 s): N_w = 6*3600/11.3 = 1912 waves. Therefore the number of overtopping waves is N_{ow} = 570.

The second and last step is to obtain the maximum wave volume considering that the individual wave volumes follow a two-parameter Weibull distribution:

$P_v = 1 - \exp -(\frac{V}{a})^b$

To obtain V_max equation 7.27 of the EurOtop manual is applied. "a" follows from Figure 5.57 having a value of 0.91 and "b" is given by EA (1999) and Pearson et al (2002). Having a value of 0.85 for impulsive conditions.

$V_{max} = a(lnN_{ow})^{1/b} = 0.91(ln1912)^{1/0.85} = 8.00 \quad m^3/m$

Thus, it is shown that for a freeboard of 7.9 m, the maximum overtopping volume is of 8 m^3/m.

Then, the largest freeboard height happens for the "allowed discharge" situation and it is 8.8 meters, when added up to the water level of NAP + 4.5 m, gives a total top level of NAP + 13.3 m. Notice that the ULS situation gives a freeboard of 7 meters, but that should be added to the ULS water level situated at NAP +0.25 m.

Inside the Valmeer, the level of the structure should be at 2.1 meters over NAP -5m. Thus, TL(ESL) = NAP -2.9 m

In the following table, the summary of the final parameters used for obtaining TL and TL(ESL) are shown together with the final level at which the structure has to be built.

	Location 1	
	Sea-side	ESL's side
Design water level (NAP + m)	4.5	-5
Wave height (m)	7.9	2.6
Wave attack angle (degrees)	0	0
Top of structure (NAP + m)	TL = 13.3	TL (ESL) = -2.9

Table G.1: Structure's top levels after performing overtopping analysis

COMMENT ON OVERTOPPING CALCULATIONS:

This calculations are rather conservative since only a deterministic approach has been done. It is recommended to do an analysis taking into account wave data from buoys close to the construction site (or wave data at the position of the structure, obtained after propagation of the wave data from a further buoy). Then, create a script in which the freeboard is a variable, therefore the overtopping discharge can be obtained for each wave height (depending on the selected freeboard). Range all the obtained discharges and obtain the one with a return period of 4200 years (as mentioned in the boundary conditions). If the overtopping discharge for that return period is the same or slightly under the maximum allowed, then the adequate freeboard has been obtained. Notice that to do this the wave data needs to be corrected for climate change. With this (simple) probabilistic analysis the top levels of the structure will be obtained with more accuracy.

Appendix H

Advantages and disadvantages of the different alternatives considered for design

H.1 Introduction

In the present appendix, the information used for executing the MCA is presented.

The different categories that will be analyzed are:

- Overall dimensions
- Construction docks (temporary works)
- Construction method
- Best alternative regarding head loss
- Life span
- Reliability/availability of flood defense gates
- Construction time
- Construction costs

Then for each category and alternative, the advantages and disadvantages will be exposed. In the following sections, a brief explanation about what's included in each category is given to then point out each alternative's pros and cons.

H.2 Dimensions

Dimensions refer to the overall dimensions of the civil work. Also the dimensions of the powerhouse are compared for different alternatives. The assumption is that larger dimensions mean larger costs (larger dry-dock, more material used, longer construction time).

- Alternative 1: Largest concrete structure of them all. The own structure has to be stable on its own. It takes all the sea loads. It's length is around 85 meters. However, if overall dimensions are compared, this alternative is the smallest one.
- Alternative 2: Smaller power plant of them all. Only stands within the Valmeer, not having to resist water head differences. The largest load is the hydraulic load. Second most important load is the wind waves generated inside the Valmeer. However, a part from the power house, an abutment containing the main gates needs to be constructed at the sea-side which will increase overall dimensions. Still, this alternative is the smaller of all if we don't consider the dike (which is part of the Valmeer's ring dike).

- Alternative 3: The powerhouseis larger than Alternative 2 and smaller than Alternative 1. This is because in the one hand, the loads present for Alternative 2 are present. Plus, the power plant acts as a retaining wall. On the other hand, the hydrostatic and wave loads are assumed to be taken and dissipated by the dike. Additionally if the abutment dimensions are also considered, the total amount of concrete used is similar to the one in Alternative 1. The overall dimensions of the whole system of dam+power plant is very large. As for Alternative 2 the dike is not considered part of the alternative, Alternative 3 is the one with largest overall dimensions.

H.3 Construction docks

Construction docks will be needed for all alternatives. For the in situ alternative its use is obvious, the alternative will be built on the dry at its final position. For the prefab alternatives they will be used to construct the structure's elements to then flood them and tow the elements to its final position. It is important to mention that the prefab dry dock will depend of the construction sequence. In general terms, the dry dock for in situ construction method will be larger than the dry dock for prefab construction method.

In the present analysis, the construction dock is analyzed looking at its two main design parameters: The size and the depth at which it needs to be excavated. In the lines below this is further explained. Notice that the dry dock dimensions are interior dry dock dimensions (i.e. space needed for construction of the elements). It is done this way because the dikes around the building pit are not object of study and therefore their width is unknown. For the material use estimations an assumption of slope 1/10 for the seaside and 1/5 for the interior side is done.

H.3.1 Construction dock's size

The size of the construction dock is important for calculating the amount of water that will be infiltrated within the dock. The larger the dock, the more pumps and wells will be needed to keep the dock dry. First, regarding **in situ** construction method we have the following:

- Alternative 1 (2800 m x 125 m): Similar to Alternative 2.
- Alternative 2 (2800 m x 80 m + 2800 m x 40 m): Not much smaller than the one for Alternative 1. Nevertheless two dry docks (one at each side of the dike) will be needed. It is preferable to build just one dry dock than 2.
- Alternative 3 (2800 m x 220 m): Construction dock is in the order of two times larger. This involves more infiltration, so more wells and pumps needed as so as longer building time and construction costs.

Second, for the **prefab** method the size of the dock goes in accordance with the powerhousedimensions mentioned in Section H.2. The dimensions of the dry docks were obtained assuming that all the elements were constructed in a dry dock and then floated to position, i.e. no gates are installed in the dry docks, so once they are emptied with water, they water can't be pumped out again:

- Alternative 1 (880 m x 890 m)
- Alternative 2 (880 m x 740 m)
- Alternative 3 (880 m x 900 m)

The construction docks for Alternative 1 and 3 have similar dimensions (since the amount of concrete to be used is similar) and the dock for Alternative 2 can be smaller since the power plant will be the smaller of all. In general terms however, for prefab method the dry docks can have similar dimensions for all alternatives.

H.3.2 Construction dock's depth

The construction dock depth is limited by soil uplift (see Appendix E). However, the depth also influences piping at the dikes forming the dock and infiltration. The deeper the dock the larger head difference and therefore the more water infiltration in the dock. More infiltration means more wells and pumps and thus more costs and complications.

The depth of dock excavation only depends on the construction method used. For in situ construction, since the alternative its built at its final position, the dry dock's base must be at NAP -34 m. Whereas for the prefab method, the dry dock has to be deep enough to float the caissons inside. Therefore, the bottom of the dock will be at NAP -19 m. The largest caissons have a draught of 18 m.

H.4 Construction method

For each Alternative 2 construction methods are considered: in situ and prefab. In this section the focus will be on the general complications that may arise when building each alternative rather than accurately explaining how each alternative will be built. Due to time limitations this will be done for the alternatives that passed the first loop of functional design (see Appendix I). The aspects of construction that will be analyzed are the following ones:

- General characteristics of building in situ vs prefab.
- Elements transportation.
- Elements connection. Also the connection at the abutments will be considered.
- Necessity for special machinery.
- Penstock installation method.
- Fill material considerations.

In the following page, a table comparing the different alternatives is given. Notice that for the comparison, plus and minus symbols were used. Their meaning is as follows:

- Plus (+): This symbol indicates a positive characteristic.
- Minus (-): This symbol indicated a negative characteristic.
- Plus/Minus (+/-): This symbol indicates a neutral characteristic

There can be some very positive or negative characteristics, this will be noted with a double symbol (++ or –). To facilitate the visualization of which alternative has more positive characteristics than other, the positive characteristics have been colored with green color and the negative with red color. Neutral is black.

Criteria for construction method	1 Construction is flood defense (independently stable)				2 Construction does not form the flood defense (the dam does)				3 Construction forms flood defense in combination with the dam (stabil only i.c.w. dam)			
	1a In situ		1b Prefab		2a In situ		2b Prefab		3a In situ		3b Prefab	
General characteristics of building in situ vs prefab	Controled environment in dry construction dock. Foundation is done over the sand bed in situ which eases the work as so as the machinery used.	+	Precise preperation of the foundation surface (small tollarances). Avoid soil accretion in the bed after dredging.	-	Controled environment in dry construction dock. Foundation is done over the sand bed in situ which eases the work as so as the machinery used.	+	Precise preperation of the foundation surface (small tollarances). Avoid soil accretion in the bed after dredging.	-	Controled environment in dry construction dock. Foundation is done over the sand bed in situ which eases the work as so as the machinery used.	+	Precise preperation of the foundation surface (small tollarances). Avoid soil accretion in the bed after dredging.	-
Elements transportation	No floating nor transport of elements once constructed	+	Complex maneuvering of the elements. Top caisson has to be floated with a freeboard of 5 m for positioning on top of bottom caisson. Favourable weather conditions needed. Temporary dock can be constructed next to final structure's position. Towing distance is minimal. Situated within the Valmeer to avoid dredging an access channel form dock to construction site.	+/-	No floating nor transport of elements once constructed	+	Complex maneuvering of the elements. Favourable weather coditions needed. Temporary dock can be constructed next to final structure's position. Towing distance is minimal. Situated within the Valmeer to avoid dredging an access channel form dock to construction site.	+/-	No floating nor transport of elements once constructed	+	Complex maneuvering of the elements. Favourable weather coditions needed. Temporary dock can be constructed next to final structure's position. Towing distance is minimal. Situated within the Valmeer to avoid dredging an access channel form dock to construction site.	+/-
Elements connection. Including connection to abutments	No elements connection needed. Power plant part of a large block	+	Difficult connection between the elements (both horizontal an vertical). Largest elements to position from all alternatives.	-	No elements connection needed. Power plant part of a large block	+	Connection between elements less critical than alternative 1b since power plant is smaller and horizontal joints don't need to be waterproof. In case there are vertical joints these need to be waterproof and the connection between elements to the penstock allows for tiny tolerances	+\-	No elements connection needed. Power plant part of a large block	+	Difficult connection between the elements (both horizontal and vertical) mainly because apart from the power plant, the abutment and penstock need to be positioned and connected to each other. Tolerances are critical for this positioning	-
Necessity for special machinery	No specific machinery needed	+	Specific machinery needed to transport and position elements	-	Specific machinery needed to pass the penstock throught the sand dune. Very difficult operation.	- -	Specific machinery needed to transport and position elements	-	No specific machinery needed	+	Specific machinery needed to transport and position elements	-
Penstock installation method	Penstock is installed within the concrete structure so it is founded completely on concrete	+	Penstock is installed within the concrete structure so it is founded completely on concrete	+	Penstock needs special foundations when out of the power plant. It is founded on sand. However, in situ construction eases this	-	Special foudation has to be placed before the penstock is installed. Tolerances are critical. Very complicated penstock installation.	- -	Penstock needs special foundations when out of the power plant. It is founded on sand. However, in situ construction eases this	-	Special foudation has to be placed before the penstock is installed. Tolerances are critical. Very complicated penstock installation	- -
Fill material (as part of the sand dune included as an element of the construction) considerations	No fill material needed.	+	No fill material needed.	+	No fill material needed. Sand dune is already in position when the power plant is constructed	+	No fill material needed. Sand dune is already in position when the power plant is constructed	+	Filling material needs to be carefully place to not damage the penstock and other elements	-	Filling material needs to be carefully place to not damage the penstock and other elements. Besides, in open waters this operation is riski since water currents can take the fill particles away from its position	- -

H.5 Best alternative regarding head loss

Power generation depends mainly on water head difference available and head losses during transport of water. Since the water head difference is constant for all alternatives, the focus will be on head losses. These losses can come from having a large penstock length, bends at the pipe, small sections (with large fluid velocity) and inlet/outlet geometries. The most relevant aspects for comparison between alternatives are: penstock's length and inlet/outlet geometry. The penstock is largest for both Alternative 2 and 3, however increasing the length doesn't affect as much as the losses in the inlet to the power plant (see sections D, D.2 and D.3) .

For Alternative 1, both for in situ and prefab methods, the inlet design can be accurately done. For Alternative 2 and 3, a similar situation applies since the inlet is constructed in the abutment. However there are more limitations for geometry at the abutments. Greater losses will be expected for alternatives 2 and 3.

H.6 Lifespan

The materials used for building the power plants are the same, so lifetimes of the materials can be assumed identical. However, ensuring maintenance of the most of the elements is crucial for enlarging the service life of the structure. Therefore, the most accessible alternative regarding maintenance the better. In this matter, Alternative 1 is way more favourable than the other two alternatives. First, Alternative 1 is more compact than the other alternative and has all the elements closer positioned one to another. This eases the maintenance labour . Second, not having a large penstock under a dike is way more favourable for maintenance purposes.

H.7 Availability of flood defense gates

This section has been looked at because of the literature reviewed on the Eastern Schedlt barrier. In this project, the gates are mounted in two independent pillars and over a sill beam. Differential settlements that go over the tolerances could make the gate's to not close (see Figure H.1). However, in the present project the gates will always close.

Figure H.1: Settlements affection to closing operation for the Eastern Scheldt barrier.

Alternative 1 has attached the gates, pillars and sill beam to the main structure (see Figure H.2), so differential settlements will not affect the closing operation. The same happens for alternatives 2 and 3 since the gates' structure is constructed on continuous abutments.

Figure H.2: Settlements affection to closing operation for the Alternative 1.

H.8 Construction time

Construction time affects costs, the larger you take, the more expensive it is. Equipment and human labor are paid by the hour so this is something that needs to be reduced at maximum.

The aim of this thesis is not to calculate exactly how much time takes to build an alternative nor trying to reduce it. However, it is important to get a feeling about which alternatives would take longer time to be constructed. The aspects that where analyzed are the following:

- Dry dock dimensions: the larger and the deeper the dry dock the more time its construction will take.
- Transportation of elements: For in situ construction there is no transport of the structure since it is built in place. However, this extra time needs to be accounted for for in situ method. The elements need to be transported from the dry dock to their final position.
- Repetition factor: A high repetition factor will be translated into lower man-hours (van der Hoorst, 2016).

In the following table, the issues regarding construction time are shown:

Criteria for construction time	1 Construction is flood defense (independently stable)				2 Construction does not form the flood defense (the dam does)				3 Construction forms flood defense in combination with the dam (stabil only i.c.w.			
	1a In situ		1b Prefab		2a In situ		2b Prefab		3a In situ		3b Prefab	
Dock's size	Area: 2800 m x 125 m = 350.000 m2 Bottom: NAP -34 m	-	880 m x 890 m = 783.200 m2 Bottom: NAP -19 m	+	2800 m x 80 m + 2800 m x 40 m = 336.000 m2 Bottom: NAP -34 m	-	880 m x 740 m = 651.200 m2 Bottom: NAP -19 m	+	2800 m x 220 m = 616.000 m2 Bottom: NAP -34 m	-	880 m x 900 m = 792.000 m2 Bottom: NAP -19 m	+
Transportation of elements needed?	No elements transportation and placing	+	Elements need to be transported. Not many elements in comparison with alternatives 2 and 3 (2 x 56)	+\-	No elements transportation and placing	+	Elements need to be transported. More elements than for alternative 1 (3 x 56)	-	No elements transportation and placing	+	Elements need to be transported. More elements than for alternative 1 (3 x 56)	-
Amount of different elements	No different elemens to be constructed as for alternatives 1 and 2. Repetition factor is large.	+	Repetition factor is high since there are 56 identical caissons. Only two caissons types.	+	4 different elements (in-/putlet abutment, power plant, penstock and sand fill).	-	Repetition factor is high since there are 56 identical caissons. Three types of caissons. Power plant caisson smaller than the ones for alternative 1	+\-	4 different elements (in-/putlet abutment, power plant, penstock and sand fill)	-	Repetition factor is high since there are 56 identical caissons. Three types of caissons. Power plant caisson smaller than the ones for alternative 1 and larger than alternative 2	-

H.9 Costs

Costs are the most deciding factor when building a civil work. Sometimes it is combined with MCA in order to perform a cost/value analysis. For this project, a cost estimation good enough for comparison between alternatives would require lots of time. So costs calculation won't be included. However, the most deciding factors regarding costs are shown in this section. This information will be used to assess which alternatives can be more expensive in comparison with each other.

For looking at costs, the following table has been used:

Criteria for construction costs	1 Construction is flood defense (independently stable)		2 Construction does not form the flood defense (the dam does)		3 Construction forms flood defense in combination with the dam (stabil only i.c.w.	
	1a In situ	1b Prefab	2a In situ	2b Prefab	3a In situ	3b Prefab
Expensive	Building pit + dewater system	Special towing and positioning vessels; Foundation done by special vessel.	Building pit + dewater system. Double than alternative 1 since size is tripled; special penstock foundation; Boring penstock through sand dune;	Special towing and positioning vessels; Foundation done by special vessel. More elements than for alternative 1	Building pit + dewater system. Double than alternative 1 since size is tripled; special penstock foundation;	Special towing and positioning vessels; Foundation done by special vessel. More elements than for alternative 1.
Cheap	In situ construction; No floating nor elements transportation; No special foundation for penstock;	Fast elements construction in dry dock; Smaller building pit.	In situ construction; No floating nor elements transportation; No fill material needed.	Fast elements construction in dry dock; Smaller building pit. More elements involved though.	In situ construction; No floating nor elements transportation;	Fast elements construction in dry dock; Smaller building pit. More elements involved though.

Appendix I

Extended construction method for Alternative 1. Both in situ and prefab construction methods

I.1 Introduction

At this appendix, the reader can find the extended construction methods used for constructing the following alternatives:

- Alternative 1, in situ method
- Alternative 1, prefab method

All this information will be used to develop the MCA in the second loop of Chapter 6 (Functional design). The different construction methods are shown below.

I.2 In situ construction method

This method is used to construct a dry environment. The idea is to construct a permeable water barrier to then dry the inside of the basin and work there in dry conditions. Previous structures were already built in the dry using impermeable dikes as barriers. For instance, the Haringvlietdam was built in a building pit surrounded by dikes made out of coal waste. This material was able to resist the current velocities and was a good base for then placing sand on top. However, the wash from the waves caused fairly gentle slopes (Deltadienst of Rijkswaterstaat, 1973).

Figure I.1: Plan view of the building pit used to construct the Haringvlietdam

First, a list containing the main construction sequence is shown below. Afterward, a further description of the construction methods is given. Drawings of the construction sequence are shown in Section 7.1

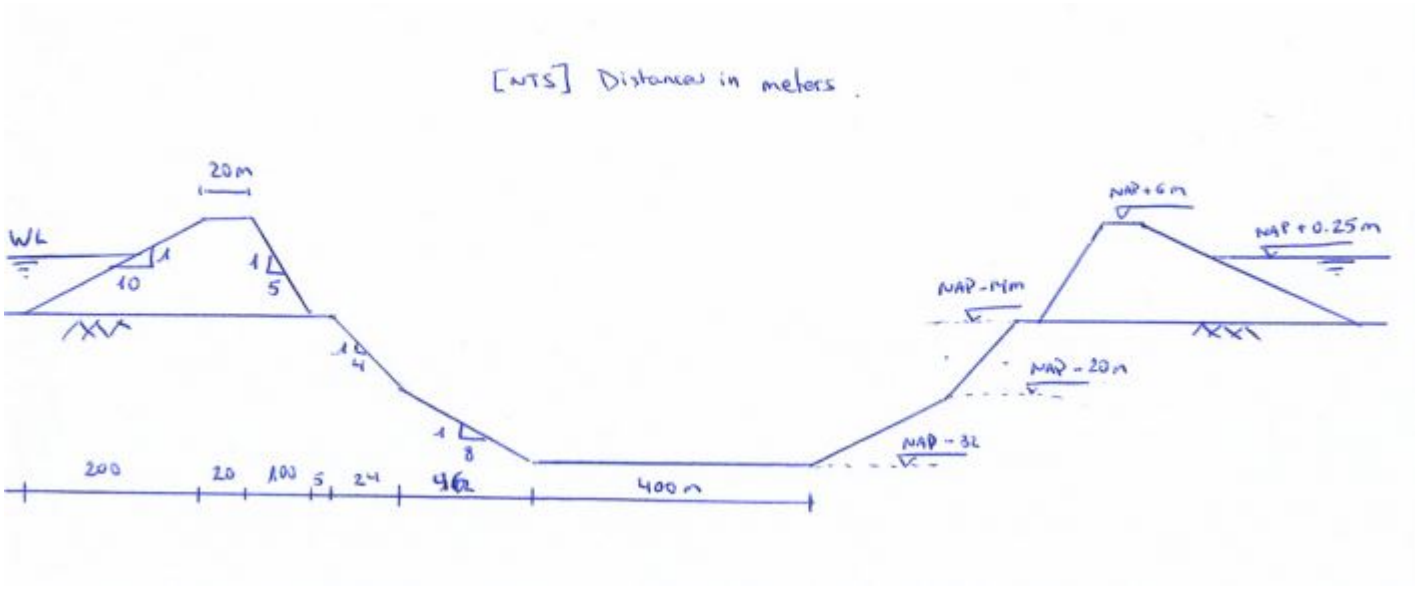

Figure I.2: Caption

1. (Temporary) access roads construction.
2. Dry dock construction.
   (a) Dredging + dike formation
   (b) Installation of seepage reduction screens
   (c) Wells installation and dewatering
3. Piping protection installation. 1^{st} extension.
4. Power plant construction in situ (Concrete works)
5. Gates installation and sand refill next to the plant and bed protection installation at both sides of the plant
6. Main gates installation and disassembly of dry dock
7. Extension of the rest of the piping protection (final positioning towards Valmeer side)
8. Road deck installation
9. works finalization

The works begin with the dry dock construction. The dock's interior dimensions will be 2800 m x 125 m (350.000 m^2). The dike will be constructed with the sand removed from the interior of the pit. The dock will be dredged using trailing suction hopper dredgers which will allow for both excavation and deposition of the dredged sand to build the dikes. It is estimated that a total of 10.607.000 m^3 of sand will be dredged and a total of 22.780.000 m^3 of sand will be needed for the dikes. Giving a sand deficit of 7.200.000 m^3 of sand that will need to be taken from the sea or from the inside of the Valmeer (not object of this thesis to indicate where to get this sand from). The assumed dredging and dikes' geometries are shown below:

Once the dikes are constructed, the wells can be installed to keep the water level below NAP -34.5 m. Additionally, to pump out the water within the dock, large pumps will be needed. There will be pumps placed on every well (perspomp in dutch terminology). From a simple Darcy's law calculation, and assuming that the material in the area is sand with a permeability of 10^{-4}, the amount of water that will be infiltrated in the dry dock is 6115 m^3/h (1.70 m^3/s). This discharge can be provided with 153 40 m^3/h wells (installed every 44 meters) or with 61 100 m^3/h wells (installed every 110 meters). Additionally to the water infiltration, the wells must evacuate the expected rainwater. It is been proved that the dewatering of the pit should be possible. However, further research is recommended to look for other methods for dewatering or reduce the

water infiltration discharge into the dock (for instance, by making more impermeable dock's dikes).

Meanwhile, the dock is being pumped out, access roads will be built to bring all the necessary machinery and materials to carry on the construction of the structure in the dry.

When the dry dock has no water, the first step is to extend the power plant's piping protection. As its length is circa 250 m, and the bottom width of the dry dock is 125 meters, only a first installation will be done. The rest will be installed after the structure is finished. This will not be a problem if the rest of the piping protection is installed with a water level of NAP -5m in the Valmeer. This is because then, the piping distance will be circa 75m, so the structure itself will avoid piping.

Now it is time to erect the power plant. Construction will start from the foundation. The foundation is a shallow foundation that will be installed over the sand bed. Preliminary calculations show that the bearing capacity of the sand (assumed to be 400 $kN/m^2/m$, Hydraulic Structures Manual (2018)) is enough to support the weight of the structure ($\approx$ 250 $kN/m^2/m$). From there, the structure will be erected taking into account the following phases (See Chapter 7 for a graphical representation of the construction method):

1. Erection of the concrete volute pump caisson in which the turbines will be installed. This includes the FSI, draft tube. and the room where a maintenance horizontal gate will be installed.
2. Penstock supporting element: this structure will be used to later build the penstock on top of it
3. Erection of vertical walls.
4. Penstock construction: Using steel profiles and reinforced concrete, the penstock is built. It can also be prefabricated and then situated over the supporting structure. However, in this case, the placing tolerances are minimum.
5. Room for spherical valve. A space to install and maintain this valve will be constructed.
6. Shaft room. The space to install the shaft that connects the turbine to the generator will be built. The generator will be fitted in this room.
7. Sea-side inlet structure: This inlet structure will provide a space so that water enters from the sea to the penstock. This inlet structure will be surrounded by a rubber profile that will ensure water tightness when the main gate is closed.
8. Pier for cylinders. The piers where the cylinders are going to be installed are erected after the inlet is finished.
9. Powerhouse construction. The powerhouse is constructed over the shaft room. Inside, most of the elements needed to open/close all gates are situated. A so as a traveling crane that will be used for maintenance of the turbines and generators.
10. Road. The access road will be constructed on top of the structure. This access road will allow public and staff traffic on it. It will be prefabricated and transported to position using cranes from within the building pit.
11. Main gate's installation. The main gates will be installed at its position. Then, the cylinders will also be installed and attached to the gate. These elements will be installed from the road previously positioned.
12. Finishing works. The necessary works for finishing the structure will be done. Painting, lights, alarms, sidewalks, connection of the road with powerhouse, bed protection, etc.

After the powerhouse construction is done (step 9 above), the bed protection will be installed. This bed protection comprises the rocks needed to avoid soil erosion at the inlets/outlets. Filter layers will be installed so that the sand under the bed protection don't pass through the bed protection.

Afterward, the building pit will be cleaned up so that the water can be let in.

The following step is then breaching the dry dock to let water within it. This operation needs to be done once the Valmeer dikes are finished. In this way, the water level inside the Valmeer can be kept at NAP -5 m and piping under the structure is avoided. The water levels then will be at NAP -5 m at Valmeer-side and NAP

+0.25 at sea-side.

To install the rest of the piping protection, a new dredging has to be done. The sand can be momentarily placed next to the dredging area so that later can be put back into position. Now there will not be a risk of uplift since the water levels are high. This dredging will be done down to NAP -34m. The new piping protection is laid over the previously installed one. Once in position, the previously dredged sand is put back into position.

Other methods for constructing a dry dock such as the cellular sheet piles use were developed in the past. In the following picture we can see an example of the use of this technique to build the Olmsted Locks and Dam:

Figure I.3: Cellular sheet pile building pit for the construction of the Olmsted Locks and Dam

It is important to notice that due to the large water level difference (around 34 meters during construction), this method will require the installation of a huge cellular/double sheet pile. Thus requiring large sheet pile lengths (larger than 50 m). That is why this cellular method has not been considered.

I.3 Floating caisson construction method

This method consists of constructing parts of the structure in a dry-dock, or inland, and then transporting them to its final position. This method was already used to build the piers of the Eastern Scheldt Barrier. These were built in different dry docks that were flooded once finished. Afterward, the piers had to be tugged into position and lowered on the seabed carefully.

Figure I.4: Eastern Scheldt construction yards. One compartment flooded.

For the present project, it has been estimated that a total of 56 (50 m x 84 m x 18.4 m) elements will be constructed to place on top of the seabed (These will be called "bottom caissons"). On top of these elements, other 56 (50 m x 84 m x 18.1 m) elements will be placed (These will be called "top caissons"). This will provide a dry area where the different necessary elements of the power plant will be built/transported. After the two elements are positioned, the rest of the structure can be finished in situ. The construction steps for this method are explained in the following bullet points. Then, the specifics of the method will be further explained.

1. (Temporary) access roads construction.
2. Dry dock construction.
   (a) Dredging + dike formation
   (b) Wells installation and dewatering
3. Bottom caisson construction
4. Bed preparation for positioning bottom caisson
5. Bottom caisson towing and positioning
6. Top caisson construction
7. Top caisson positioning
8. Bed protection installation and sand fill around structure (where needed)
9. Construction access roads to structure
10. In situ construction of the rest of the structure and elements
11. Works finalization

In the following lines, a more extended explanation of each phase is given.

As for the in situ method, dry docks need to be built. In this case to prefabricate the caisson elements. For the present project the next layout has been selected:

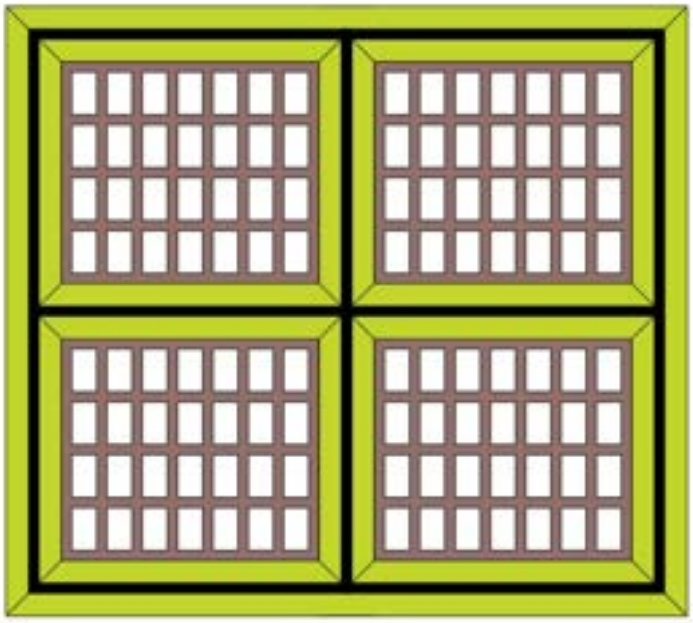

Figure I.5: Different compartments for elements construction

Twenty-six bottom caissons will be constructed in one compartment. Once they are finished, the dock will be filled with water and the elements will be towed to its position. Then, in another compartment, the top caissons are being built. These are transported to position once the previous bottom caissons are properly placed. The same applies for the other two compartments.

To build the dry dock, the same technique explained for the in situ construction method is used (see Section I.2). The only difference is that this dock will only be excavated to NAP -19 m since the caissons will have a draught of around 18 meters. The interior dimensions of each compartment are of 510 m x 440 m (224400 m^2) if we want to construct 7 x 4 segments at once. This allows having a distance of 20 m between different elements and between the elements and the dike. For a total of 4 compartments, the total area needed to construct the elements is 4 $\times$ 224400 m^2 = 893.600 m^2. This is a huge dry dock. In comparison with the one needed for the in situ construction method this dock is (893.600 m^2 / 350.000 m^2) 2.5 times bigger than the dock for in situ construction. However, these dimensions can change according to the construction technique used. If, for instance, the dry dock area is reduced by four (see Figure I.6), so that the prefab dry dock is smaller than the in situ one, some gates must be installed in the dry dock so that this can allow for controlled fill and empty operation. This is not a simple operation taking into account the with of the dikes (circa 320 m) If only two compartments are left, the 16 first bottom caisson elements will be built, then the compartment is flooded and the caissons towed into position. Meanwhile, in the other compartment, the top caissons are constructed. After all the bottom caissons are towed out the compartment, the gates can be closed and the water is then pumped out. This will allow us to construct another batch of elements (3 batches of 16 elements and one of 8 are needed in total). The same happens for the compartment of the top caissons. In this way, the individual interior dry dock dimensions can be reduced to 370 m x 335 m. Now the dry dock for in situ method is (350.000 m^2 / 247.900 m^2) 1.4 times larger than the one used for prefab construction method.

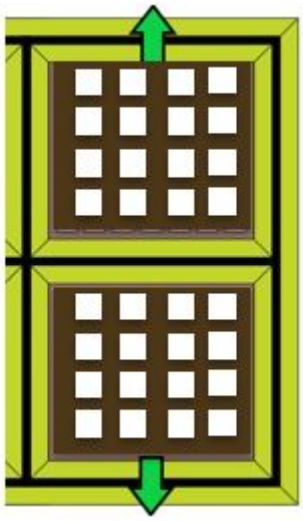

Figure I.6: Different compartments for elements construction. Dry dock needs to have gates (represented by green arrows).

Within the dry dock, both bottom and top caissons will be built. In the following lines, the geometry of the caissons is defined. These caissons' stability is ensured while floating, being transported and when positioned. This can be checked in Appendix J

The bottom caisson's geometry is shown in the figures below. In these figures, the reader can see a 3D representation of the caissons without the lid (for a better understanding of the caisson's shape) together with the sections performed. Section 1 is a vertical section through line 1 (ZX plane in figure J.10). Section 2 is a vertical section through line 2 (ZY plane in figure J.10). Section 3 is a horizontal section through line 3 (XY plane in figure J.10).

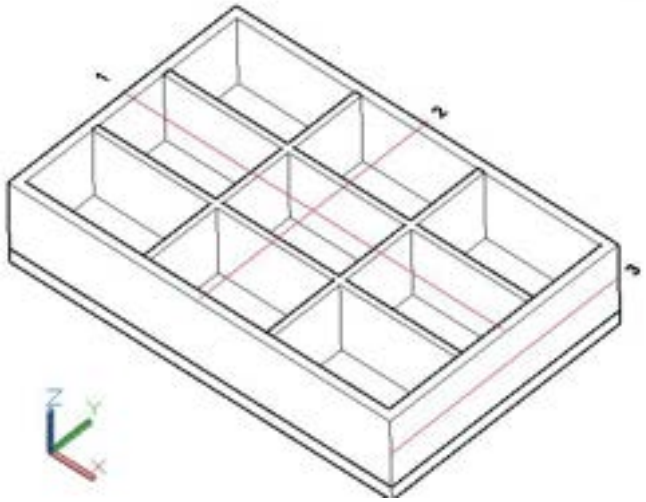

Figure I.7: 3D view of the bottom caisson. Notice that the top lid is not represented here.

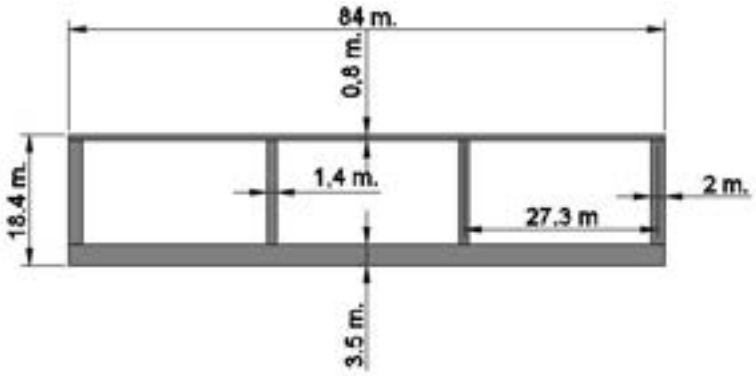

Figure I.8: Section 1 from figure J.10

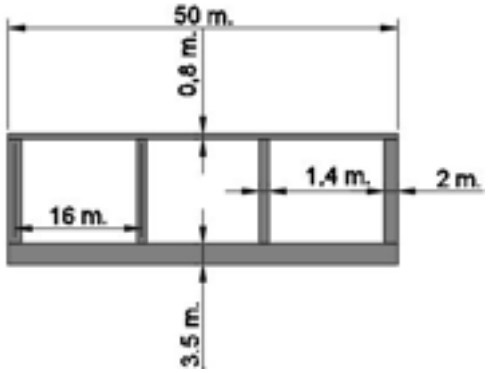

Figure I.9: Section 2 from figure J.10

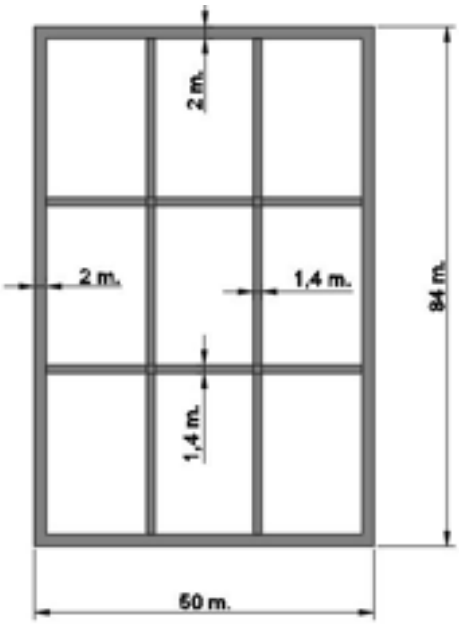

Figure I.10: Section 3 from figure J.10

The element's draught is 18 m (0.4 m freeboard). The necessary ballast water volume to safely lower the element is 29000 m^3.

The top caisson's geometry is shown in the figures below. In these figures, the reader can see a 3D representation of the caissons without the lid (for a better understanding of the caisson's shape) together with the sections

performed. Section 4 is a vertical section through line 4 (ZX plane in figure J.10). Section 5 is a vertical section through line 5 (ZY plane in figure J.10). Section 6 is a horizontal section through line 6 (XY plane in figure J.10).

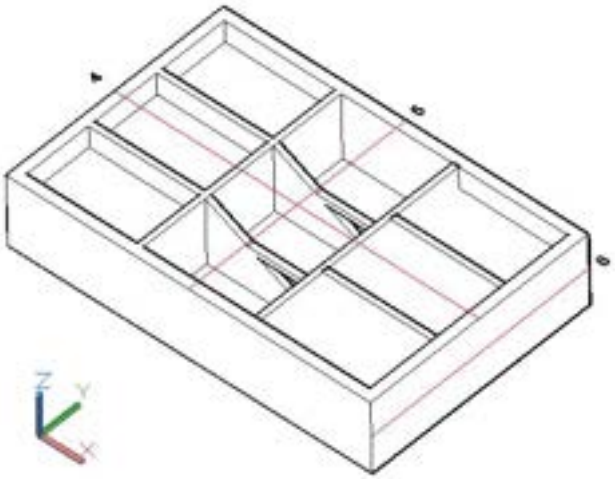

Figure I.11: 3D view of the top caisson. Notice that the top lid is not represented here.

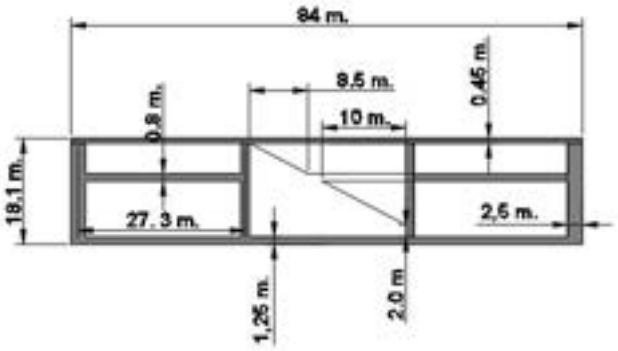

Figure I.12: Section 4 from figure J.10

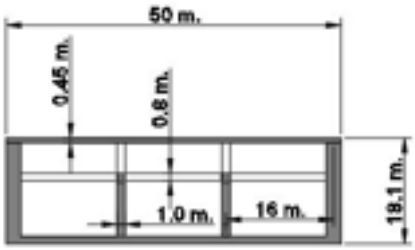

Figure I.13: Section 5 from figure J.10

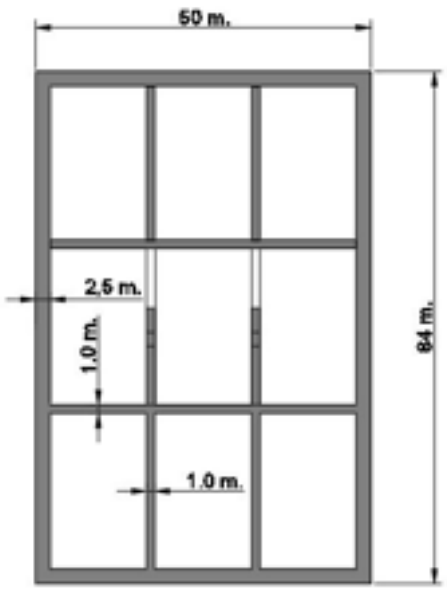

Figure I.14: Section 6 from figure J.10

The element's draught is 13.4 m (4.7 m freeboard). This is necessary to place the top caisson over the bottom caisson. During transport, a freeboard of 4.7 can cause some problems. However, the water ballast compartments can be filled with 1680 m^3 of water to transport the elements with a 0.1 m freeboard. The necessary ballast water volume to safely lower the element is 29000 m^3.

The erection of the caissons will be done using traveling formwork.

To ensure a watertight connection between the horizontal elements, GINA gasket as so as OMEGA joints will be installed on the elements (Walter el al., 1997). In the first figure the rubber profile is shown in positioned around the caisson element. Below the cut of the first figure is shown.

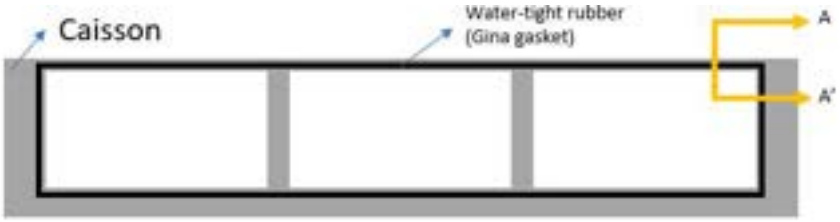

Figure I.15: GINA placement around caisson. 84 m long side.

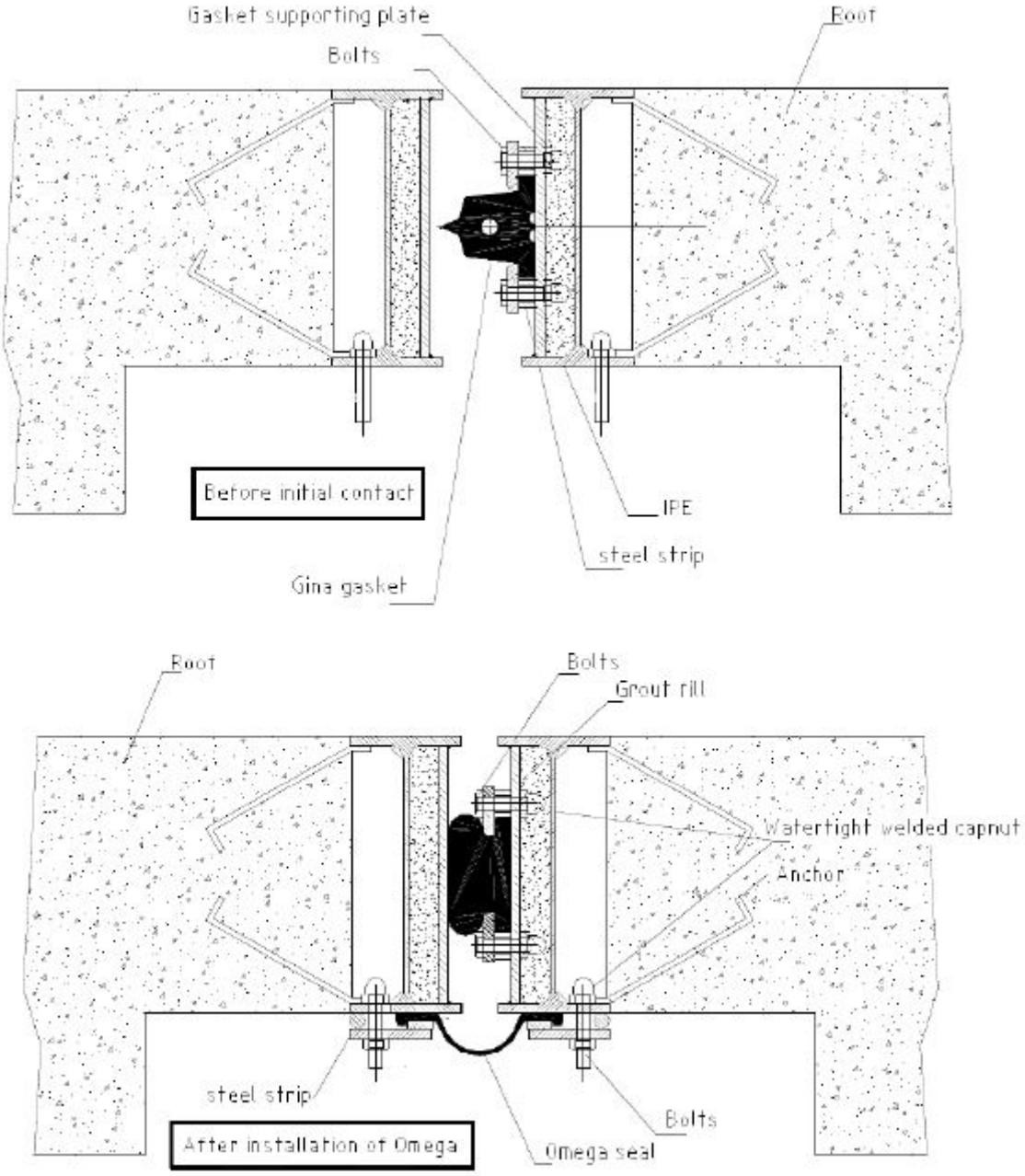

Figure I.16: GINA gasket representation. From cut AA' in figure I.15. Source: Van Lagen (2016)

To ensure vertical water-tightness, slots will be designed that will help to lower the elements to the adequate position. In the figures below the reader can see the top view and a cut o these slots.

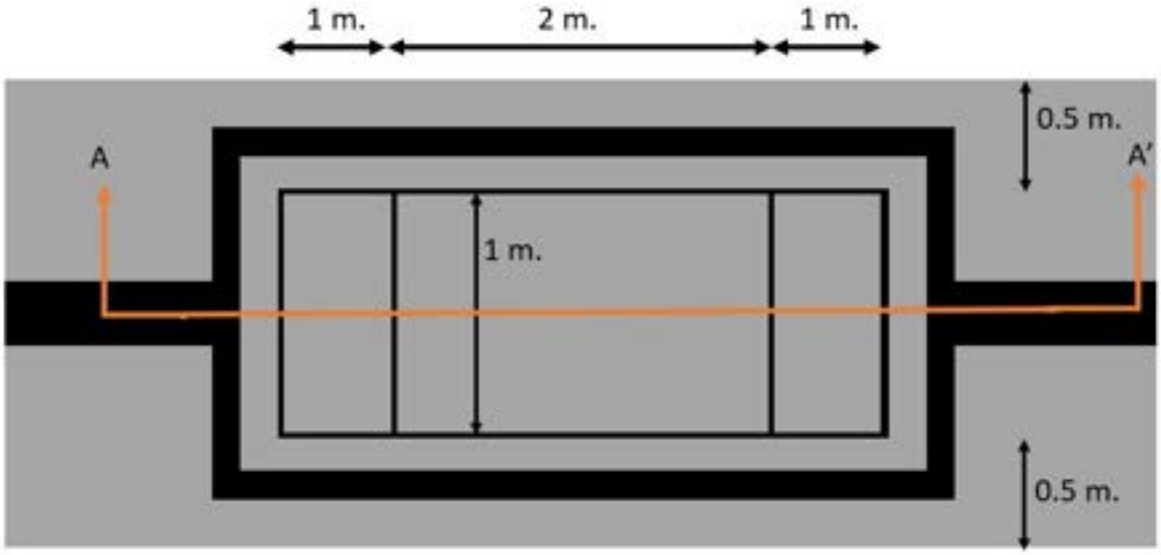

Figure I.17: Top view of the slot present in the bottom caissons.

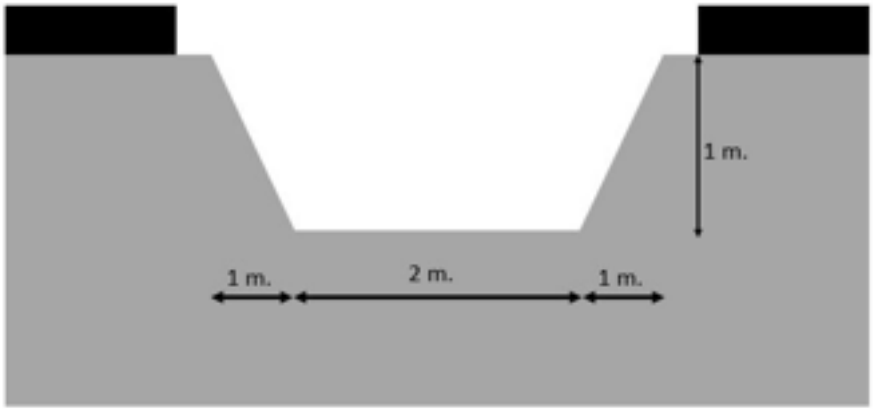

Figure I.18: Vertical cut of the bottom caisson's slots. Cut AA' in figure I.17

The top caisson will have extensions so that the top and bottom caissons can be connected as:

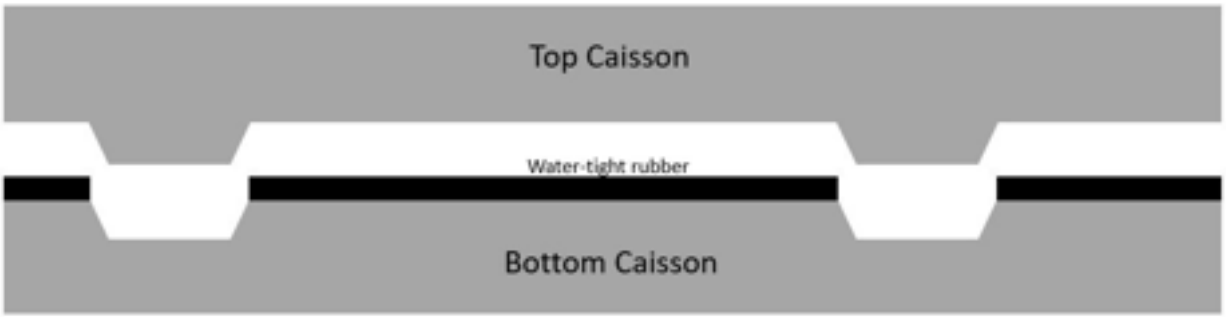

Figure I.19: Side view of bottom and top caisson connection.

Once the elements are constructed, the dock is filled with water and the elements are towed to the final position by tugboats (see Appendix J to see how the floatability of the caissons is ensured). When they are in position,

a special vessel will lower the elements on top of the bed. Which was already prepared.

The bed preparation starts by dredging the channel over which the foundation and elements will be placed. After dredging the channel, the piping protection and then gravel foundation can be positioned. This requires special machinery. Once the foundation is in position, the first caisson can be lowered on top of it. The channel may need extra dredging once the trench is finished to avoid soil sedimentation on it. The trench geometry is as follows:

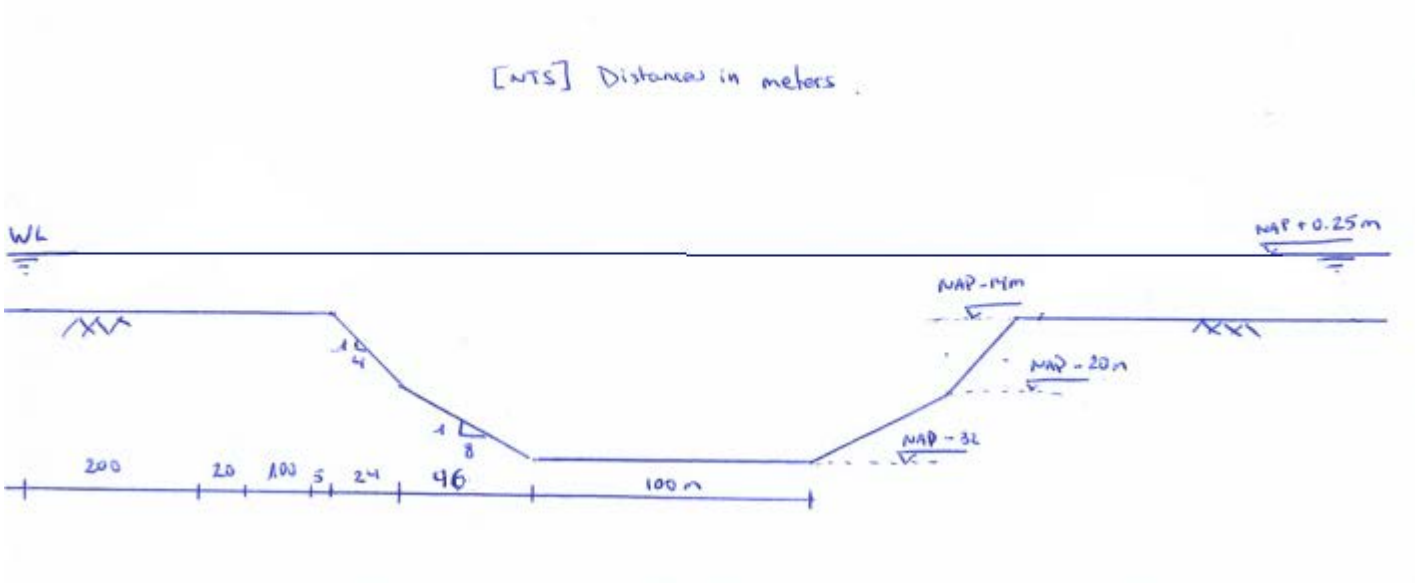

Figure I.20: Trench cross section

After the bottom caisson is placed, there is still 15.8 m of water (During average tidal conditions) on top of it to bring the top element and position it on top. This will leave a gap of 2.4 meters between the bottom and top elements. During average high tide, this gap raises to 3.4 meters, enough to position the top element without damaging the caisson below.

After the elements are positioned, the trench can be refilled with sand and the bed protection can be put in position. The final geometry would be like this:

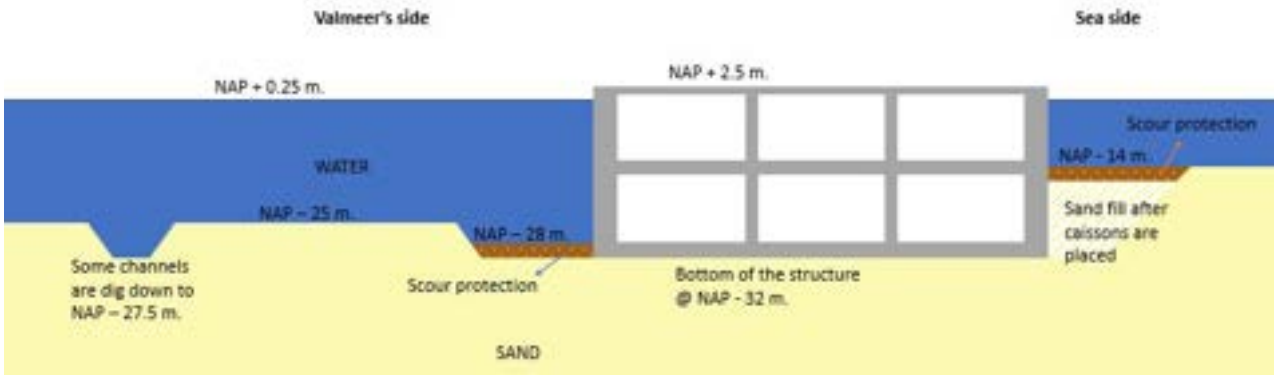

Figure I.21: Geometry after filling in the trench

At this point, the rest of the elements can be either towed or built in situ inside the caissons. For that, temporary roads will be constructed to reach the structure.

After all the in situ work is done, the final elements need to be installed (electrical groups, tension lines, cables, lights, paint, etc) and the work site will be cleaned up.

Appendix J

Caissons' stability during transport, immersion and in position

J.1 Introduction

Here, the main calculations and their steps are performed. The caisson is assumed to be constructed using reinforced concrete with a unit weight of 25 kN/m^3. The salt-water unit weight is of 10 kN/m^3. This is used for both buoyancy calculations and ballast water.

J.2 Bottom caisson

As in the previous appendix, the bottom caisson's geometry is shown in the figures below. In these figures, the reader can see a 3D representation of the caissons without the lid (for a better understanding of the caisson's shape) together with the sections performed. Section 1 is a vertical section through line 1 (ZX plane in figure J.10). Section 2 is a vertical section through line 2 (ZY plane in figure J.10). Section 3 is a horizontal section through line 3 (XY plane in figure J.10).

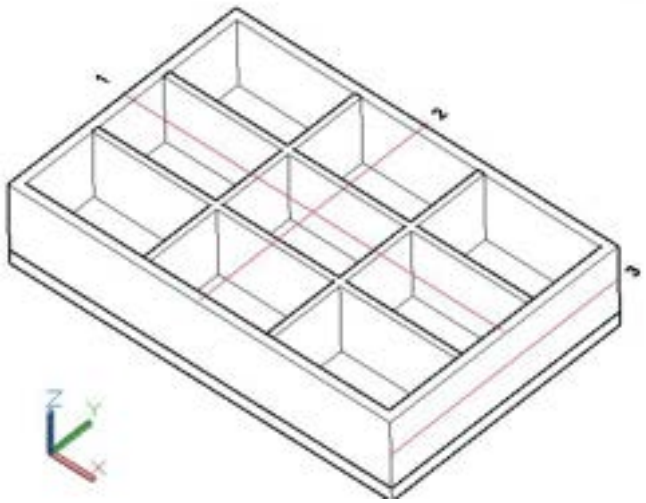

Figure J.1: 3D view of the bottom caisson. Notice that the top lid is not represented here.

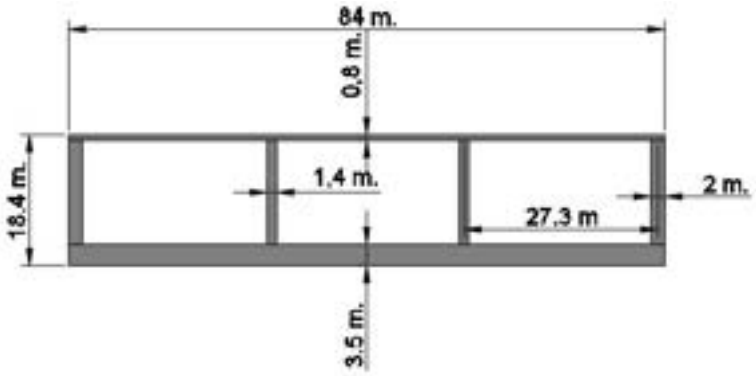

Figure J.2: Section 1 from figure J.10

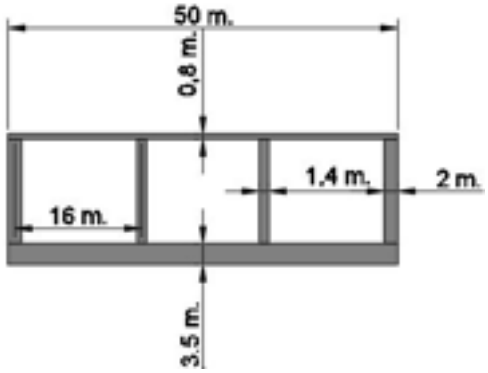

Figure J.3: Section 2 from figure J.10

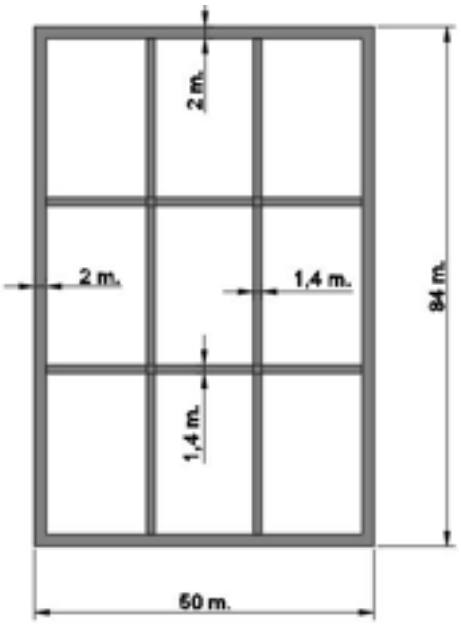

Figure J.4: Section 3 from figure J.10

From the above geometry, the geometrical properties are as follows:

CAISSON'S GEOMETRICAL PROPERTIES			
Exterior volume	Vt = L*W*H	77280	m3
Top surface=bottom surface	St = L*W	4200	m2
Surface for water storage	Sw	3344	m2
Mid-solid-Surface	Sm	856	m2
Height for water storage	Hw = H-Cs-Ci	13.9	m
Volume for storage	Vsto = Sw*Hw	46482	m3
Storage for ballast	Vb = nx*ny*lx*ly*Hw	46482	m3
Volume of solid	Vs = Vt-Vsto	30798	m3
Interior caisson length (x)	lx	25.333	m
Interior caisson length (y)	ly	22.000	m
Exterior wall area	Aext	4931	m2
Interior wall area	Aint	10451	m2
Bottom Slab area	Aslabb	938	m2
Top slab area	Aslabt	268	m2
Total wall volume	Vwall	11898	m2
Total slabs volume	Vslabs	18900	m2

Figure J.5: Geometrical properties of the bottom caisson used for upcoming calculations

J.2.1 Floatability

The first important check is to see if the caisson floats. As the dimensions of the caisson are already given, the draught must be computed from equilibrium between the buoyancy force and the caisson weight. This is calculated during the towing journey, when the caisson travels without any ballast.

The weight of the caisson is calculated with this formula

$$F_W = V_s \times \gamma_{Reinf-concrete} = 769960kN$$

Let's note that as we don't know yet the amount of reinforcement, the reinforced concrete unit weight of $25kN/m^3$ has been used.

The buoyancy force is then calculated according to formula

$$F_b = V_{sub} \times \gamma_w$$

where V_{sub} is the volume immersed and expressed as $L \times W \times d$ and where d is the draught.

As we know that F_b must be equal to $769960kN$, the the draught is obtained from equilibrium and equals to 18.3m and the freeboard is then 0.1m. A low value is recommended to ease the towing operation.

Floating static stability

As mentioned before, during towing the caisson is transported without ballast, so the following calculations will only consider the caisson self weight. In order to assess the static stability of the floating body, three points have to be considered :

- The centre of buoyancy C: Point of application of resultant buoyant force.
- The centre of gravity G: Point of application of the weight resultant force.
- The metacentre M: Point of intersection between KG and vertical line through C. If it is above G, the structure will be stable while floating.

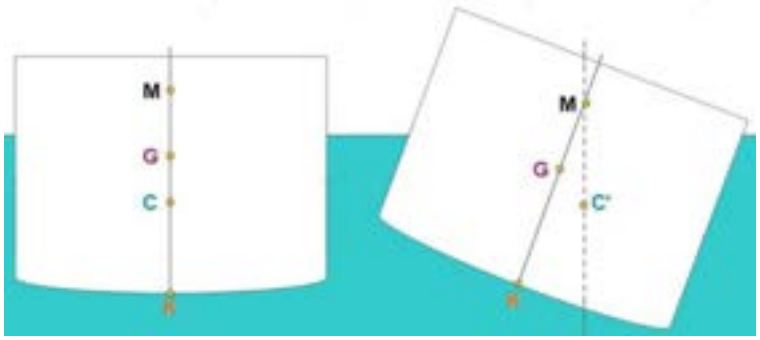

Figure J.6: Floating body static stability (Wikimedia commons, 2017)

To take safety into account, the caisson is stable if $GM > 0,5m$

The position of the gravity centre, the buoyancy centre and the metacentre are calculated according to these formulas:

$$KG = \frac{\Sigma V_i e_i \gamma_i}{\Sigma V_i \gamma_i} = \frac{\Sigma V_i e_i}{\Sigma V_i} = \frac{Ci/2 \cdot Ci \cdot L \cdot W + (Ci + (H - Ci - Cs)/2) \cdot (H - Cs - Ci) \cdot Sm + (H - Cs/2) \cdot Cs \cdot L \cdot W}{Ci \cdot L \cdot W + Cs \cdot L \cdot W + (H - Cs - Ci) \cdot Sm} = 7$$

$$KC = \frac{d}{2} = 9.2m$$

$$CM = \frac{I}{V_{sub}} = \frac{1/12 \cdot L \cdot W^3}{d \cdot L \cdot W} = 11m$$

Then, the metacentric height is computed

$GM = KC + CM - KG = 13.2m > 0.5m$ the structure is the stable while floating.

Floating dynamic stability

The impact of waves during the towing journey also has to be considered. As a rule of thumb, the caisson is dynamically stable if :

$$L_{wx} < 0,7 \times L = 59m$$
$$L_{wy} < 0,7 \times W = 35m$$

If the wave height during construction is lower than 35 meters, the position of the caisson relative to the direction of the waves can be anything. If the wave length is between 35 and 59 meters, while towing the element, the L dimension will ave to be aligned with the direction of the waves to ensure the above equilibrium conditions. Finally, the wave length cannot be larger than 59 meters during the construction operation.

In addition to that, to check the dynamic instability due to wave natural oscillation period, the polar moment of inertia has to be computed :

$$I_p = L \times W \times \frac{L^2 + W^2}{12} = 3344600m^4$$

The polar inertia radius and the natural oscillation period are then :

$$j = \sqrt[2]{\frac{I_p}{A_c}} = 28.2m$$

where A_c is the concrete cross section area $A_c = L \cdot W$

The wave oscillation period has to be smaller than the natural oscillation period in order to have the caisson stable. The natural oscillation period is calculated as:

$$T_o = \frac{2\pi j}{\sqrt{GM \times g}} = 15.6s$$

This means that for floating the caisson and transporting it, the wave period during towing must be lower than 15.6 seconds. In that case, the dynamic stability criterion will be fulfilled and the transportation of the caisson can be done with any trouble. This won't be a problem since the wave period for a return period of 1/1000 years is 11.3 seconds.

Keep in mind that the wave height at the work area has to be smaller than 1.5m during transport and positioning operations. This is because after performing some simulations, Esteban et al. (2009) found that the wave height could be up to 1.5 m without causing risk or damage to the caisson during installation.

Overall stability

The bottom caisson top level when positioned is at NAP -15.6 m. This means that the caisson is completely submerged and that the wave forces the caisson will feel are negligible. Furthermore, all the caisson is surrounded by the same water pressures, so the resultant of these forces will be zero. For these reasons, the bottom caisson, once in position, will be considered to be stable against sliding, overturning and vertically. Vertical stability is ensured since the caisson is less heavy than the Alternative 1 and 2 previously calculated. Thus, the bearing capacity of the soil will be enough to support the bottom caisson.

The only calculation that will be done in this section is the needed ballast water to keep the structure stable on the floor. This comes from having a safety factor of 1.05 (Lecture notes Bored and Immersed Tunnels, CIE5305) against uplift. So, the ballast water weight can be computed from: $F_{ballast} = 1.05 \cdot F_W - F_b = 1.05 \cdot F_W - F_W = 0.05 \cdot F_W = 38500kN$. Which, translated to water volume it is 3850 m3 of water.

J.3 Top caisson

As done in the preceding appendix, the top caisson's geometry is shown in the figures below. In these figures, the reader can see a 3D representation of the caissons without the lid (for a better understanding of the caisson's shape) together with the sections performed. Section 4 is a vertical section through line 4 (ZX plane in figure J.10). Section 5 is a vertical section through line 5 (ZY plane in figure J.10). Section 6 is a horizontal section through line 6 (XY plane in figure J.10).

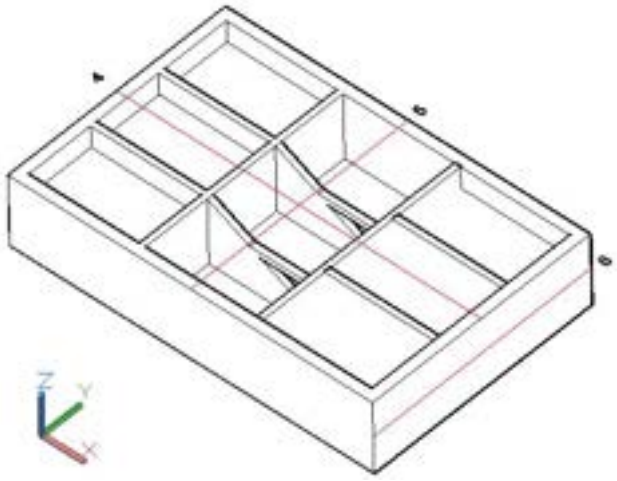

Figure J.7: 3D view of the top caisson. Notice that the top lid is not represented here.

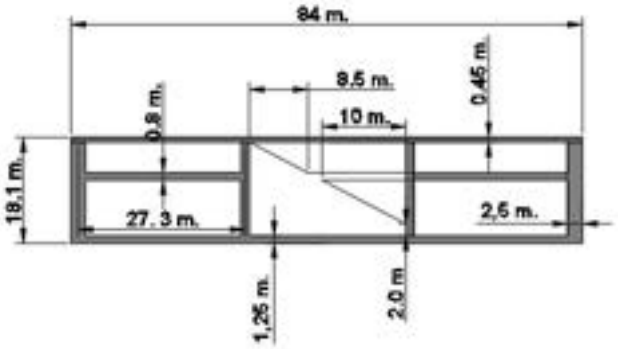

Figure J.8: Section 4 from figure J.10

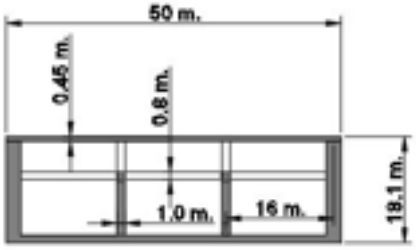

Figure J.9: Section 5 from figure J.10

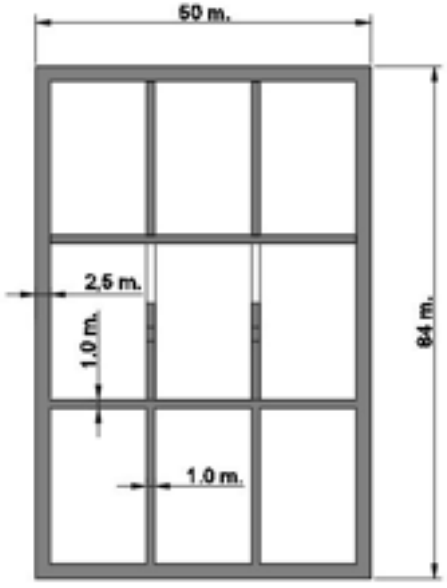

Figure J.10: Section 6 from figure J.10

From the above geometry, the geometrical properties are as follows:

CAISSON'S GEOMETRICAL PROPERTIES			
Exterior volume	Vt = L*W*H	76020	m3
Top surface=bottom surface	St = L*W	4200	m2
Surface for water storage	Sw	3344	m2
Mid-solid-Surface	Sm	856	m2
Height for water storage	Hw = H-Cs-Ci	15.6	m
Volume for storage	Vsto = Sw*Hw	52166	m3
Storage for ballast	Vb = nx*ny*lx*ly*Hw	52166	m3
Volume of solid	Vs = Vt-Vsto	23854	m3
Interior caisson length (x)	lx	25.333	m
Interior caisson length (y)	ly	22.000	m
Exterior wall area	Aext	4851	m2
Interior wall area	Aint	10281	m2
Bottom Slab area	Aslabb	402	m2
Top slab area	Aslabt	268	m2
Total wall volume	Vwall	13354	m2
Total slabs volume	Vslabs	10500	m2

Figure J.11: Geometrical properties of the top caisson used for upcoming calculations

J.3.1 Floatability

As it was already done for the bottom caisson, the first important check is to see if the caisson floats. As the dimensions of the caisson are already given, the draught must be computed from equilibrium between the buoyancy force and the caisson weight. This is calculated during the towing journey, when the caisson travels without any ballast.

The weight of the caisson is calculated with this formula

$$F_W = V_s \times \gamma_{Reinf-concrete} = 596340kN$$

Let's note again that as we don't know yet the amount of reinforcement, the reinforced concrete unit weight of $25kN/m^3$ has been used.

The buoyancy force is then calculated according to formula

$$F_b = V_{sub} \times \gamma_w$$

where V_{sub} is the volume immersed and expressed as $L \times W \times d$ and where d is the draught.

As we know that F_b must be equal to $596340kN$, the the draught is obtained from equilibrium and equals to 14.2 m, giving a freeboard of 3.9m. Notice that the top caisson needs some clearance to float above the bottom caisson and then sink on top of it. A freeboard of 3.9 meters gives an space between bottom and top caisson of 4.1 meters. Enough to place one caisson above the other and then proceed to safely lower the element on top of the bottom element.

Floating static stability

As mentioned before, during towing the caisson is transported without ballast, so the following calculations will only consider the caisson self weight. In order to assess the static stability of the floating body, three points have to be considered :

- The centre of buoyancy C: Point of application of resultant buoyant force.
- The centre of gravity G: Point of application of the weight resultant force.
- The metacentre M: Point of intersection between KG and vertical line through C. If it is above G, the structure will be stable while floating.

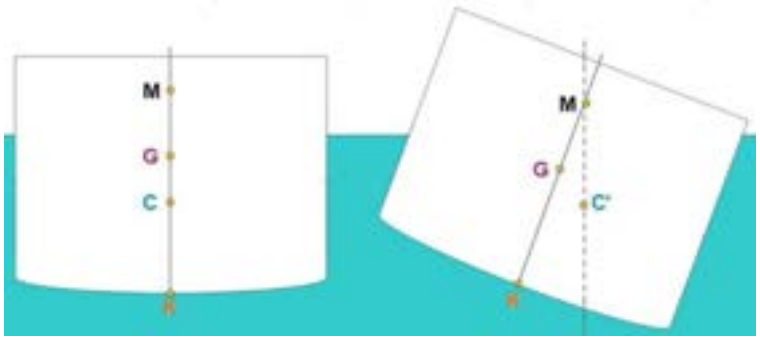

Figure J.12: Floating body static stability (Wikimedia commons, 2017)

To take safety into account, the caisson is stable if $GM > 0,5m$

The position of the gravity centre, the buoyancy centre and the metacentre are calculated according to these formulas:

$$KG = \frac{\Sigma V_i e_i \gamma_i}{\Sigma V_i \gamma_i} = \frac{\Sigma V_i e_i}{\Sigma V_i} = \frac{Ci/2 \cdot Ci \cdot L \cdot W + (Ci + (H - Ci - Cs)/2) \cdot (H - Cs - Ci) \cdot Sm + (H - Cs/2) \cdot Cs \cdot L \cdot W}{Ci \cdot L \cdot W + Cs \cdot L \cdot W + (H - Cs - Ci) \cdot Sm} = 8$$

$$KC = \frac{d}{2} = 7.1m$$

$$CM = \frac{I}{V_{sub}} = \frac{1/12 \cdot L \cdot W^3}{d \cdot L \cdot W} = 15$$

Then, the metacentric height is computed

$GM = KC + CM - KG = 13.3m > 0.5m$ the structure is the stable while floating.

Floating dynamic stability

This section coincides witht the previous one, so the reader can go thought it easily. Notice that this is convenient since it means that the sea conditions for both caissons have to be the same for placing the elements.
The impact of waves during the towing journey also has to be considered. As a rule of thumb, the caisson is dynamically stable if :

$$L_{wx} < 0,7 \times L = 59m$$

$$L_{wy} < 0,7 \times W = 35m$$

If the wave height during construction is lower than 35 meters, the position of the caisson relative to the direction of the waves can be anything. If the wave length is between 35 and 59 meters, while towing the element, the L dimension will ave to be aligned with the direction of the waves to ensure the above equilibrium conditions. Finally, the wave length cannot be larger than 59 meters during the construction operation.

In addition to that, to check the dynamic instability due to wave natural oscillation period, the polar moment of inertia has to be computed. It can be computed from the addition of the moment of inertia around the x-axis and y-axis:

$$I_p = I_x + I_y = \frac{1}{12} \times L^3 \times W + \frac{1}{12} L \times W^3 = \frac{L \times W}{12} \times (L^2 + W^2) = 3344600m^4$$

The polar inertia radius and the natural oscillation period are then :

$$j = \sqrt[2]{\frac{I_p}{A_c}} = 28.2m$$

where A_c is the concrete cross section area $A_c = L \cdot W$
The wave oscillation period has to be smaller than the natural oscillation period in order to have the caisson stable. The natural oscillation period is calculated as:

$$T_0 = \frac{2\pi j}{\sqrt{GM \times g}} = 15.6s$$

This means that for floating the caisson and transporting it, the wave period during towing must be lower than 15.6 seconds. In that case, the dynamic stability criterion will be fulfilled and the transportation of the caisson can be done with any trouble. This won't be a problem since the wave period for a return period of 1/1000 years is 11.3 seconds.

Keep in mind that the wave height at the work area has to be smaller than 1.5m during transport and positioning operations. This is because after performing some simulations, Esteban et al. (2009) found that the wave height could be up to 1.5 m without causing risk or damage to the caisson during installation.

Overall stability

The caissons will have to be stable to wave attack during the construction time (assumed to be 20 years). This is a rather conservative assumption since the time that the caissons will be positioned empty (only ballast) will be less than the construction time. The yearly failure probability for the caissons is defined as 0.5% (p=1/200 = 0.005). Therefore, the design wave height and period will have a return period of:

$$R = \frac{1}{1 - \Big(1 - p\Big)^n}$$

Where n is the duration of the construction works (n = 20 years). FInally, the return period for the wave height during construction is:

$$R = \frac{1}{1 - \Big(1 - 0.005\Big)^{20}} = 10\,years$$

The design wave height, period and water level will then be H_s = 5.3 m, t_p = 8.6 s and WL = NAP +3.3 m respectively. As it was already done for the regular conditions case in Appendix L.6.1. Both these cases return period coincides.
After the caissons are all placed and completely ballasted with sea water, during construction, the worst condition that can occur is having the design wave height and the water level. This is because during construction the caissons will be empty and surrounded by the same water level at all sides. For this situation the sliding stability should be checked. In order to check it, the frictional resistance has to be higher than the sum of all the horizontal forces.

The sum of the horizontal force and vertical forces and the frictional resistance follows from the formulations used in Appendix L and results in:

Downward force: selfweight + ballast - buoyancy	F_wPositioned	410282	kN	applied @	0	m from center of BOS
Hydrostatic force (sea)	F_hs	89303	kN	applied @	6.3	m from BOS
Hydrostatic force (ESL)	F_hv	89303	kN	applied @	6.3	m from BOS
Horizontal wave force p1(Sea)	F_ws1	441	kN	applied @	19.6	m from BOS
Horizontal wave force p3 (Sea)	F_ws2	2088	kN	applied @	9.5	m from BOS
Horizontal wave force p1-p3 (Sea)	F_ws3	2929	kN	applied @	12.6	m from BOS
Vertical wave force pu (Sea)	F_ws4	4639	kN	applied @	14.0	m from center of BOS

Figure J.13: Forces acting on the caisson.

$$\Sigma F_h = h_{hs} - F_{hv} + F_{ws1} + F_{ws2} + F_{ws3} = 5457kN$$

$$\Sigma F_v = F_{caisson} + F_{ballast} - F_{buoyancy} - F_{ws4} = 405643kN$$

$$R_{friction} = \mu \times \Sigma F_v = 243386kN$$

where μ is the friction coefficient and is equal to 0,6 for this case.

$243386kN > 5457kN$ so the caisson is stable.

Overturning stability

This is considered when the caisson is fully ballasted with sand. This has to be checked in the worse case which is at the section of the fuel tank when it is empty. This criterion is ok if the eccentricity e smaller than 1/6 of the total length.

e is calculated according to this formula

$$e = \frac{|M|}{\Sigma F_v} = \frac{h_{hs} \cdot 6.3 - F_{hv} \cdot 6.3 + F_{ws1} \cdot 19.6 + F_{ws2} \cdot 9.5 + F_{ws3} \cdot 12.6 + F_{ws4} \cdot 14.0}{405643} = 0,32m$$

where M is the moment calculated at the centre of the floor slab.

$0,6m < 84/6 = 14m$ so this criterion is fulfilled.

Soil bearing capacity

The maximum pressure applied by the caisson in case of completely filled compartments should not exceed the bearing capacity of the subsoil of 400| : KN/m^2. which means that $\sigma_{kmax} < 400\ KN/m^2$. This maximum pressure happens when the caissons are in position and when the buoyancy is minimum. That is, when the water level is minimum. For the caissons that happens right after they are positioned and there is low tide (water level at NAP -1.25m). The equilibrium of the structure in the use phase was already done in Appendix L.6.1. There the weight of the structure is maximum and therefore the conditions more unfavourable so no calculations will be done for the bearing capacity of having only caissons. If the soil resist the loads later on, when the caissons are place it will also resist.

Appendix K

Different elements of the Valmeer's hydro pump storage station

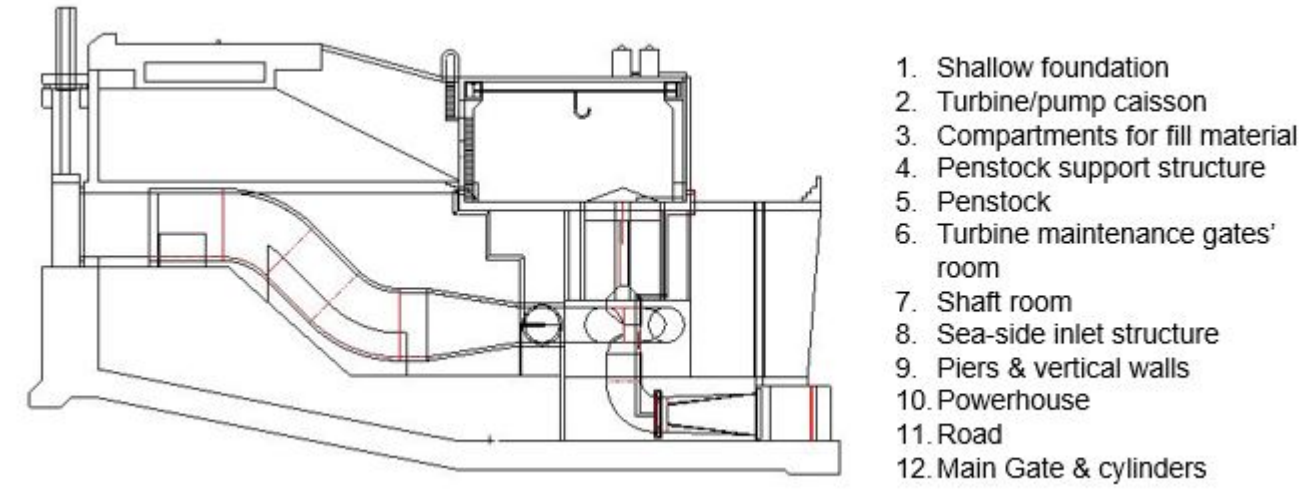

Figure K.1: General cross section and list of elements

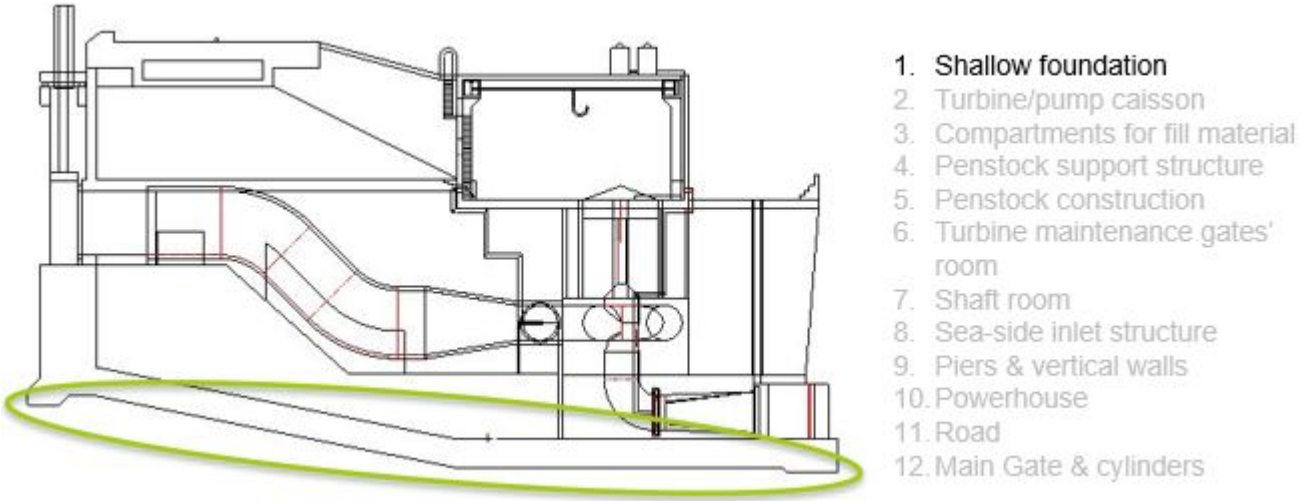

Figure K.2: General cross section showing shallow foundation

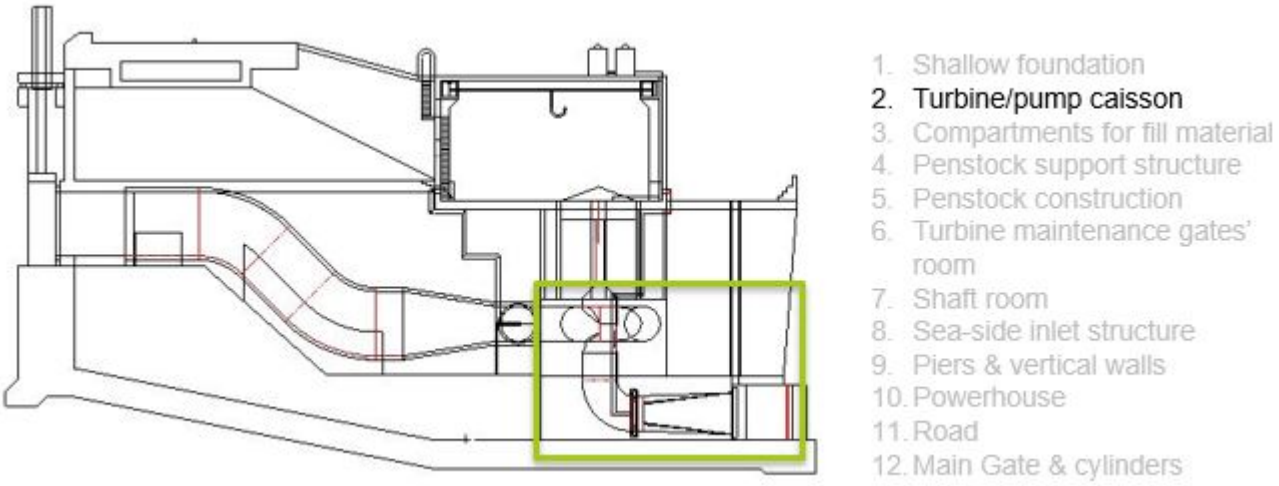

Figure K.3: General cross section showing turbine/pump caisson

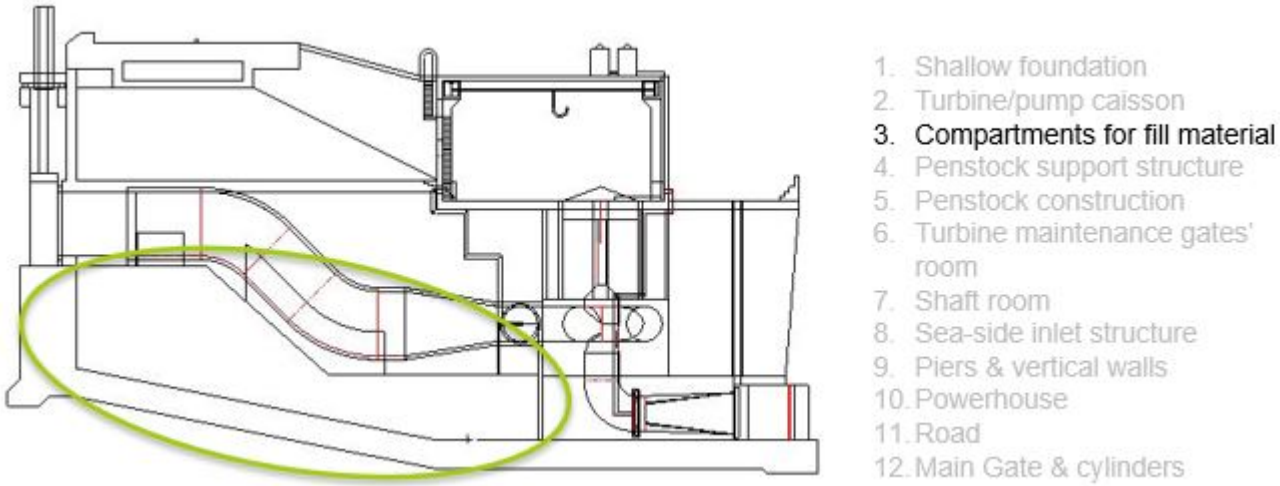

Figure K.4: General cross section showing compartments for fill material

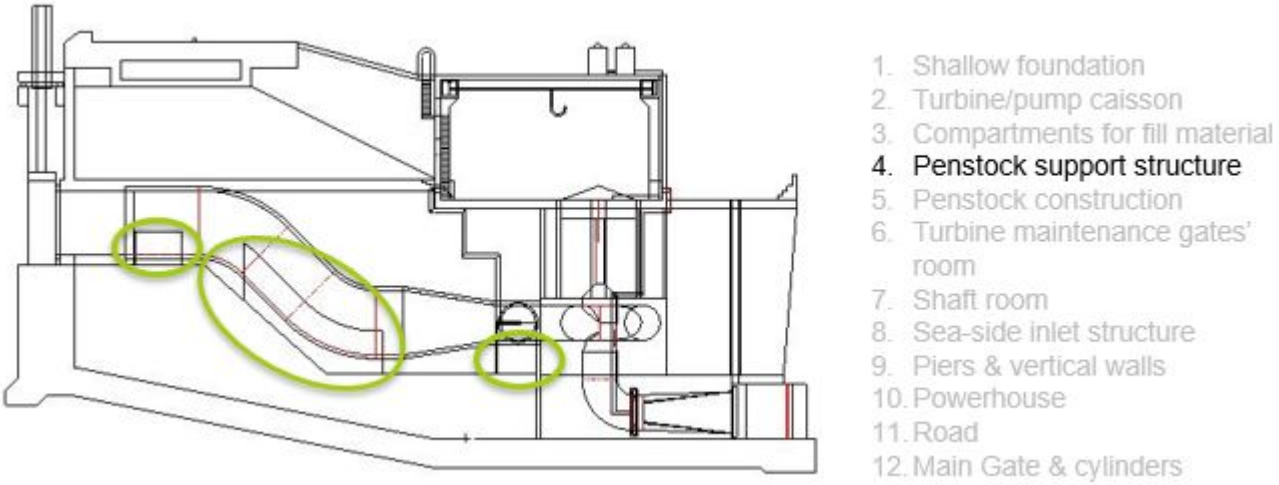

Figure K.5: General cross section showing penstock support structure

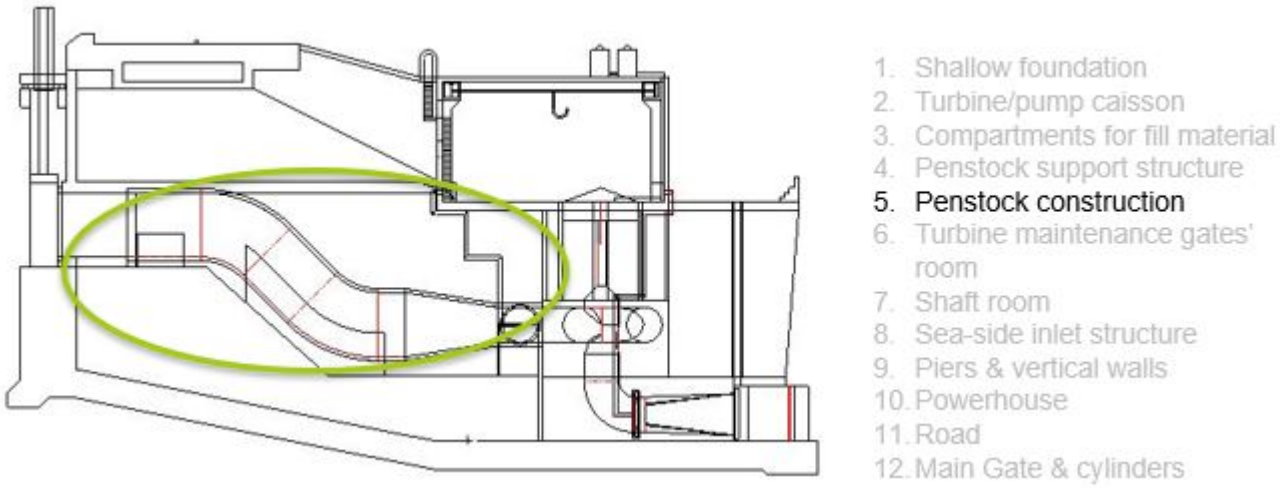

Figure K.6: General cross section showing penstock

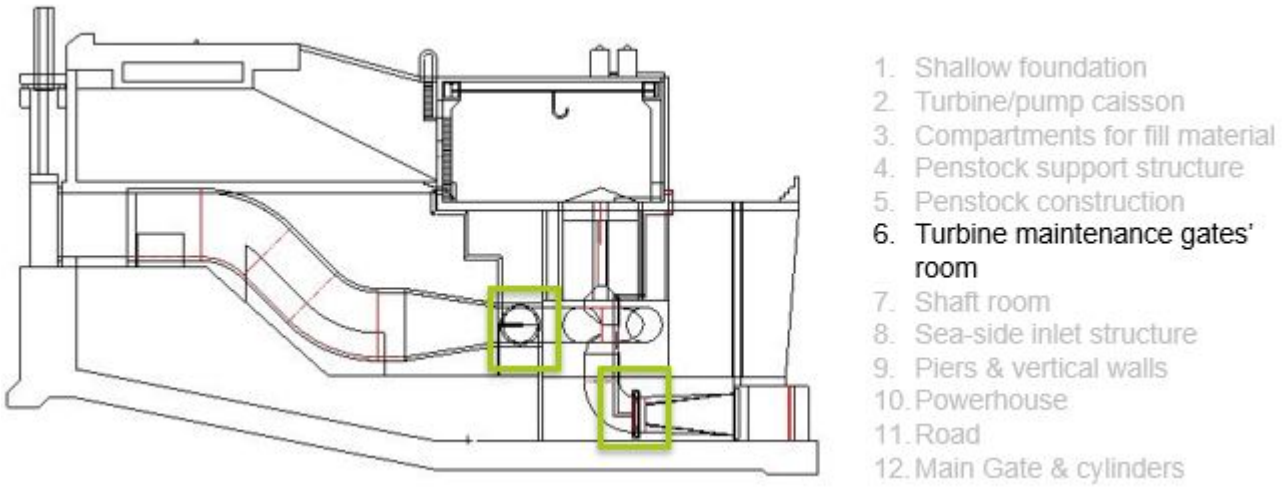

Figure K.7: General cross section showing gates for turbine maintenance of pump/turbine

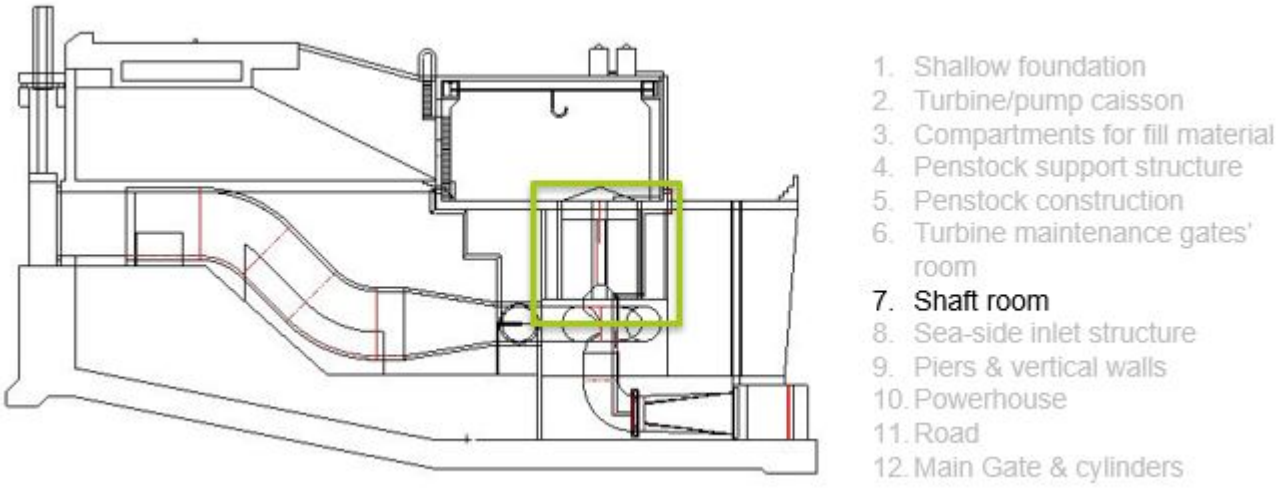

Figure K.8: General cross section showing the shaft room

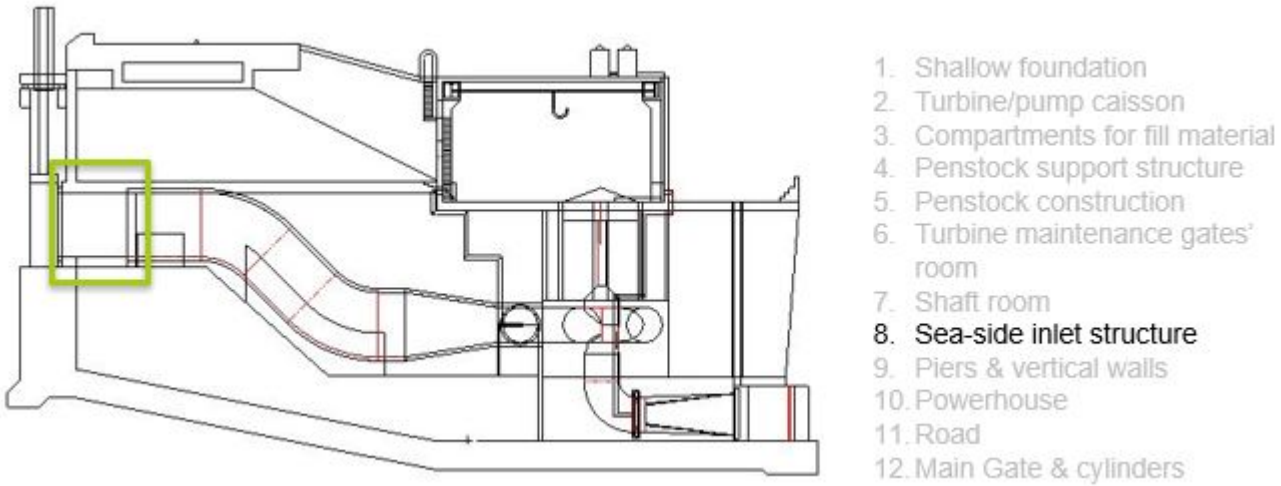

Figure K.9: General cross section showing sea-side inlet structure

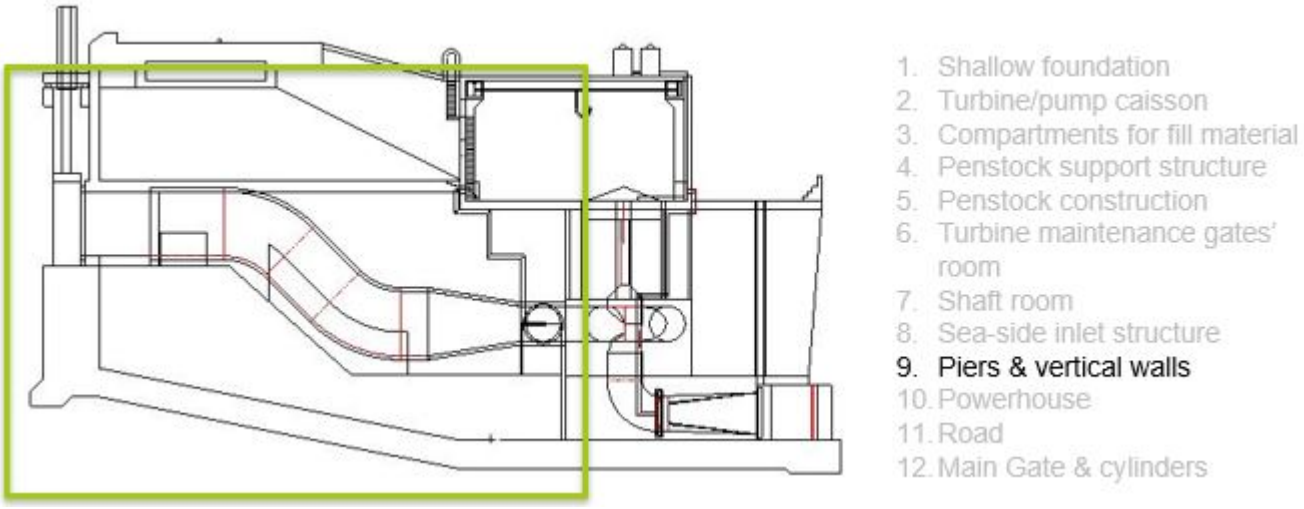

Figure K.10: General cross section showing piers and vertical walls. These can be seen properly in the 3D Figure 7.6

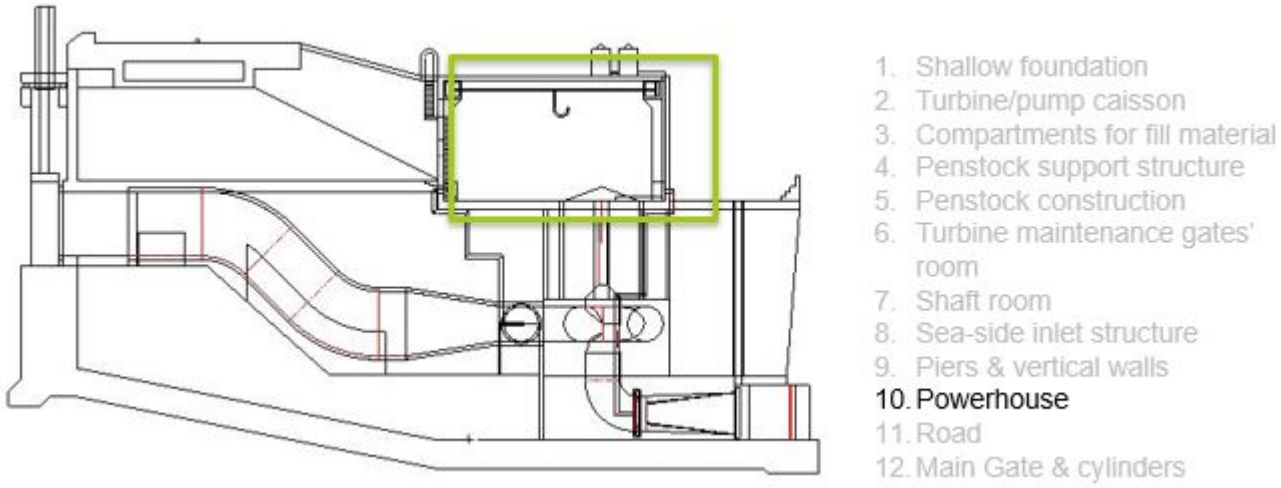

Figure K.11: General cross section showing powerhouse

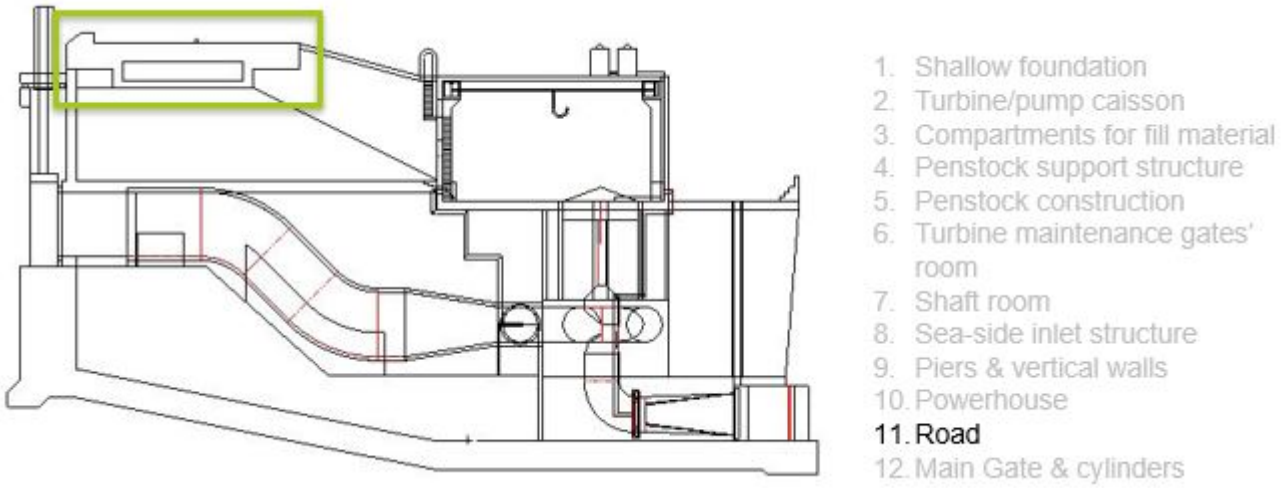

Figure K.12: General cross section showing the road deck

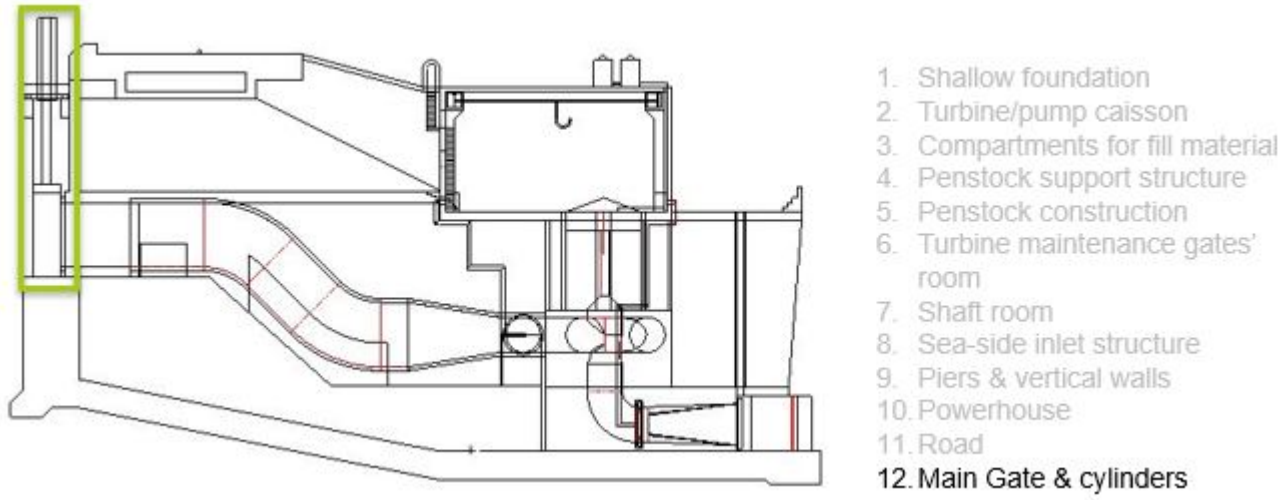

Figure K.13: General cross section showing the main gate and cylinders

Appendix L

General stability of the alternatives

L.1 Introduction

In this appendix, the different alternatives, together with the calculations performed for stability and head loses will be shown. First, the theoretical background that has been followed for ensuring that the structure is stable is presented. After that, the different groups of alternatives are shown ("construction is a flood defense (Alternative 1)", "the construction is not a flood defense (Alternative 2)" and "the construction is part of a flood defense in combination with the dike (Alternative 3)"), and the stability calculations are performed in order to provide initial realistic overall measures for the different power plant's alternatives. Notice that the calculations for each alternative was done by iterating in an excel spreadsheet. Below, only the result of those iterations is shown. For a detailed stability calculation the reader is referred to Chapter 7.2.

The calculations were performed using an excel spreadsheet, so that iteration of the values could be easily done until stability (horizontal, vertical and rotational stability) is achieved.

L.2 Theoretical background for stability and head loses

L.2.1 Inventory of forces acting on the structure

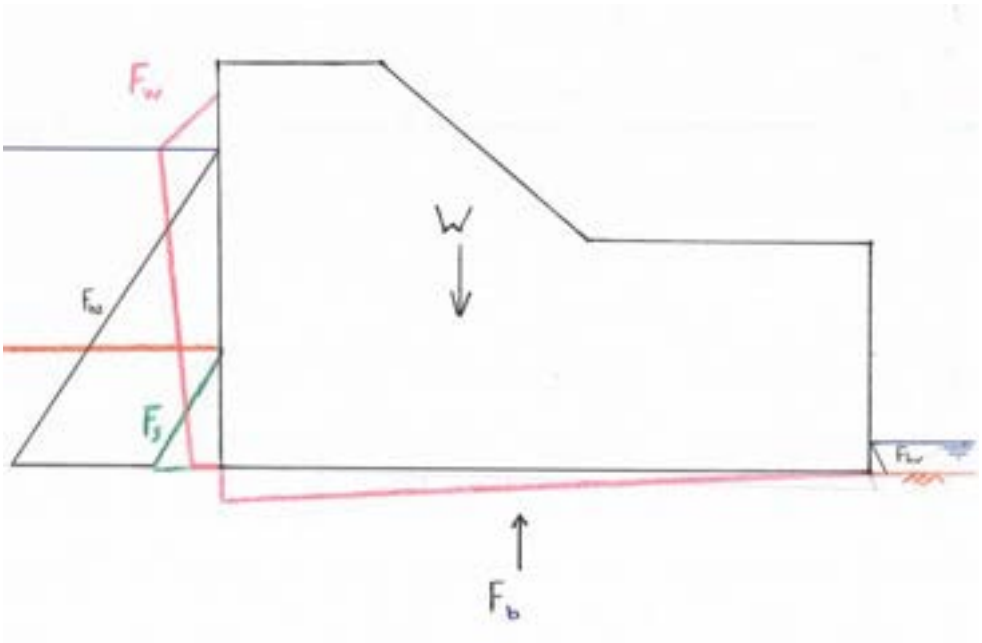

Figure L.1: Sketch showing the forces acting on the structure

Where:

- Hydrostatic force: Represented in blue. There is presence of this force at both sides of the structure. These forces depend of the water depth.
- Soil force: Represented in green. This load comes from the submerged weight of the soil located next to the structure.
- Wave loading: Represented in red. This is calculated for the design wave height and design levels. It was obtained using Goda (1974) formulation.
- Selftweight: Represented with a W. It is obtained by multiplying the area of concrete present in a section of the structure times the reinforced concrete unit weight.
- Buoyancy: Water upwards pressure at each side of the structure is considered for this calculation.

In the following lines, it is shown how to obtain the numerical values for the present pressures.
The hydrostatic pressure can be calculated as:

$$F_h = \gamma_w \cdot h \quad [kN/m^2] \tag{L.1}$$

In a similar manner, the soil load can be obtained as:

$$F_s = \gamma_s \cdot h_{soil} \cdot k \quad [kN/m^2] \tag{L.2}$$

Where k is the soil pressure coefficient. This coefficient, according to Rankine's theory, has to limits: active and passive coefficients. The active coefficient is used to calculate soil pressures acting on a wall when the wall is displacing away from the soil. On the other hand, the passive coefficient is used to calculate soil pressures on a wall that is being pushed towards the soil. If the structure within the soil is at rest (no displacements at all), the neutral soil pressure coefficient is used. In the following figure, a representation of the active, neutral and passive coefficients as a function of soil displacement (relative to the structure within the soil) is shown:

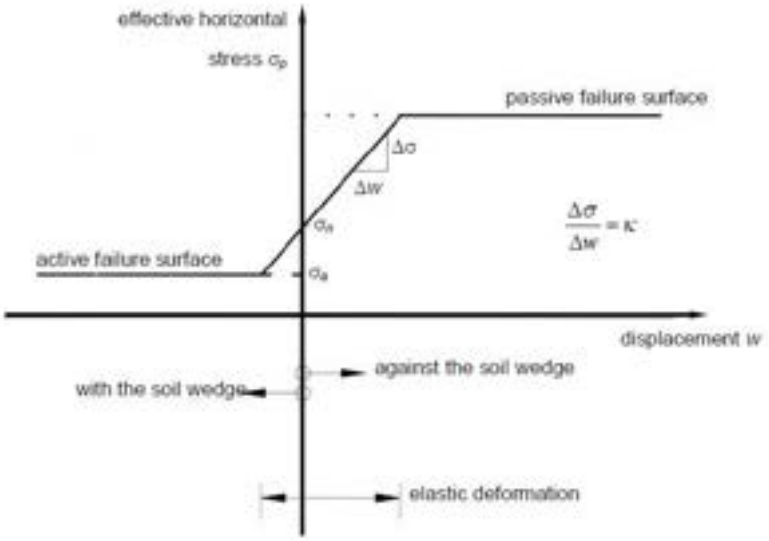

Figure L.2: Soil pressure vs displacement diagram for a spring supported beam. Source: CIE4363 reader, 2018 (TU Delft)

Following Rankine's theory, the active and passive soil coefficient can be calculated as:

$$k_a = \frac{1 - sin(\phi)}{1 + sin(\phi)} \quad [-] \tag{L.3}$$

$$k_p = \frac{1 + sin(\phi)}{1 - sin(\phi)} \quad [-] \tag{L.4}$$

The neutral soil coefficient can be calculated using Jaky's formula (1944):

$$K_0 = 1 - sin(\phi) \tag{L.5}$$

This equation is used for its simplicity and because its results are a good representation of true stress ration in soils (Michalowski, 2005).

The buoyancy force calculation is shown in the following sketch:

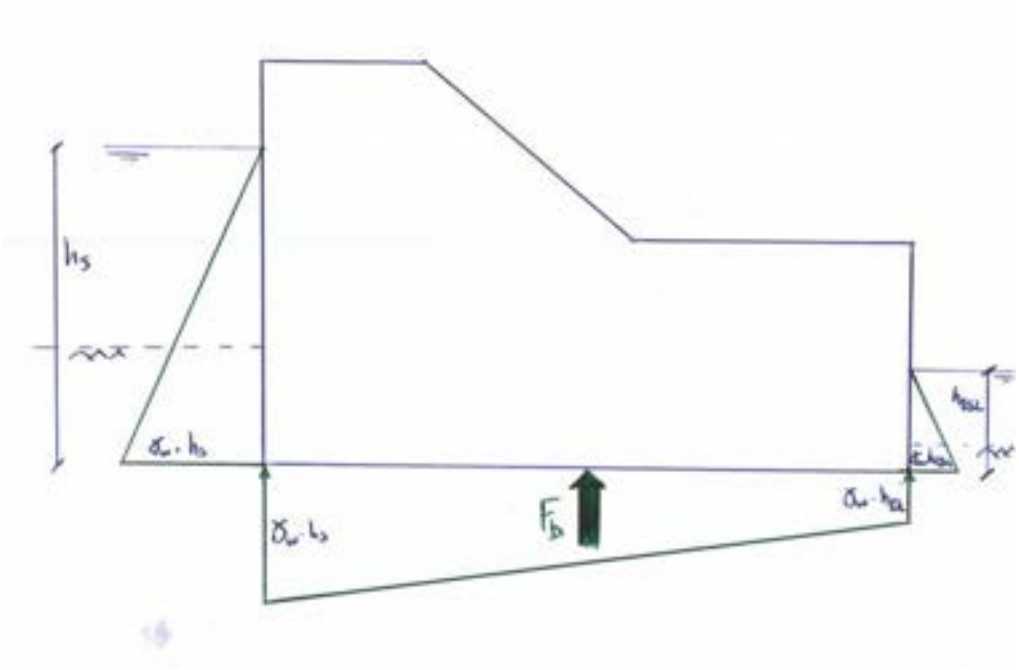

Figure L.3: Model used for the calculation of the buoyant force.

Therefore, as the buoyancy force is assumed to be linear from one side to the other of the structure, the equation of the area of a trapezoid can be used to obtain the buoyant force:

$$F_b = \frac{1}{2} \cdot \left(h_{ESL} + h_{sea}\right) \cdot \gamma_w \cdot L \quad [kN/m^2] \tag{L.6}$$

Where L is the length of the structure.

Finally, the wave pressures were obtained using Goda (1974) formulation. Goda developed this formulation for breaking and non-breaking waves hitting a caisson on a rockfill sill. The structure object of design for this thesis has a vertical face were waves hit. This is similar to the caisson situation. However, this structure won't be over a sill but embedded in the soil. This is assumed to give more conservative estimates. Meaning that the actual wave loads the structure will support will be lower than the calculated ones from Goda's formulation since for the real situation, wave loading will be damped by the soil around the structure.

Other formulations for non-breaking waves suck as Sainflou have been considered. According to the Hydraulic Structures Manual, 2019 this method overestimates wave forces for steep waves, which might reach the structure. Due to this overestimation, the Goda method has been used.

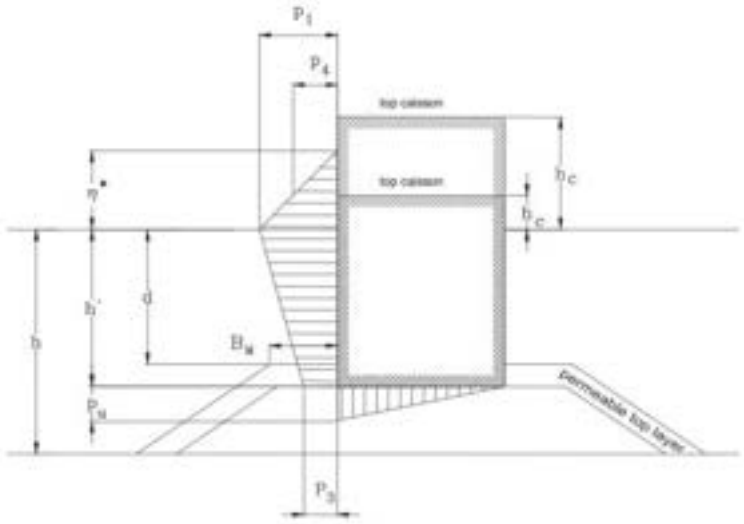

Figure L.4: Wave pressure distribution according to Goda, based on: TAW (2003)

$$p_1 = \frac{1}{2}(1 + cos\beta)(\lambda_1\alpha_1 + \lambda_2\alpha_* cos^2\beta)\rho g H_d \quad [kN/m^2] \tag{L.7}$$

$$p_3 = \alpha_3 p_1 \quad [kN/m^2] \tag{L.8}$$

$$p_4 = \alpha_4 p_1 \quad [kN/m^2] \tag{L.9}$$

$$p_u = 0.5(1 + cos\beta)\lambda_3\alpha_1\alpha_3\rho g H_d \quad [kN/m^2] \tag{L.10}$$

In which:
$\eta = 0.75(1 + cos\beta)\lambda_1 H_d$
β = angle of the incoming wave respecting the normal to the structure $\alpha_1 = 0.6 + 0.5\left[\frac{4\pi h/L_d}{sinh(4\pi h/L_d)}\right]^2$
$\alpha_2 = min\left[\frac{(1-d/h_d)(H_D/d)^2}{3}, \frac{2d}{H_d}\right]$
$\alpha_3 = 1 - (h'/h)\left[1 - \frac{1}{cosh(2\pi h/L_d)}\right]$
$\alpha_4 = 1 - \frac{h'_c}{\eta'}$
$h'_c = min(\eta', h_c)$
$\lambda_1, \lambda_2, \lambda_3$ = factors dependent on the shape of the structure and on wave conditions. For vertical walls and non-breaking waves: $\lambda_1 = \lambda_2 = \lambda_3 = 1$.
h_b = water depth at a distance $5H_d$ from the wall.
H_D = design wave height
L_D = design wave length
d = water depth above the top of the sill
h' = water depth above the wall foundations plane
h = water depth in front of the sill

L.2.2 Stability

In this section the horizontal, vertical and rotational stability calculations are described. For this calculations, a shallow foundation has been assumed (which viability will have to be checked later on). This has been assumed from experts recommendations, current similar structures' foundation techniques and for time-limits for the present thesis. An accurate soil profile definition at the worksite is recommended together with calculations to check whether shallow foundation is possible and if not, what other foundations should be used.

Horizontal stability

The structure has to resist to the lateral forces acting on it. For that, the resultant of its vertical force times the friction coefficient (between structure's base material and seabed material) has to be larger than the resultant

of the lateral forces. The friction coefficient has been considered to be 0.6, taking into account that the base of the structure (concrete) will be placed over a gravel bed.

$$\sum H \leq \eta \cdot \sum V \tag{L.11}$$

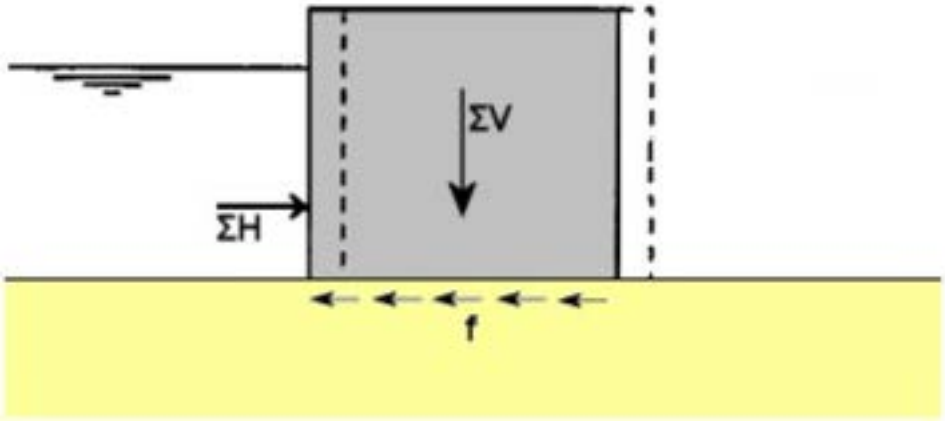

Figure L.5: slip-off principle sketch. Source: Hydraulic Structures Manual

Rotational stability

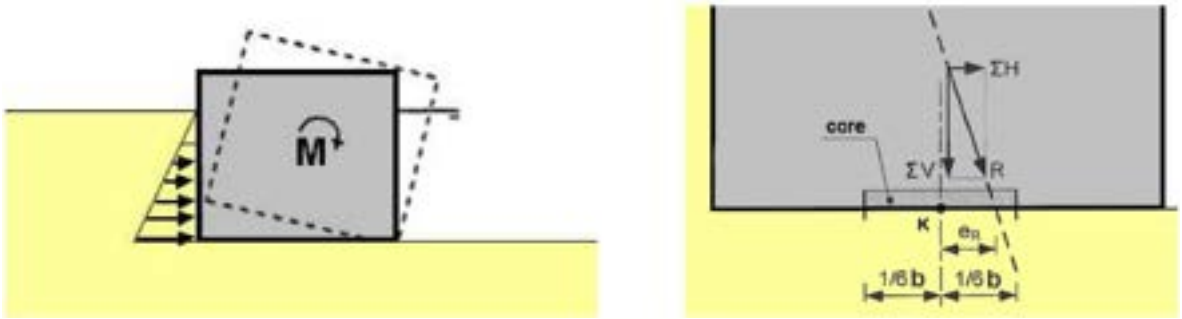

Figure L.6: Rotational stability sketch.Source: Hydraulic Structures Manual

Soils can only take compression stresses. Sands and no cohesive materials cannot provide negative stress. Therefore, the stresses can only be positive. That is the case when the resulting force intersects the core of the structure. The core is defined as the area extended 1/6 of the base to both sides of the center of the structure (see Figure L.41). In equation form:

$$e_R = \frac{\sum M}{\sum V} \leq \frac{1}{6} b \quad [m] \tag{L.12}$$

The forces acting on the structure are the same as for the horizontal stability. Nonetheless, now the distance at which the force is acting is of importance to calculate the rotational moment.

Vertical stability

The vertical effective stress from the loads acting on the structure should not exceed the maximum soil bearing capacity ($\sigma_{k,max} < p'_{max}$). Otherwise the soil will collapse. The maximum load on the soil is calculated as:

$$\sigma_k, max = \frac{F}{A} + \frac{M}{W} = \frac{\sum V}{b \cdot l} + \frac{\sum M}{\frac{1}{6} l b^2} \quad [kN/m^2] \tag{L.13}$$

On the other hand, as the soil cannot take negative stresses, the minimum load acting on the soil has to have a positive sign ($\sigma_k, min > 0$. Only compressive stresses allowed). The minimum soil load is calculated as:

$$\sigma_k, max = \frac{F}{A} - \frac{M}{W} = \frac{\sum V}{b \cdot l} - \frac{\sum M}{\frac{1}{6} l b^2} \quad [kN/m^2] \tag{L.14}$$

The bearing capacity can be calculated according to the Brinch Hansen method. As a rule of thumb, the bearing capacity of densely packed sand is often assumed to be 400 kN/m^2 in accordance with the Dutch Handboek Funderingen (CUR, 2010) (Hydraulic Structures Manual, 2018). For this preliminary calculations, the soil bearing capacity will be taken as 400 kN/m^2. This is quite conservative but due to lack of accurate soil information, the rule of thumb value will be assumed and further research in this topic is recommended.

Piping

Groundwater flow under structures is caused by a potential difference across the structure. That is, due to a water level difference at both sides of the structure. There are two basic conditions that have to be met so that piping occurs (Hydraulic Structures Manual, 2018):

1. The duration of the water level difference has to be sufficiently long to start this mechanism.
2. Sand particles should have the possibility to extrude. That is, if the ground level at land side of the structure is high enough, piping becomes unlikely, as if the ground had a sufficiently strong surface.

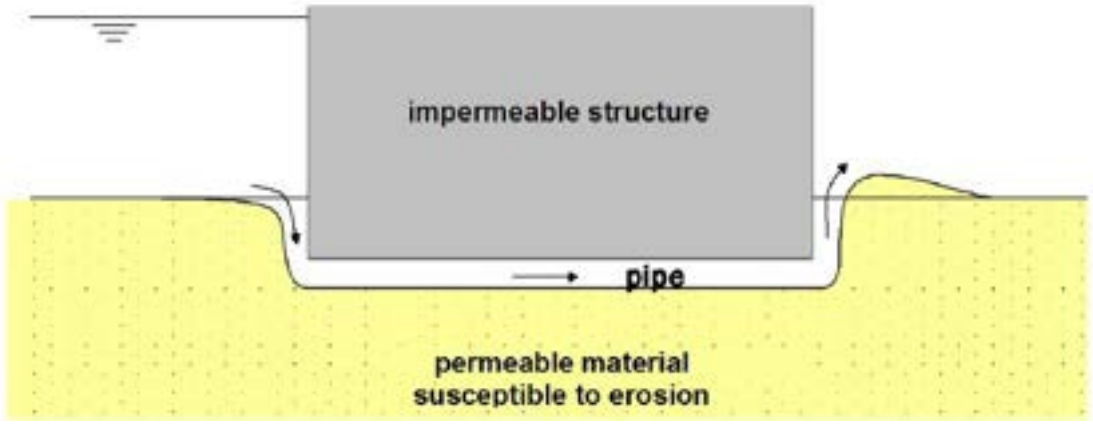

Figure L.7: Piping mechanism sketch. Source: Hydraulic Structures Manual

There are some empirical formulations to check if piping will occur. For this report, the Lane formulas will be used. Lane extended Bligh's theory and concluded that vertical parts of the structure are less likely to lead to pipe than horizontal parts. For that reason, the seepage length according to Lane is:

$$L = \sum L_{vert} + \sum \frac{1}{3} L_{hor} \quad [m] \tag{L.15}$$

In order to not have piping, the criterion to be met is the following one:

$$L \geq \gamma \cdot C_L \cdot \delta H \quad [m] \tag{L.16}$$

Where:

- L [m] = Total seepage distance.
- C_L [-] = Lane's constant, depends on soil type. See table below.
- ΔH [m] = Head difference across the structure
- γ [-] = Safety factor (1.5)
- i_{max} [-] = Maximum allowed hydraulic gradient = δH / L

In the following table, the Lane's constant and maximum hydraulic gradient are given for different types of soil:

Soil type	C_L	i_{max}
Very fine sand / silt / sludge	8.5	11.8%
Fine sand	7.0	14.3%
Middle fine sand	6.0	16.7%
Coarse sand	5.0	20.0%
(fine) Gravel (+sand)	4.0	25.0%

The Hans Sellmeijer (1988) formulation gives a more accurate piping description when compared to Lane's theory. Anyways, it won't be in this report since it requires a large amount of soil information.

Scour protection

The presence of a structure on the water along with waves and currents, creates local velocity fields that can erode the soil in the vecinity of the structure. Scour can be avoided using granular filters, geotextile or and more or less impermeable layers such as asphalt (Hydraulic Structures Manual, 2018). As mentioned before, the scour can be cause by waves or currents:

Scour of sand beds, induced by waves

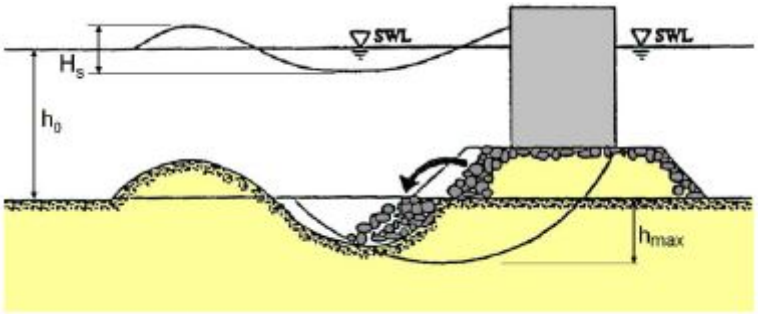

Figure L.8: Bottom scour induced by waves before breakwater

Xie (1981) proposed a simple equation for scour near vertical or steeply sloping impermeable structures, related to the wave height, water depth and wave length:

$$h_{max} = 0.4 \cdot H \cdot \left(sinh\left(\frac{2 \cdot \pi \cdot h_0}{L_{wave}} \right) \right)^{-1.35} \tag{L.17}$$

This equation is valid for both fine and course sediments with regular waves. Regular waves won't be present at the study area, but the formulation will be used to obtain a first estimate of the scour protection needed.

Scour of sand beds, induced by currents

Bed protection prevent structural damages due to soil erosion. Turbulence at the end of the scour protection could cause scour holes. If this holes are large enough, and a critical slope 1:n_s is exceeded, the bed protection will fall into the scour whole and failure of the structure will occur. For a first estimate, the required length of the bottom protection can be calculated with:

$$L \geq \gamma \cdot n_s \cdot h_{max} \tag{L.18}$$

Where:

- γ [-] = safety factor (¿ 1.0)
- 1:n_s [-] = average slope of the slide plane
- h_{max} [m] = maximum scour depth

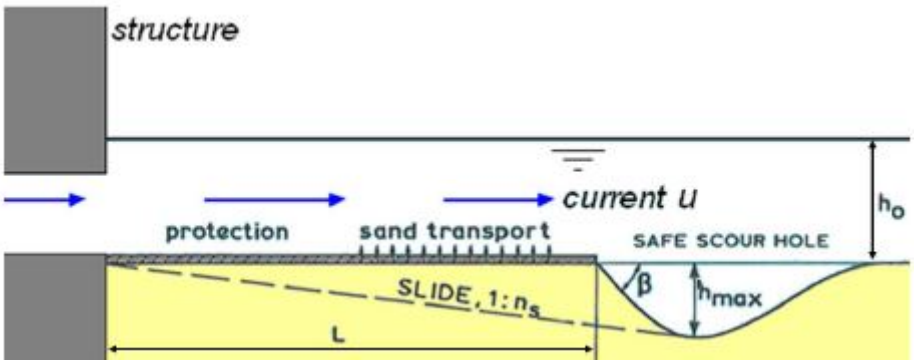

Figure L.9: Length of bottom protection

The values of n_s can vary considerably. It ranges from 6 for densely packed soil to 15 for loosely packed material.

The maximum depth of scour can be calculated from Herman Breusers of Deltares (1991), but the method is tedious and requires lots of information (Hydraulic Structures Manual, 2018). Therefore, assuming that no sediment is coming from upstream (clear water scour), the maximum equilibrium depth can be obtained using a much more simple formulation (see Equation L.19). This assumption is accepted as true since the water will come out of the power plant, where sediment is not allowed in.

$$\frac{h_{max}}{h_0} = \frac{0.5 \cdot \alpha \cdot u - u_c}{u_c} \; for \; 0.5 \cdot \alpha \cdot u > 0 \tag{L.19}$$

Where

- h_{max} [m] = maximum depth of the scour hole (equilibrium depth)
- h_0 [m] = initial water depth
- u [m/s] = depth-averaged flow velocity at the end of the scour protection
- u_c [m/s] = critical velocity regarding begin of motion of sand particles
- α [-] = turbulence coefficient, depending on the upstream disturbance. The valu of α is in the order of 3.

The critical velocity for inutiation of sand transport can be calculated with the Shields equation:

$$u_c = C\sqrt{\Psi_c \cdot \Delta \cdot D_{50}} \tag{L.20}$$

Where:

- D_{50} [m] = median nominal diameter of sand particles at the end of the scour protection.
- C [$\sqrt{m}$/s] = Chézy coefficient
- Δ [-] = relative density: $\Delta = \frac{\rho_s - \rho_w}{\rho_w}$
- Ψ_c [-] = Shields (stability) parameter (see Figure L.10)

The Chézy coefficient can be calculated with:

$$C = 18 \cdot log\Big(\frac{12 \cdot R}{k_r}\Big) \tag{L.21}$$

Where

- k_r [m] = equivalent bed roughness:
  $k_r \approx 2D_{n50}$ for narrowly graded gravel and rock
  $k_r \approx 3D_{n50}$ for widely graded gravel and rock
  $k_r \approx 1$ to 5 dm for sand

- R [m] = hydraulic radius of the flow channel at the end of the scour protection:
  R = wet area/ wet circumference of the flow channel
  $R \approx h_0$ for wide channels

The shields parameter depends of the dimensionless grain diameter: $d_* = D_{50} \cdot \sqrt[3]{\frac{\delta \cdot g}{\nu^2}}$ where ν is the kinematic viscosity [m^2/s]. In the following figure, the relationship between the shields parameter and dimensionless grain diameter is shown:

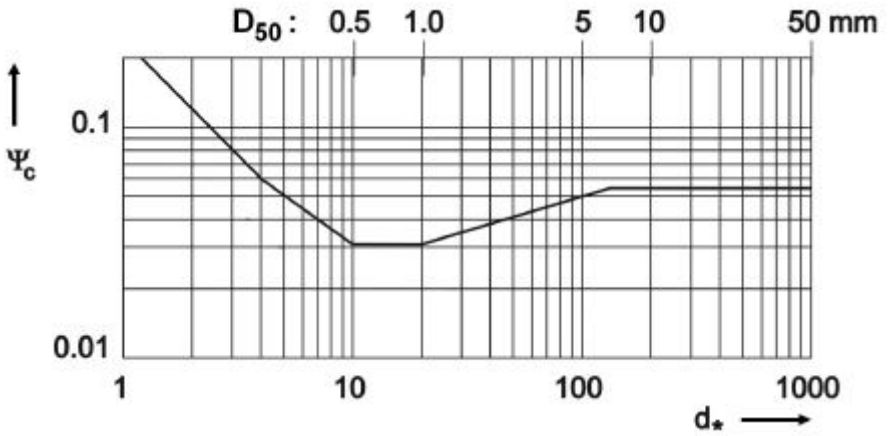

Figure L.10: Relation between the Shields parameter and d_* or d_{50} for determining the scour depth under usual conditions (after Schiereck & Verhagen, 2016)

So, for the present case, the turbined water will come into the Valmeer at a specific velocity. This velocity could be enough to erode the sand particles around the structure and cause failure of it. For the present geometry, the velocity at the entrance to the Valmeer (averaged over the cross-section) would be around:

$$v = \frac{Q}{A} = \frac{60}{13.5 \cdot 6.1} = 0.73 m/s$$

L.3 Alternative 1: Power Plant as storm surge barrier. In situ.

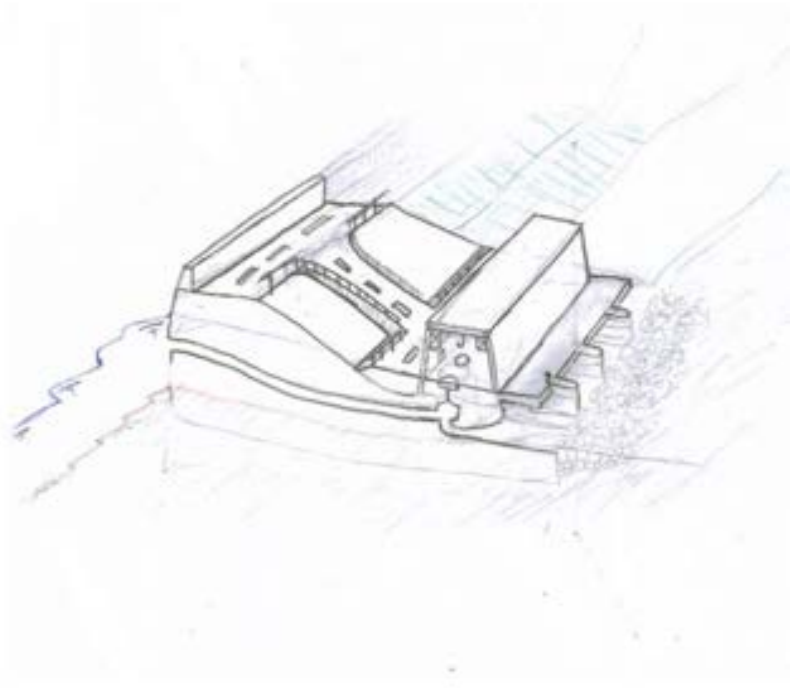

Figure L.11: 3D conceptual design of the power station. Cut showing the interior of the whole water defence plus power station.

First, the top levels of the structure are calculated from an overtopping calculation. In the Appendix **??** the full calculations are shown. In the next table the results of those calcualations are shown:
Now that the ground and water levels, as so as wave height and period are defined, the stability calculations can be performed. For the structure to be stable, the requirements for horizontal stability and rotational stability have to be met (see Section L.2).

The load case having storm surge conditions and a low water level within the Valmeer is used for the first stability calculations. This load case can be seen below:

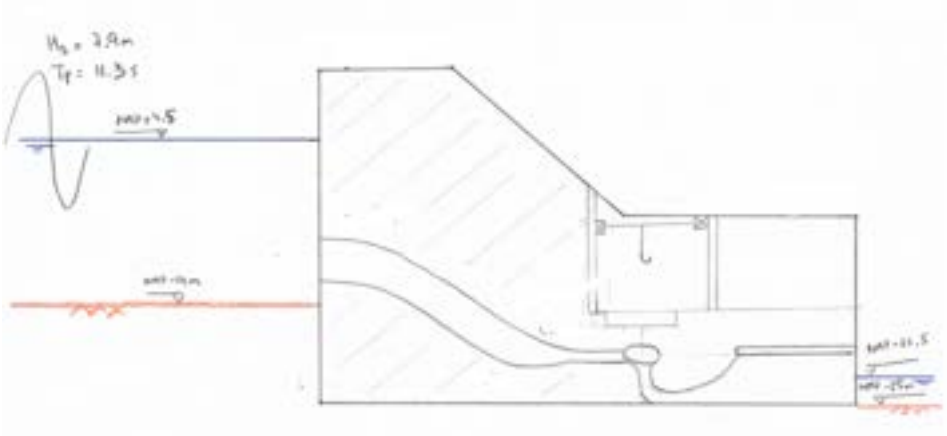

Figure L.12: Caption

L.3.1 Overall stability

In the present section, the results of the calculations for ensuring stability are shown. The forces acting on the structure can be seen in Figure L.1. The weight of the structure and length of it are iterated until the adequate weight and dimensions are obtained. Then, the design will be done considering those weight and dimensions of the structure, this process is iterative and only the results are shown in these sections. In the following lines, the initial geometrical data for each location as so as design storm are shown. Then, the stability calculations are presented.

In the table below, the geometry and wave forces necessary for performing stability calculations are given:

GEOMETRY			
Design water level at sea	WL-sea	4.5	m +NAP
Design water level at ESL	WL-valmeer	-22.5	m +NAP
Ground level at sea	GL-sea	-14	m +NAP
Ground level at ESL	GL-Valmeer	-34	m +NAP
Bottom of structure	Bot	-34	m +NAP
Width of structure	b (L next sheet)	84	m
Design wave at sea	H_s	7.9	m
Design wave length at sea	L_s	139	m
TopLevel of structure at sea	TL_sea	12.75	m +NAP
TopLevel of structure at ESL	TL_ESL	-4.5	m +NAP
Cross section area	A	1884.4	m2

Figure L.13: Structure's and surrounding geometry when in Location 1

This geometry defines the value of the loads since they depend on: water level, ground level, wave loading and geometry of the alternative. Therefore, now we can calculate the different loads. For the self-weight calculation, reinforced concrete has been considered ($\gamma_c = 25$ kN/m^3). The area that has that reinforced concrete is represented in Figure D.1 with dashed lines. So the weight of the turbine's concrete casing and the one of the maintenance rooms is not included in the calculations. Notice that the loads are given per meter width of structure.

FORCES						
Weight	W	47109	kN/m	applied @	0.0	m from center of BOS
Buoyancy force	F_b	21000	kN/m	applied @	0	m form center of BOS
Hydrostatic force (sea)	F_hs	7411	kN/m	applied @	6.2	m from BOS
Hydrostatic force (ESL)	F_hv	661	kN/m	applied @	3.8	m from BOS
Horizontal wave force p1(Sea)	F_p1	358	kN/m	applied @	24.3	m from BOS
Horizontal wave force p3 (Sea)	F_p3	831	kN/m	applied @	10.2	m from BOS
Horizontal wave force p1-p3 (Sea)	F_p1-p3	199	kN/m	applied @	13.6	m from BOS
Vertical wave force pu (Sea)	F_pu	1684	kN/m	applied @	14.0	m from center of BOS
Horizontal soil force (sea)	F_sh	883	kN/m	applied @	6.7	m from BOS
						*BOS = Base of Structure

Figure L.14: Forces acting on the structure when in Location 1

For a weight of 37000 kN/m, the structure is stable as it can be seen below:

STABILITY CHECKS			
Horizontal stability			
Resulting horizontal force (→)	H	10464	kN
Resulting vertical force (↓)	V	17557	kN
friction coefficient	μ	0.6	[-]
check	H<μ*V?	YES	
Rotational stability			
Resulting overturning moment	M	86231	kNm
Resulting vertical force (↓)	V	17557	kN
	er = M/V	4.9	m
check	er < b/6?	YES	
Load acting on the soil			
Resulting vertical force (↓)	V	17557	kN
Resulting overturning moment	M	80347	kNm
Structure's base area	A	72	m2/m
Structure's base section modulus	W	864	m3/m
Maximum load acting on the soil	σk_max	337	kN/m2/m
Minimum load acting on the soil	σk_min	151	kN/m2/m
Soil bearing capacity	σ_soil	400	kN/m2/m
checks	σk_min > 0?	YES	
	σk_max < σ_soil?	YES	

Figure L.15: Stability checks when structure's in Location 1

Piping is the same for Alternative 1 and 3, since for Lane, the total seepage distance depends on the head difference across the structure (see Section L.2.2), which is the same for Alternative 1 and 3. Alternative 2 don't have any head difference at the sides of the structure. For that reason, piping won't be a failure mechanism in this alternative.

Therefore, considering gravel as foundation material, the piping calculations are as follows:

PIPING			
seepage distance	L>gamma*Cb*deltaH	144	**m**
safety factor	gamma	1.5	
Lanes' constant	Cl	4	
differential head	deltaH	24	**m**
Max allowed hydraulic gradient	deltaH/L	16.7%	

Figure L.16: Seepage length calculation. Notice that this calculation is valid for all locations and for both Alternative 1 and 3.

To avoid piping, sheet piles could be placed under the structure. However, taking into account the base's length, 20 sheetpiles of 6 meters would be needed. When taking constructability into account, this is not a good option because the sheet piles would be needed for the more than 2700 meters long power station. However, a large impermeable layer using geotextiles can be installed at the seabed.

The next step is to calculate the scour wholes and the bed protection next to the structure. In the following table, all the necessary input as so as the calculation results are shown:

SCOUR OF SAND BED, INDUCED BY WAVES			
Incident wave height	H	7.9	m
Incident wave length	L	123	m
Water depth before the structure	h0	20	m
Maximum scour hole depth	h_max	2.4	m
SCOUR OF SAND BED, INDUCED BY CURRENTS			
Safety factor	γ	1.2	[-]
Avg. slope of the slide plane	n_s	10	[-]
Water depth before the structure	h0	18.5	m
Velocity at the end of scour protecti	u	0.75	m/s
Turbulence coefficient	α	3	[-]
Median nominal diameter	D_50	0.001	m
Relative density	ρ	0.6	[-]
Shield's stability parameter	ψ_c	0.1	[-]
Hydraulic radius of flow channel	R	20	[m]
Equivalent bed roughness	k_r	0.003	[m]
Chezy coefficient	C	88.256	[-]
Critical velocity for beginning of mc	u_c	0.684	m/s
Maximum scour hole depth	h_max	0.646	m
Length for scour protection	L	7.748	m

Figure L.17: Scour calculations

As we can see above, the maximum scour whole in front of the structure is of 2.4 meters during design storm. However, notice that the calculations assumed a storm duration enough for eroding all the scour hole. That means that in reality the hole could not be as big as the calculations show. Even though with this assumption we ensure that the actual hole won't be as big as the design one. So we are on the safe side. Important since the failure of this structure would lead to disastrous consequences regarding flood security.

Besides, the needed protection length for the exit of turbines water is of 7.7 meters. Notice that the velocity considered was the water velocity at the exit of the outlet and not at 7.7 m from the exit. This assumption is done to simplify the calculations. On the one hand, this distance will reduce the water speed but on the other hand, since turbulence is not accounted for, the local velocities at the scour whole 7.7 m form the structure can be similar to the one at the exit of the structure.

L.4 Alternative 2: The construction is not a flood defense

This alternative aims to have a small and simple powerhouse. The idea around this alternative is to use a dike surrounding the whole Valmeer and then installing the power plant within the ESL.

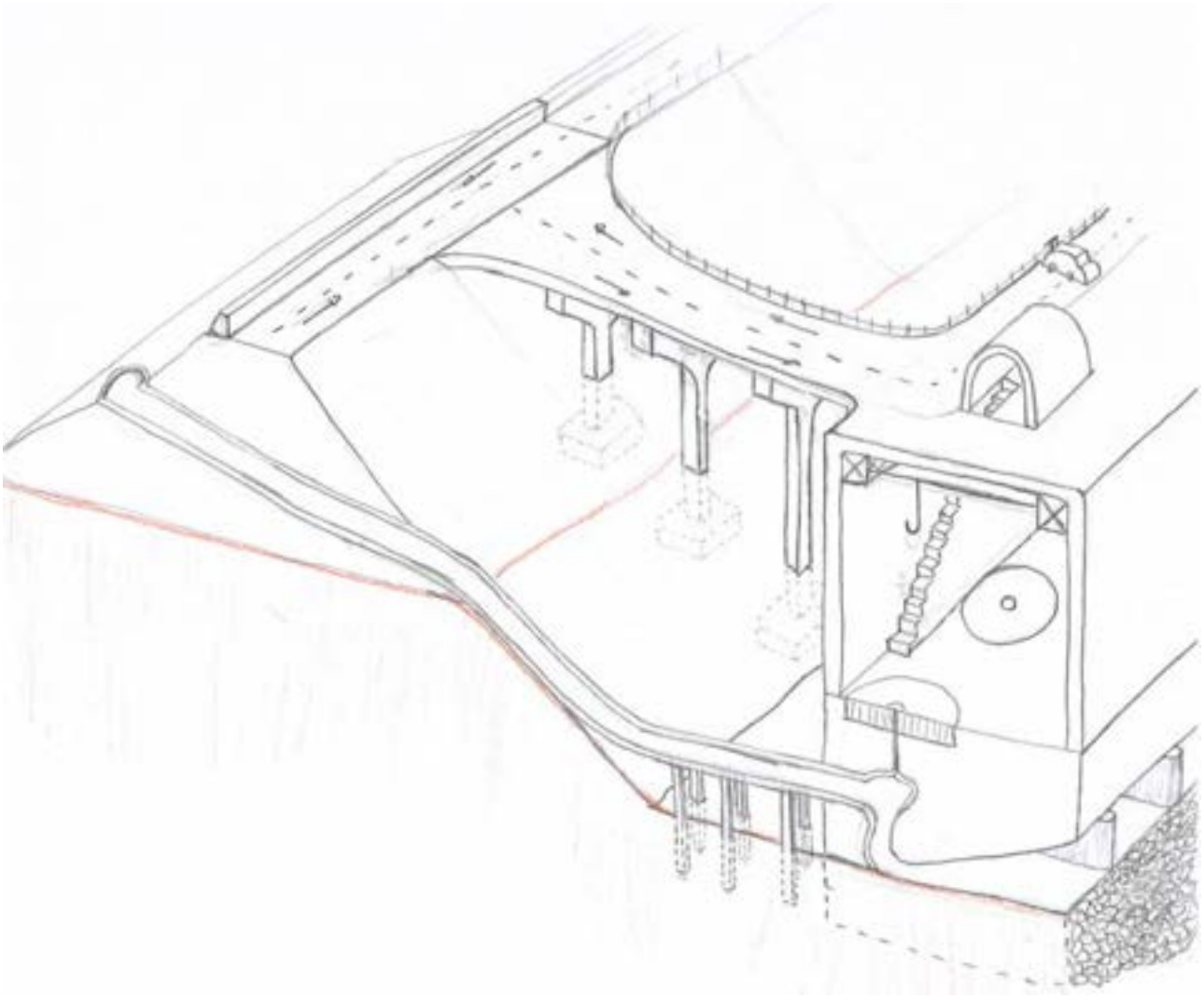

Figure L.18: 3D representation of Alternative 2.

This is an attractive alternative since the power station design could be very simple, having always the same water level all around and not being exposed to large waves the structure's overall stability would be easy to meet. However, to realise this alternative, the pipe reaching the pump/turbines will need to be very large. This means that head losses could be a limiting factor for this alternative. Besides, constructability issues might appear (see appendixH)

L.4.1 Overall stability

The next geometry provides stability of the whole design:

GEOMETRY			
Design water level at sea	WL-sea	-5	m +NAP
Design water level at ESL	WL-valmeer	-5	m +NAP
Ground level at sea	GL-sea	-34	m +NAP
Ground level at ESL	GL-Valmeer	-34	m +NAP
Bottom of structure	Bot	-34	m +NAP
Width of structure	b (L next sheet)	41	m
Design wave at sea	H_s	2.6	m
Design wave length at sea	L_s	42	m
TopLevel of structure at sea	TL_sea	-4.5	m +NAP
TopLevel of structure at ESL	TL_ESL	-4.5	m +NAP
Cross section area	A	529.6	m2

Figure L.19: Structure's and surrounding geometry when in Location 1

This geometry defines the value of the loads since they depend on: water level, ground level, wave loading and geometry of the alternative. Therefore, now we can calculate the different loads. For the self weight calculation, reinforced concrete has been considered. Notice that the loads are given per meter width of structure.

FORCES						
Weight	W	13240	kN/m	applied @	0.0	m from center of BOS
Buoyancy force	F_b	11890	kN/m	applied @	0	m form center of BOS
Hydrostatic force (sea)	F_hs	4205	kN/m	applied @	9.7	m from BOS
Hydrostatic force (ESL)	F_hv	4205	kN/m	applied @	9.7	m from BOS
Horizontal wave force p1(Sea)	F_p1	30	kN/m	applied @	33.2	m from BOS
Horizontal wave force p3 (Sea)	F_p3	47	kN/m	applied @	16.0	m from BOS
Horizontal wave force p1-p3 (Sea)	F_p1-p3	226	kN/m	applied @	21.3	m from BOS
Vertical wave force pu (Sea)	F_pu	30	kN/m	applied @	6.8	m from center of BOS
Horizontal soil force (sea)	F_sh	0	kN/m	applied @	0.0	m from BOS
						*BOS = Base of Structure

Figure L.20: Forces acting on the Alternative 2

These forces, as we can see below, are balanced and make the structure stable. The calculations for horizontal, rotational, vertical stability, piping and scour protection are shown below:

STABILITY CHECKS			
Horizontal stability			
Resulting horizontal force (→)	H	333	kN
Resulting vertical force (↓)	V	1320	kN
friction coefficient	μ	0.6	[-]
check	H<μ*V?	YES	
Rotational stability			
Resulting overturning moment	M	6759	kNm
Resulting vertical force (↓)	V	1320	kN
	er = M/V	5.1	m
check	er < b/6?	YES	
Load acting on the soil			
Resulting vertical force (↓)	V	1320	kN
Resulting overturning moment	M	6759	kNm
Structure's base area	A	41	m2/m
Structure's base section modulus	W	280	m3/m
Maximum load acting on the soil	σk_max	56	kN/m2/m
Minimum load acting on the soil	σk_min	8	kN/m2/m
Soil bearing capacity	σ_soil	400	kN/m2/m
checks	σk_min > 0?	YES	
	σk_max < σ_soil?	YES	

Figure L.21: Stability checks when structure's for Alternative 2

For this alternative, it is also critical the bending moment that the maintenance room is going to hold. A representation of this is shown in the following figure:

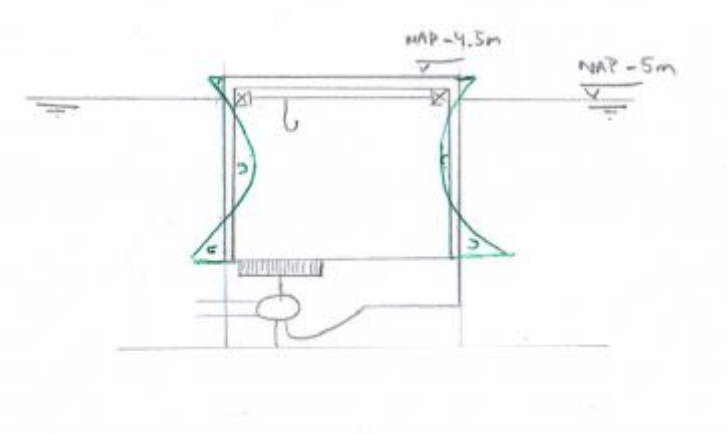

Figure L.22: Caption

L.4.2 Bed Protection

Regarding bed protection, the bed protection used for the previous alternative can be used. The velocity at which the water enters the Valmeer is the same as for that alternative. So the 7.7 meters bed protection still has to be applied.

However, the scour whole in front of the structure can be now calculated as:

SCOUR OF SAND BED, INDUCED BY WAVES			
Incident wave height	H	2.6	m
Incident wave length	L	42	m
Water depth before the structure	h0	20	m
Maximum scour hole depth	h_max	0.0	m

Figure L.23: Scour depth whole in front of structure

So no scour hole will develop during design conditions.

L.5 Alternative 3: The construction is part of the flood defense in combination with the dike

This alternative is a mix of the two previous structure, so for that reason and due to time limit, the structure will be considered to have lengths and weights that range between the previous two. Therefore, the weight of this structure for stability is between 47109 kN/m and 13240 kN/m. In the same way, the length for stability will be between 84 m and 24 m.

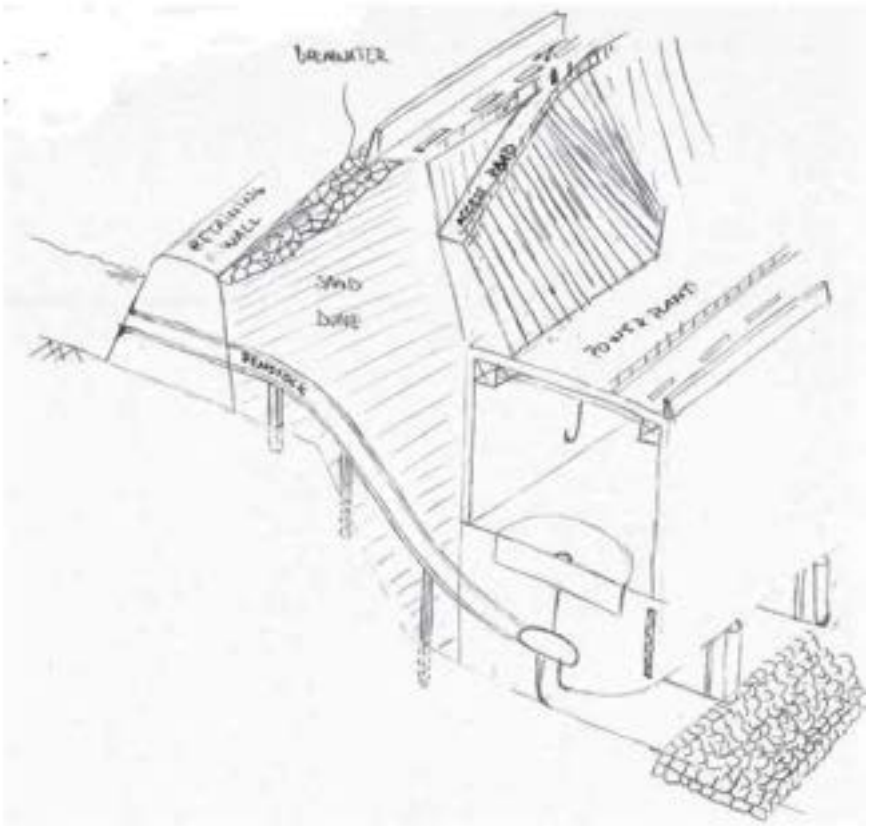

Figure L.24: 3D representation of Alternative 3

The next step is to calculate the scour wholes and the bed protection next to the structure. Again, this calculations are the same for this alternative as for Alternative 1. Therefore, the reader is referred to Figure L.17 to check the scour calculations.

The head loss however, is similar to the one in Alternative 2. The only different parameter in both alternatives is pipe's length, but from Alternative 2 to 3 this change is negligible.

L.6 Stability calculations for the chosen alternative

In Section 6.4 can be seen that the chosen alternative is Alternative 1 built in situ. In the present section, the Alternative 1 is shown after some design loops have been performed. This is because the iterations were done using an excel spreadsheet. So several design loops have been done. The formulation used to check to structure's stability is the one present in Appendix L, already used for checking the general stability of the alternatives 1, 2, and 3. Now, however, the plant's elements and weight are better defined. The final cross section can be seen below (To see the different elements of the plant, the reader is referred to Appendix K.):

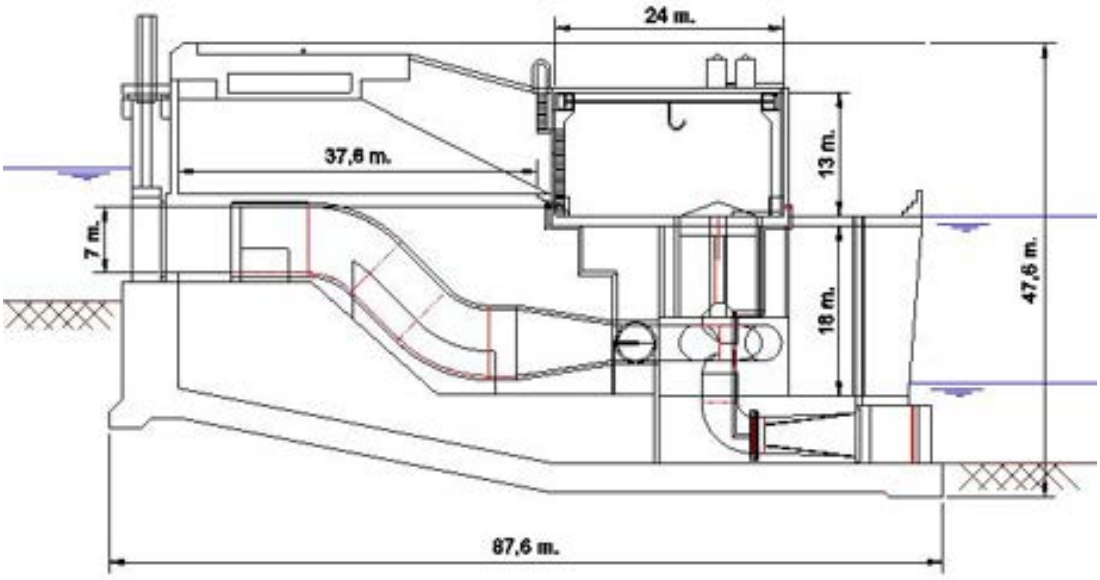

Figure L.25: Cross section showing final power plant's design

The calculations performed for the alternative include the following sections:

- Horizontal stability
- Rotational stability
- Vertical stability
- Piping protection
- Bed protection at the in-/outlet of the structure

Notice that the present appendix collects the results of design iterations. First, knowing that the final plant's length would be 84 meters (it is enough to host all the elements of the plant and in the initial stability calculations the plant was stable for a length of 84 meters), the minimum weight for making the structure stable was calculated. This was calculated by looking at the minimum weights per meter that the structure needed to be stable regarding horizontal, vertical and rotational stability. The horizontal stability was found to give the largest weight and therefore it was the critical check.

For that reason then, in the following lines, the horizontal stability calculations are first shown. There, the procedure to arrive to the stable weight of 37400 kN/m is shown. Afterwards, the checks for rotational and vertical stability are done.

The weight of the plant was obtained from the volumes of the elements of the power plant. These volumes come from the 3D model done. Remember that the model represents 3 modules of the structure. Accounting for a total of 148 meters. The total number of modulus needed for the total structure is 56. The model is composed of 178236 m^3 of reinforced concrete, 56115 m^3 of compartments which will be filled with sand and 1631 m^3 of steel elements such as cables, tubes and gates. Therefore, the structure's weight per meter is:

$$W_{structure} = \frac{178236m^3 \cdot 25kN/m^3 + 56115m^3 \cdot 17kN/m^3 + 1631m^3 \cdot 75kN/m^3}{148} = 37379kN/m \approx 37400kN/m^3$$

L.6.1 Horizontal stability

Sketch failure mechanism

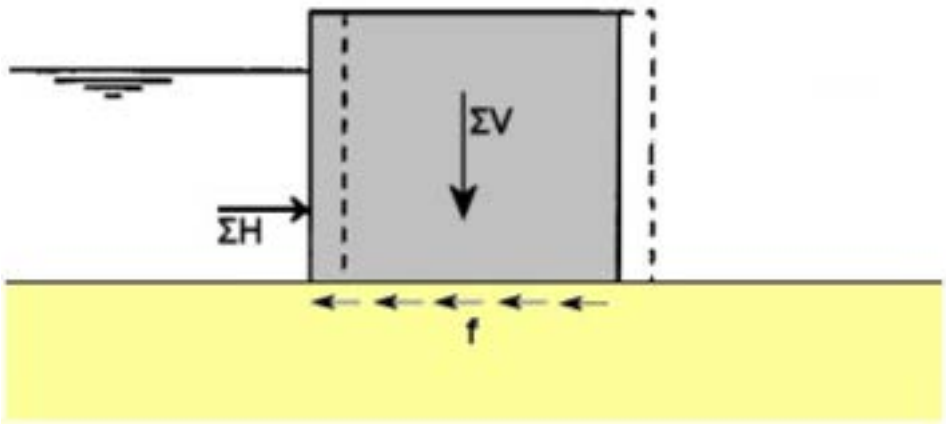

Figure L.26: slip-off principle sketch. Source: Hydraulic Structures Manual

$$\sum H \leq f \cdot \sum V \tag{L.22}$$

Critical load case

Two models of forces were considered to find the worst-case scenario for horizontal stability. The worst-case comes when the resultant horizontal forces are maximum and the resultant vertical forces are minimum. In the first load case considered, the head difference is governing (maximum lateral loads but maximum vertical load, buoyancy force is minimum) and in the second, maximum wave height does (not maximum horizontal forces, but minimum resultant vertical force, buoyancy is maximum). At first glance, the first load case seems to be more critical, since the head difference is maximum and quite large, however, buoyancy might play an important role reducing the weight of the structure and therefore the two load case s are studied:

1. Regular working conditions: In this load case , the maximum water head difference is present. For these working conditions, the design water level and wave height will have a return period of 10 years.

2. Storm surge conditions: In this load case , the wave loading is maximum. The design wave height will have a return period of 1000 years

These two load case s will be considered to check horizontal stability of the structure. The goal is to see which load case gives the larger structure dimensions and weight and then use that weight for design. Thus, making sure that the structure will hold the forces present at any future condition.

In the following lines, the stability calculations are shown for both load case s.

Regular working conditions

Water level at Valmeer is at NAP -22.5m for providing potential energy to the water. The head difference is maximum at this stage. The design wave and water level are the ones corresponding to 1/10 years

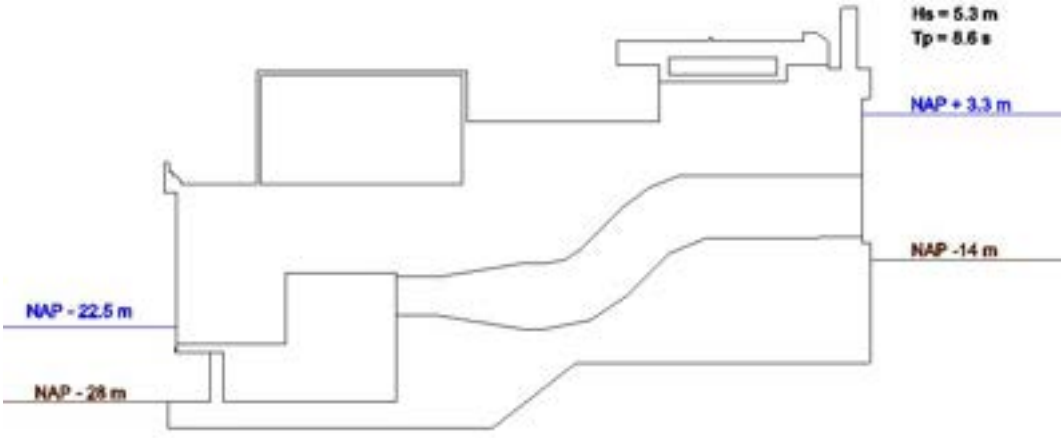

Figure L.27: load case regular conditions

The first step is to obtain the wave forces. From Goda, 1974 and using the following input values, the different wave pressures can be calculated:

Goda, 1974. Input values.		
β	30.00	degrees (NNW)
λ1	1	Vertical wall
λ2	1	and non
λ3	1	breaking waves
hb, water depth @ 5H from wall	22.49	m
Hd	5.3	m
Ld	88	m
d	17.3	m
h'	35.3	m
h	20.76	m
hc	9.45	m

Figure L.28: Input values for Goda, 1974

By pluggin-in these values in equations L.7, L.8, L.9 and L.10 the wave pressures can be obtained:

Goda, 1974. Output values.		
p1	32.00	kN/m2
p3	1.09	kN/m2
p4	0.00	kN/m2
pu	1.09	kN/m2
η	7.4	m
α1	0.6470	[-]
α2	0.0072	[-]
α3	0.0341	[-]
α4	0.0000	[-]
hc*	7.4	m

Figure L.29: Wave pressures. Goda, 1974.

In the following figure the pressures as so as the dimensions considered for the present load case can be seen:

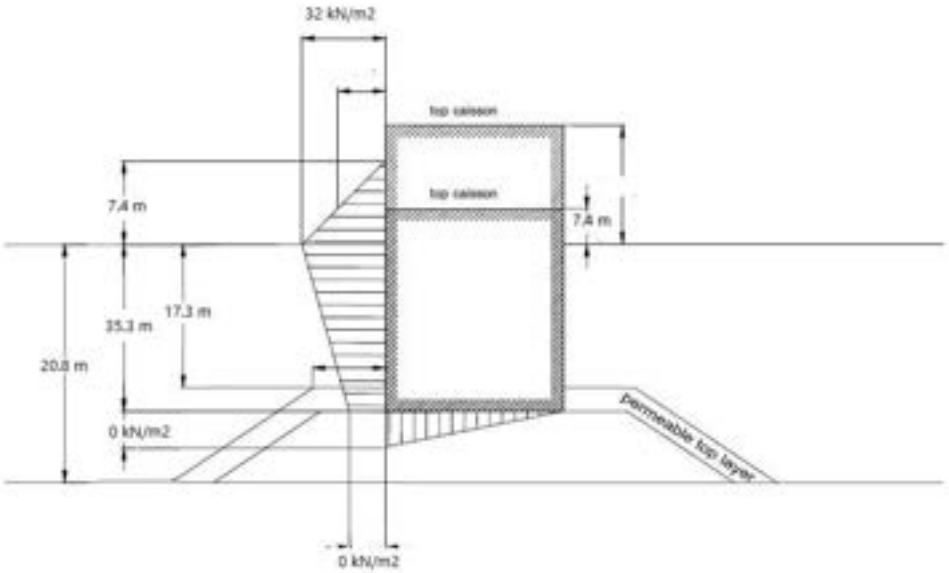

Figure L.30: Graphical representation of wave pressures

Once the wave pressures are obtained, the wave forces as so as the hydrostatic force, soil force, selfweight and buoyancy forces can be calculated (see Section L.2). The forces are obtained per meter width of element:

FORCES				
Weight	W	31000 kN/m	applied @	0.0 m from center of BOS
Buoyancy force	F_b	18816 kN/m	applied @	0 m from center of BOS
Hydrostatic force (sea)	F_hs	6230 kN/m	applied @	11.8 m from BOS
Hydrostatic force (ESL)	F_hv	451 kN/m	applied @	3.2 m from BOS
Horizontal wave force p1(Sea)	F_p1	119 kN/m	applied @	37.8 m from BOS
Horizontal wave force p3 (Sea)	F_p3	39 kN/m	applied @	17.7 m from BOS
Horizontal wave force p1-p3 (Sea)	F_p1-p3	546 kN/m	applied @	23.5 m from BOS
Vertical wave force pu (Sea)	F_pu	46 kN/m	applied @	14.0 m from center of BOS
Horizontal soil force (sea)	F_sh	715 kN/m	applied @	6.0 m from BOS

*BOS = Base of Structure

Figure L.31: Forces considered for overall stability of the structure

A representation of the above forces is shown below:

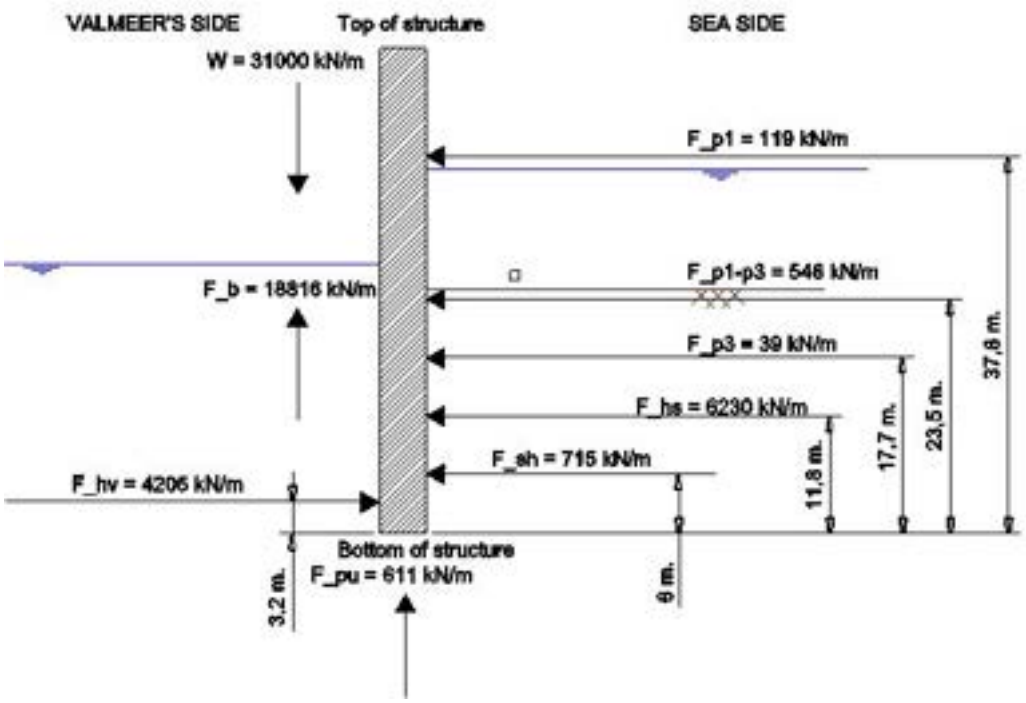

Figure L.32: Forces considered for overall stability of the structure. Graphic representation

Taking this into account and following the formulations shown in Section L.2.2 the stability calculations are done. For that, first the resultant horizontal and vertical force has to be computed:

$\sum H = F_{p1} + F_{p1-p3} + F_{p3} + F_{hs} + F_{sh} - F_{hv} = 7243kN/m$

$\sum V = W - F_b - F_{pu} = 12138kN/m$

From Section L.2.2, the horizontal stability is met if:

$\sum H \leq \nu \cdot \sum V; 7243kN/m \leq 0.6 \cdot 12138kN/m = 7283kN/m$

Thus, horizontal stability is ensured.

Storm surge conditions.

Water level at Valmeer is at NAP -5m for providing maximum lateral stability. The design wave and water level are 1/1000 years.

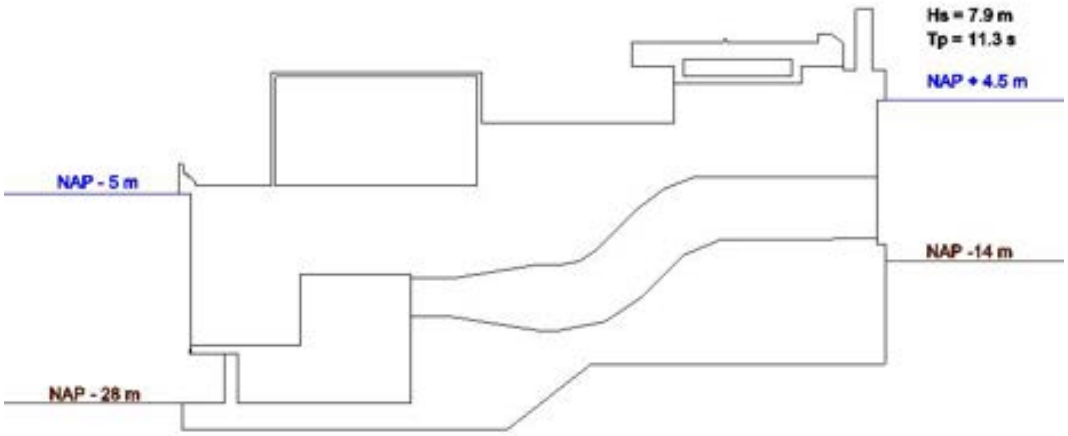

Figure L.33: load case storm surge situation

The first step is to obtain the wave forces. From Goda, 1974 and using the following input values, the different wave pressures can be calculated:

Goda, 1974. Input values.		
β	30.00	degrees (NNW)
λ1	1	Vertical wall
λ2	1	and non
λ3	1	breaking waves
hb, water depth @ 5H from wall	24.05	m
Hd	7.9	m
Ld	123	m
d	18.5	m
h'	36.5	m
h	22.2	m
hc	8.25	m

Figure L.34: Input values for Goda, 1974

By pluggin-in these values in equations L.7, L.8, L.9 and L.10 the wave pressures can be obtained:

Goda, 1974. Output values.		
p1	52.55	kN/m2
p3	16.53	kN/m2
p4	13.34	kN/m2
pu	16.52	kN/m2
η	11.1	m
α1	0.7126	[-]
α2	0.0140	[-]
α3	0.3146	[-]
α4	0.2538	[-]
hc*	8.3	m

Figure L.35: Wave pressures. Goda, 1974.

In the following figure the pressures as so as the dimensions considered for the present load case can be seen:

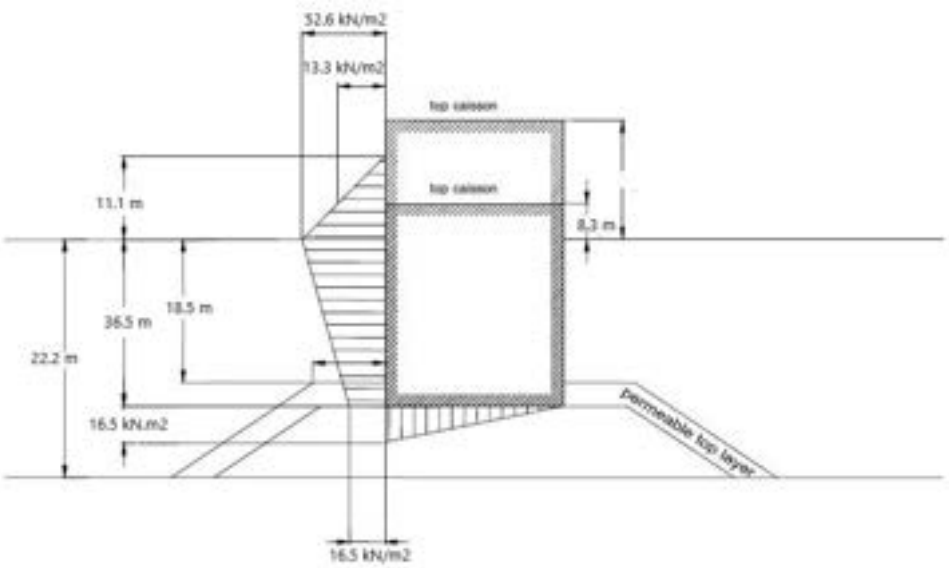

Figure L.36: Graphical representation of wave pressures for the design storm surge situation

Once the wave pressures are obtained, the wave forces as so as the hydrostatic force, soil force, selfweight and buoyancy forces can be obtained (see Section L.2). The forces are obtained per meter width of element:

FORCES				
Weight	W	37400 kN/m	applied @	0.0 m from center of BOS
Buoyancy force	F_b	26670 kN/m	applied @	0 m from center of BOS
Hydrostatic force (sea)	F_hs	6661 kN/m	applied @	12.2 m from BOS
Hydrostatic force (ESL)	F_hv	3645 kN/m	applied @	9.0 m from BOS
Horizontal wave force p1(Sea)	F_p1	291 kN/m	applied @	40.2 m from BOS
Horizontal wave force p3 (Sea)	F_p3	603 kN/m	applied @	18.3 m from BOS
Horizontal wave force p1-p3 (Sea)	F_p1-p3	657 kN/m	applied @	24.3 m from BOS
Vertical wave force pu (Sea)	F_pu	694 kN/m	applied @	14.0 m from center of BOS
Horizontal soil force (sea)	F_sh	715 kN/m	applied @	6.0 m from BOS

*BOS = Base of Structure

Figure L.37: Forces considered for overall stability of the structure

A representation of the above forces is shown below:

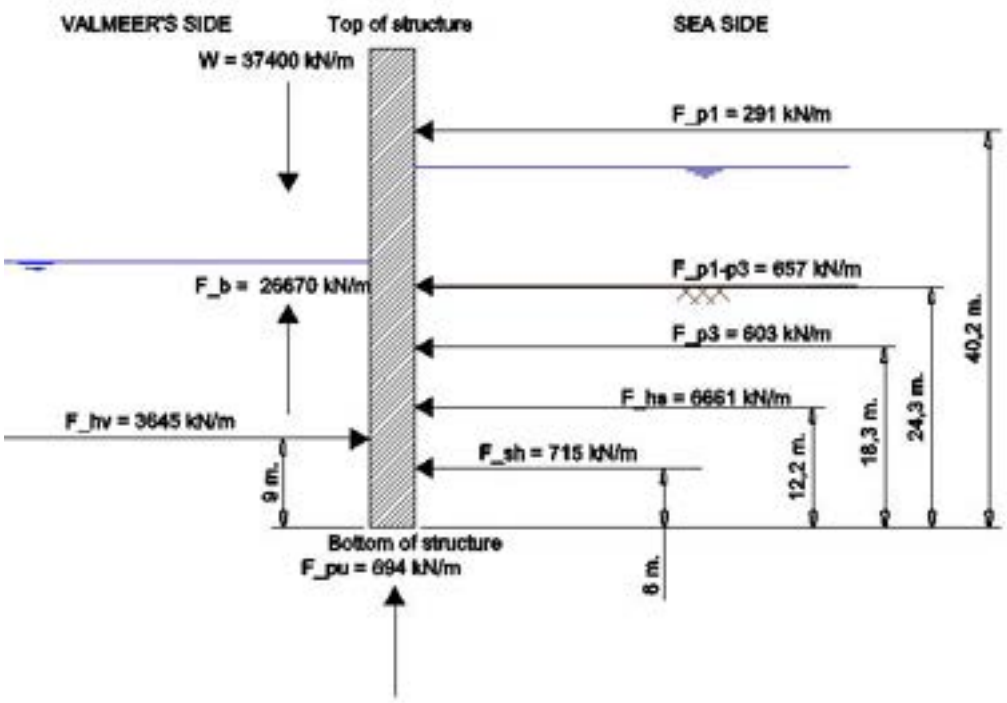

Figure L.38: Forces considered for overall stability of the structure. Graphic representation

Taking this into account and following the formulations shown in Section L.2.2 the stability calculations are done. For that, first the resultant horizontal and vertical force have to be computed:

$\sum H = F_{p1} + F_{p1-p3} + F_{p3} + F_{hs} + F_{sh} - F_{hv} = 5976kN/m$

$\sum V = W - F_b - F_{pu} = 10036kN/m$

From Section L.2.2, the horizontal stability is met if:

$\sum H \leq \eta \cdot \sum V; 5976kN/m \leq 0.6 \cdot 10036kN/m = 6022kN/m$

Thus, horizontal stability is ensured.

Conclusions from horizontal stability checks

The initial assumption that the regular conditions load case would be more critical due to the head difference is not true. Head difference plays an important role because of the large hydrostatic loads that are created. However, large head difference also means less buoyancy (see Equation L.6 to see how buoyancy is calculated), which in turn, resulted to be disadvantageous for the structure's stability (the horizontal stability check was found to be the most critical for stability, therefore the less buoyancy the better). For this reason, for each load case , the stability calculations have been obtained for a varying water level within the Valmeer.

The results are the following for both Regular and storm surge conditions:

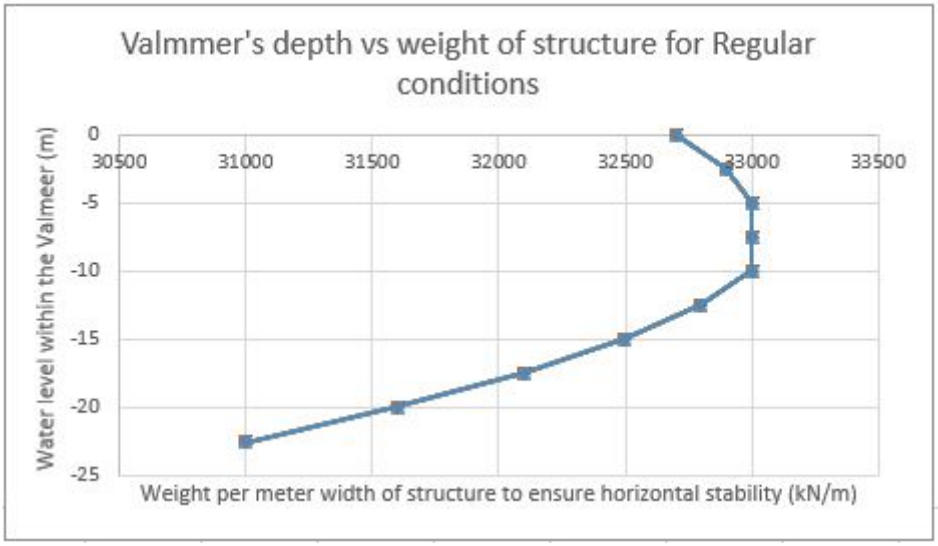

Figure L.39: Valmeer's depth vs weight of structure for Regular conditions

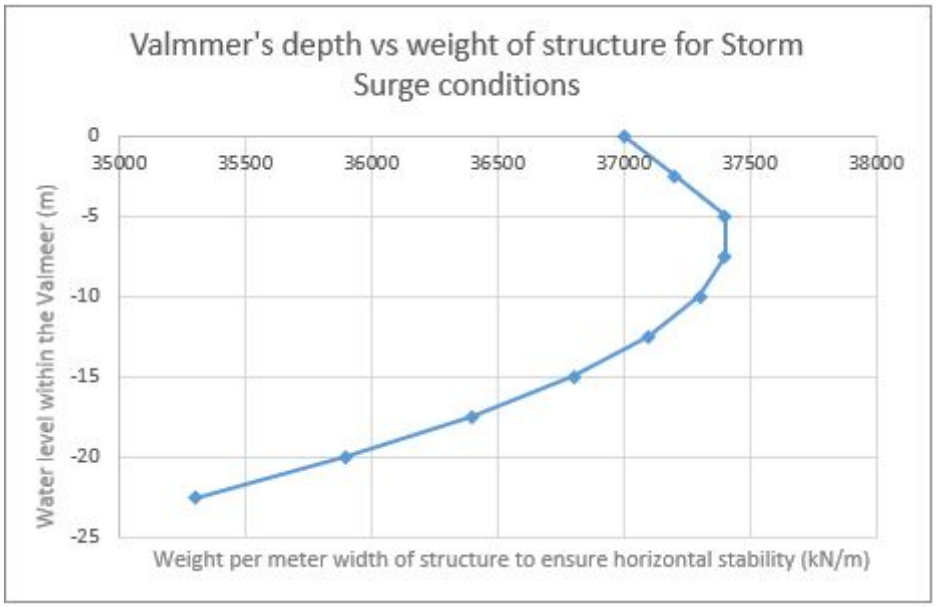

Figure L.40: Valmeer's depth vs weight of structure for Regular conditions

In these figures, it can be seen that the buoyancy influence in stability is noticeable. To the surprise of the author, the structure is more stable (less weight needed for stability) when the water level differences between the sea and the Valmeer are maximum. The worst-case scenario happens for storm surge conditions and a water level inside the Valmeer between NAP -5 m and NAP -7.5 m. For these water levels, the contribution of the lateral load by raising the water within the Valmeer is counteracted by the large buoyancy force product of having such high water levels within the Valmeer. Therefore a large weight per unit meter of structure is needed for the structure to be stable. When the water level goes higher (in the real case cannot go higher than NAP -5 m, but it is interesting to see what would happen), the water inside the Valmeer seems to counteract the loss of weight from the buoyant forces by an increase in lateral load. The opposite happens when the water level drops below NAP -7.5m. The low water level inside the Valmeer causes loss in lateral stability but, in turn, the loss in buoyant force is more critical and makes the structure more stable (less weight is needed for stability).

The selected weight per meter that the structure needs to have to be stable is then the corresponding to storm surge conditions (H_s = 7.9 m, T_p = 11.3s) and a water level within the Valmeer between NAP -5 m and NAP -7.5 m. The weight per meter needed for stability is then 37400 kN/m.

Another interesting conclusion is that the water level within the Valmeer don't have to be raised to NAP -5 m in order to have more favourable conditions to hold back the storm surge, as it was expected since the beginning. It was demonstrated above that the most favourable case for providing lateral stability to the structure is when the water level in the Valmeer is minimum (NAP -22.5 m). This means that the water level of the Valmeer can be lowered to NAP -22.5 m in order to resist better the loads and to increase the storing capacity of runoff water of the Valmeer. Then maybe the pumps would not need to be used until a really large river discharge is present. However, lowering the water level at maximum during storm surge conditions is not a good strategy regarding piping (see piping protection Section L.6.4 below). This is not in the scope of this thesis and therefore no further mentions about it will be done.

From now on, the storm surge conditions can happen together with having water levels within the Valmeer between NAP -5 m and NAP -22.5 m.

L.6.2 Rotational stability

Sketch failure mechanisms

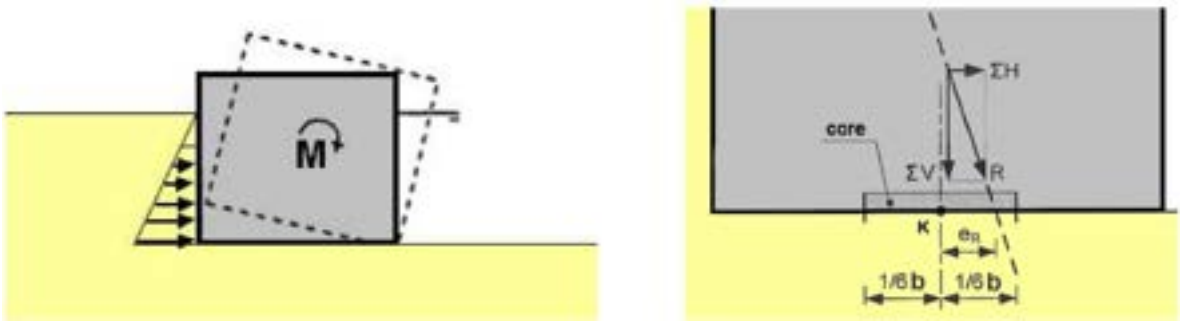

Figure L.41: Rotational stability sketch.Source: Hydraulic Structures Manual

$$e_R = \frac{\sum M}{\sum V} \leq \frac{1}{6} b \quad [m] \tag{L.23}$$

Critical load cases

Now that the worst-case for selecting the weight of the structure was developed, in the following sections, the checks showing that the other stability requirements are met are shown.

In the present section, the worst-case loading regarding rotational stability is considered. Rotational stability is more critical when the rotational moment is maximum and the vertical resultant force is minimum. Maximum rotational moment happens when the head difference is maximum (only lateral loads are considered) but minimum vertical resultant force happens when the water levels at both sides of the structure are maximum. Using the experience gained in the previous check, the rotational stability checks will be done for the storm surge case and different water levels within the Valmeer.

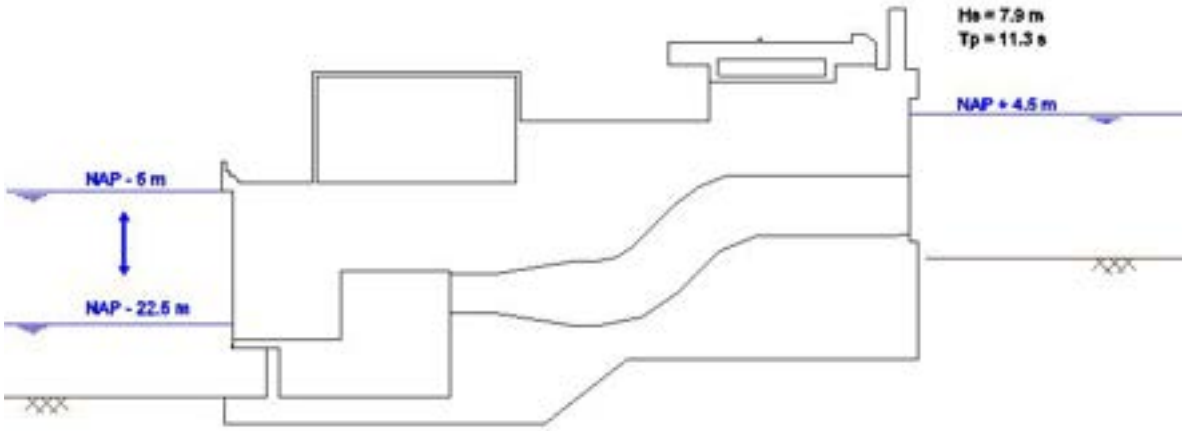

Figure L.42: load case considered to check whether rotational stability is met

In the following lines, first a figure considering the safety factor against rotational stability for each water level will be shown. Then, the rotational stability calculations will be shown for the worst case scenario.

Safety factor against rotational stability for storm surge conditions and different water levels inside the Valmeer

Rotational stability checks are done following the formulation present in Section L.2.2. There, it can be seen that:

$e_R = \frac{\sum M}{\sum V} \leq \frac{1}{6}b \quad [m]$

Therefore, the e_R will be used as the design unit. e_R has been calculated for storm surge conditions and the different water levels that can be present within the Valmeer. The safety factor (SF) has been defined as:

$SF = \frac{b/6}{e_R}$

This means that for the limit of $b/6 = e_R$, the safety factor will be one, as the e_R value decreases, the safety factor increases (as expected). The results of the analysis can be observed below:

Figure L.43: Safety factor against rotational stability

As we can see above, the worst-case scenario happens when the water level within the Valmeer is at NAP -5m (it is actually at NAP -2.5 m, but this water level is not allowed within the Valmeer). This coincides with

the worst case scenario for horizontal stability. Below, the calculation performed are shown for the worst-case scenario.

Notice that again, the safety factor increases with depth, due to the contribution of the buoyant force. For water levels above NAP -5 m, the safety factor decreases until a water level of NAP -2.5 m, when it start to increase again. For depths lower than NAP -5 m (any level of the possible ones) the structure is more safe regarding rotational stability.

Wort-case scenario for rotational stability check

The worst-case scenario happens for the following conditions:

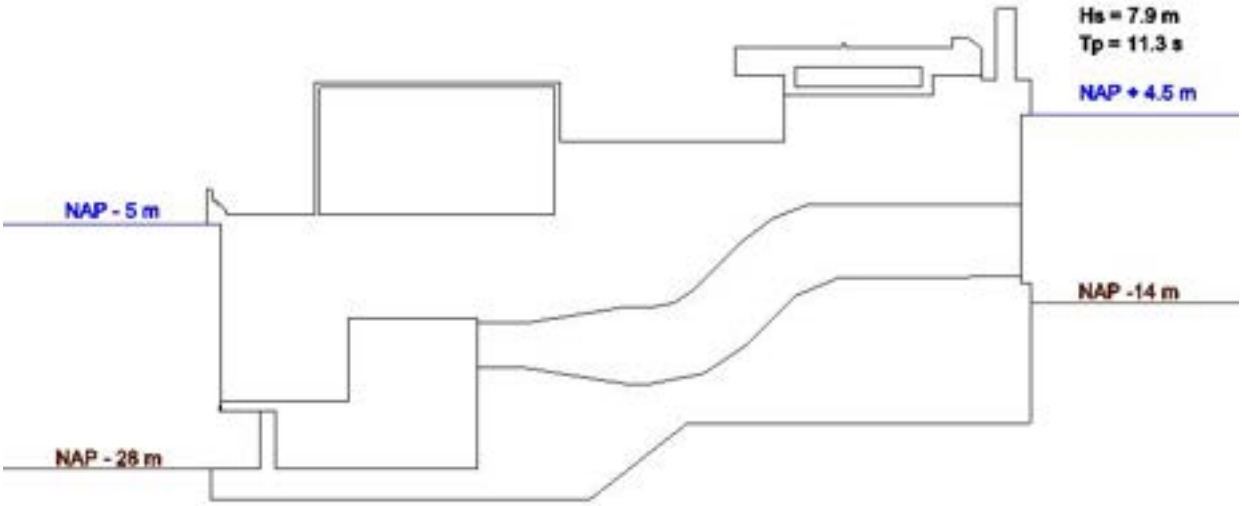

Figure L.44: Worst-case scenario for rotational stability

As the load case is the same as the one used for horizontal stability, the loads follow from there:

FORCES				
Weight	W	37400 kN/m	applied @	0.0 m from center of BOS
Buoyancy force	F_b	26670 kN/m	applied @	0 m from center of BOS
Hydrostatic force (sea)	F_hs	6661 kN/m	applied @	12.2 m from BOS
Hydrostatic force (ESL)	F_hv	3645 kN/m	applied @	9.0 m from BOS
Horizontal wave force p1(Sea)	F_p1	291 kN/m	applied @	40.2 m from BOS
Horizontal wave force p3 (Sea)	F_p3	603 kN/m	applied @	18.3 m from BOS
Horizontal wave force p1-p3 (Sea)	F_p1-p3	657 kN/m	applied @	24.3 m from BOS
Vertical wave force pu (Sea)	F_pu	694 kN/m	applied @	14.0 m from center of BOS
Horizontal soil force (sea)	F_sh	715 kN/m	applied @	6.0 m from BOS

*BOS = Base of Structure

Figure L.45: Forces considered for overall stability of the structure

Following Section L.2.2, the rotational stability is met if:

$$e_R = \frac{\sum M}{\sum V} \leq \frac{1}{6}b \quad [m]$$

Where $\sum M$ comes from calculating the rotational moment around the center of the base of the structure. The distances can be seen both in figures L.31 and L.32:

$$\sum M = h_{hs} \cdot 12.2 - F_{hv} \cdot 9.0 + F_{p1} \cdot 40.2 + F_{p3} \cdot 18.3 + F_{p1-p3} \cdot 24.3 + F_{pu} \cdot 14.0 + F_{sh} \cdot 6.0 = 100927 kNm/m$$

And the resultant of the vertical forces is:

$\sum V = W - F_b - F_{pu} = 10036kN/m$

Therefore, we can check:
$e_R = \frac{\sum M}{\sum V} \leq \frac{1}{6}b \quad [m] = \frac{100927}{10036} \leq \frac{1}{6} \cdot 84; 10.1m \leq 14m$

Thus, rotational stability is ensured.

L.6.3 Vertical stability

Sketch of failure mechanism

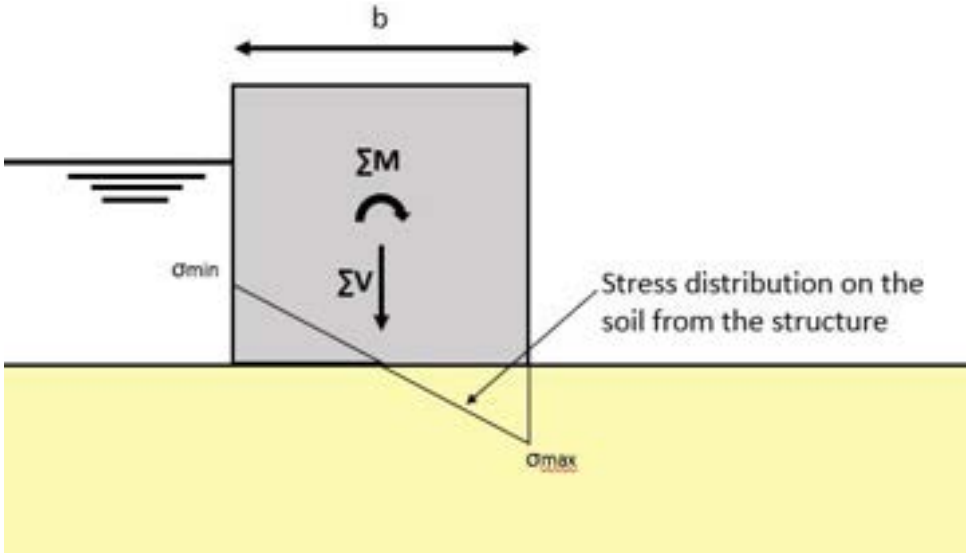

Figure L.46: Vertical stability sketch

The vertical effective stress from the loads acting on the structure should not exceed the maximum soil bearing capacity ($\sigma_{k,max} < p'_{max}$). Otherwise the soil will collapse. The maximum load on the soil is calculated as:

$$\sigma_k, max = \frac{F}{A} + \frac{M}{W} = \frac{\sum V}{b \cdot l} + \frac{\sum M}{\frac{1}{6}lb^2} \quad [kN/m^2] \tag{L.24}$$

On the other hand, as the soil cannot take negative stresses, the minimum load acting on the soil has to have a positive sign ($\sigma_k, min > 0$. Only compressive stresses allowed). The minimum soil load is calculated as:

$$\sigma_k, max = \frac{F}{A} - \frac{M}{W} = \frac{\sum V}{b \cdot l} - \frac{\sum M}{\frac{1}{6}lb^2} \quad [kN/m^2] \tag{L.25}$$

Worst load cases for vertical stability

This section will check if the maximum and minimum soil pressure stay below the 400 kN/m^2 (densely packed sand bearing capacity assumption from CUR, 2010) limit and above zero (no tensile stresses can develop in the soil).

The maximum soil pressure happens when the vertical resultant force and the rotational moment are maximum. The vertical force is maximum just after finishing of the structure construction. Since water is not surrounding the structure and therefore no buoyant force makes the structure "lighter". Maximum rotational moment happens for the case of having storm surge and a water level within the Valmeer of NAP -22.5 m. Therefore, a calculation only including selfweight will be done and then another calculation will be done for the case of having storm surge and a water level within the Valmeer of NAP -22.5 m.

The minimum soil pressure happens when the vertical resultant force is minimum and the rotational moment is maximum. The vertical force is minimum for the case when maximum water levels are present at both sides of the structure. The maximum rotational moment happens when the structure is subjected to storm surge conditions and the water level within the Valmeer is maximum. Therefore again, the case of having storm surge conditions will have to be checked for the different water levels inside the Valmeer.
Therefore, the following loadcases will be considered:

- The structure has just been constructed and there is not water around it.
- Storm surge and water level within Valmeer between NAP -5m and NAP -22.5m.

Maximum pressure acting on the soil

First, the vertical stability is calculated for the case when the structure has just been constructed and there is no water surrounding it. The structure's selfweight was 37400 kN/m. Therefore, the pressure over the soil comes from dividing the weight by the length of the structure:

$\sigma_k, max = \frac{37400kN/m}{84m} = 445kN/m2$

As we can see, if the whole weight of the structure is present, the soil will fail in compression. However, the road will be installed after the structure is surrounded by water. From Sagemo & Storck (2013) we know that the installed bridge weight per meter is 24.71 tons/m, which results in:

$24.71tons/m \cdot 1000kg/ton \cdot 10kN/kg = 2471kN/m$

Now the soil pressure is computed as:

$\sigma_k, max = \frac{37400kN/m - 2471kN/m}{84m} = 416kN/m2$

Which still not feasible. One more thing can be done though. The power plant contains some compartments that will be filled with sand (to provide more weight and therefore stability). These compartments can be filled up after the water is surrounding the structure since they are only needed for providing stability during the design storm situation. The weight of each of these compartments can be calculated from:

$W_{compartment} = V_{compartment} \cdot \gamma_{sand} = 6235m^3 \cdot 17kN/m^3 = 105995kN$

The volume is obtained from the AutoCAD model and the unit weight has been assumed. The weight per meter of structure is then computed as:

$$W_{compartmentPerMeter} = \frac{W_{compartment} \cdot N_{compartments}}{Width_{plant}} = \frac{105995 \cdot 9}{148} = 6445kN/m$$

The width of the compartment has also been calculated from the AutoCAD model. Thus, if the compartments are empty and only filled in after the bulding pit is flooded, the "dry" weight of the structure is now:

$W_{structure} = 37400kN/m - 2471kN/m - 6445kN/m = 28484kN/m$. Giving now a soil pressure of:

$\sigma_k, max = \frac{28484kN/m}{84} = 339kN/m^2$

Now, the soil can take the pressure of the structure.
The other load case comprise the maximum rotational moment. That load case can be sen below:

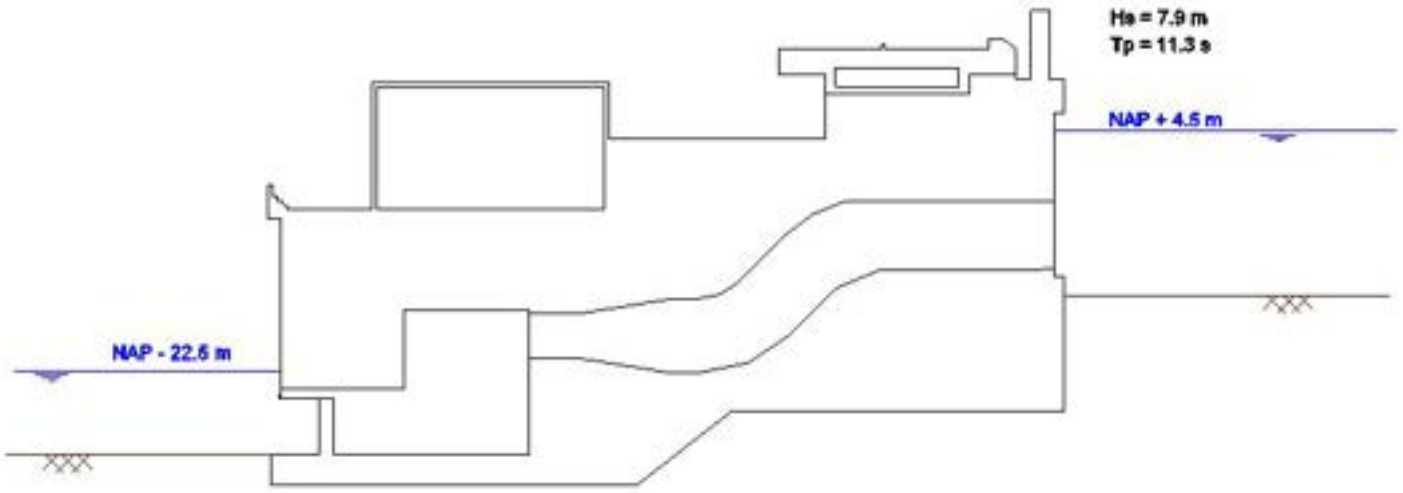

Figure L.47: load case for maximum rotational moment. Storm surge and low water level within Valmeer.

The wave pressures coincide with the ones used for horizontal stability. This is because wave pressures depend on the geometry of the sea-side of the structure, the water level and wave characteristics. This is the same for the load case of having storm surge. However, the different water levels considered for horizontal stability gives different forces. These are shown below:

FORCES				
Weight	W	37400 kN/m	applied @	0.0 m from center of BOS
Buoyancy force	F_b	19320 kN/m	applied @	0 m from center of BOS
Hydrostatic force (sea)	F_hs	6661 kN/m	applied @	12.2 m from BOS
Hydrostatic force (ESL)	F_hv	451 kN/m	applied @	3.2 m from BOS
Horizontal wave force p1(Sea)	F_p1	291 kN/m	applied @	40.2 m from BOS
Horizontal wave force p3 (Sea)	F_p3	603 kN/m	applied @	18.3 m from BOS
Horizontal wave force p1-p3 (Sea)	F_p1-p3	657 kN/m	applied @	24.3 m from BOS
Vertical wave force pu (Sea)	F_pu	694 kN/m	applied @	14.0 m from center of BOS
Horizontal soil force (sea)	F_sh	715 kN/m	applied @	6.0 m from BOS

*BOS = Base of Structure

Figure L.48: Forces present in the storm surge and water level within the Valmeer at NAP -22.5 m

Following Section L.2.2 the maximum soil pressure can be calculated with Equation L.24:

$$\sigma_k, max = \frac{F}{A} + \frac{M}{W} = \frac{\sum V}{b \cdot l} + \frac{\sum M}{\frac{1}{6} l b^2} \quad [kN/m^2]$$

Where:
$\sum V = W - F_b - F_{pu} = 17386 kN/m$ $b = 1m$; since the analysis is per meter width of structure $L = 84m$
$\sum M = h_{hs} \cdot 12.2 - F_{hv} \cdot 3.2 + F_{p1} \cdot 40.2 + F_{p3} \cdot 18.3 + F_{p1-p3} \cdot 24.3 + F_{pu} \cdot 14.0 + F_{sh} \cdot 6.0 = 132303 kNm/m$

After pluggin in the above values into Equation L.24, the maximum load acting on the soil is:

$\sigma_k, max = 319 kN/m^2/m$

Minimum pressure acting on the soil

Following Section L.2.2 the minimum soil pressure can be calculated with Equation L.25:

$$\sigma_k, max = \frac{F}{A} - \frac{M}{W} = \frac{\sum V}{b \cdot l} - \frac{\sum M}{\frac{1}{6} l b^2} \quad [kN/m^2]$$

To obtain the minimum pressure, the load case of having storm surge will be checked for finding the minimum stability for different water levels inside the Valmeer. The following has been done using Equation L.25:

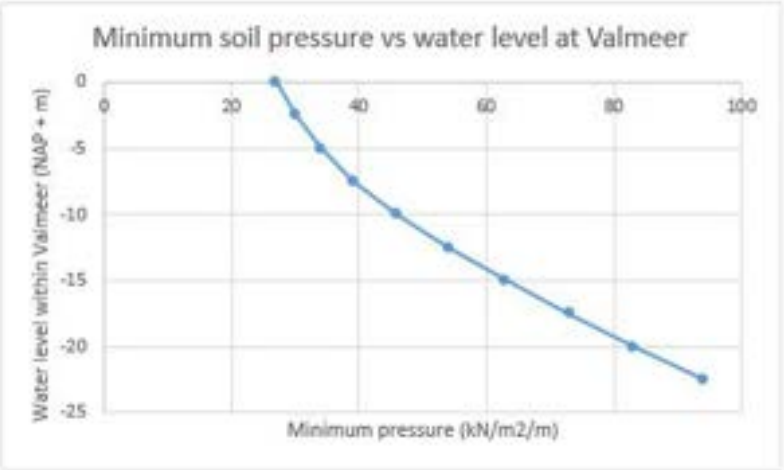

Figure L.49: Minimum soil pressure depending on water level at Valmeer

It can be observed that in this case, the minimum pressure increases when increasing the depth of the Valmeer. Again the contribution of the buoyant force is governing.

L.6.4 Piping protection

The piping calculations have been done following Lane's formula. As stated in Appendix L there are another more accurate formulations such as the Hans Sellmeijer formulation (1988) but they require more soil information. As this is not available and the present design is conceptual, Lane's theory will be used. The formulation can be seen below. For a better definition of the theoretical background of these formulas, the reader is referred to Appendix L.

$$L \geq \gamma \cdot C_L \cdot \delta H \quad [m]$$

$$L = \sum L_{vert} + \frac{1}{3} \sum L_{hor} \quad [m]$$

In this case, it is easy to find the critical load case since according to Lane's formula the piping length depends mainly on the head difference. So the larger head difference that the system will face will be used for the piping calculation. The maximum head difference will happen for the conditions of storm surge and low water level. This conditions are taken as design conditions beacause it is a possible situation and the wordt one. Further research is recommended on this aspect, since by managing water levels within the Valmeer a reduction in pipin protection can be achieved (see piping conclusions below). Below the design water levels are shown:

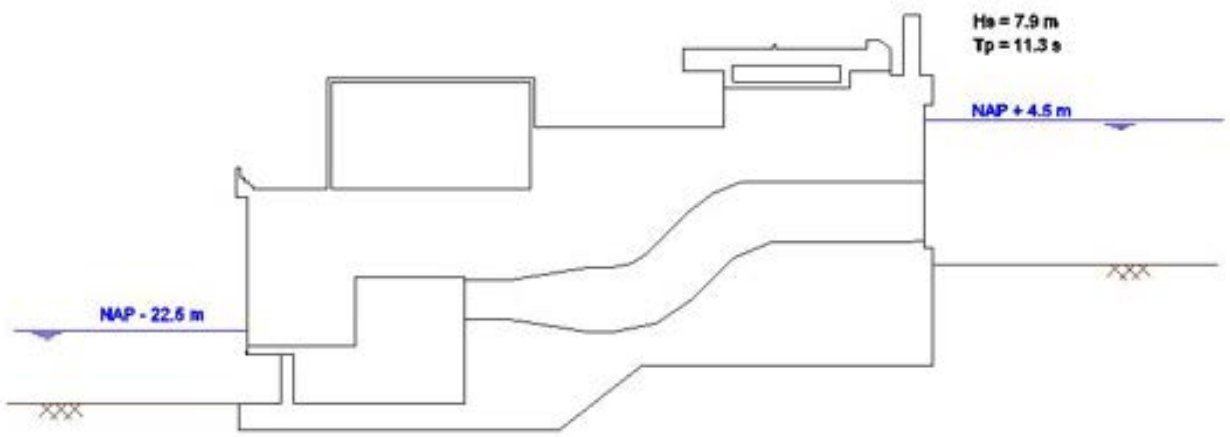

Figure L.50: load case for piping calculations. Storm surge and low water level within Valmeer.

Assuming that the soil below the structure is "middle fine sand" and following lane's formulation the seepage length is then:

$L = 1.5 \cdot 6 \cdot (4.5 - (-22.5)) = 243m$

Middle fine sand was considered (C_L in the above equation is equal to 6), therefore the maximum allowed hydraulic gradient is (from the table in Section L.2.2) 16.7%. The actual hydraulic gradient is:

$i_{actual} = \frac{4.5-(-22.5)}{243} = 11.1\%$ Therefore the maximum allowed is not reached.
The total protection length can be obtained from Equation L.15, also shown in the beginning of this section. At the sea-side of the structure, 18 meters of vertical protection will be installed, on the Valmeer's side another 4 meters of vertical protection are applied. Then, 243 - 4 - 18 = 221 meters are still needed. Since these will be installed horizontally, Lane recommends $L_{hor} = 3 \cdot L = 3 \cdot 221m = 663$ meters of horizontal piping protection. Equation L.15 is then: $L = 18 + 4 + \frac{1}{3} \cdot 663 = 243m$ which meets Lane's formulation. The total piping length protection is then 663 + 18 + 4 = 685 meters long without applying any other measures. Below, different strategies are recommended to reduce the piping protection length.

Conclusions from the piping calculations

Having a shallow foundation gives the above-calculated necessary piping length protection without applying extra measures. Here recommendations are given to reduce the piping protection. First, some alternative techniques using sheet pile walls and diaphragm walls are give. Then, the advantages and disadvantages of those techniques are explained. To finish, a recommendation is given to change the design load case.

According to Lane's theory, the vertical screens are more effective against piping than the horizontal ones (L_{hor} is divided over 3). Therefore the following strategies are recommended:

- Installation of 32 m long sheet pile wall (or diaphragm wall) down to the impermeable clay layer. This would stop piping since water won't pass through the impermeable clay layer. However, digging sheet pile walls this depth could not be possible. Then diaphragm wall could be a better option but the slurry pressure to counterbalance the water pressures before reaching the clay layer needs to be approximately 640 kN/m^2. A big advantage of this method is that the seepage within the building dock would be significantly reduced. Easing the dewatering process.
- Installation of 20 m long sheet pile wall (or diaphragm wall). This technique won't avoid fully piping but it will reduce the amount of piping protection needed. Different techniques can be applied:
  - 2 lines of 20 meters sheet piles: 2x20m sheet pile reduces protection to L = 2x20x2 + 18 + 4 + 1/3 * 423, having then 423 m of horizontal protection. Sheet pile area needed = 110.560 m2 (2 x 2764 m x 20m) [16 football fields].

- 3 lines of 20 meters sheet piles: 3x20m sheet pile reduces protection to L = 3x20x2 + 18 + 4 + 1/3 * 303. having then 303 m of horizontal protection. Sheet pile area needed = 165.840 m2 (3 x 2764 m x 20m) [24 football fields].
- 4 lines of 20 meters sheet piles: 4x20m sheet pile reduces protection to L = 4x20x2 + 18 + 4 + 1/3 * 190. having then 190 m of horizontal protection. Sheet pile area needed = 221.120 m2 (4 x 2764 m x 20m) [32 football fields].
- 5 lines of 20 meters sheet piles: 5x20m sheet pile reduces protection to L = 5x20x2 + 18 + 4 + 1/3 * 63 , having then 63 m of horizontal protection. Which would be provided just with the base of the structure, so no extra horizontal protection would be installed. However, a huge amount of steel would be needed and installing 5 sheet pile files would be very expensive. Sheet pile area needed = 276.400 m2 (5 x 2764 m x 20m) [40 football fields].

GENERAL DRAWBACKS:
The installation of the sheet pile walls need a precise placing operation but according to professionals it can be done.

Furthermore, the more sheet piles installed under the structure, the better regarding buoyancy because the water pressures will take longer to develop because of the influence of the impermeable screen that the sheet piles create. In Figure 7.22 the effect of the sheet piles installation under the structure is already mentioned. However, this issue should be further researched to see the effects in buoyant forces.

As a last remark, the design water levels for piping can be different because during storm conditions the water level in the Valmeer can be raised to increase protection against piping by reducing the water head difference. Then, the other design condition will be the daily situation. But it would be interesting to check whether piping will occur in daily situations. For daily conditions, during 2 hours a day the water level difference is 22.5 metes. Additional research should be done to Figure out adequate strategies to reduce the piping protection. This is not the main focus of this thesis, so for this thesis, the following piping protection is recommended (without doing any costs analysis, just considering the a short horizontal piping length and not the largest number of sheet piles to be installed due to the problem of increasing buoyancy):

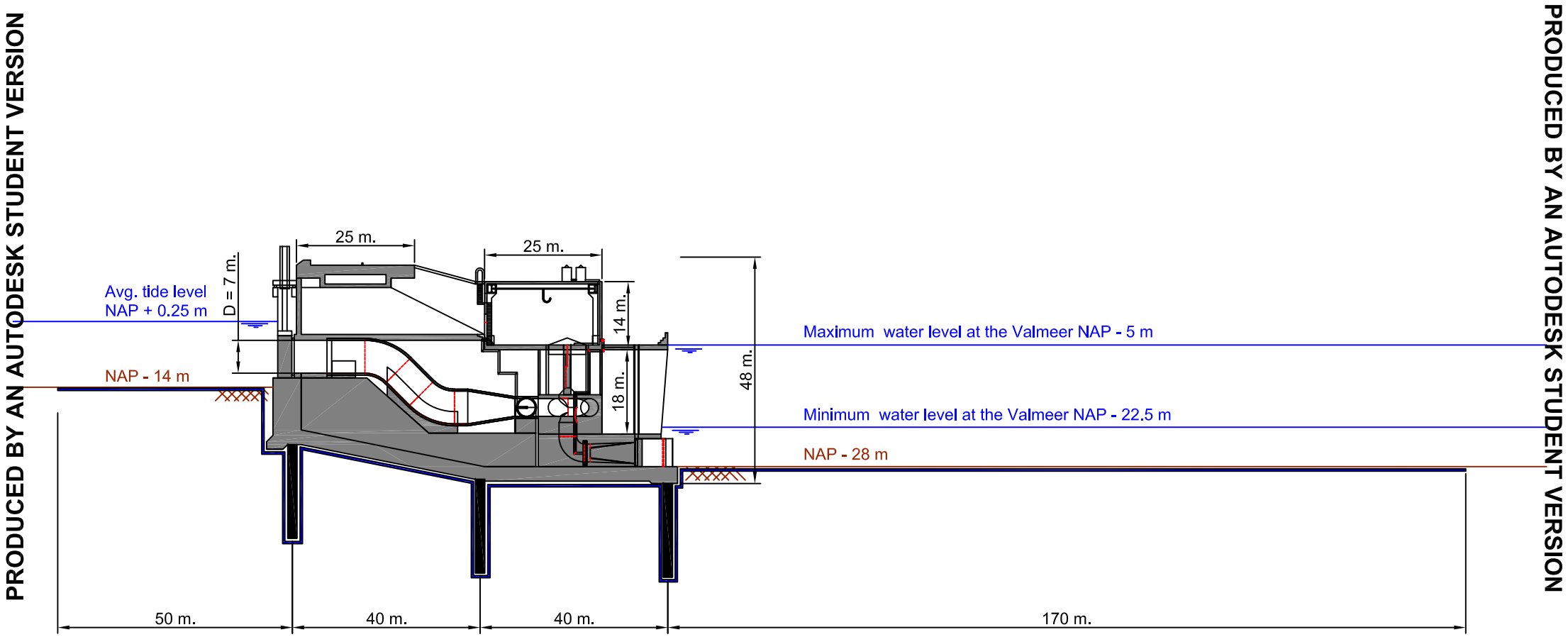

PRODUCED BY AN AUTODESK STUDENT VERSION

PRODUCED BY AN AUTODESK STUDENT VERSION

L.6.5 Bed protection at the in-/outlet of the structure

Bed protection is needed for two different phenomena. The scour holes which develop by the action of waves on vertical walls and the erosion of the bed caused by water flows velocities. This happens when water leaves the Valmeer during pumping (or enters during turbining). For these last cases, the following two scenarios will be considered:

1. Maximum discharge leaving the Valmeer. Erosion at sea-side of the structure.
2. Maximum discharge entering the Valmeer. Erosion at Valmeer-side of the structure

The scour depth due to wave action is already calculated in Figure L.17. The wave conditions of the final structure coincides with the ones of preliminary calculations. Therefore, a scour hole of 2.4 meters is expected to happen during critical conditions (if the storm duration is long enough for the hole to develop).

In the following lines, the reasoning for obtaining the bed protection length from flow velocities is shown.

Maximum discharge leaving the Valmeer

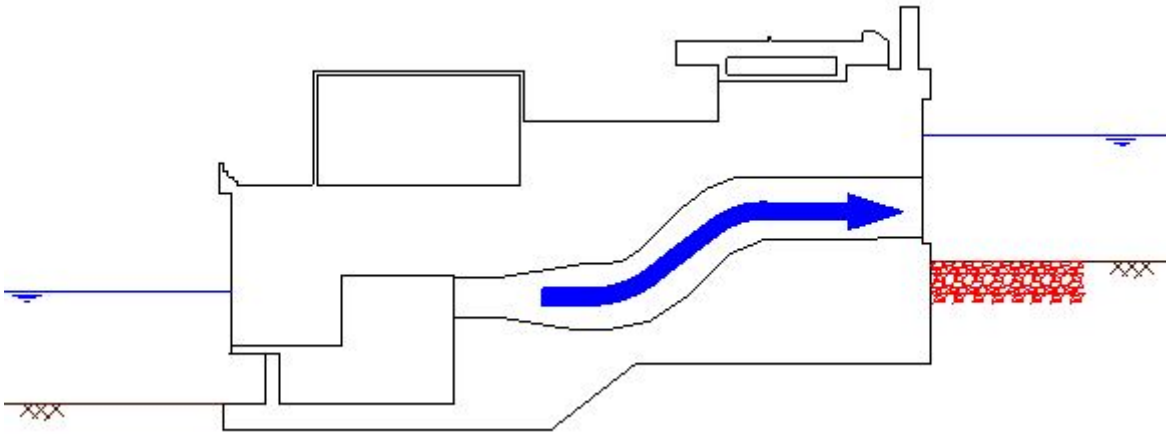

Figure L.51: Representation of water leaving the Valmeer. The bed protection zone is signaled in red color.

When water is leaving the Valmeer it is exited by pipes with a diameter of 7 meters. The flow velocity at this pipe is then calculated as:

$v = \frac{Q}{A} = \frac{60}{\pi \cdot 7^2/4} = 1.6 m/s$

To reduce this velocity at the exit, 3 pipes are diverted into a rectangular "inlet structure" with dimensions of 37 m × 7 m. Ideally, the "inlet structure" would reduce the flow velocity to:
$v = \frac{Q}{A} = \frac{60 \cdot 3}{37 \cdot 7} = 0.70 m/s$

However, the velocity reduction won't happen instantaneously. For that reason, a reduction in flow velocity of a 25% with respect to the velocity at each tube is assumed for the socour calculations. Then, the design velocity of the water leaving the Valmeer will be 0.75 × 1.6 m/s = 1.2 m/s.

Following Equation L.20, the critical velocity for initiation of motion of the sand particles (D_{50} = 1 mm) at the end of the bed protection is calculated:

$u_c = 88.3\sqrt{0.1 \cdot 0.6 \cdot 0.001} = 0.70 m/s$

Then, the maximum scour hole depth is calculated as:

$h_{max} = 18.5 \cdot \frac{0.5 \cdot 3 \cdot 1.2 - 0.70}{0.70} = 1.6 m$

Check $0.5 \cdot \alpha \cdot u > 0$: $0.5 \cdot 3 \cdot 1.2 = 1.8 > 0$.

Finally, the bed protection length is at least:

$L \geq 1.2 \cdot 10 \cdot 1.6 = 19.6m \approx 20m$

Therefore, at the sea-side, the bed protection length has to be of 20 m.

Maximum discharge entering the Valmeer

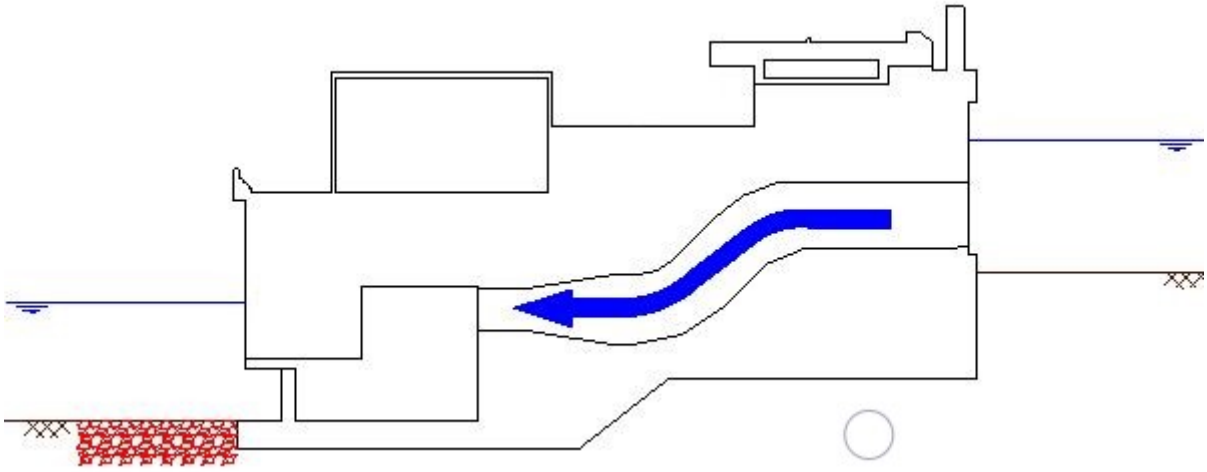

Figure L.52: Representation of water coming into the Valmeer. The bed protection zone is signaled in red color.

The water enters the Valmeer at a lower velocity that it exites. The draft tube is designed to reduce the flow velocity at maximum in order to maximize the kinetic energy obtained at the turbine. The flow velocity is calculated from the geometry of the formed suction intake (see Figure C.7):

$v = \frac{Q}{A} = \frac{60}{13.3 \cdot 6} = 0.75m/s$
The critical velocity for initiation of motion for the sand particles present at the end of the bed protection is the same as for the previous case: 0.70 m/s.
In this case though, due to the reduction of the flow velocity, the maximum scour hole depth is:

$h_{max} = 18.5 \cdot \frac{0.5 \cdot 3 \cdot 0.75 - 0.70}{0.70} = 0.66m$

Check $0.5 \cdot \alpha \cdot u > 0$: $0.5 \cdot 3 \cdot 0.75 = 1.1 > 0$.

Finally, the bed protection length is at least:

$L \geq 1.2 \cdot 10 \cdot 0.66 = 7.7m \approx 8.0m$

Therefore, inside the Valmeer, the bed protection length has to be of 8 m.

L.7 Strength calculations

The reinforcement calculations include the following:

- Gate design
- Reinforcement of the main wall

Each item above will be part of a different section. Within a section, the worst load case will be shown with a sketch. Then the forces will be calculated and the gate geometry and necessary reinforcement will be shown. No more strength calculations are added due to time limitations and lack of academic interest.

L.7.1 Gate Design

Vertical lift gates have been chosen for the Valmeer's pump storage station. The information for selection a gate has been obtained from Daniel & Paulus (2018). Vertical lift gates allow for large spans, which in this case was very convenient to reduce the number of installed gates. 54 gates are installed along 2,7 kilometers of plant. A drawback of this is that cylinders able to lift up heave gates are needed. However, these gates have similar dimensions to the Oosterschelde Barrier. Thus, its realization is possible. Besides, vertical lift gates just need a pier in which to lift and a cylinder, all in the vertical direction, leaving space in the back for the penstock and the access road. Maintenance, reparation, or replacing operations are simple in comparison with other gates suited for large spans such as sector gates. Finally, the simplicity of vertical gates make them relatively cheap in comparison with sector or rotatory gates.

This structure is composed of gates with dimensions of 38 m (width) $\times$ 9 m (height). The top of the gate is at NAP -3 m and the bottom at NAP -12 m. This gate is supported by the inlet structure behind it. Its span is 36.5 m and 7.5 m in the horizontal and vertical direction respectively. The span can be reduced by constructing two vertical walls between the penstocks exit that are shown in Figure L.53 below. However, then this wall would need to have the strength to handle the forces acting on the wall. This strength would have to be checked for both compression and buckling. For this reason, and because vertical lift gates can have large spans, the span of 36.5 meters is chosen for design. In the Figure L.53 below, an schematization of the gate is shown:

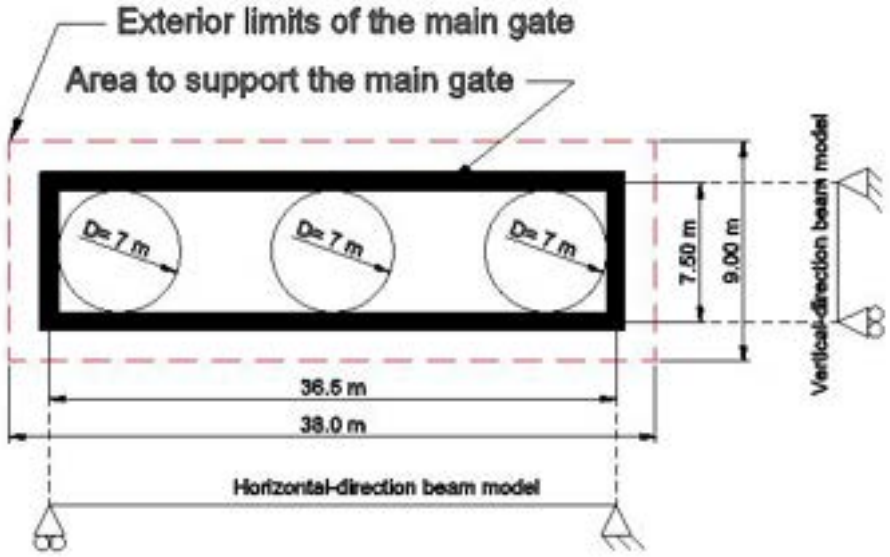

Figure L.53: Schematization of the main gate. Showing the beam-model used for bending moment and shear force diagrams calculation

The worst-case scenario that the gate will be under during its lifetime is the one where the design storm surge is present (H_s = 9m, T_p = 11.3 s, WL = NAP + 4.5 m):

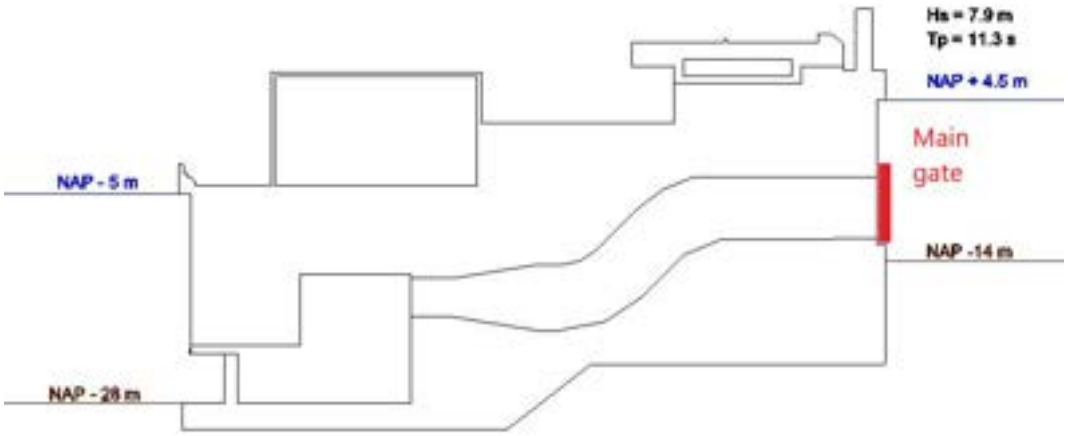

Figure L.54: load case storm surge situation

Therefore the wave pressures can be obtained from Figure L.36. For the gate design, the interest is on the pressures at the top (NAP -3 m) and bottom (NAP -12 m) of the gate. In the following image these pressures are shown:

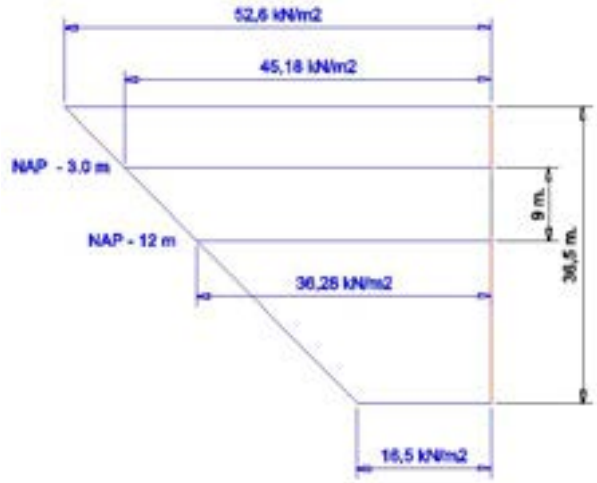

Figure L.55: Wave pressures at the top and the bottom of the gate

Therefore we have the following wave pressures at the top and bottom of the gate:

$P_{wTOP} = 45.12kN/m^2$
$P_{wBOT} = 36.28kN/m^2$

Furthermore, the hydrostatic pressures can be calculated from:

$P_{hTOP} = \gamma_w \cdot h_{top} = 10 \cdot (4.5 - (-3)) = 75kN/m^2$
$P_{hTOP} = \gamma_w \cdot h_{bot} = 10 \cdot (4.5 - (-12)) = 165kN/m^2$

Then, the resultant pressures at the top and bottom of the structure follow from:

$P_{top} = P_{wTOP} + P_{hTOP} = 45.12 + 75 \approx 120kN/m^2$
$P_{bop} = P_{wBOT} + P_{hBOT} = 36.28 + 165 \approx 201kN/m^2$

The pressures can be added since both wave and hydrostatic pressure are linear. Then the pressures acting on the gate are as follow:

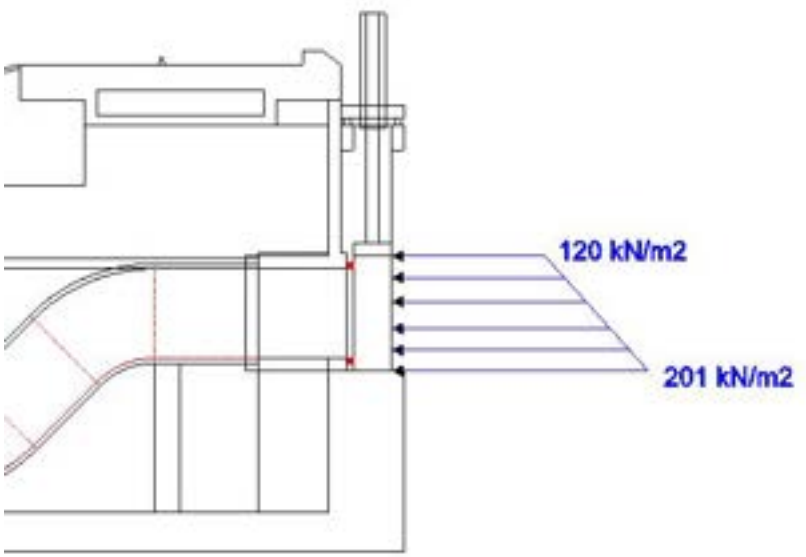

Figure L.56: Resultant pressure acting on the gate. The gate supports are shown in red

The above load case results in different loads for each direction (width or height) of the gate. In the following figure, this is shown in a sketch:

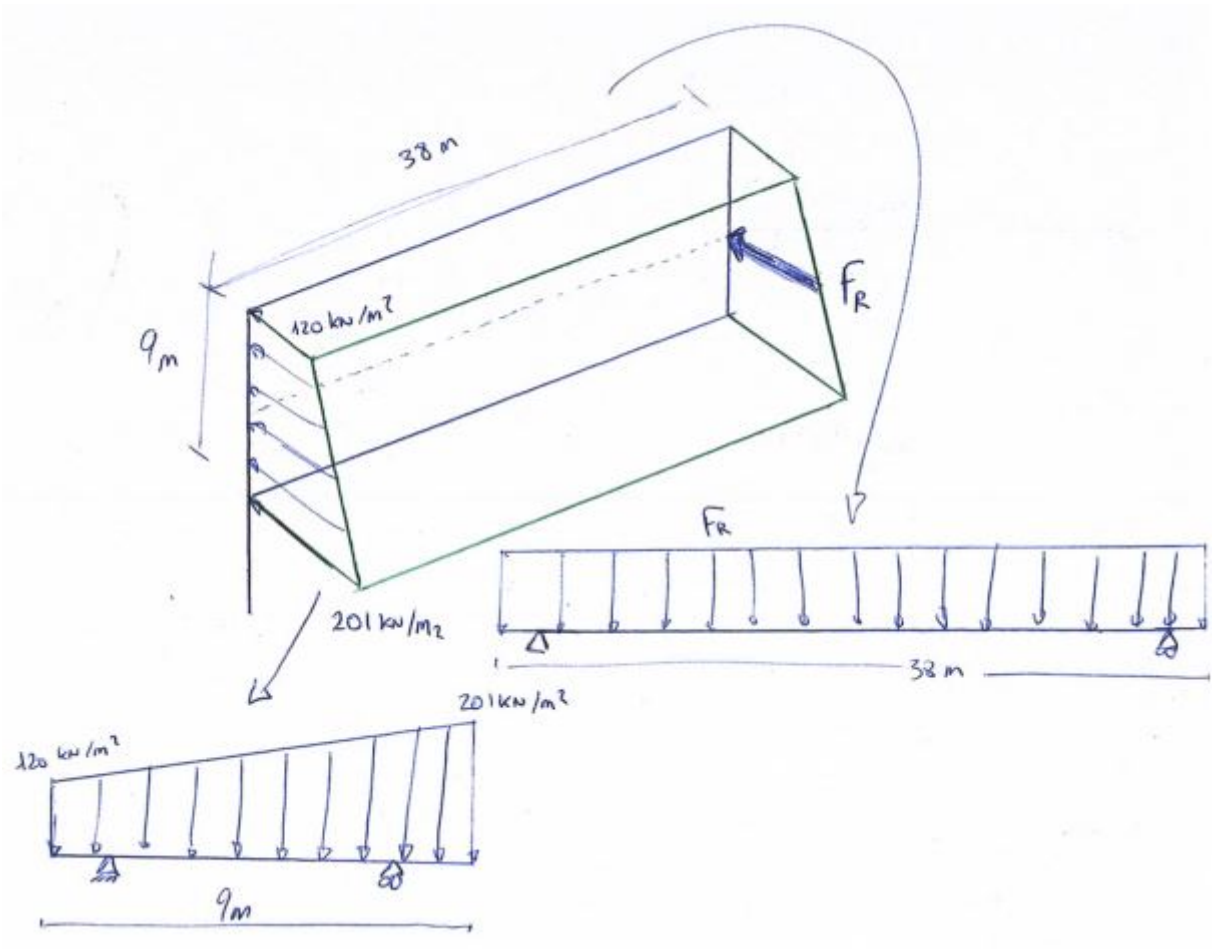

Figure L.57: Differentiation between height and length direction for loadcases

Width direction section modulus needed

For the length direction, the load case comes from obtaining the resultant force for the pressures acting on the gate and then distribute that force over the width direction. Again a safety factor of 1.5 is applied to the load. The resultant force from the load case in Figure L.56 is calculated as:

$F_R = 1.5 \cdot \frac{120+210}{2} \cdot 9 = 2167 kN/m$ Notice that this load is per meter width of gate. The load case for the width direction of the gate is then the following one:

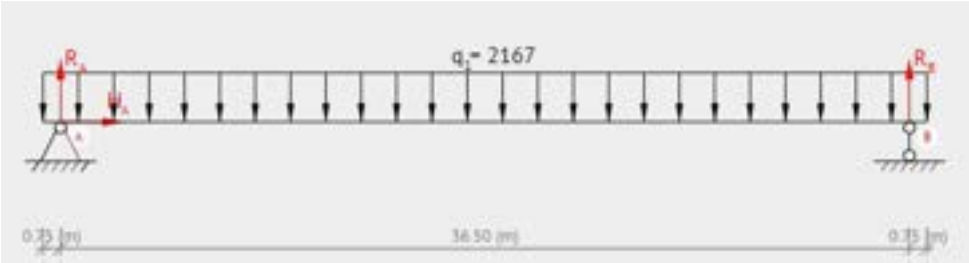

Figure L.58: load case for horizontal girders design. Source: https://beamguru.com/

From the above loadcase, the bending moment diagram is obtained together with the maximum bending moment:

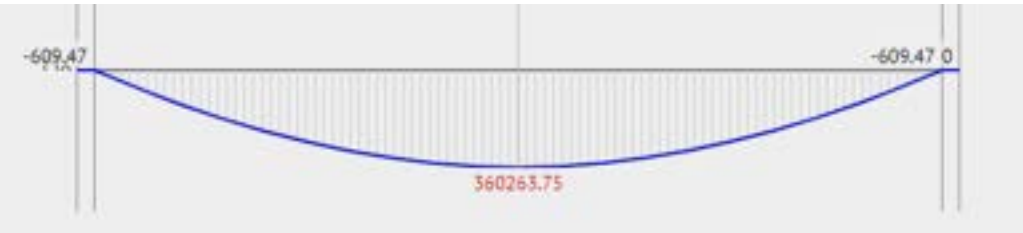

Figure L.59: Bending moment diagram. Source: https://beamguru.com/

Therefore, the design bending moment is $M_d = 360264$ kNm. The section modulus needs to resist the bending moment and comes from assuming that the gate's steel yields at 240 N/mm^2 (using steel S275):

$W = \frac{M_d}{\sigma_{steel}} = \frac{360264 \times 10^6 Nmm}{240 N/mm^2} = 1501 \times 10^6 mm^3$

Height direction section modulus needed

For the height direction, the bending moment can be calculated from a beam analysis considering a pin support and roller support. These supports have been considered since the gate is simply supported on the sides. Notice that a safety factor of 1.5 has been applied to the pressures calculated above and that the analysis is done per meter width of the gate. The loading condition is as follows:

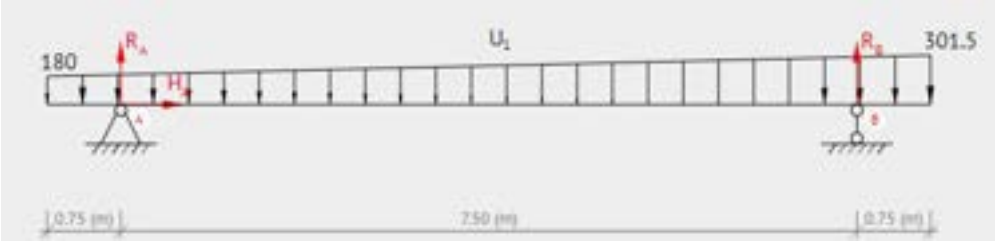

Figure L.60: load case for vertical girders design. Source: https://beamguru.com/

From the above loadcase, the bending moment diagram is obtained together with the maximum bending moment:

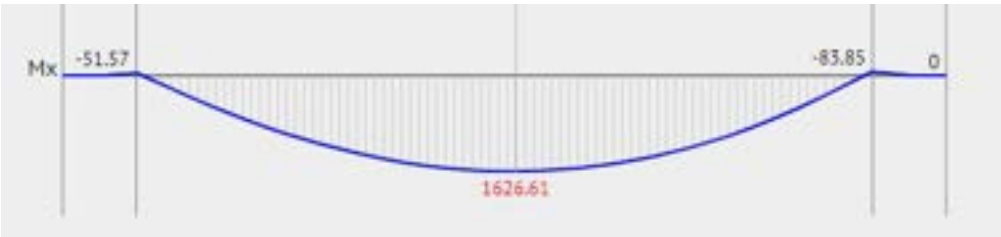

Figure L.61: Bending moment diagram. Source: https://beamguru.com/

Therefore, the design bending moment is $M_d = 1627$ kNm/m. Notice that the moment is given per meter width of structure. From the bending moment, the section modulus needed to resist the bending moment is calculated considering that the steel of the gate yields at 240 N/mm^2. Therefore:
$W = \frac{M_d}{\sigma_{steel}} = \frac{1627 \times 10^6}{240} = 6.78 \times 10^6 mm^3/m$ this result is still per meter width of the gate, therefore the total section modulus can be calculated as:

$$W = 6.78 \times 10^6 mm^3/m \cdot 38m = 258 \times 10^6 mm^3$$

Gate design

From the previous sections, it is known that the gate cross-section will have to have the following section modulus depending on its direction:

- Horizontal direction $1501 \times 10^6 mm^3$
- Vertical direction $258 \times 10^6 mm^3$

The gate's section modulus has been obtained following the method taught in the Hydraulic Structures slides of the TU Delft. In the following lines, the theoretical background to obtain the section modulus is shown:

First, the gate's design idea can be seen below:

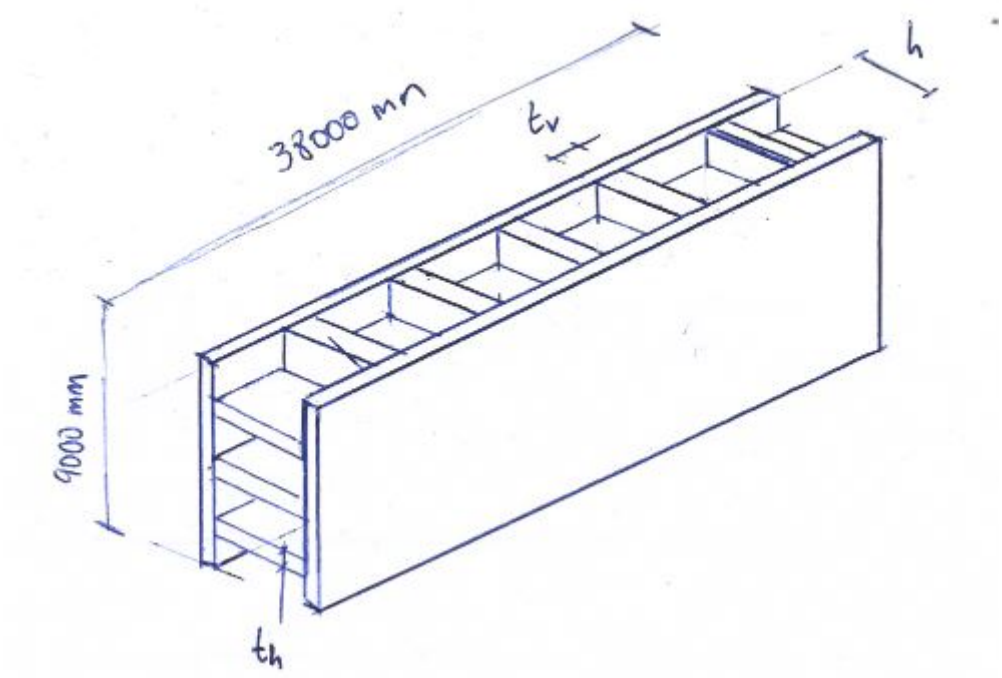

Figure L.62: Gate general design

The gate is formed by two steel plates and some girders (web of a beam) that unite the plates. The plates are the same thicknesses to ease its production. The front plate will take the water forces and transmit them to

the girders and rear plate. The rear plate also has the function of ensuring that the gate is water-tight. In the figure below, a schematization of the gate model used for obtaining the section modulus is shown:

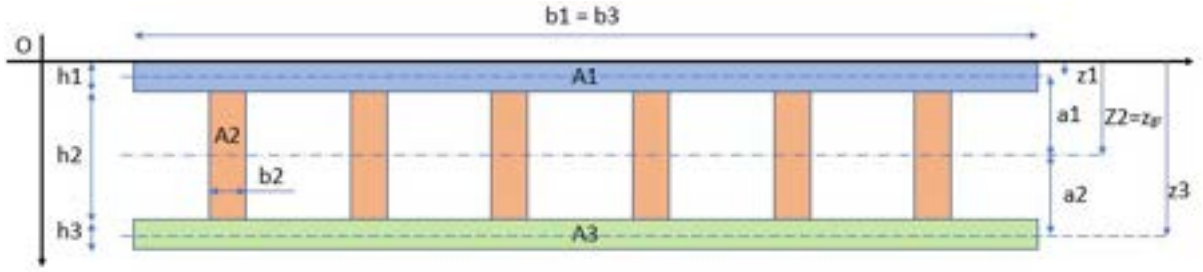

Figure L.63: Schematization of the gates's geometry and geometrical characteristics

The front plate is element 1 in the figure above. Element 2 is composed of the girders and element 3 is the rear plate. Notice that due to the symmetry of the gate, the center gravity line of the whole section coincides with the of the girders (or webs, element 2 in the figure above). So, $a_2 = 0$ mm.

To obtain the section modulus of the gate, the total modulus of inertia of the gate is obtained by using the Steiner's theorem:

$$I_{total} = \sum_{i}^{n} \left(I_i + a_i^2 \cdot A_i \right) \, mm^4 \tag{L.26}$$

Where:

- I_i: Moment of inertia of each element. For rectangular sections it is calculated as $I_i = 1/12 \cdot b_i h_i^3$. Notice that the element two is an addition of smaller elements A_{2i} and its moment of inertia is calculated from multiplying the numbers of elements by the moment of inertia of a single element.
- A_i: Area of each element. For rectangular sections it is calculated as $A_i = b_i h_i$. Notice that the element two is an addition of smaller elements A_{2i} and its area is calculated from multiplying the numbers of elements by the area of a single element.
- a_i: Distance from the gravity center of each element to the gravity center of the whole element. It is calculated as $a_i = z_{gr} - z_i$. The calculation of z_{gr} is shown below.

$$z_{gr} = \frac{\sum_i^n z_i \cdot b_i \cdot h_i}{A_{total}} \tag{L.27}$$

Where A total is the total cross-sectional area of the gate.

Once the total moment of inertia of the gate is knonw, the section modulus at the top and bottom fiber of the gate can be obtained from:

$$W_{up} = \frac{I_{total}}{h_{up}} \tag{L.28}$$

$$W_{down} = \frac{I_{total}}{h_{down}} \tag{L.29}$$

h_{up} and h_{down} are defined in the following figure:

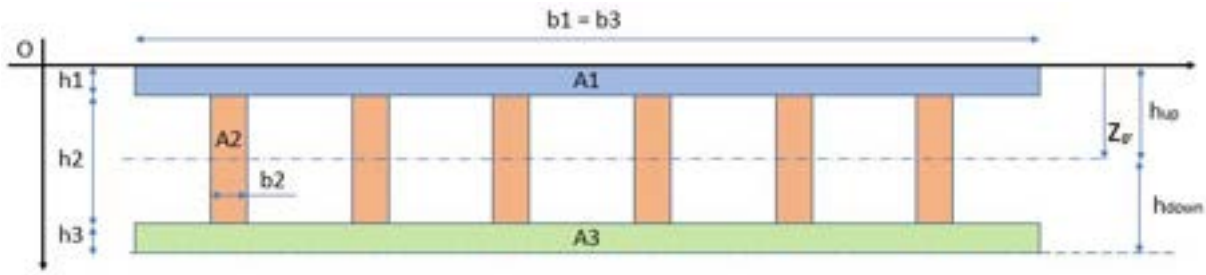

Figure L.64: graphical representation of h_{up} and h_{down}

And the stress at those fibers is then:

$$\sigma_{up} = \frac{M_{Ed}}{W_{up}} \tag{L.30}$$

$$\sigma_{down} = \frac{M_{Ed}}{W_{down}} \tag{L.31}$$

This steel stress must be lower than the yield stress of the steel, which for the design of this gate is 240 N/mm^2.

Since the horizontal dimension is more critical (it has a way larger span compared to the vertical dimension: 38 meters and 9 meters span respectively), the geometry for the vertical section will be calculated and then a check will be done to see if the horizontal section needs reinforcement. The design of the gate will be composed of two steel plates connected by steel flanges. The analyzed thicknesses of the plates are 20, 40, 60 and 80 mm. In the following lines, the calculation for obtaining the required section modulus for a gate composed of two steel plates of 20 mm is shown. The aim of this is showing how the calculations were done.

First, for the horizontal direction (vertical cross-section), the geometry must have a section modulus larger than $1501 \times 10^6 mm^3$ to resist the design bending moment. The following geometry will be studied:

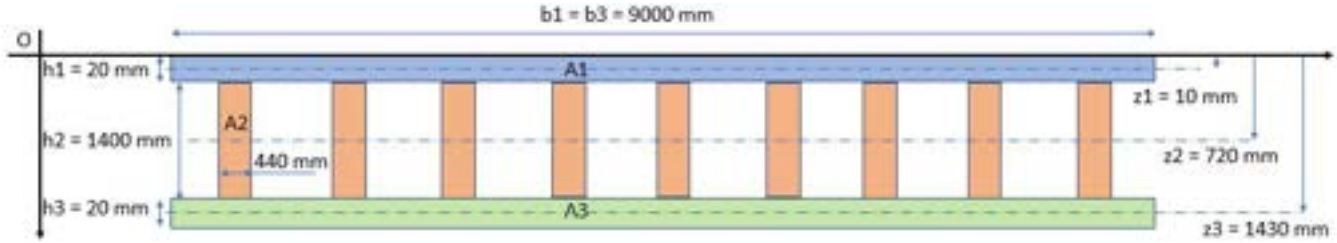

Figure L.65: Gate's geometry able to bear the design bending moment.

Then the area of each element and the total area is:

$$A_1 = h_1 \cdot b_1 = 20 \cdot 9000 = 180000\ mm^2$$

$$A_2 = h_2 \cdot b_2 \cdot n_{girders} = 1400 \cdot 440 \cdot 9 = 5544000\ mm^2$$

$$A_3 = h_3 \cdot b_3 = 20 \cdot 9000 = 180000\ mm^2$$

$$A_{total} = A_1 + A_2 + A_3 = 5904000\ mm^2$$

Now, the moment of inertia of each element is calculated as:

$$I_1 = \frac{1}{12} \cdot b_1 \cdot h_1^3 = \frac{1}{12} \cdot 9000 \cdot 20^3 = 6.000 \times 10^6\ mm^4$$

$$I_2 = n_{girders} \cdot \frac{1}{12} \cdot b_2 \cdot h_2^3 = 9 \cdot \frac{1}{12} \cdot 440 \cdot 1400^3 = 9.055 \times 10^1 1\ mm^4$$

$$I_3 = \frac{1}{12} \cdot b_3 \cdot h_3^3 = \frac{1}{12} \cdot 9000 \cdot 20^3 = 6.000 \times 10^6\ mm^4$$

To calculate the total moment of inertia of the section, the Steiner's theorem is used. To use it, first the a_i term, and therefore z_{gr} in Equation L.27 is calculated:

$$z_{gr} = \frac{\sum_{i=1}^{n=3} z_i \cdot b_i \cdot h_i}{A_{total}} = \frac{\sum_{i=1}^{n=3} z_i \cdot A_i}{A_{total}} = \frac{10 \cdot 180000 + 720 \cdot 5544000 + 1430 \cdot 180000}{5904000} = 720\ mm$$

Then, a_i is defined as:

$$a_1 = abs(z_{gr} - z) = abs(720 - 10) = 710\ mm$$

$$a_2 = abs(z_{gr} - z) = abs(720 - 720) = 0\ mm$$

$$a_3 = abs(z_{gr} - z) = abs(720 - 1430) = 710\ mm$$

The Steiner theorem can now be applied:

$$I_{total} = \sum_{i=1}^{n=3} \left(I_i + a_i^2 \cdot A_i\right) = \left(6.000 \times 10^6 + 710^2 \cdot 180000\right) + \left(9.055 \times 10^1 1 + 0^2 \cdot 5544000\right) + \left(6.000 \times 10^6 + 710^2 \cdot 180000\right) =$$

$$= 1.087 \times 10^1 2 \ mm^4$$

And finally, the section modulus at the top and bottom fiber (which will be the same due to the symmetry of the section) is:

$$W_{up} = \frac{I_{total}}{h_{up}} = \frac{1.087 \times 10^{12} \ mm^4}{1440 - 720} = 1.509 \times 10^9 \ mm^3$$

$$W_{down} = \frac{I_{total}}{h_{down}} = \frac{1.087 \times 10^{12} \ mm^4}{1440 - 720} = 1.509 \times 10^9 \ mm^3$$

Therefore, the section modulus of the gate is larger than the critical one ($1.501 \times 10^9 \ mm^3$). We can conclude that the gate's section is adequate and the stress at the top and bottom fiber will be of:

$$\frac{M_{Ed}}{W_{up}} = \frac{3.603 \times 10^{11} \ [Nm]}{1.509 \times 10^9 \ [mm^3]} = 238.6 N/mm^2$$

This formulations where introduced in an spreadsheet to play with the values and find different sections that could take the bending moment. In the following lines only the result of other geometries having a section modulus greater than $1501 \times 10^6 mm^3$ for different thicknesses of plate and different girder geometries are shown below:

PLATE 20 MM					
Number of flanges	h	th	Gate's area (m2)	t/h ratio	space between flanges (mm)
9	1000	920	8.640	0.92	90
9	1200	620	7.056	0.52	427.5
9	**1400**	**440**	**5.904**	**0.31**	**630**
12	1000	690	8.640	0.69	90
12	1200	470	7.128	0.39	420
12	**1400**	**330**	**5.904**	**0.24**	**630**

Figure L.66: Different geometries when installing steel plates of 20 mm

PLATE 40 MM					
Number of flanges	h	th	Gate's area (m2)	t/h ratio	space between flanges (mm)
9	1000	830	8.190	0.83	191.25
9	1200	530	6.444	0.44	528.75
9	**1400**	**360**	**5.356**	**0.26**	**720**
12	1000	620	8.160	0.62	195
12	1200	400	6.480	0.33	525
12	**1400**	**270**	**5.256**	**0.19**	**720**

Figure L.67: Different geometries when installing steel plates of 40 mm

PLATE 60 MM					
Number of flanges	h	th	Gate's area (m2)	t/h ratio	space between flanges (mm)
9	1000	720	7.560	0.72	315
9	1200	440	5.832	0.37	630
9	**1400**	**280**	**4.608**	**0.20**	**810**
12	1000	540	7.560	0.54	315
12	1200	330	5.823	0.28	630
12	**1400**	**210**	**4.608**	**0.15**	**810**

Figure L.68: Different geometries when installing steel plates of 60 mm

PLATE 80 MM					
Number of flanges	h	th	Gate's area (m2)	t/h ratio	space between flanges (mm)
9	1000	600	6.480	0.60	450
9	1200	340	5.112	0.28	742.5
9	**1400**	**190**	**3.843**	**0.14**	**911.25**
12	1000	450	6.480	0.45	450
12	1200	250	5.040	0.21	750
12	**1400**	**140**	**3.792**	**0.10**	**915**

Figure L.69: Different geometries when installing steel plates of 80 mm

As we can observe, the minimum area for the gate (and therefore the cheapest) always happen for the maximum ”h” value and 12 flanges instead of 9. However, the difference between having 9 or 12 flanges its negligible. In fact, for the 20 and 60 mm gate the cross-section area is the same for both 9 and 12 flanges. Then, to avoid buckling (high t/h ratio) and to ease the gate construction (less flanges to attach results in cheaper gate), 9 flanges will be installed.

From above it can also be observed that the thicker the plate, the lower the area of the gate can be. This can be easily seen in the plot below:

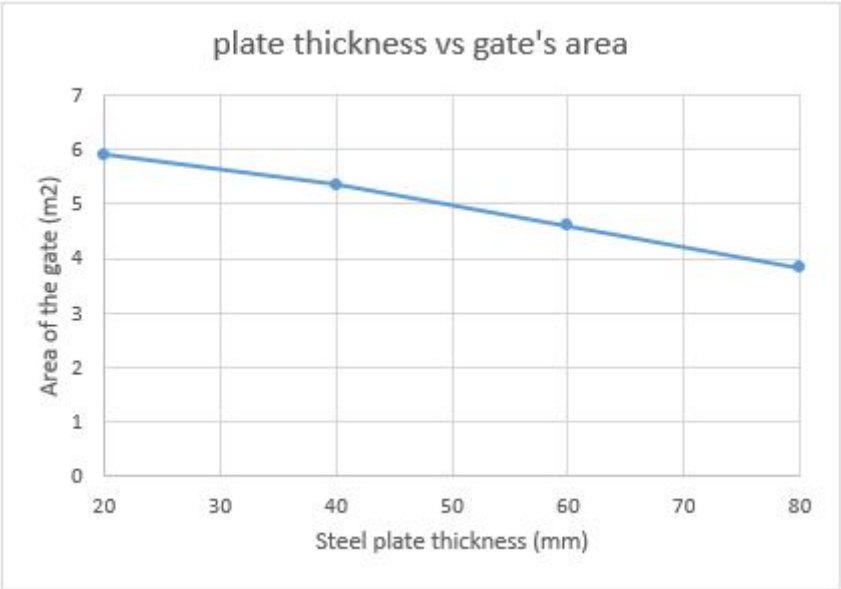

Figure L.70: Plate thickness versus gate area

However, the t/h ratio also becomes smaller for larger steel plate thicknesses as we can see below:

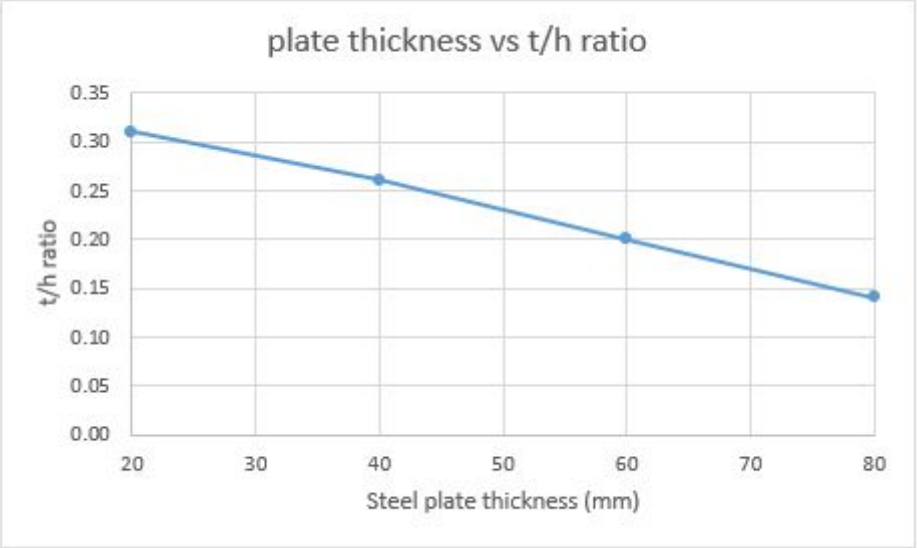

Figure L.71: Plate thickness versus gate area

Therefore, the chosen plate thickness will be of 60 mm since the area is quite low and at the same time the t/h ratio of 0.2 will allow the gate to not buckle.

For the vertical direction of the gate, using two steel plates of 60 mm each, separated by 1400 mm is already enough for achieving the needed section modulus of $258 \times 10^6 mm^3$. The section modulus in the vertical direction becomes $3200 \times 10^6 mm^3$, way more than needed. However, it is recommended to install flanges of some thickness to increase the buckling stability of the horizontal flanges.

Notice that due to the huge span of the gate, a section modulus of $1501 \times 10^6 mm^3$ is only needed at the midsection, so a second design loop considering that the flange height can decrease while approaching the sides of the gate is shown below

The above bending diagram (see Figure L.59 will be divided between 3 sections. Before, we considered that

the whole gate was subjected to a bending moment of 360263.75 kNm. However, now the aim is to consider 3 different bending moments for 3 different areas. For doing this, first, the bending moments are calculated at 4 and 11 meters from the support:

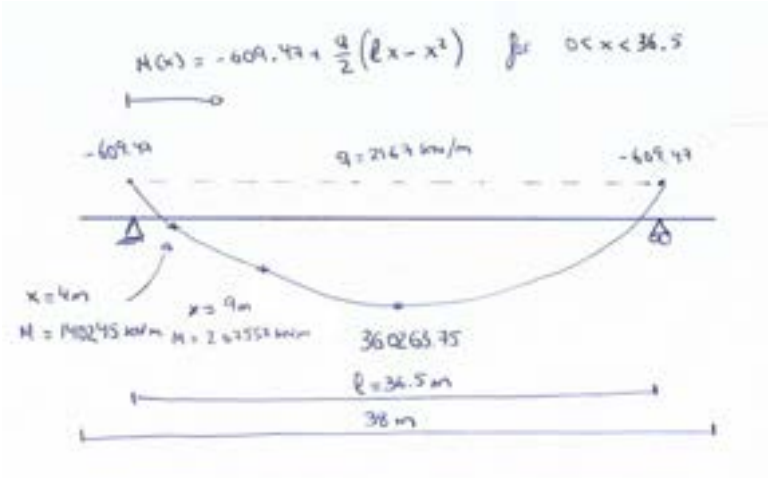

Figure L.72: Bending moment at 4 and 9 meters from the support

Then, we can divide the above bending moments over the length of the gate. In the following image, the previous model considering just the maximum bending moment and the new model considering 3 different gate sections is shown:

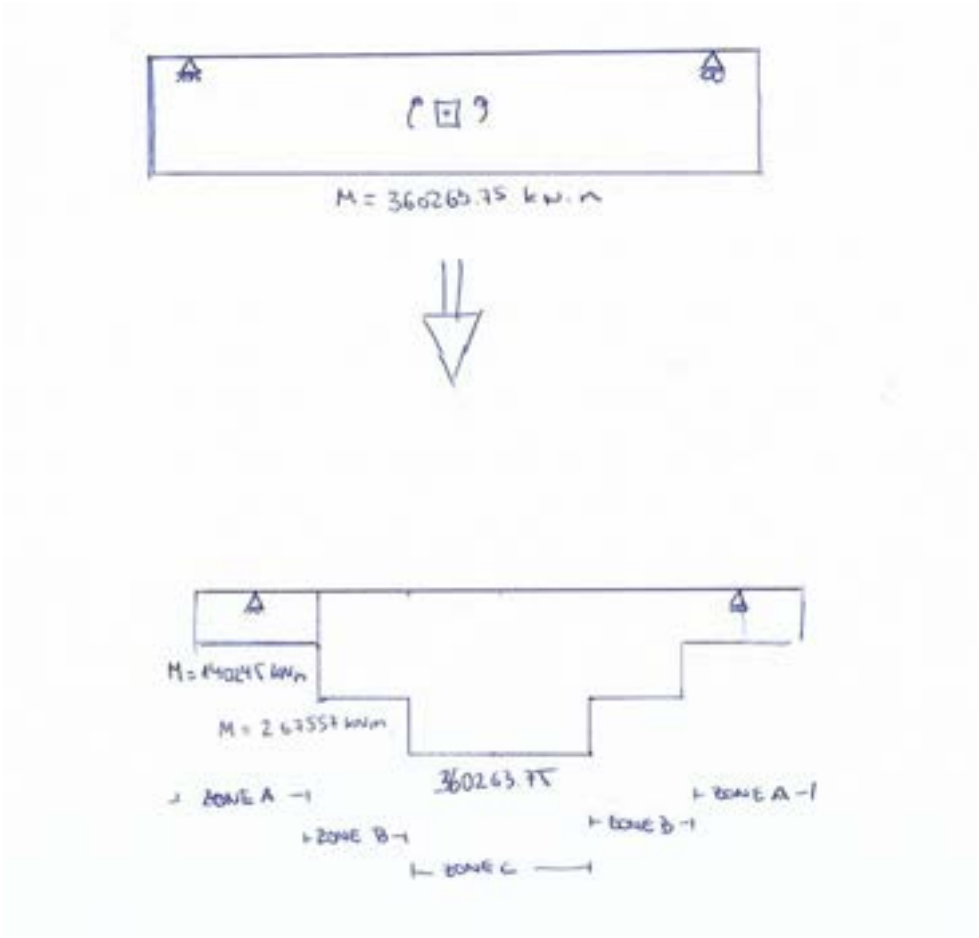

Figure L.73: Initial model considered and final model considered for gate design

The needed section modulus at each zone is as follows:

Zone A: $W_A = \frac{M_{dA}}{\sigma_{steel}} = \frac{140245 \times 10^6 Nmm}{240 N/mm^2} = 584 \times 10^6 mm^3$
Zone B: $W_A = \frac{M_{dB}}{\sigma_{steel}} = \frac{267557 \times 10^6 Nmm}{240 N/mm^2} = 1114 \times 10^6 mm^3$
Zone C: $W_A = \frac{M_{dC}}{\sigma_{steel}} = \frac{360264 \times 10^6 Nmm}{240 N/mm^2} = 1501 \times 10^6 mm^3$

The steel plate used for design will still be the 60 mm one. Besides, the width of the flange is fixed to be 280 mm so only the height of the flange will change. The height is varied instead of the width because at zone A, reducing the flange of 280 mm can be problematic for buckling. This change for each zone is as follows:

- Zone A: $h_{fA} = 750mm$
- Zone B: $h_{fB} = 1150mm$
- Zone C: $h_{fC} = 1400mm$

So instead of having a box-like gate, the gate will be like:

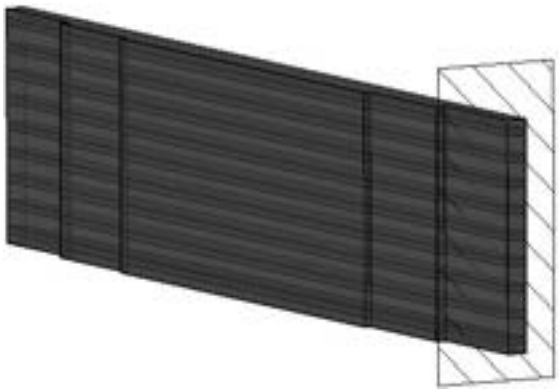

Figure L.74: 3D representation of the gate.

In the picture above, we can see an area that represents the cut below:

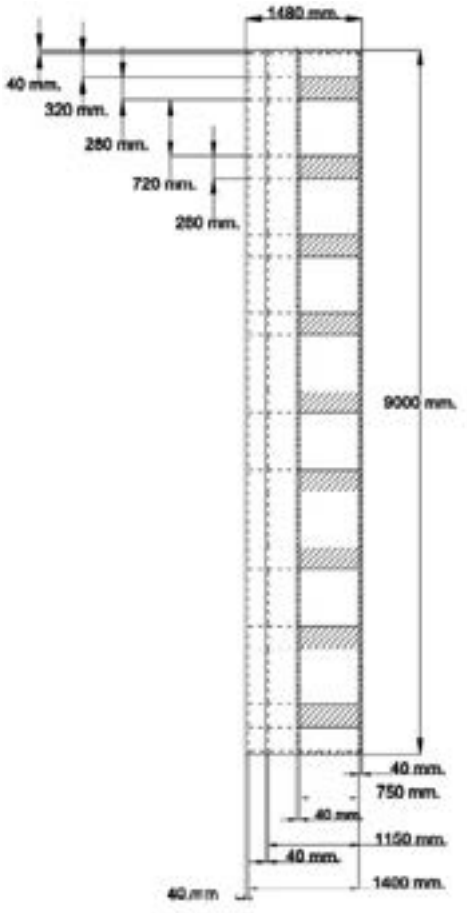

Figure L.75: Gate's vertical cross-section including measurements

The forces are transmitted to the pillars as shown in this image:

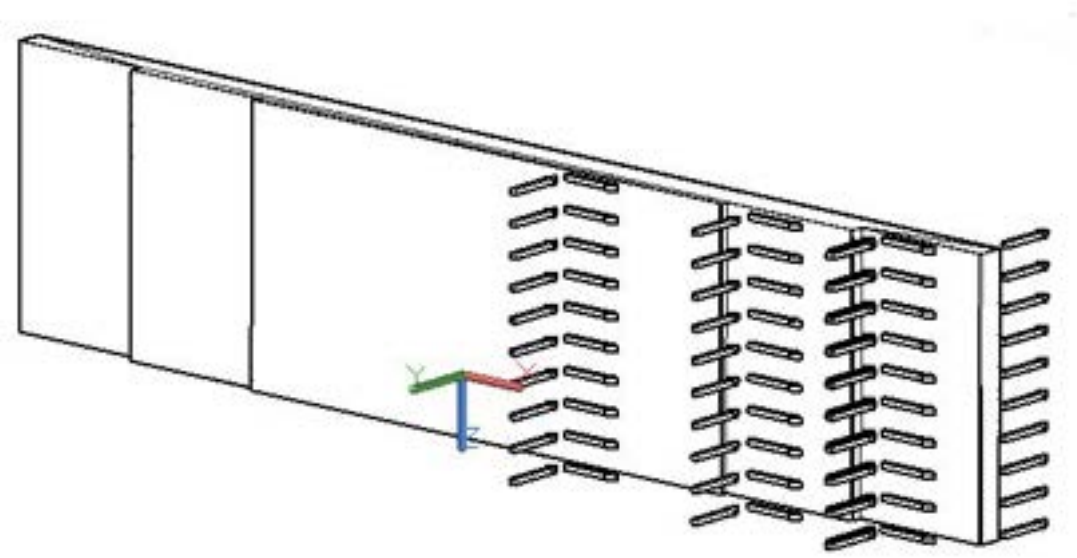

Figure L.76: Flow of forces acting on the gate

The forces acting perpendicularly to the gate are transmitted via the horizontal flanges to the sides, where the forces are transmitted to the structure.

With this last figure, the gate design is complete.

L.7.2 Reinforcement of the water-retaining wall

The present section includes the flow of forces for the "skeleton" of the structure (see Figure **??**). This skeleton is composed by the piers, the wall between the piers that stops the water from passing into the Valmeer, the vertical walls and horizontal slabs, and finally the caisson for the turbine, where the last forces will be transmitted to the ground. In this section, reinforcement calculations for the wall between the piles are included.

To calculate reinforcement, the structure is subjected to the larger load that can happen during its lifetime. That is, during storm surge conditions. The water level inside the Valmeer don't play an important role for the reinforcement of the sea-side part of the structure. They will play an important role in the reinforcing of the Valmeer-side part. However, for the purpose of this thesis and time limitations, this loads won't be considered.

In the following figure, the loads considered for the design of each element is shown.

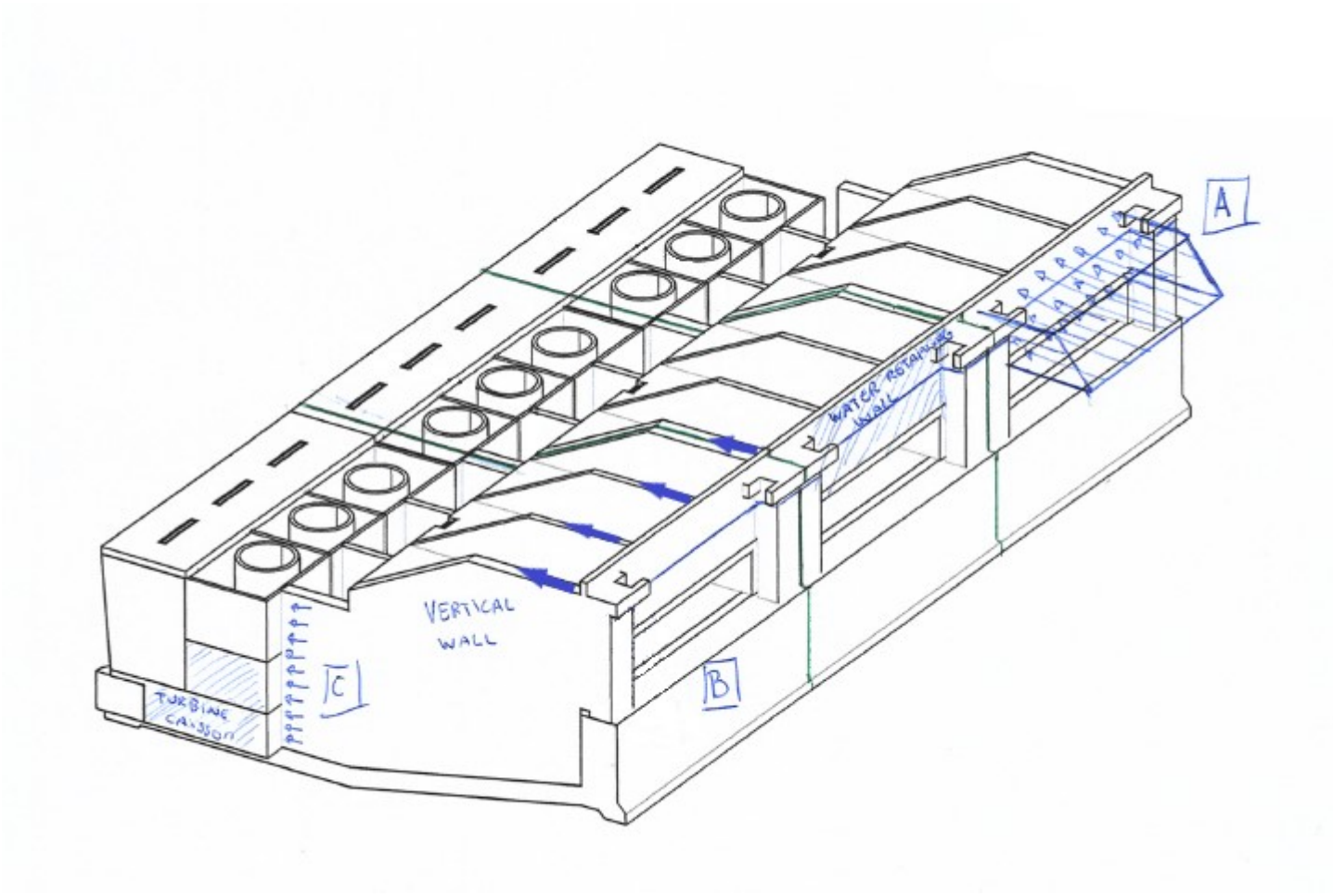

Figure L.77: General view of the loads considered for reinforcement calculations

The above A, B and C areas mean the following:

- A: the load comes from the combination of the hydrostatic load and wave pressures present during storm surge conditions (H_s = 9m, T_p = 11.3 s, WL = NAP + 4.5 m). This wall will be analyzed considering a beam model solved with the MatrixFRAME software. The load considered in the beam model will be the resultant of the wave pressures acting on the water retaining wall. The beam will be modeled as a beam with fixed-end supports (at the thick walls behind the pillar) and fixed pin supports in between (at the walls between the pillars). This model is conservative. All the resultant force from the pressures acting on the wall is assumed to be applied in a 1 m width strap which will be modelled as a beam. Actually, in a meter strap, just the force from the pressures acting in one meter width should be taken into account.

The problem here is what strap needs to be considered for the design. the point of maximum pressures (and therefore forces) is at the bottom of the wall, however, the bending moment will not be the maximum ones since the structure is fixed at the bottom. The largest bending moment in the wall will happen at a point where the pressure is large and the wall span is also large. That can be somewhere in the middle of the wall and at a place next to the top of the wall (see Figure L.78 below). A realistic model would include a plate analysis having three fixed-ends (the sides are connected to the pillars and the bottom part to the inlet structure) and a free one (the top level is free) having the actual total pressures acting on it. However, this is more time consuming and is recommended to be done when the design of the structure is at a further stage. As the calculation is already conservative, no safety factor will be applied to the load.

- B: the load comes from the support reaction forces obtained from A. The support forces will be transferred to the vertical walls as a load per meter of wall height. A strut and tie model will be used to transfer the loads from B to C and find the critical tension areas that will need reinforcement.
- C: the load comes from the above-mentioned strut and tie model and again, a strut and tie model will be considered for the turbine caisson. Above this caisson, in Figure L.77 we can see a vertical wall which will be calculated using beam model with a point load (which acts at the position of the vertical wall).

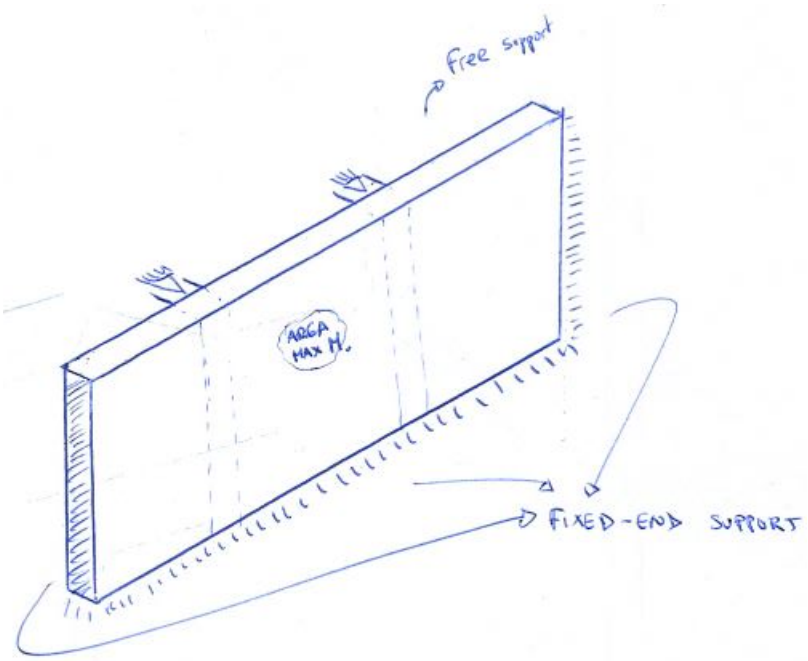

Figure L.78: Possible point of maximum positive bending moment. Representation of the water retaining wall.

Design of the water retaining wall

The water retaining wall has to stand the storm surge pressures. These were already calculated before and can be checked in Figure L.35. For this wall however, some forces change. F_{p1} remains the same and can be taken from Figure L.45. However, the rest of the wave pressures and the hydrostatic load acting on the water retaining wall give another force. This force can be calculated from the following pressures:

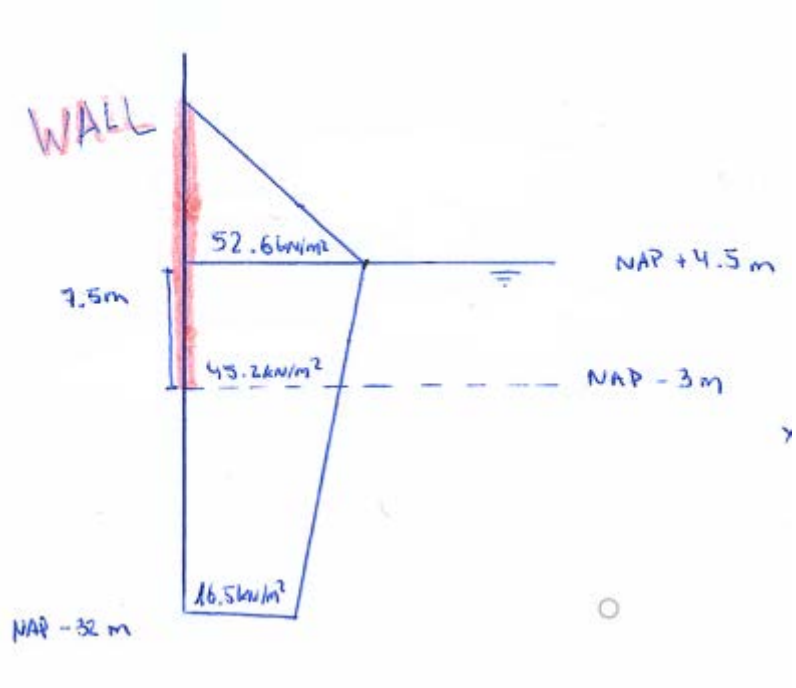

Figure L.79: Wave pressures acting on the wall

The wave pressure at the bottom part of the wall, which is situated at NAP -3m, follows from:

$p_{wallBOTTOM} = 52.6 - \frac{52.6-16.5}{32+4.5} \cdot 7.5 = 45.2kN/m^2$

With that pressure know, it can be added to the hydrostatic force and the total pressure at the bottom of the water retaining wall is $42.5kN/m^2 + 10kN/m^3 \cdot (4.5+3)m = 120kN/m^2$. The pressure distribution together with the resultant forces is then:

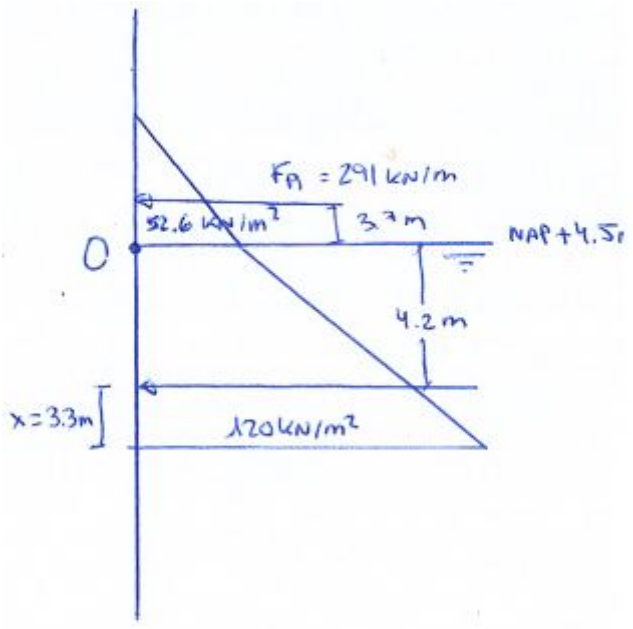

Figure L.80: Pressure distribution acting on the wall

The forces acting on the wall were calculated from:

$F = \frac{120+52.6}{2} \cdot 7.5 = 647kN/m$ and it is applied at: $x = \frac{7.5 \cdot (120+2 \cdot 52.6)}{3 \cdot (120+52.6)} = 3.3m$ from the bottom part of the

water retaining wall. Thus, the application point is at NAP + 0.3 m.

Finally, these system of forces is equivalent to this following one:

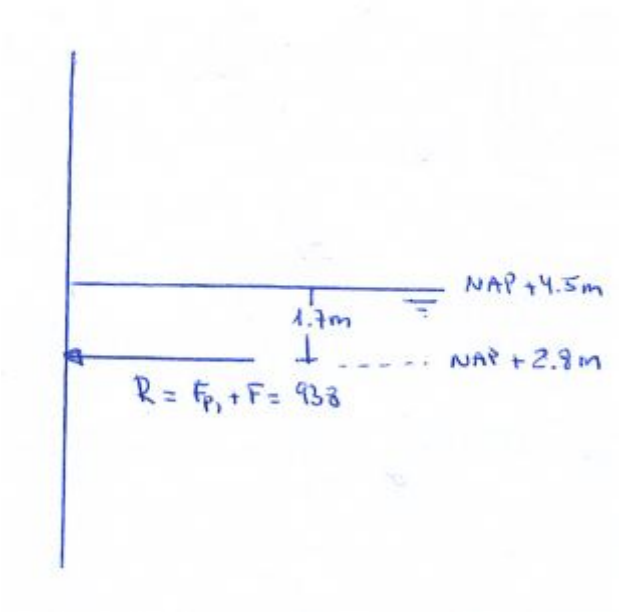

Figure L.81: Resultant system of forces equivalence

Where the point at which the resultant force is applied comes from the moment equilibrium around the NAP + 4.5m point (0 in the figure above):

$M_0 = -291kN/m \cdot 3.7m + 647kN/m \cdot 4.2m = (291kN/m + 647kN/m) \cdot x; x = 1.7m$ Then, the point of application of the force is 1.7 meters below NAP + 4.5m. Thus, it is applied at NAP + 2.8 m.

This load (R in Figure L.81), distributed over the width of the water retaining wall and will be used for the bending moment calculation. The safety factor applied to the load is 1.5 (as it was already done for the gate design). However, remind that this is conservative, since a more realistic model of the wall is the one shown in Appendix L.6 Figure L.78 and not considering a beam. The load case introduced in MatrixFrame is shown below:

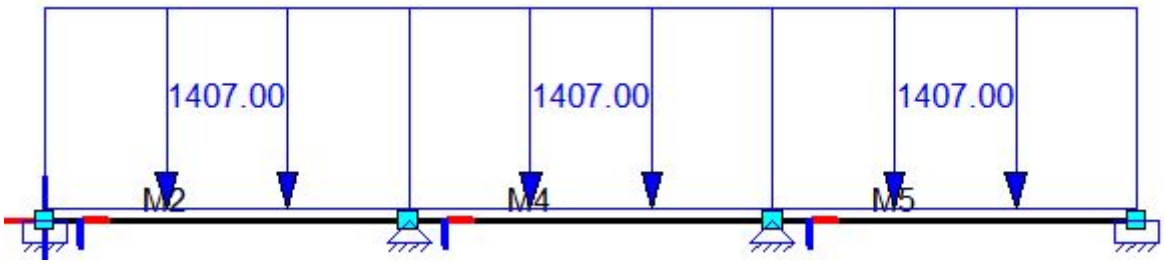

Figure L.82: Load case from MatrixFrame

The beam considered for design has fixed ends and fixed pin support in between. The cross-section is a 19.3 m wide (height of the water retaining wall) and 1 m in height (the thickness of the water-retaining wall is of 1 meter). Notice that the cross-section geometry doesn't affect the bending moment but will be considered later on for the reinforcement calculations. The resulting bending moment from MatrixFrame is as follows:

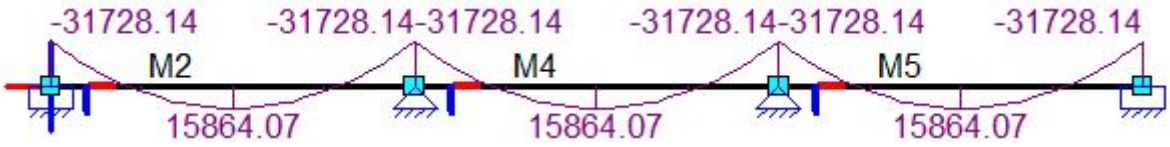

Figure L.83: Bending moment diagram from MatrixFrame

Therefore, the design bending moment for the water retaining wall is 31728 kNm (negative bending moment at the position of the walls). The shear diagram also follows from MatrixFrame:

Figure L.84: Shear force diagram from MatrixFrame

The reinforcing calculations follow from the "Eurocode 2: Design of concrete structures". The reinforcement needed for bending strength is calculated as:

$$A_s = \frac{1}{F_{yd}}\left(\frac{M_{Ed}}{z} + N_{Ed}\right) \tag{L.32}$$

Where:

- A_s: area of reinforcing steel needed.
- f_{yd}: steel's design yield strength. Defined as the steel characteristic yield strength over the material safety factor (f_{yk} / 1.15).
- M_{Ed}: Design bending moment at the considered section.
- z: Moment arm. It is calculated using Equation L.33 below.
- N_{Ed}: Design axial force. Zero for the load case considered.

$$\frac{z}{d} = \frac{1}{2}\left(1 + \sqrt{1 - 2k}\right) \tag{L.33}$$

Where:

- d: distance from the most exterior compression fiber to the center of the rebar's position.
- k: calculated with Equation L.34 below. It must be lower than 0.295.

$$k = \frac{M_{Ed}}{bd^2 f_{cd}} \tag{L.34}$$

Where:

- b: wall's height. Distance from top to bottom of the wall.
- h: wall's thickness.
- f_{cd}: design concrete cylinder strength. Calculated as characteristic cylinder strength over the material safety factor (f_c / 1.5).

Before digging into the above reinforcement calculations, first the concrete cover is calculated. The concrete cover is calculated from:

$$c = c_{min} + \Delta c_{dev} \tag{L.35}$$

Where:

- c_{min}: minimum concrete cover, follows from the exposure class and the structural class.
- Δc_{dev}: allowance in design for deviation. The Eurocode 2 recommends to use 10 mm for this value.

The "water retaining wall" is exposed to cyclic water level differences and to direct wave action. For that reason, the exposure class is XS3 (risk of chloride corrosion (seawater) & cyclic wet and dry conditions). The structural class is defined in the Eurocode 2 as 4 for a service life of 50 years. For a service life of 100 years that this design is done, the structural class is increased by 2. Other factors such as applying a concrete class larger than C45/55 would reduce the structural class (concrete class C35/40 selected). However, these factors don't apply to the present design. Thus, the structural class is 6 and from Table 4.4N of the Eurocode 2, the minimum cover is then 55 mm. The final concrete cover is thus:

$c = c_{min} + \Delta c_{dev} = 55 + 10 = 65\ mm$

The reinforcement calculations can now follow. The needed information for equations L.34, L.33, and L.32 is found below:

- M_{Ed} = 31728 kNm $\approx 3.2 \times 10^4$ kNm.
- b = 19.3 m.
- d = h - c - $\phi_{rebar}/2$ - $\phi_{stirrup}$ = 1000 - 65 - 20/2 - 20 = 905 mm.
- f_{cd} = 35 MPa / 1.5 = 23.3 MPa.
- f_{yd} = 500 MPa / 1.15 = 435 MPa.

Thus, the needed reinforcement area can be calculated:

$$k = \frac{M_{Ed}}{bd^2 f_{cd}} = \frac{3.2 \times 10^7 [Nm]}{19.3[m]905^2[mm^2]23.3[N/mm^2]} = 0.019$$

$$\frac{z}{d} = \frac{1}{2}\Big(1 + \sqrt{1-2k}\Big);\ z = d \cdot \frac{1}{2}\Big(1 + \sqrt{1-2k}\Big) = 1909 \cdot \frac{1}{2}\Big(1 + \sqrt{1-2\cdot 0.087}\Big) = 864 \quad mm$$

$$A_s = \frac{1}{f_{yd}}\Big(\frac{M_{Ed}}{z} + N_{Ed}\Big) = \frac{1}{435}\Big(\frac{2.3 \times 10^10}{864} + 0\Big) = 85198\ mm^2$$

That this steel area can be provided with 272 20 mm rebars. However, the minimum and maximum reinforcement area requirement needs to be checked. You can see it below:

$$A_{smin} = 0.26\frac{f_{ctm}}{f_{yk}}bd = 0.26\frac{3.2[MPa]}{500[MPa]}19300[mm]1909[mm] = 61308\ mm^2 \tag{L.36}$$

$$A_{smax} = 0.04 \cdot b \cdot hmm^2 = 0.04 \cdot 19300 \cdot 1000 = 772000\ mm^2 \tag{L.37}$$

As it is shown above, the area of steel used is larger than the minimum requirement and lower than the maximum requirement. Thus, the section's reinforcement is adequate to uphold the bending moment.

Regarding shear force resistance, the first thing to check is whether if the section itself (only concrete) has enough shear resistance to support the shear forces. This is done again, following the Eurocode 2 formulation:

$$V_{Rd,c} = C_{Rd,c}k(100\rho_l f_{ck})^{1/3}b_w d \tag{L.38}$$

Where:

- $V_{Rd,c}$: shear resistance without applying extra shear reinforcement.
- $C_{Rd,c}$: coefficient derived from tests. 0.12 is recommended.
- k: size factor $1 + \sqrt{200/d}$.
- ρ_l: longitudinal reinforcement ratio (¿0.02).

- f_{ck}: characteristic concrete compressive strength.
- b_w: smallest web width.
- d: effective height of cross section.

By plugging in the correct values we have:

$V_{Rd,c} = C_{Rd,c}k(100\rho_l f_{ck})^{1/3}b_w d = 0.12(1 + \sqrt{200/905})(100\frac{A_s}{bd}35)^{1/3}19300 \cdot 906 \approx 7930000N$

which is lower than the shear force at the section (11572000 N). Thus, additional shear reinforcement should be applied. Again, the Eurocode 2 formulation is followed and the resistance is calculated from:

$$V_{Rd,s} = \frac{A_{sw}}{s} z f_{ywd} cot\phi \tag{L.39}$$

Where:

- $V_{Rd,s}$: Shear resistance including shear stirrups.
- A_{sw}: steel area provided by the stirrups.
- s: stirrups spacing.
- f_{ywd}: stirrup's yield strength.
- ϕ: angle of positioning of the stirrups.

If we use 20 mm stirrups with a spacing of 50 mm between then it is demonstrated below that the shear force can now be resisted:

$V_{Rd,s} = \frac{A_{sw}}{s} z f_{ywd} cot\phi = \frac{2*314[mm]}{50[mm]} 870[mm] \cdot 500/1.15 \cdot cot(21.8) = 11760000N$

This value is now greater than the shear force at the section and therefore the shear reinforcement calculations are finished.

The necessary reinforcement for both bending and shear is shown in the figures below:

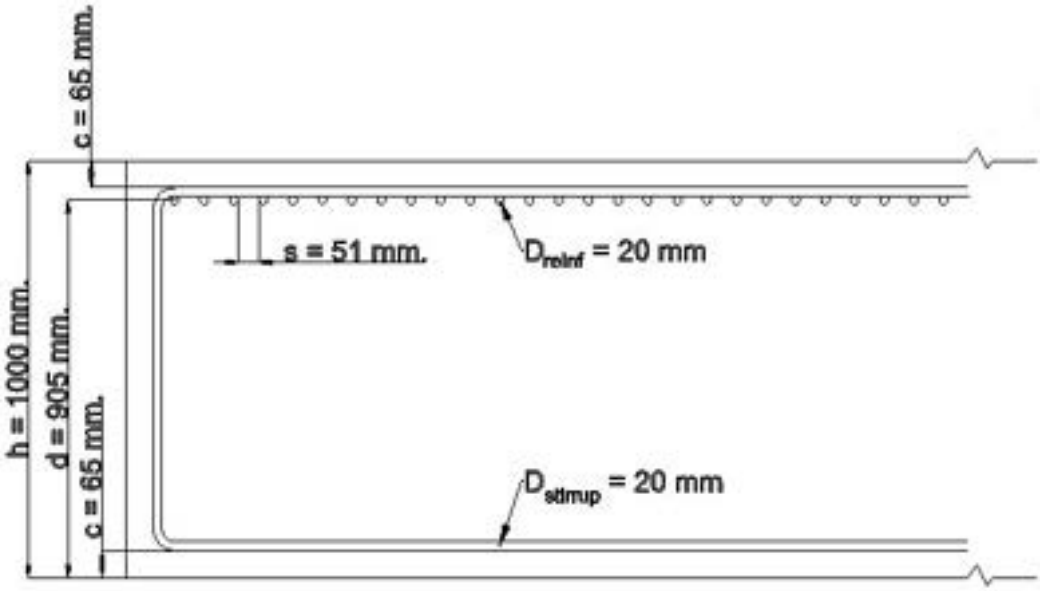

Figure L.85: Reinforcement needed to resist the design bending moment. Vertical cut of the water-retaining wall.

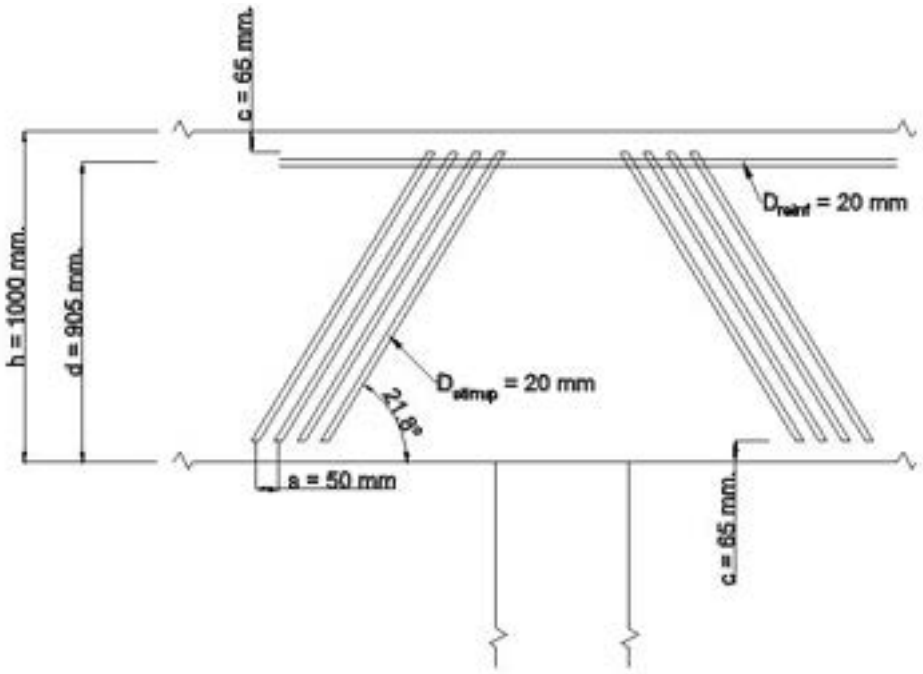

Figure L.86: Reinforcement needed to resist the design shear force. Horizontal cut of the water-retaining wall. Notice that the angle is not represented with its actual tilting to better fir the bars.

With these figures, the reinforcement of the water retaining wall against bending moment and shear force is ensured. As a last remark, notice that the reinforcement should attend to minimize the economic costs of the materials. This is not done here since the aim was to show that the wall can stand the forces present and don't need additional prestressed concrete or other techniques to bear the loads.

Design of the vertical wall

The forces for calculating the reinforcement of the vertical wall comes from the reaction forces of the above load case (see Figure L.82). Notice that these forces are calculated per meter width of the water retaining wall. The reaction force from MatrixFrame are:

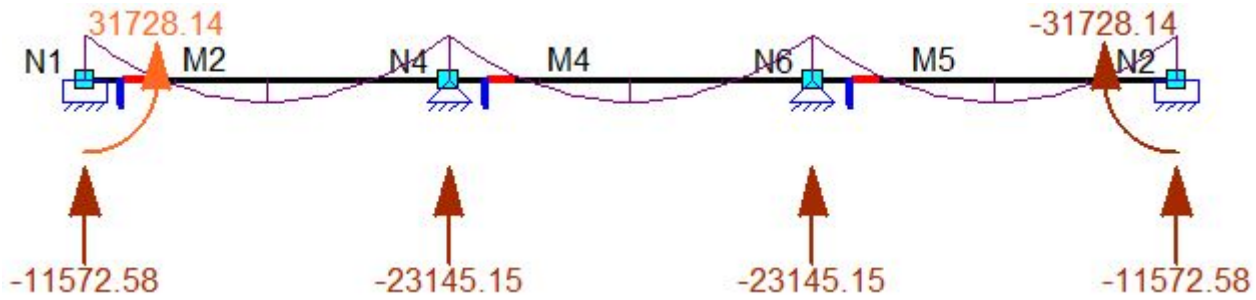

Figure L.87: Reaction forces from the load case shown in Figure L.82 for vertical wall design

The vertical wall design is not includeded in this thesis.

Appendix M

Comparative analysis between the Pump storage station and other renewable energy technologies

M.1 Introduction

In this appendix, the Valmeer's pump hydro storage station characteristics will be compared to other renewable energies. In the LCA this comparison was already made comparing CO_2 emissions per kWh of electricity produced. In the present analysis, costs per MW of power installed are analyzed for different renewable energy technologies. It would be more realistic to compare costs per GWh of electricity produced, but that information is harder to find. And this is just a brief appendix to give an idea to the reader about how the Valmeer's hydro pump storage station ranges among other renewable electricity technologies in terms of costs per MW.

The Valmeer's basin will take around 20 km^2 of land and the current construction costs estimation is at 1.23 billion €. This estimation has been taken from the DELTA21 report. There, it is stated that the entire cost of the plan would be 3.7 billion €. According to the DELTA21 initiators, 2/3 of these costs are allocated to water safety and 1/3 to energy generation. Please notice that the actual costs of constructing the Valmeer's pump hydro storage plant has not been calculated in this thesis and that is why the previous estimation will be used.

For each renewable energy generation technology, a table with the data and its source and a graph showing the cost per MW in comparison with the Valmeer's plant is shown.

M.2 Solar photovoltaic

Name	Country	Capacity (MW)	Costs (M€)	Source	cost/MW (euro/MW)
Noor Abu Dhabi	United Arab Emirates	1177	786	forbes.com; techspot.com	667,799
Longyangxia Dam Solar Park	China	850	850	originenergy.com.au	1,000,000
Kamuthi	India	648	613	originenergy.com.au	945,988
Kurnool Ultra Mega Solar Park	India	1000	903	originenergy.com.au	903,000
Extremadura	Spain	590	300	pv-magazine.com	508,475
Cestas solar farm	France	300	360	pv-magazine.com	1,200,000
Neuhardenberg solar park	Germany	145	280	wikipedia	1,931,034

Figure M.1: Comparison euros per MW installed

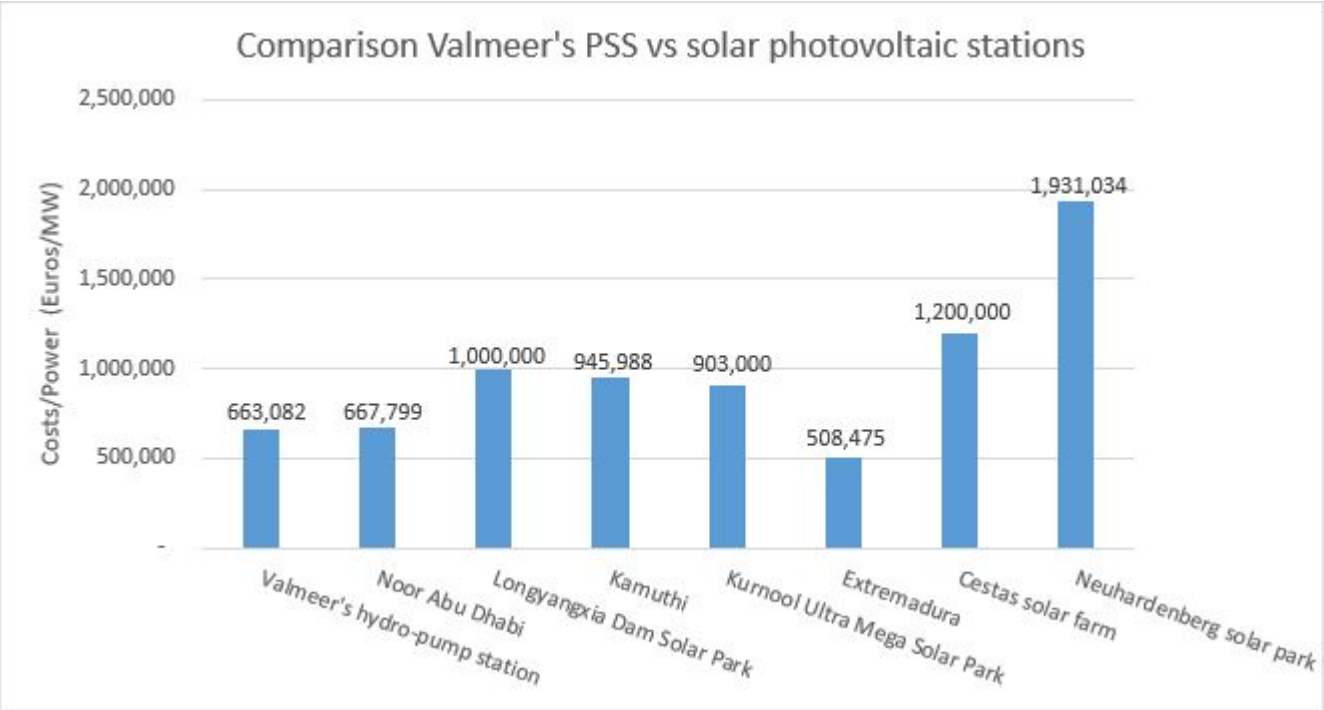

Figure M.2: Comparison euros per MW installed

M.3 Offshore wind

Name	Country	Capacity (MW)	Costs (M€)	Source	cost/MW (euro/MW)
Anholt offshore wind farm	Denmark	400	1350	Wikipedia	3,375,000
Gemini offshore Wind farm	Netherlands	600	2800	geminiwindpark.nl/	4,666,667
London array	England	630	2130	wikipedia.org	3,380,952
Gwynt y Mor	Wales	576	2000	wikipedia.org	3,472,222
Race Bank Wind Farm	England	573	1077	cleantechnica.com	1,879,581

Figure M.3: Comparison euros per MW installed

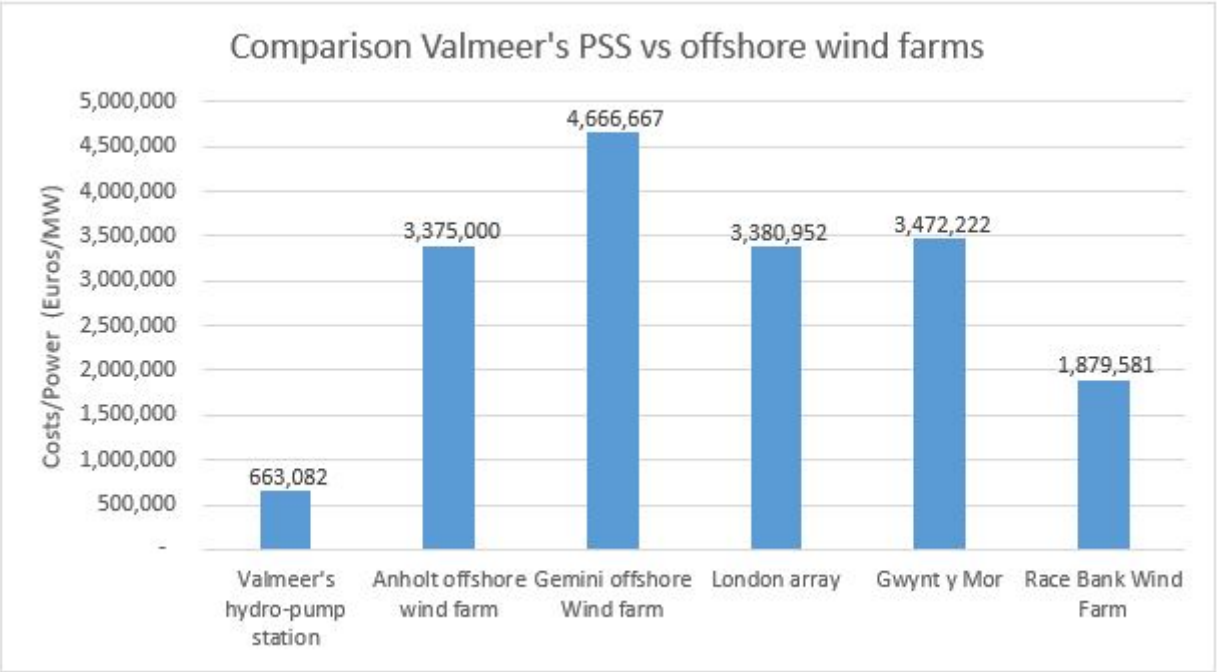

Figure M.4: Comparison euros per MW installed

M.4 Onshore wind

Name	Country	Capacity (MW)	Costs (M€)	Source	cost/MW (euro/MW)
Alta Wind Energy Center	US	1547	2590	wikipedia.org	1,674,208
Whitelee Wind Farm	Scotland	322	354	energy-uk.org.uk	1,099,379
Macarthur Wind Farm	Australia	420	898	reneweconomy.com.au	2,138,095
Shepherds Flat Wind Farm	US	845	1796	tramsmissionhub.com	2,125,444

Figure M.5: Comparison euros per MW installed

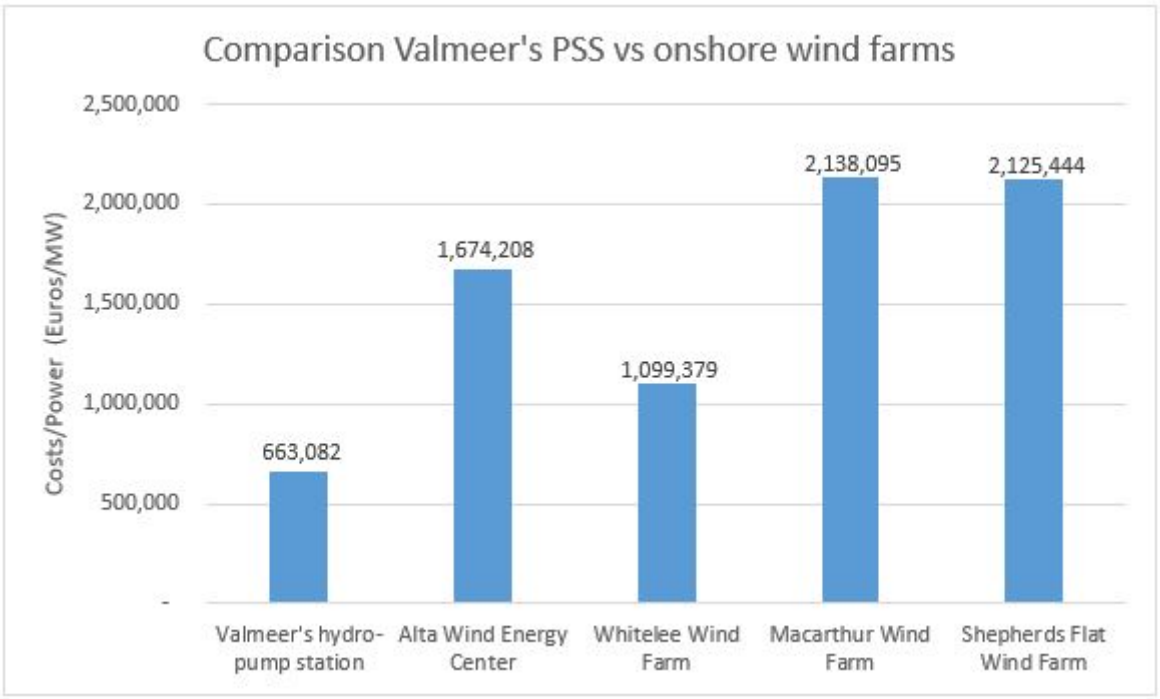

Figure M.6: Comparison euros per MW installed

M.5 Tidal energy

Name	Country	Capacity (MW)	Costs (M€)	Source	cost/MW (euro/MW)
Swansea bay lagoon	England	320	1300	Appendix A of this thesis	4,062,500
La rance tidal power station	France	240	910	Appendix A of this thesis	3,791,667
sihwa lake tidal power station	South korea	245	500	Appendix A of this thesis	2,040,816
Annapolis tidal station	Canada	20	30	Appendix A of this thesis	1,500,000

Figure M.7: Comparison euros per MW installed

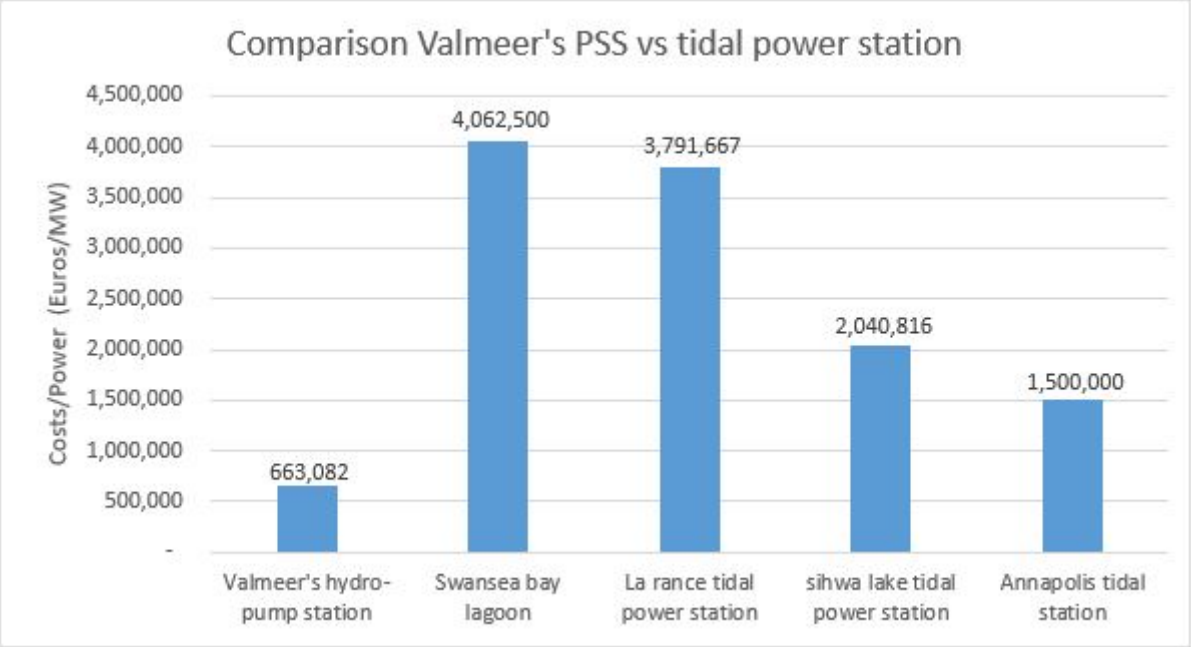

Figure M.8: Comparison euros per MW installed

M.6 Alpine pump storage stations

Name	Country	Capacity (MW)	Costs (M€)	Source	cost/MW (euro/MW)
Bath county PSS	USA	2100	1441	elperiodicodelaenergia.com	686,190
Tianhuangping PSS	China	1836	973	elperiodicodelaenergia.com	529,956
Dinorwig PSS	UK	1728	501	elperiodicodelaenergia.com	289,931
Goldistal PSS	Germany	1806	600	wikipedia.org	332,226
Raccoon mountain PSS	US	1652	1000	wikipedia.org	605,327

Figure M.9: Comparison euros per MW installed

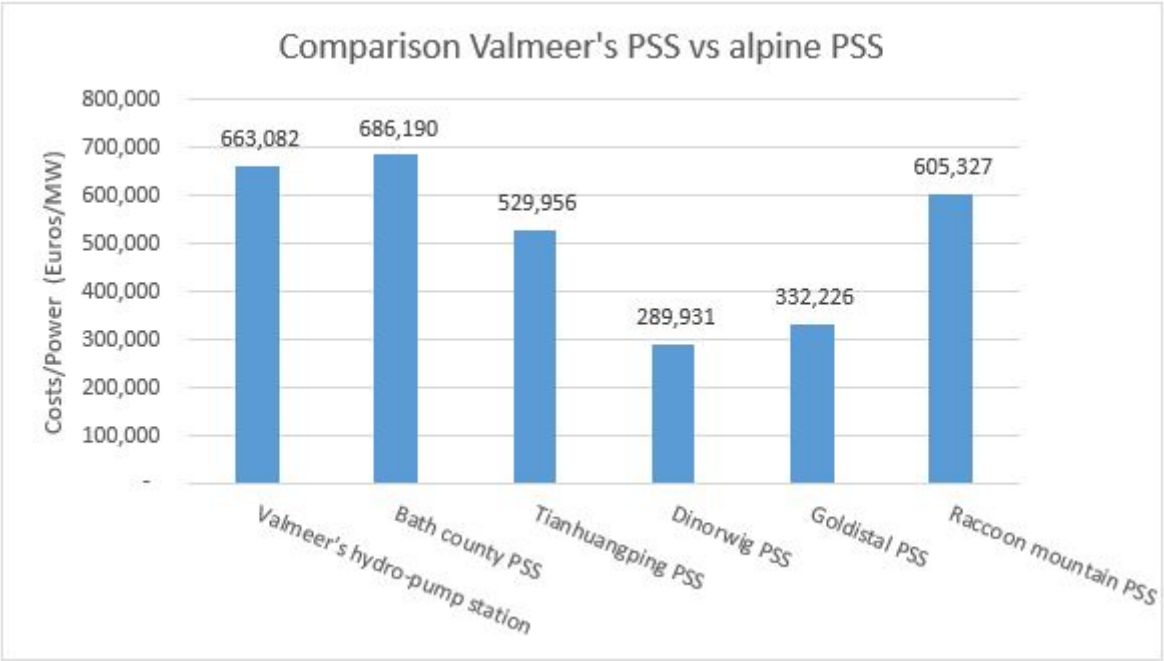

Figure M.10: Comparison euros per MW installed

M.7 Conclusion

As we can see above, the Valmeer's hydro pump storage station ranges better than most of the renewable energy technologies. Regarding costs per MW it is more efficient than wind and tidal energy. When compared against alpine pump storage stations, it ranges below the Bath county and Raccoon ones which are quite old already. Against the newly built alpine pump storage it ranges worst but this is expected since it is the same technology but with lower head difference for electricity generation. Finally, when compared with solar energy, only the Spanish station from Extremadura ranges better. However, against German solar (which could have similar conditions to dutch solar) it ranges better.

This shows that the Valmeer's plant is a good alternative for producing renewable energy in the Netherlands. Besides, in the Valmeer's plant, the cost of storing electricity is already accounted for, something that it cannot be done for solar, wind and tidal energy. But as said in the introduction of this appendix, this is just a fast type of comparing alternatives. Just to have a general idea of the costs per MW.

Appendix N

LCA year-by-year emissions

In this appendix, the emissions per year of the Valmeer's hydro pump storage station are shown. First, a graph is shown and then all the figures are given per year.

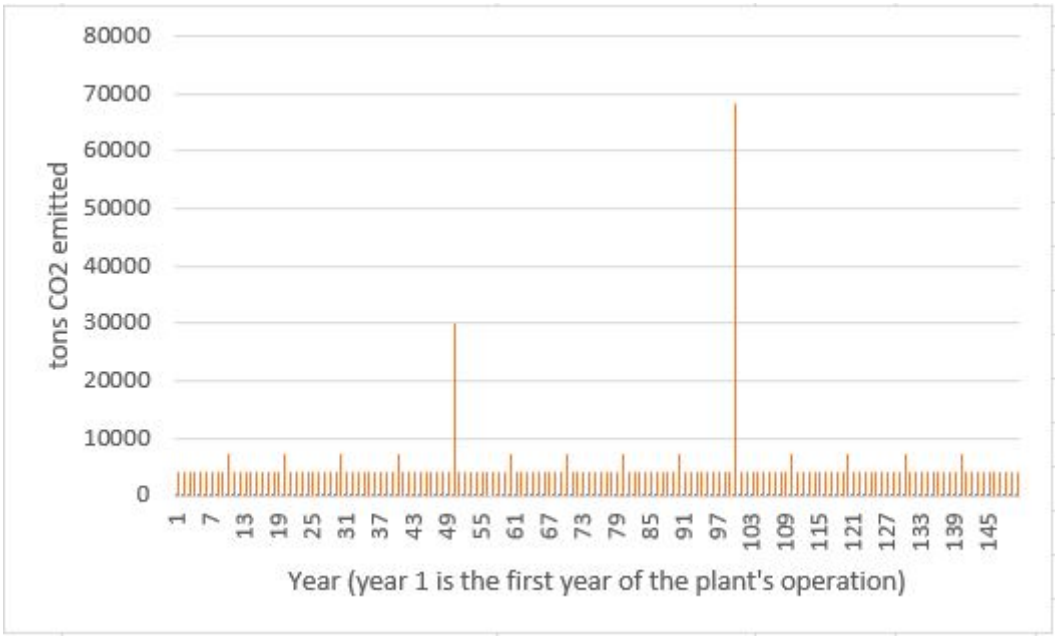

Figure N.1: Yearly CO_2 emissions

In short, the yearly emissions comes from the difference of energy consumed to power the pumps minus the energy obtained from turbining water into the Valmeer. Then, every 10 years maintenance of the pumps/turbines, main gates and turbine gates is taken into consideration. Every 50 years the turbine/pumps as so as the turbine gates will be replaced and finally, at year 100, the main gates will be replaced. The emissions at year 50 are only the emissions from energy consumption because then the structure is considered to be dismantled. Therefore, it makes no sense to perform maintenance in that last year.

Yearly CO_2 emissions of the plant

Year	Tons of CO2
0	610,373
1	4,188
2	4,188
3	4,188
4	4,188
5	4,188
6	4,188
7	4,188
8	4,188
9	4,188
10	7,239
11	4,188
12	4,188
13	4,188
14	4,188
15	4,188
16	4,188
17	4,188
18	4,188
19	4,188
20	7,239
21	4,188
22	4,188
23	4,188
24	4,188
25	4,188
26	4,188
27	4,188
28	4,188
29	4,188
30	7,239
31	4,188
32	4,188
33	4,188
34	4,188
35	4,188
36	4,188
37	4,188
38	4,188
39	4,188
40	7,239
41	4,188
42	4,188
43	4,188
44	4,188
45	4,188
46	4,188
47	4,188
48	4,188
49	4,188
50	30,017
51	4,188
52	4,188
53	4,188
54	4,188
55	4,188
56	4,188
57	4,188
58	4,188
59	4,188
60	7,239
61	4,188
62	4,188
63	4,188
64	4,188
65	4,188
66	4,188
67	4,188
68	4,188
69	4,188
70	7,239
71	4,188
72	4,188
73	4,188

74	4,188
75	4,188
76	4,188
77	4,188
78	4,188
79	4,188
80	7,239
81	4,188
82	4,188
83	4,188
84	4,188
85	4,188
86	4,188
87	4,188
88	4,188
89	4,188
90	7,239
91	4,188
92	4,188
93	4,188
94	4,188
95	4,188
96	4,188
97	4,188
98	4,188
99	4,188

100	68,266
101	4,188
102	4,188
103	4,188
104	4,188
105	4,188
106	4,188
107	4,188
108	4,188
109	4,188
110	7,239
111	4,188
112	4,188
113	4,188
114	4,188
115	4,188
116	4,188
117	4,188
118	4,188
119	4,188
120	7,239
121	4,188
122	4,188
123	4,188
124	4,188
125	4,188

126	4,188
127	4,188
128	4,188
129	4,188
130	7,239
131	4,188
132	4,188
133	4,188
134	4,188
135	4,188
136	4,188
137	4,188
138	4,188
139	4,188
140	7,239
141	4,188
142	4,188
143	4,188
144	4,188
145	4,188
146	4,188
147	4,188
148	4,188
149	4,188
150	4,188